ESTABLISHMENT OF UREOLYTIC BIOFILMS AND THEIR INFLUENCE ON THE PERMEABILITY OF PULSE-FLOW POROUS MEDIA COLUMN SYSTEMS

by

Laura Allison Wheeler

A thesis submitted in partial fulfillment
of the requirements for the degree

of

Master of Science

in

Chemical Engineering

MONTANA STATE UNIVERSITY
Bozeman, Montana

January 2009

APPROVAL

of a thesis submitted by

Laura Allison Wheeler

This thesis has been read by each member of the thesis committee and has been found to be satisfactory regarding content, English usage, format, citation, bibliographic style, and consistency, and is ready for submission to the Division of Graduate Education.

Dr. Robin Gerlach

Approved for the Department of Chemical and Biological Engineering

Dr. Ronald Larsen

Approved for the Division of Graduate Education

Dr. Carl A. Fox

STATEMENT OF PERMISSION TO USE

In presenting this thesis in partial fulfillment of the requirements for a master's degree at Montana State University, I agree that the Library shall make it available to borrowers under rules of the Library.

If I have indicated my intention to copyright this thesis by including a copyright notice page, copying is allowable only for scholarly purposes, consistent with "fair use" as prescribed in the U.S. Copyright Law. Requests for permission for extended quotation from or reproduction of this thesis in whole or in parts may be granted only by the copyright holder.

Laura Allison Wheeler

January 2009

ACKNOWLEDGEMENTS

I would like to thank everyone who lent support and advice during the preparation of this thesis. First, I would like to thank my committee, Dr. Robin Gerlach, Dr. Ron Larsen, and Dr. Al Cunningham for their guidance throughout the writing process. I would like to especially thank all the people who proofread the document: Dr. Robin Gerlach, Erin Field, Stacy Parks, and Natasha Mallette. Thanks to Adie Phillips for teaching me proper lab technique. Special thanks to Dr. Andy Mitchell for taking SEM and stereoscope images of the beads and columns. Thanks to Chris Groth for answering endless questions about the tubing and the column building process. Special thanks to Logan Schultz and Betsey Pitts for their help with calculating direct counts. Thank you to everyone at the CBE, especially John Neuman, for providing me with emergency supplies and making me feel like part of a family.

Lastly, I would like to thank my mom, my dad, and Glenn; I would be nothing without your love and support.

TABLE OF CONTENTS

TABLE OF CONTENTS-CONTINUED

LIST OF TABLES

LIST OF TABLES-CONTINUED

Table Page

LIST OF TABLES-CONTINUED

Table Page

LIST OF FIGURES

LIST OF FIGURES-CONTINUED

Figure Page

LIST OF FIGURES-CONTINUED

Figure Page

LIST OF FIGURES-CONTINUED

Figure Page

LIST OF FIGURES-CONTINUED

Figure Page

LIST OF FIGURES-CONTINUED

Figure Page

LIST OF FIGURES

Figure Page

LIST OF FIGURES-CONTINUED

Figure Page

ABSTRACT

As the population of the world has increased, energy consumption and greenhouse gas emissions have increased as well. One possible way to reduce the amount of greenhouse gases emitted into the atmosphere is through the geologic sequestration of carbon dioxide. During geologic sequestration, supercritical carbon dioxide is injected into different types of underground formations. Inherent cracks in these formations may lead to the upward leakage of CO_2, and a controllable engineered strategy is needed to reduce this potential leakage. Currently, biomineralization has been used in many different environmental applications but not for the sequestration of carbon dioxide. The goal of this research is to establish biofilm communities of ureolytic bacteria that promote $CaCO_3$ precipitation in a pulse-flow porous media column system with the intent of reducing the porosity and permeability of the porous media.

Pulse-flow column systems were inoculated with different species of ureolytic bacteria: *S. pasteurii*, *B. sphaericus* #21776, or *B. sphaericus* #21787. The bacteria were allowed to grow in the column for five days before a calcium-containing medium was introduced. Flow rate, pH, ammonium concentration, calcium concentration, culturable bacteria, and protein concentration were monitored over the course of the entire experiments. It was shown that all ureolytic species were capable of growing, utilizing urea, and creating an environment that facilitated calcium carbonate precipitation in 1mm diameter glass bead packed columns at room temperature and atmospheric pressure. To better understand the effect of pore space on biomineralization columns packed with 0.1 mm diameter glass beads were constructed and inoculated with *S. pasteurii*. Within days of calcium introduction, the permeability of the columns was reduced to the point where no more fluid would drain from the column.

These results indicate that the ureolytic bacteria are capable of surviving, facilitating calcium carbonate precipitation, and reducing the permeability of the pulse-flow porous media column system. While further study is needed, the precipitation of calcium carbonate through ureolysis may offer a controllable engineered strategy to reduce the permeability of underground formations used for geologic sequestration.

INTRODUCTION

The research described in this thesis is part of a project sponsored by Zero Emissions Research and Technology (ZERT). ZERT is funded by the United States Department of Energy, under award number DE-FC26-04NT42262 (1). ZERT is dedicated to reducing the amount of greenhouse gas emissions in the atmosphere through geologic storage/sequestration and developing technology that can ensure the reliability of that storage (1). The project described in this thesis was undertaken by the Center for Biofilm Engineering (CBE) at Montana State University and studied the potential role of biofilms in carbon capture and sequestration.

The increase in the world's population, from about 6 billion in 1999 to a projected 9.2 billion in 2050 (2) means that energy consumption, and therefore carbon emissions, will increase as well. Based on data from 2004 obtained from the United Nations Statistics Division (3), the United States leads the world in carbon emissions with 5.9 billion metric tons released into the atmosphere - a 19.6% increase since 1990. Other nations are not far behind: China released 5 billion metric tons - a 108.7% increase, India released 1.3 billion metric tons - a 96.9% increase, and Japan released 1.3 billion tons - a 12.4% increase. Figure 1 shows CO_2 emissions per capita for the world in 2004.

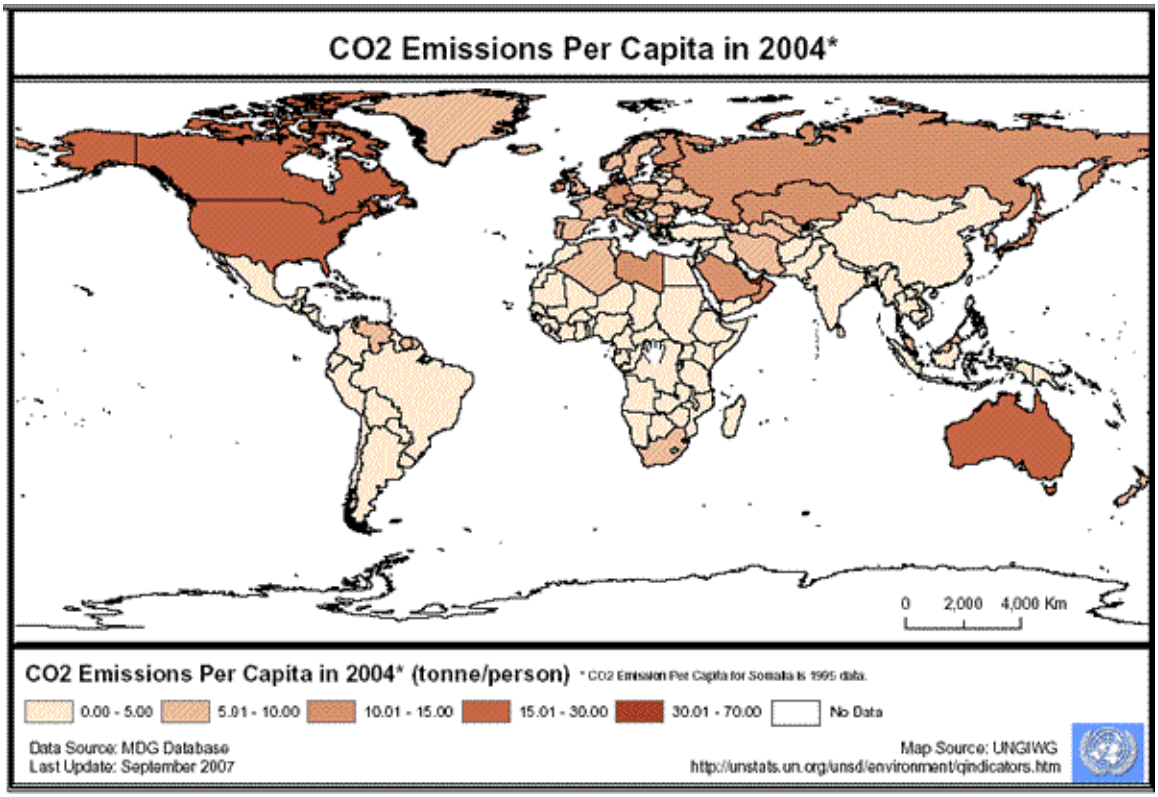

Figure 1: CO_2 emissions per capita for 2004 (3).

Carbon dioxide has long been considered a primary contributor to global warming and the need to reduce its concentration in the atmosphere to pre-industrial levels might be necessary for maintaining the health of the planet.

Geologic Sequestration

Geologic sequestration of carbon dioxide is just one strategy to reduce the emission of greenhouse gases into the atmosphere due to the combustion of fossil fuels. Sequestration involves the injection of supercritical CO_2 into oil bearing formations, deep un-mineable coal seams, and deep saline aquifers as shown in Figure 2 (5).

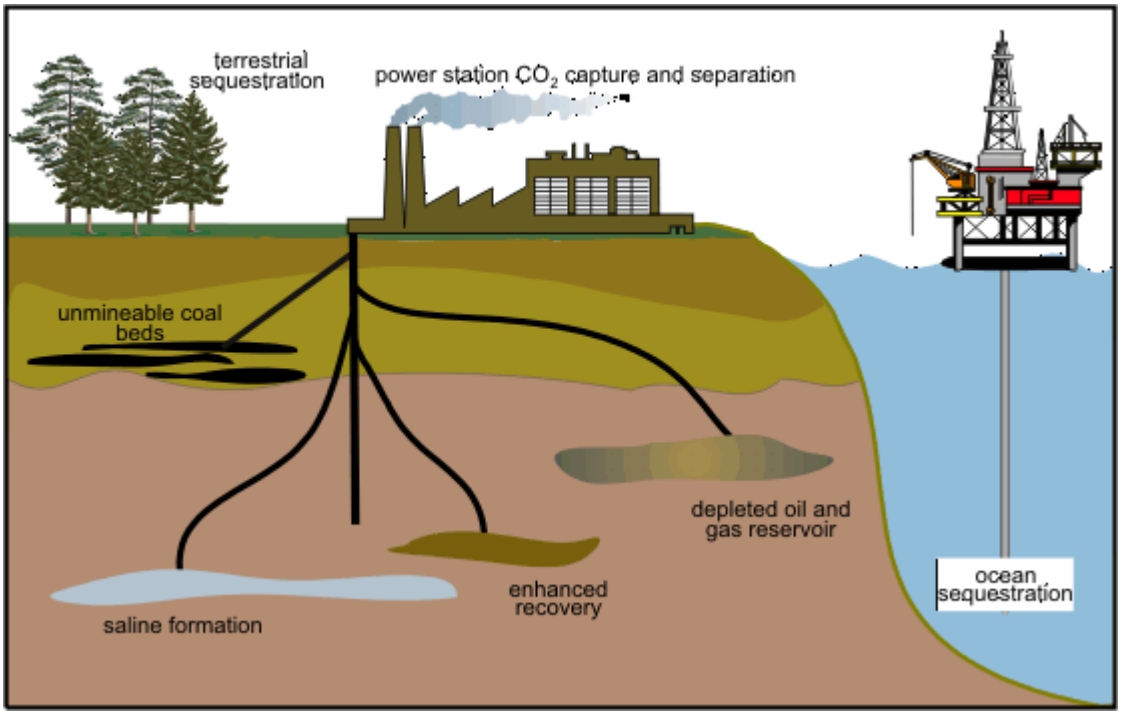

Figure 2: Possible CO_2 trapping formations include saline aquifers, unmineable coal seams, the sea, and oil bearing formations (10).

The injection of the supercritical CO_2 can cause regions of elevated pressure to form near the injection wells. Pressure gradients formed by this process may cause upward leakage of CO_2. Leakage of CO_2 may also be caused by cracks and fractures already present in the sequestration site, and by the inherent permeability of the CO_2 trapping formation. It is critical to develop methods to reduce CO_2 leakage to make geologic sequestration of CO_2 a possible mechanism to reduce the amount of greenhouse gases in the atmosphere.

It is also possible to sequester carbon dioxide in other areas. Currently the Norwegian oil company Statoil is taking carbon dioxide from gas production in the Sleipner West Field and injecting it 1000 m beneath the seabed of the Norwegian North Sea. About 2800 tons are injected into the sandstone formation every day (6). The success of Statoil's underwater sequestration program is dampened by the cost of the

project. "This approach isn't the first people are likely to turn to, but it will be one of the key solutions if emission reductions are really going to bite," says Mr. Torp, manager of the saline aquifer carbon dioxide storage project (6). Even though the cost is currently prohibitive (6), sequestration may become a viable solution to reducing the amount of greenhouse gases in the atmosphere.

Ureolysis and Carbonate Biomineralization

The relationship between bacterial activity and carbonate mineral precipitation has long been recognized in modern and ancient sedimentary environments (7). In 1889, reports of $CaCO_3$ precipitation in the presence of urea decomposition were published by Murray and Irvine (27). According to Ehrlich, G.A. Nadson in 1899 (and again in 1903) was the first to provide extensive evidence that bacteria could precipitate $CaCO_3$ (14). Nadson not only identified several organisms capable of precipitating $CaCO_3$, he also proved that $CaCO_3$ precipitation was not dependent on a certain group of bacteria but rather on the environmental or surrounding conditions (14). Since Nadson's discovery in the early 1900s, researchers have identified many more bacteria capable of $CaCO_3$ precipitation, and have found many scenarios where $CaCO_3$ precipitation can be used for benefit.

It has been hypothesized that almost all bacteria are capable of $CaCO_3$ production because precipitation occurs as a byproduct of common metabolic processes such as photosynthesis, sulfate reduction, and urea hydrolysis (8). The urease enzyme (e.g. urea amidohydrolase; EC 3.5.1.5) is common in many microorganisms and ureolysis can be

induced in a lab setting by adding urea (8). One mol of urea is hydrolyzed intracellularly to 1 mol of ammonia and 1 mol of carbamate (equation 1), which spontaneously hydrolyzes to form an additional 1 mol of ammonia and carbonic acid (equation 2). These products subsequently equilibrate in water to form bicarbonate, 2 mol of ammonium, and 2 mol of hydroxide ions (equations 3 and 4). The latter give rise to a pH increase, which in turn can shift the bicarbonate equilibrium, resulting in the formation of carbonate ions (equation 5), which in the presence of soluble calcium ions precipitate as $CaCO_3$ (equation 6) (8). Equation 7 is an overall reaction for the system, showing that urea and calcium are added to the system, and ammonium and calcium carbonate are products.

$CO(NH_2)_2 + H_2O \rightarrow NH_2COOH + NH_3$ (1)

$NH_2COOH + H_2O \rightarrow NH_3 + H_2CO_3$ (2)

$H_2CO_3 \leftrightarrow HCO_3^- + H^+$ (3)

$2NH_3 + 2H_2O \leftrightarrow 2NH_4^+ + 2OH^-$ (pH increase) (4)

$HCO_3^- + H^+ + 2OH^- \leftrightarrow CO_3^{2-} + 2H_2O$ (5)

$CO_3^{2-} + Ca^{2+} \leftrightarrow CaCO_3$ (carbonate precipitation) (6)

$CO(NH_2)_2 + 2H_2O + Ca^{2+} \rightarrow 2NH_4^+ + CaCO_3$ (overall reaction) (7)

Calcium carbonate is an appropriate mineral to use for the reduction of porosity of underground formations for many reasons. Ca^{2+} is one of the most abundant cations and carbonate ions (HCO_3^- and CO_3^{2-}) are some of the most abundant anions in most subsurface waters (9). In order to produce the most mineral mass, utilizing elements

already present in the subsurface is a more efficient method than adding another chemical. Injection of supercritical CO_2 into the underground formations will also make more carbonate ions by the dissolution and disassociation of CO_2, which in turn will be used to precipitate more mineral (as seen in the above equations).

Bacterial calcium carbonate precipitation results from both passive and active nucleation. Passive carbonate nucleation occurs from metabolically driven changes in the bulk fluid environment surrounding the bacterial cells. This increases the mineral saturation and induces nucleation (11). In the ureolysis driven system, this occurs from an increase in pH due to ammonification (12). Active carbonate nucleation occurs when the bacterial cell surface is utilized as the nucleation site. The cell clusters exhibit a net electronegative charge which favors the adsorption of Ca^{2+} ions. The Ca^{2+} ions attract CO_3^{2-} and HCO_3^- ions, which will eventually form calcium carbonate precipitates (8, 13).

Although it is known that there are many different types of bacteria capable of calcium carbonate precipitation, it has been hypothesized that there are specific attributes of certain bacteria that promote and affect $CaCO_3$ precipitation more than others (8). It has already been noted that cell walls have an inherent electronegative charge that affect the binding of certain ions (29), but the extracellular polymeric substance (EPS) associated with biofilms may also be involved. Biofilm cells are contained in the EPS matrix and may use it as an attachment device, for structural support, and/or protection (30). The EPS matrix is composed primarily of polysaccharides and, depending on the side chains attached to the polysaccharides (e.g. carboxyl groups, pyruvate, phosphate, or

sulfate), the matrix can exhibit an overall negative charge (30). This negative charge is important in trapping metal ions within the EPS matrix (28).

One of the primary applications of biomineralization is the plugging of porous media with applications leaning toward bioremediation (31). Because plugging of porous media can occur in many different environmental locations and involve many different factors, such as soil alkalinity, temperature, and pressure, it is important to monitor the effectiveness of the bacteria's ability to precipitate out calcium carbonate in each different environmental situation. Research done by Ferris et al. (2003) showed that the hydrolysis of urea by *Bacillus pasteurii* (now reclassified as *Sporosarcina pasteurii* (4)) is temperature dependent and that the highest calcite precipitation rates occurred near the point of critical saturation (31). It also highlighted the fact that calcite precipitation is kinetically dependent on saturation state and independent of temperature (31). This research by Ferris et al. (2003) emphasized the impact of environmental conditions on calcite precipitation that were previously noticed by Nadson, as recorded by Ehrlich (14).

Members of the genus *Bacillus* are Gram-positive, rod-shaped, endospore-forming bacteria commonly found in soil (15). *Bacillus pasteurii*, a member of this genus, converts urea to ammonium carbonate more actively than any other known bacterium (15). Therefore, *B. pasteurii* and other members of the *Bacillus* genus are incorporated into studies to determine their influence on calcium carbonate precipitation in various environments. Experiments performed by Stocks-Fischer et al. (1999) indicated that urease activity at high pH in *B. pasteurii* favored calcium carbonate precipitation (12). Upon examination of the sand grains from columns used in the

experiment, bacterial cells were shown encased in calcite crystals, which indicated that the bacteria acted as a nucleation site for the mineralization process, an example of active nucleation (12).

Another study conducted by Hammes et al. (2003) looked at strain specific $CaCO_3$ precipitation. Isolates collected from various soil locations in Belgium yielded some crystal growth and urease activity and, when sequenced, showed that all the isolates were closely related to one another and the group *Bacillus sphaericus*. Other close relatives of the group are *Bacillus pasteurii*, *Bacillus psychrophilus*, *Bacillus globisporus*, *Planococcus okeanokoites*, and *Filibacter limicola* (8).

Bioremediation

Bacteria have the largest surface area to volume ratio of any life form (11) and have a net electronegative charge (29). The combination of the large surface area and net negative charge facilitates the binding of dissolved metal ions on the surface of the bacteria. This immobilization of metal ions and their transformation into mineral deposits could lead to the use of biomineralization techniques for bioremediation applications such as removing harmful contaminants from groundwater and converting toxic chemicals from mining sites to less harmful compounds. In order to determine the maximum amount of calcium carbonate that can be precipitated under extreme conditions, the effect of common contaminants on the kinetics of the process have to be considered.

Certain bacteria are capable of surviving in very harsh environments, and some prefer an extreme pH and higher temperatures. The normally slow production of toxic chemicals at mining sites can be accelerated by the presence of chemolithotrophs which oxidize Fe^{2+} to Fe^{3+} and sulfur to SO_4^{2-}. A specific chemolithotroph, *Thiobacillus ferrooxidans*, oxidizes iron and sulfur, but is also capable of immobilizing the portion of metal leachate it comes in contact with, eventually encapsulating itself in a mineral phase of mainly iron oxides (11). By showing that mineral formation can occur under extreme or toxic conditions, biomineralization can be viewed as a possible mechanism for cleaning up hazardous environments.

When used in bioremediation work, bacteria are often in the presence of toxic substances, and it is important to know if these toxic substances inhibit the effectiveness of the bacteria. Biomineralization could also be a possible clean-up solution for aquifers where the groundwater is contaminated with divalent metals (Pb^{2+}, Zn^{2+}, Ba^{2+}, and Cd^{2+}) and radionuclides (^{90}Sr and ^{60}Co) as a result of Department of Energy activities (16, 17, 31). Coprecipitation of calcium carbonate offers a means of slowing the transport of the above contaminants into the subsurface. Fujita et al. (2000) proves that there are ureolytic bacteria capable of precipitation inherent in the contaminated aquifers (16). The strategy is to accelerate the precipitation process by adding urea, thus slowing the transport of harmful chemicals in the subsurface.

As a follow up to the work done on aquifers and groundwater by Fujita et al. (2000), Mitchell and Ferris (2006) looked at the effect of ^{90}Sr on crystal size and morphology of the calcium carbonate precipitated out by the bacteria. Mitchell and

Ferris found that crystal diameter increased over a number of days in strontium free solutions, but remained constant for the first six days in a strontium inclusive solution (17). Crystal size was also smaller in the strontium inclusive experiments, indicating that strontium inhibited crystal growth. These smaller crystals were also more soluble than the larger ones (17). Even though the crystal size and solubility were different in the presence of strontium, over 99% of calcium was precipitated and strontium coprecipitated, so it is unlikely that the effectiveness of strontium immobilization was affected (17). This research shows that the presence of toxins can slow down bacterial processes, but not to the point where calcium precipitation is halted.

Biomineralization may also have a place in an industrial setting. Wastewater associated with industrial processes often has high concentrations of dissolved calcium which can lead to clogging in downstream processes. The current approach to this problem is to add chemicals that increase the pH of the wastewater and to add sand grains as nucleation sites for $CaCO_3$ precipitation (8). The addition of ureolytic bacteria could be an easier and more efficient method for removing the excess calcium in the water; ureolysis would be induced with the addition of urea, and calcium carbonate would precipitate. An experiment performed by Hammes et al. (2003), showed that up to 85% of calcium was removed from industrial wastewater using this method (32).

The use of bacteria in bioremediation processes has potential to be more environmentally friendly, efficient, and cost effective. The use of inherent bacteria eliminates the need for the addition of bacteria and costly reagents. Biomineralization

has the potential to be used in the remediation of many contaminated sites and aquifers across the United States.

Enhanced Oil Recovery

With the price of oil reaching record highs, enhancing the amount of oil recovered from reservoirs has become paramount. Current oil production methods recover anywhere from 8% to 30% of the oil present in a reservoir (18, 33), and enhanced oil recovery accounts for 4% of the nation's oil production (35). One method used to enhance oil recovery involves introducing a fluid into the subsurface reservoir through several injection wells. The fluid is injected at or above the inherent formation pressure and as it flows through the formation it drives the oil upwards the wells (19). This method of oil recovery is not as effective because the permeability of the subsurface regions are not uniform and the driving fluid will move through regions of higher permeability first, bypassing the regions of lower permeability and any oil contained in those regions (19). Biomineralization could be an effective solution to this problem; selectively closing off regions of higher permeability after the oil contained in them has been recovered, allowing the oil in the lower permeability regions to be collected.

Oil bearing formations can also lie on top of zones of water. Because water is less viscous than oil, it is easier to pump (20). Wells that have poor oil recovery will eventually produce just water after several years (20). Plugging these subsurface water zones via biomineralization could be a simple method for alleviating the problem.

Both MacLeod et al. (18) and Ferris et al. (19) have demonstrated that the plugging of the higher permeability zones by microbial mineral precipitation and the flow of the fluid to zones of lower permeability is possible, which indicates that this method could be a potential avenue for enhanced oil recovery. However, plugging of the formation by biomineralization is not a perfect method for enhancing oil recovery. High velocity flow and pressure conditions could damage the bacterial colonies, rendering this method unusable (19). While there are certain drawbacks, biomineralization could enhance oil recovery in many regions.

Microbial Concrete Remediation

Concrete and steel are arguably the most widely used construction materials in the world today. Steel bars are embedded in concrete to produce stronger building structures and the concrete provides the added benefit of protecting the steel bars from the elements (21). When cracks appear in the concrete, the possibility for corrosion of the embedded steel arises which could eventually ruin the integrity of the structure. Without immediate attention, the cracks can expand and cause extensive damage.

Current forms of concrete crack remediation are structural epoxy, resins, epoxy mortar, and other synthetic filler agents (22). These synthetic solutions often need to be applied more than once as the cracks expand. Clearly there is a need for an effective, long-term, environmentally safe method to repair cracks in concrete structures.

Several research groups have investigated the possibility of biomineralization as an effective method to remediate cracks and fissures in concrete structures.

Ramachandran et al. (2001) demonstrated that cracks filled with a mixture of *B. pasteurii* (now reclassified as *Sporosarcina pasteurii* (4)) and sand showed a significant increase in compressive strength and stiffness, compared to cracks without cells. Microscopy confirmed the presence of calcite crystals and cells near the surface of the cracks (22).

Other groups have noted that biomineralization can be used in the conservation of ornamental limestone statues or carvings, similar to its use in concrete remediation. *Myxococcus xanthus* is capable of precipitating calcium carbonate. The $CaCO_3$ cements pre-existing calcite grains on the pore walls of the limestone without completely plugging the pore. The resulting crystals are strongly attached and more resistant to stress than were the pre-existing calcite grains (23).

Microbial Dust Suppression

Dust contamination at construction sites, quarries, and unpaved roads has long been a problem. Effective dust control can reduce human respiratory problems, vehicle accidents due to poor visibility and road conditions, impacts on fish, aquatic life, vegetation, water quality, vehicle and equipment wear and damage, and unpaved road maintenance costs (45, 46).

Past methods of dust control fall into four categories: agronomic, surface penetration, admixture, and surface blanket (48). Surface penetration methods include some of the more widely known treatments for dust suppression such as applying water, used oil, and chemicals directly onto the soil surface (48). Because of possible side effects of this approach such as runoff toxicity, pollution, contamination, and method

effectiveness, an economical and environmentally friendly method for dust suppression is needed.

Bang and colleagues from the South Dakota School of Mines and Technology have proposed a method for dust suppression that makes use of microbial calcite precipitation (40). This group has already proven that microbes are capable of cementing fine dust particles and plugging cracks on the soil surface (12, 22, 24, 25, 40). Based on this observation, it is believed that this could be a controllable, engineered strategy for dust suppression.

OBJECTIVES

The project described in this thesis is designed to meet a portion of the Zero Emissions Research and Technology (ZERT) sponsored project undertaken by the Center for Biofilm Engineering to reduce potential leakage of carbon dioxide during geologic carbon sequestration. From the literature review, it is apparent that the idea of microbial calcite precipitation is not new and has applications in many different aspects of science and engineering. However, it has never before been used as a potential barrier in the geologic sequestration of carbon dioxide.

The specific objectives of this research were:

1. To establish biofilm communities of ureolytic bacteria that promote $CaCO_3$ precipitation in a pulse-flow porous media column system.

2. To reduce the permeability of porous media using ureolytic biofilms and calcium carbonate precipitation.

MATERIALS AND METHODS

Column System Design

The column system used in this research was modified from a previous column experiment. In the previous column system (Figure 3), the media was added to the system manually, increasing the potential for contamination in the media bottle and in the columns. The new column system was designed as a closed system instead of an open system because a closed system will reduce the potential for contamination and because the new system facilitates a quicker sampling procedure. The new system was built using the paper by Vandevivere and Baveye (1992) as a guideline (26).

Figure 3: Picture of old column system. Medium was added to the system by hand, exposing the columns to daily contamination.

The system consisted of glass columns all with an inner diameter of 1 cm and a length of 40 cm. The columns were cut by Bridger Glass (Bozeman, MT) from a single length of glass tubing.

The beads used in the columns were all purchased from Biospec Laboratories (Bartlesville, OK). The beads are glass with diameter sizes of 1 mm, 0.5 mm, and 0.1 mm.

500 mL of medium were placed in a 1L Pyrex media bottle outfitted with a two holed, size 8, rubber stopper and connected to the top of the glass column via size 16 Norprene or Tygon tubing. A plunger-less 10 mL Fisher brand plastic syringe filled to the 5 mL mark with glass wool served as an air vent (Figure 4). A standard bacterial vent had been used before, but it was not able to stand up to long sterilization times in the autoclave, and was therefore replaced with the glass wool-filled syringes.

Figure 4: Pyrex media bottle with glass-wool filled syringe air vent and half of the fluid delivery system.

In the first few trials with this column system, medium was taken from a single bottle and delivered to the column system via a three-way splitter. The potential for back and cross contamination led to the creation of a separate media bottle and flow system for each column. At the beginning of this research, large glass flow breaks were used to prevent back contamination. However, this method did not always work, hence custom flow breaks were

made from Fisher Brand syringes. Each syringe plunger was removed and a double holed, size 4 stopper was inserted into the top of each syringe. A small glass tube was inserted into one of the holes in the stopper and the remaining hole was plugged with glass wool and sealed with WeldBond brand glue and DAP brand aquarium silicon sealant. The glass tube was connected to the media bottle using size 16 silicon tubing. The other end of the syringe was connected to the silicon tubing with a Luer-lock connector.

A two holed, size 00 black rubber stopper was fitted securely in the top of the glass column. Two small lengths of Cole Parmer 1/16 in inner diameter Teflon FEP tubing were threaded through the holes. One piece of the FEP tubing was connected to a glass-wool-filled syringe air vent. The other piece of FEP tubing was connected to a three-way “T” connector (Figure 5). A small septum was attached to the “stem” end of the T connector and was used during inoculation and while packing the sterilized beads tightly into the column. The long length of tubing attached to the other end of the “T” connector connected to the Luer-lock end of the syringe flow break.

Another “T”-connector with a septum was placed in line near the media bottle outlet in order to sample the media daily.

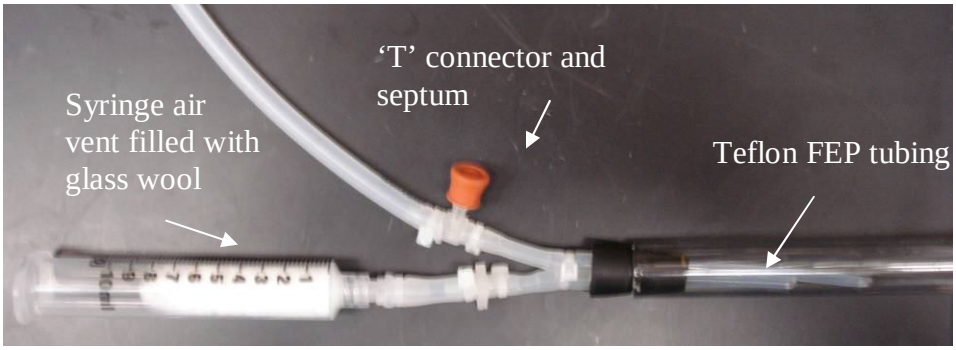

Figure 5: Influent section of glass columns. Septum is used during inoculation and during packing the sterilized porous media in the column.

A single holed size 00 black rubber stopper was fitted securely in the bottom of the column. A small piece of Cole Parmer 1/16 in inner diameter Teflon FEP tubing is threaded through the hole and cut so it is flush with the top of the stopper. This piece of FEP tubing is connected to size 14, 16, and 15 silicon tubing via tubing connectors. A 5.5 cm length of glass tubing is connected to the piece of size 15 silicon tubing and is connected securely to a glass funnel (Figure 6). A large piece of tubing is wrapped around the top part of the funnel to ensure that the glass piece is securely connected.

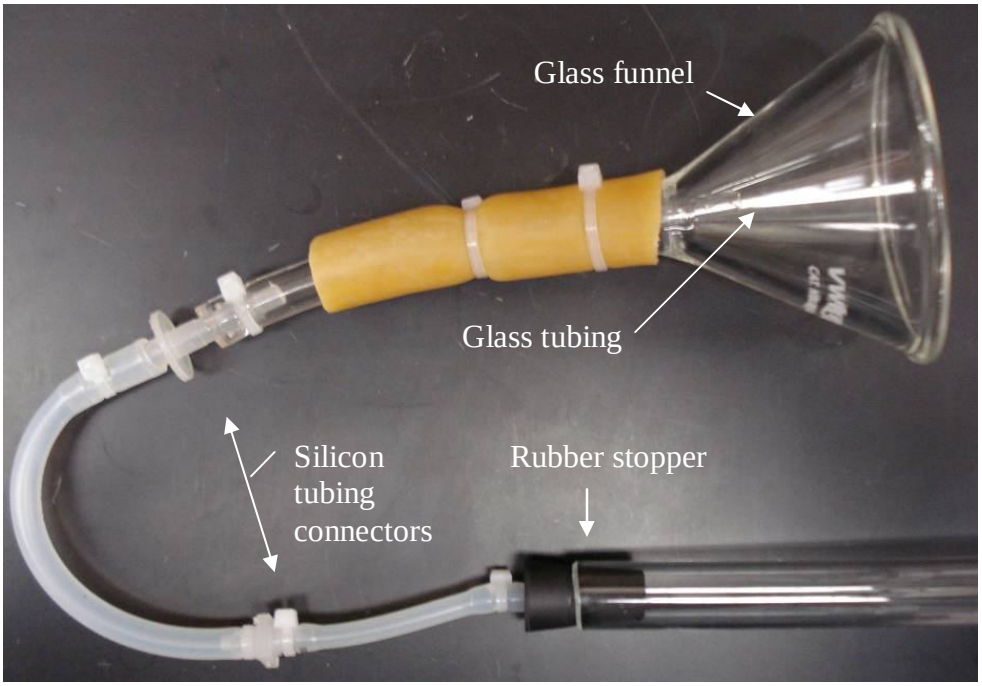

Figure 6: Effluent section of column. Fluid is drained from the column, passes out through the funnel, and into a 15 mL centrifuge tube.

Once the column system was assembled, all tubing connections were secured with cable ties. The columns were attached to a steel rack with cable ties, and the tubing was run through a Cole-Parmer Masterflex cartridge pump. The media bottles, and the tubing attached to them, were elevated so that the flow breaks were able to remain upright to prevent back contamination of the system. Tube clamps were installed in line on the effluent collection system to control the draining of media from the column (Figure 7).

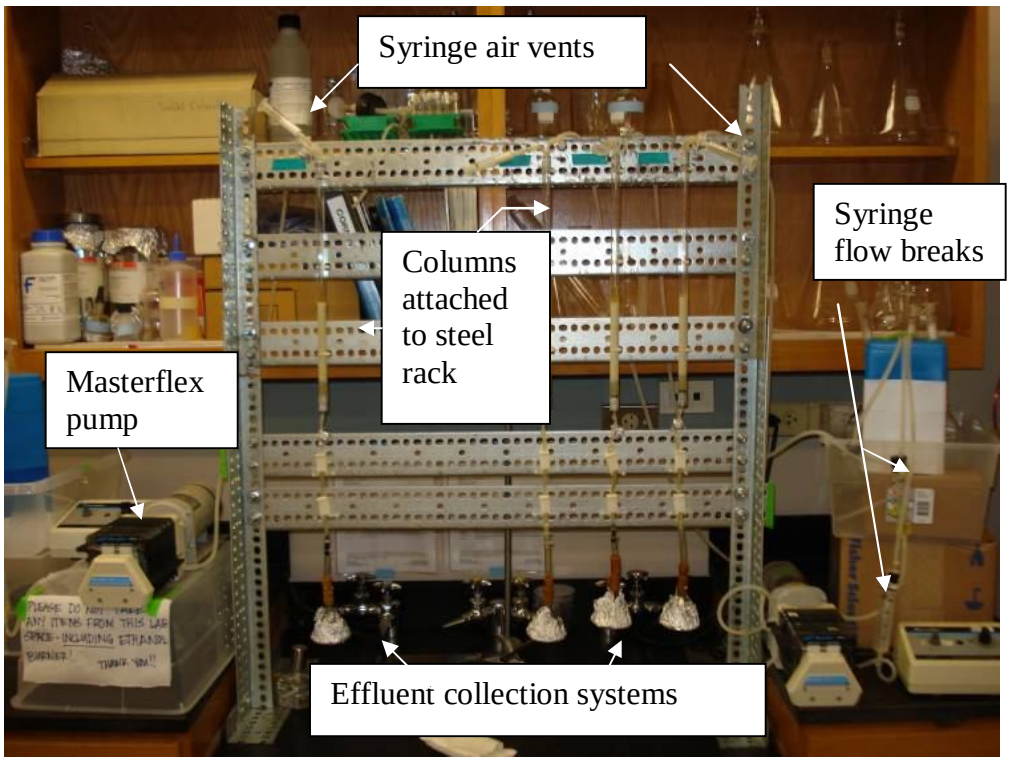

Figure 7: Column system fully assembled on steel rack and attached to media bottles.

Prior to sterilization, the columns were partially assembled on the rack. A funnel was used to pack the column with 1.0 mm diameter beads to a glass bead bed height of 15 cm as measured from the bottom of the column. Once the beads were in the column, the column was tapped gently to help settle the beads.

Figure 8: The bottom 3 cm of a 0.1 mm diameter bead column. The column is packed with 1 cm of 1 mm diameter beads, 1 cm of 0.5 mm beads, and 13 cm of 0.1 mm beads.

Then, the rubber stopper and tubing were attached to the top of the column. When the 0.1 mm beads were used in the column, a base layer of 1 cm of 1 mm beads and 1 cm of 0.5 mm beads were put in place before the remaining 13 cm was filled with the 0.1 mm beads (Figure 8).

Once the system was assembled, the entire apparatus was placed in a large autoclave tub with test tube racks in the bottom. The test tube racks ensured that the equipment would be separated from the water that accumulated in the autoclave tub during the autoclave process. The system was autoclaved on a dry cycle for 45 minutes.

The media bottle stopper complete with air vent and fluid delivery apparatus was autoclaved separately in a 1L Pyrex media bottle on a dry cycle for 25 min.

After the system was sterilized and all the stoppers were secured with parafilm, the columns were filled with calcium-free medium. Medium was poured into a shallow glass dish and pulled up into a 30 mL syringe with a 23G 1 inch long needle. Medium was injected into the column via the septum and the column was inverted carefully from side to side until the beads were packed in the column without any air bubbles. The column was then reattached to the steel rack.

If the column contained 0.1 mm beads, a septum was installed at the effluent end of the column near the rubber stopper. The column was attached to the steel rack prior to packing. The media was injected slowly through septum at the bottom of the column so it rose up through the bead pack. The column was tapped lightly on the side to make sure the beads packed evenly.

Preparation of Growth Medium and Bacterial Inoculum

Calcite Mineralizing Medium (CMM) was prepared according to the procedure outlined in a 1996 paper by Ferris and Stehmeier (20) with the following modifications: a plus (+) after the CMM indicates the inclusion of calcium in the medium and a minus (-) indicates the exclusion of calcium.

The medium was composed of the following ingredients:

Table 1: Recipe for the preparation of calcite mineralizing medium (CMM).

Ingredient	**Concentration (g/L)**
Difco Nutrient Broth	3
Urea	20
Ammonium Chloride	10
Sodium Bicarbonate	2.1
Calcium Chloride Dihydrate	3.7

CMM was made in the following manner: Three grams of Difco Nutrient Broth (BD, Sparks, MD) were dissolved in 500 mL of nanopure water and autoclaved for 25 minutes. 20 grams of Urea (Fisher, Fair Lawn, NJ), 10 grams of ammonium chloride (Fisher, Fair Lawn, NJ), and 2.1 grams of sodium bicarbonate (Fisher, Fair Lawn, NJ) were dissolved in 500 mL of nanopure water on a stir plate. This solution was added to the nutrient broth after it had cooled to room temperature. The whole solution was adjusted to pH 6 +/- 0.1 using concentrated HCl. For calcium inclusive medium (CMM+), 3.7 grams of calcium chloride dihydrate (Acros, NJ, USA) was added after pH adjustment. The complete medium was filter sterilized using a SteriTop 0.22 µm vacuum filter (Fisher, Fair Lawn, NJ).

All bacteria were grown in a medium made from Brain Heart Infusion (BHI) and 2% autoclaved urea. This medium was prepared by dissolving 37 grams of BHI (Oxoid, Basingstoke, Hampshire, England) and 20 grams of urea (Fisher, Fair Lawn, NJ) in nanopure water and autoclaving for 25 minutes. There was a difference noted between solutions in which the urea had been autoclaved with the other ingredients and solutions in which the urea had been added after autoclaving. If the medium title includes "2% autoclaved urea", the urea was added to the solution prior to autoclaving.

For plate counts, a standard dilution series was made in a phosphate buffer solution (PBS, Table 2). The phosphate buffer solution was made at a 10x strength and diluted 1:10 in deionized water and autoclaved for 25 minutes. The test tubes were capped, arranged in a rack, and autoclaved prior to being filled with PBS. Once the solution and the tubes were cool, 9 mL of PBS was added to each tube in the laminar flow hood.

Table 2: Recipe for single strength phosphate buffer solution (PBS) used for plate counts.

Ingredient	**Concentration (g/L)**
NaCl (Fisher, Fair Lawn, NJ)	8.5
KH_2PO_4 (Fisher, Fair Lawn, NJ)	0.61
K_2HPO_4 (Fisher, Fair Lawn, NJ)	0.96

The dilution series was plated on BHI + 2% autoclaved urea agar plates (Table 3).

Table 3: Recipe for BHI + 2% autoclaved urea agar plates.

Ingredient	**Concentration (g/L)**
BHI (Oxoid, Basingstoke, Hampshire, England)	37
Urea (Fisher, Fair Lawn, NJ)	20
Granulated Agar (BD, Sparks, MD)	15

Bacterial Culture Methods

The three bacteria used were *S. pasteurii*, *B. sphaericus* #21776, and *B. sphaericus* #21787. *S. pasteurii* was chosen because it was known to be a strong ureolytic organism (15). The *B. sphaericus* strains were chosen because they were isolated from natural soils and are known to facilitate $CaCO_3$ precipitation. *B. subtilis* was chosen for its non-ureolytic properties and used as a control organism.

A 1 mL frozen stock of the bacterium was thawed then poured into 100 mL of the BHI and urea growth medium. The flask was placed in a G24 Environmental Incubator-Shaker from New Brunswick Scientific Co. (Edison, NJ) operating at about 150 rpm. *S. pasteurii*, *B. sphaericus* #21776, and *B. sphaericus* #21787 were grown at 30°C, and *B. subtilis* was grown at 37°C. After the cultures grew in the incubator-shaker for 24 hours, 1 mL of the culture was transferred to a new flask filled with 100 mL of the BHI and urea growth medium. The cultures were transferred twice in a 48 hours time period before being prepared for inoculation.

Inocula Preparation

45 mL from the twice-transferred cultures were poured into 50 mL Fisher Brand plastic centrifuge tubes. The tubes were centrifuged at 6000 rpm for 10 minutes in a Sorvall Instruments RC5C centrifuge using a Sorvall PTI F15S 8x50c rotor. The cells were washed with CMM- twice before they were adjusted to an optical density (OD) at 600 nm of about 0.4, measured using a 96 well plate, BioTek Synergy HT plate reader

and KC4 software. 100 μL aliquots of the desired inoculum were added to three separate wells in the 96 well plate before the plate was inserted into the reader. The inocula were poured into serum bottles, stoppered, and crimp sealed.

Column Inoculation

The medium used to pack the beads in the column was drained to just above the bead pack prior to inoculation. The desired inoculum was prepared as detailed above. A 23G 1 inch long needle was used to draw the inoculum into a 10 mL syringe. The inoculum was injected into the column and rested on top of the bead pack. Then, the inoculum was drained until it was level with the top of the bead pack. After inoculation, the columns were rested for 48 hours before the media reservoirs were connected and the pulse-flow operation began.

Daily Sampling Procedure and Tested Parameters

The medium in the columns was exchanged daily for 5 days, then the column rested for 48 hours. This pattern was in place for the duration of the experiment. The column effluent was sampled for seven different parameters. These parameters include plate counts, OD_{600}, and the Pierce-Coomassie protein assay to assess biomass, the Nessler assay to monitor ammonia production, pH measurements, and total and dissolved calcium measurements to monitor the production of calcium carbonate. During the media exchange the effluent flow rate was monitored.

Flow Rate

About 5 mL of medium were added to the columns via a Cole-Parmer Masterflex peristaltic pump. The tube clamps were released and the fluid was allowed to drain from the column until the fluid level was directly above the bead pack. A stopwatch was used to record the drainage time of each column, and the amount of fluid drained from the column was recorded. Flow rate was determined by dividing the amount of fluid by the drainage time.

Plate Counts

The first sample taken from the effluent collected in the centrifuge tube was for plate counts. A standard dilution series was made in phosphate buffer solution (PBS). Five 10 μL drops from each dilution were plated on a BHI + 2% urea agar plates. The plates were allowed to sit upright on the bench top overnight, or until the drops had fully absorbed into the agar. The plates were then turned and placed in the 30°C Labline Imperial III incubator. The plates were incubated for at a minimum of 24 hours and were generally counted the next day. Even though all dilutions were plated, the dilution that had between 10-50 colonies per drop was counted. Each of the five drops from that dilution series were counted, and an average was taken. Plate counts were calculated as follows:

$$\frac{\text{Average \# of colonies from the five drops}}{10\,\mu\text{L}} \text{ x } \frac{1000\,\mu\text{L}}{1\,\text{mL}} \text{ x dilution factor} = \text{CFU/mL}$$

Protein Analysis-Pierce Coomassie Assay

1 mL of the column effluent collected daily was placed in a 1.5 mL microcentrifuge tube and stored in the freezer. All the samples set aside for protein analysis were assayed together.

The frozen protein samples were allowed to thaw on the bench top. Once thawed, 500 µL of each sample was placed in a new microcentrifuge tube and 500 µL of 1 N NaOH was added. The samples were vortexed before they were digested at 90°C for 10 min in a Fisher IsoTemp 205 hot water bath. The samples were removed from the bath, vortexed again, and allowed to cool to room temperature. Once cooled, 70 µL of 6:10 v/v HCl was added to every sample and they were vortexed again. These samples were saved in the freezer until the actual assay was run.

Standards were made from a lab-prepared stock solution of 2 mg/mL Bovine Serum Albumin (BSA). Standards were prepared as follows (Table 4):

Table 4: Preparation of standards for Pierce-Coomassie protein assay.

Standard Identification	**Standard Concentration (µg/mL)**	**Standard/Stock to add (mL)**	**Water to Add (mL)**
Stock	2000		
A	1000	0.5 of stock	0.5
B	100	0.1 A	0.9
C	75	0.075 A	0.925
D	50	0.05 A	0.95
E	25	0.025 A	0.975
F	10	0.1 B	0.9
Blank	0	0	1.0

50 µL of each sample and standard were placed in separate wells in a 96-well plate. 150 µL of Pierce-Coomassie reagent (Pierce, Rockford, IL) was added to each well with a multichannel pipetter, then the plate was covered and allowed to sit on the

bench top for 15 minutes. The plate was inserted into the plate reader and read at 595 nm. If dilution of samples for the protein assay were necessary they were made in deionized water and performed prior to NaOH digestion.

Optical Density (OD_{600})

To measure the optical density of the biomass within the columns, 100 µL aliquots of the column effluent were placed in separate wells in a 96 well plate and read in the plate reader at 600 nm.

Nessler Assay

The sample for the Nessler Assay was taken directly from the column effluent and was not filtered before it was assayed. Because the assay was performed immediately, filtering was not necessary. There was no statistically significant difference between filtered and non-filtered samples.

A stock standard solution was made by dissolving 382 mg of ammonium chloride (Fisher, Fair Lawn, NJ) in 100 mL of deionized water in a volumetric flask to a final concentration of 1000 mg/L NH_4-N. The standards were prepared as follows (Table 5):

Table 5: Preparation of standards for Nessler assay.

Standard Identification	**Standard Concentration (mg/L of N)**	**Standard/Stock to add (µL)**	**Water to Add (µL)**
A	100	100 Stock	900
B	50	50 Stock	950
C	25	250 A	750
D	10	100 A	900
E	5	100 B	900
F	1	100 D	900
Blank	0	0	1000

The samples were diluted 1:1000 in deionized water before the assay was performed. The dilutions were done in series: a 1:10 dilution was diluted 1:10 again to make a 1:100 dilution, and the 1:100 dilution was diluted 1:10 to make a 1:1000 dilution. Higher dilutions were performed if necessary.

The miniaturized Hach Nessler Assay was performed. 250 µL of each sample and standard were placed in separate wells in a 96 well plate. 3 µL of a mineral stabilizing reagent (Hach, Loveland, CO) were added to each well. Next, 3 µL of a polyvinyl alcohol reagent (Hach, Loveland, CO) were added to each well. Finally, 10 µL of the Nessler Reagent (Hach, Loveland, CO) were added to each well using a multichannel pipetter. The 96 well plate was covered and allowed to sit on the bench top between 10 and 15 minutes, then placed in the plate reader and read at a wavelength of 425 nm.

Calcium Analysis

To determine total calcium, 4.9 mL of 1.5% ICP-MS trace metal grade HNO_3 (Fisher, Fair Lawn, NJ) was placed in a 50 mL centrifuge tube. 100 µL of the column effluent was added to the tube, and the tube was vortexed for 30 s. The solution was drawn out from the centrifuge tube using a 10 mL syringe and a 22G1 needle. A non-sterile 0.22 µm filter was used to filter the acid-effluent solution into a clean 15 mL centrifuge tube. The calcium crystals were given 2-5 minutes to dissolve prior to filtration.

To determine dissolved calcium, 4.9 mL of 1.5% ICP-MS trace metal grade HNO_3 (Fisher, Fair Lawn, NJ) was placed in a 15 mL centrifuge tube. A small amount of the effluent was drawn up into a 1 mL syringe and filtered into a microcentrifuge tube

using a 0.22 µm non-sterile filter. 100 µL of this filtered effluent was placed into the 4.9 mL of acid in the 15 mL centrifuge tube. The tube was vortexed for 30 s.

All samples were saved on the bench top and were analyzed collectively at the end of the experiment on an Agilent 7500ce ICP/MS.

pH

The pH of the column effluent was measured using a Fisher Scientific Model 50 pH/ion/conductivity meter. The meter was calibrated daily using a Fisher Scientific pH 7 stock buffer solution. While there is risk associated with a one-point calibration for pH measurements, this meter was calibrated and used multiple times a day by other group members.

Destructively Sampling the Columns

Several small autoclave trays were lined and covered completely with aluminum foil. The trays were autoclaved using the dry cycle for 20 min, and used to collect the beads during destructive sampling of the columns.

No medium was pumped into the columns on the day they were destructively sampled. Instead, the medium was completely drained from the bead pack. The rubber stopper was removed from the effluent end of the column and the beads were extruded into the foil covered trays. The beads were deposited in sections on the bottom of the trays: “top”, “middle”, and “bottom”, with “top” being the influent end of the column. A small amount of PBS was washed through the column to remove the beads stuck to the inside and these beads were saved in a 50 mL centrifuge tube. After the beads were

removed, the column was washed with a small amount of 20% ICP-MS trace metal grade HNO_3 which was saved in a 50 mL centrifuge tube. The column, tubing, and media bottle were set aside and autoclaved later to kill any remaining bacteria.

Plate Counts

Beads from each column section were placed in pre-weighed 50 mL centrifuge tubes. 10 mL of 1x PBS were added to the 50 mL centrifuge tubes and the tubes were vortexed for 30 seconds. The tubes were then placed in a small container with ice and sonicated in a Fisher Scientific FS-15 sonicator for 1 min. After sonication, the tubes were vortexed again for 30 seconds. These tubes represented the 10^{-1} dilution in the standard dilution series. The remaining dilutions were made from this 10^{-1} dilution, and drop-plated on BHI +2% autoclaved urea agar plates.

Direct Counts

1 mL of 37% filter sterilized formaldehyde was added to each dilution tube from the plate count dilution series and the tubes were saved in the refrigerator. Slides were prepared for the direct counts as follows. The filter apparatus was cleaned with ethanol and distilled water and a 0.22 µm black polycarbonate filter (GEI-W&PT, USA) was placed on the chimney stage, shiny side up. The filter was sucked down onto the stage and the chimney was put in place. The tube containing the sample was vortexed for 30 seconds and 1 mL of the sample was placed directly on the membrane. The sample was sucked down onto the filter so that the cells were deposited directly on the filter. 600 µL of a 10mg/L DAPI solution was added to the filter and allowed to sit for 7 minutes. The

excess liquid was sucked off, and the filter was washed with 2 mL of deionized water. The excess liquid was sucked off, the chimney was removed, and the membrane was placed on a clean microscope slide. One drop of type FF immersion oil was placed on top of the filter and a cover slip was placed over that. Another drop of immersion oil was placed on top of the cover slip. Twenty pictures of each slide were taken using a Nikon Eclipse E800 and DAPI filter set. The pictures were digitally counted later using MetaMorph 7.0 software. MetaMorph estimates the number of cells based on area and returns the area covered by cells in units of pixels squared. Direct counts were calculated as follows:

$$\frac{\text{cells}}{\text{pic}} \text{x} \frac{1\,\text{pic}}{1.34\text{x}10^{6}\ \text{pixels}^{2}} \text{x} \frac{1\,\text{pixel}^{2}}{4.49\text{x}10^{-3}\ \mu\text{m}^{2}} \text{x} \frac{10^{6}\ \mu\text{m}^{2}}{\text{mm}^{2}} \text{x}\ 218.8\,\text{mm}^{2}\ \text{x} \frac{\text{dil. factor}}{1\,\text{mL}} \text{x} \frac{9\,\text{mL}}{\text{gr of bds}} = \frac{\text{cells}}{\text{gr of bds}}$$

Where 218.8 mm^2 is the chimney area, the mL under the dilution factor is volume of sample that was filtered, 9 mL is the volume of the original sample, and the grams of beads is the weight of beads that was taken from each column section.

Protein

Beads from each column section were placed in pre-weighed 15 mL centrifuge tubes. 500 µL of deionized water and 500 µL of 1 N NaOH were added to the beads. The protein assay protocol described above was then followed. The supernatant was taken off the beads and saved in the freezer until the protein assay could be performed.

Calcium

Beads from each column section were placed in pre-weighed 15 mL centrifuge tubes. Two mLs of 20 % ICP-MS trace metal grade HNO_3 were placed in the 15 mL

centrifuge tubes. The tubes were then vortexed and placed in the refrigerator until the samples could be analyzed using an Agilent 7500ce ICP/MS.

Dry Weight of Beads

Beads from the plate counts, protein assay, and calcium analysis were left in the tubes after the fluid had been removed. The caps were removed from the tubes and the tubes were put in a large glass beaker and allowed to sit for 24 hours in a 100°C oven. After 24 hours, the tubes were cooled to room temperature and then weighed to obtain the "dry" weight of beads. The beads were presumed to be "dry" when they no longer stuck together and were loose in the tube.

Imaging

Bead samples were taken from each column section when the column was destructively sampled. They were allowed to air dry for 5 minutes and were then mounted on adhesive carbon tape. The samples were instantly frozen and sublimated in the cryogenic prep chamber for imaging on a JEOL Model 6100/NORAN/Röntec/Oxford Scanning Electron Microscope (SEM) at the Image and Chemical Analysis Laboratory (ICAL) at Montana State University.

Bead samples were also placed in a sterile Petri dish and imaged using a Nikon SMZ 1500 Stereoscope. The columns themselves were sometimes imaged before the beads were removed.

RESULTS AND DISCUSSION

1 mm Columns-Effluent Data

The first objective of this research project was to establish biofilm communities of ureolytic bacteria that promote $CaCO_3$ precipitation in a pulse-flow porous media column system. The ureolytic bacteria chosen for this experiment were *S. pasteurii*, *B. sphaericus* #21776, and *B. sphaericus* #21787. There were two types of control columns used in the column experiments. One type of control column was an un-inoculated column that was tested in tandem with the inoculated columns during each column trial. The other type of control column was a column inoculated with *B. subtilis*. This column was run in order to determine if a non-ureolytic organism was capable of reducing the porosity of the pulse-flow porous media column system. In order to assess how the cells were growing within the column effluent cell counts, optical density at 600 nm, and protein concentration were monitored over time.

Plate Counts

Plate counts measure the amount of culturable cells in the column effluent. There is a subtle difference between culturable and viable cells. Viable but not culturable (VBNC) cells are still alive but are incapable of growth on a typical agar plate. Culturable cells are also alive and are capable of growing on agar plates. Environmental conditions and the growth medium can affect the ability of a cell to be cultured. Just because some cells are not culturable does not mean that they are not viable.

Direct counts measure all cells present whether they are culturable, viable but not culturable, or not viable (dead). Figure 9 shows the change in plate counts over time for three duplicate S. *pasteurii* trials. The plate counts are generally at a high of 8 to 9 Log CFU/mL for the first four to six days and decrease after CMM+ appears in the column effluent. After this decline, the plate counts level out for the remainder of the experiment.

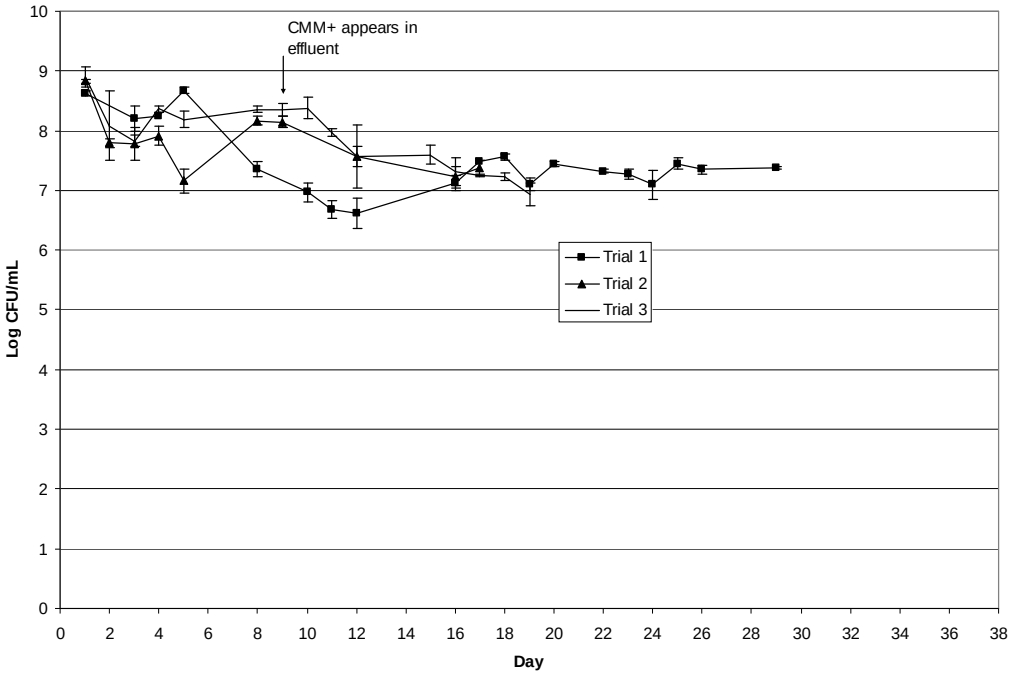

Figure 9: The change in plate counts over time for three replicate *S. pasteurii* experiments. Error bars represent one standard deviation of five measurements. Data points that appear to be missing were due to unreadable agar plates.

This decrease in culturable cells after the addition of CMM+ could be due to the cells becoming encapsulated in $CaCO_3$. As described earlier, bacterial cell walls exhibit a net electronegative charge (29) that facilitates the binding of positively charged ions (28) such as Ca^{2+}. In this thesis research, free calcium ions are added to the system. The hydrolysis of urea is an intracellular process, meaning that urea is converted inside the cell. This creates an environment that has a high pH and is suitable for calcium carbonate precipitation directly around the cell. Combined with the presence of free calcium ions in close proximity to or bound to the cell, any calcium carbonate which precipitated out could entirely surround the cell. Once the cells are encapsulated, they might not longer be culturable and might not contribute towards plate counts. It is possible, however, that the cells might still be viable. If the calcium carbonate surrounding the cells is removed, it is also possible that the cells might again be culturable. In Figure 9, the plate counts tend to level out at a value of approximately 7-7.5 Log CFU/mL, indicating a steady-state between cell growth and detachment within the columns.

Figure 10 shows the change in plate counts over time for two *B. sphaericus* #21776 trials. The trend observed in the three *S. pasteurii* trials is also observed here: the plate counts start out high for the first two or three days and decrease over time. Unlike the *S. pasteurii* trials, however, there is no noticeable decrease in plate counts with the addition of CMM+. This could be due to the fact that while *B. sphaericus* #21776 is ureolytically active, it does not exhibit the same degree of ureolytic activity that *S. pasteurii* does. It is possible that *B. sphaericus* #21776 does not convert urea at the same rate as *S. pasteurii*. This will be discussed in more detail in a later section. Because of

slow urea conversion, there may not be as much $CaCO_3$ precipitating out in this column system and not as many of the *B. sphaericus* #21776 cells are becoming encased in the precipitate.

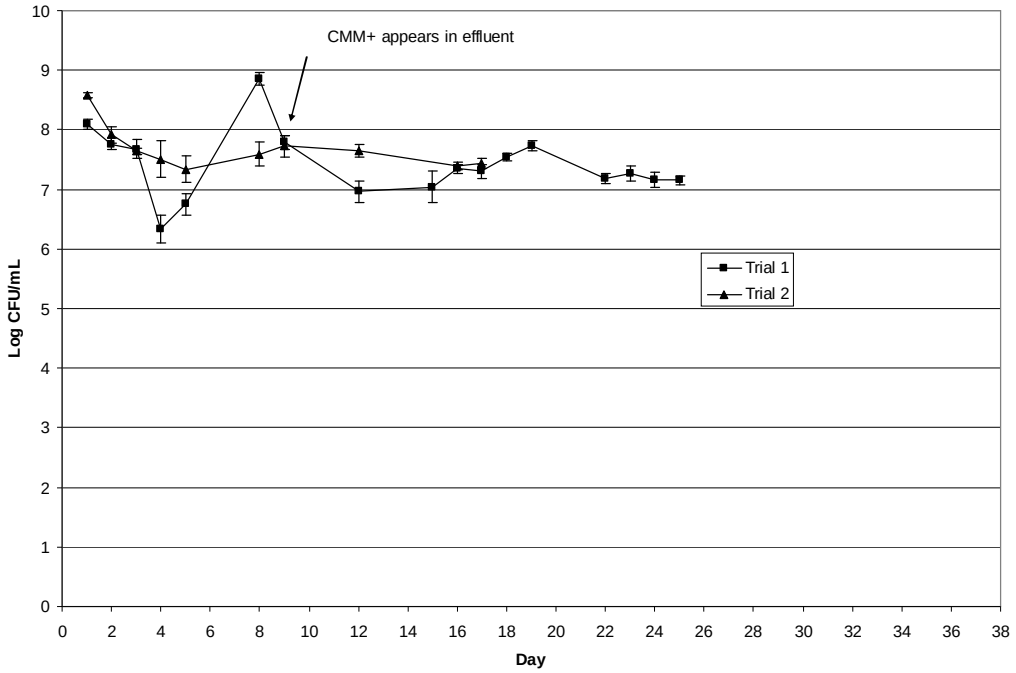

Figure 10: The change in plate counts over time for two replicate *B. sphaericus* #21776 experiments. Error bars represent one standard deviation of five measurements. Data points that appear to be missing were due to unreadable agar plates.

Since not as many cells are encased, more cells would still be culturable and would be accounted for in plate counts, resulting in the higher cell numbers even after the addition of CMM+. The plate counts tend to level off at a value of 7-7.5 log CFU/mL, the same value at which the plate counts for the *S. pasteurii* trials stabilized at. This indicates a steady state between cell growth and detachment within the columns.

Figure 11 shows the change in plate counts over time for the two *B. sphaericus* #21787 trials. The trend observed for the three replicate *S. pasteurii* trials and the two replicate *B. sphaericus* #21776 trials is not wholly observed here: the plate counts begin to decrease from day one and continue to decrease throughout the duration of Trial 1. For Trial 2, the plate counts decrease for the first five days then level out for the rest of the experiment. Unlike the *S. pasteurii* trials, there is no noticeable decrease in plate counts with the addition of CMM+. This could be due to the fact that while *B. sphaericus* #21787 is known to be ureolytically active, it does not exhibit the same degree of ureolytic activity as *S. pasteurii* or *B. sphaericus* #21776. It is possible that *B. sphaericus* #21787 does not convert urea as quickly as *B. sphaericus* #21776 or *S. pasteurii*. Because of possible slow urea conversion, there may not be as much $CaCO_3$ precipitating out in this column system and consequently not as many of the *B. sphaericus* #21787 cells are becoming encased in the precipitate. Since not as many cells are becoming encased, there would be more culturable cells present. This results in the higher numbers seen for the plate count data, even after the addition of CMM+ in Trial 2. The rapid decrease in plate counts seen in the first 13 days of Trial 1 could indicate that the *B. sphaericus* #21787 cells are not stressed and are not detaching from the column. This means that there are fewer cells in the daily column effluent samples available to grow on the agar plates. The plate counts tend to level off at a value of 6-6.5 log CFU/mL for the first trial, a lower value than what has been recorded previously. It also takes this first column 15 days to reach a steady state value between cell growth and

detachment. The plate counts for Trial 2 reach a steady state between cell growth and detachment at a value of 7-7.5 CFU/mL. This value is reached within 8 days.

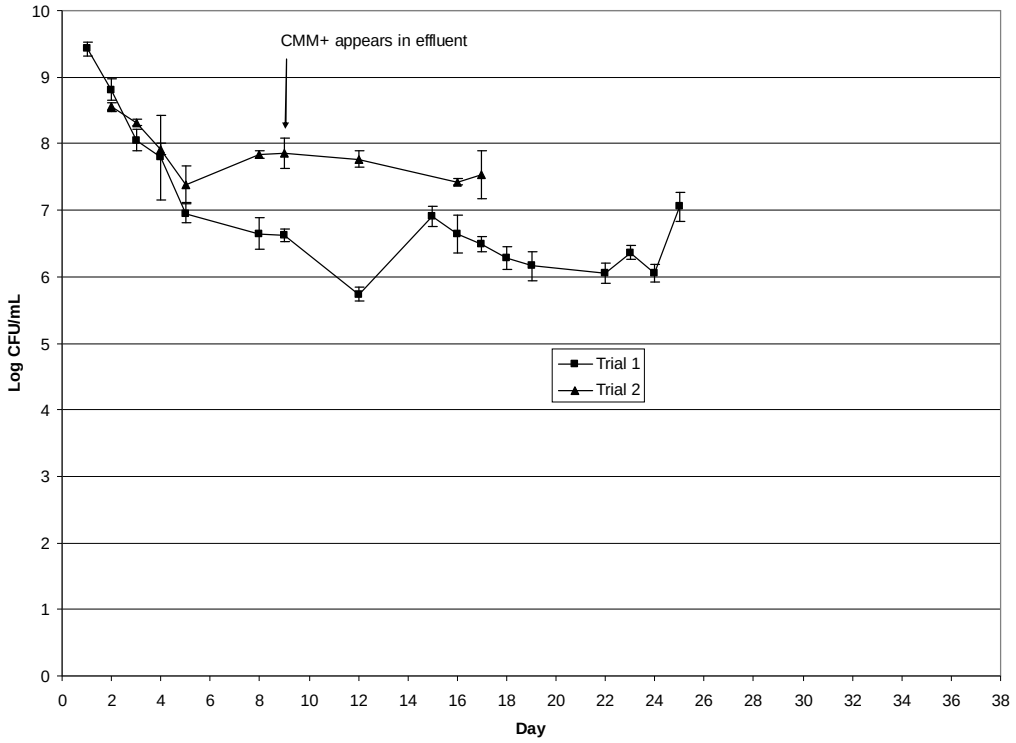

Figure 11: The change in plate counts over time for two replicate *B. sphaericus* #21787 experiments. Error bars represent one standard deviation of five measurements. Data points that appear to be missing were due to unreadable agar plate.

Figure 12 shows the change in plate counts over time for *B. subtilis*. *B. subtilis* is a non-ureolytic organism and is included in these tests as a control organism. *B. subtilis* should be capable of growing in the CMM- and CMM+, but will not be able to utilize and convert urea. Therefore the pH of the system should not increase, ammonium will not be produced, and calcium carbonate will not precipitate out. *B. subtilis* also prefers to grow at 37°C while the other bacteria in this study prefer to grow at 30°C.

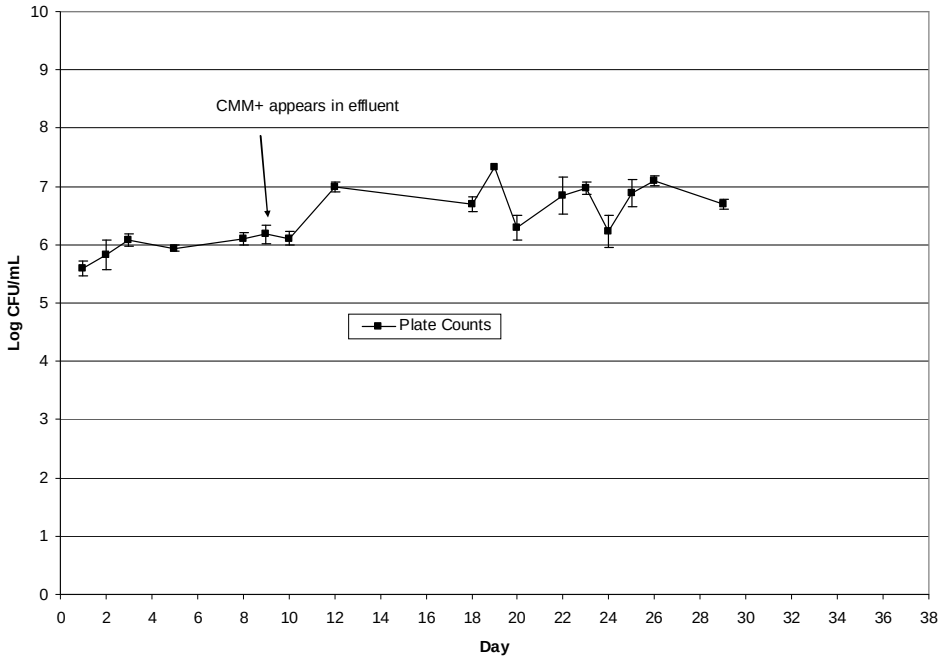

Figure 12: The change in plate counts over time for the only B. subtilis experiment. Error bars represent one standard deviation of five measurements. Data points that appear to be missing were due to unreadable agar plates.

In Figure 12, the plate counts for *B. subtilis* start out relatively low, around 5.5 log CFU/mL, and increase over the course of the experiment to a steady state value between cell growth and detachment at approximately 7 log CFU/mL. A noticeable increase occurs after CMM+ appears in the column effluent. The low starting value of the plate counts may be due to the fact the bacteria are not growing at their optimal temperature and are not able to utilize urea, one of the main ingredients in the growth medium, resulting in slower cell growth. The slow increase in culturable cells over time indicates that *B. subtilis* was able to adapt to the pulse-flow system environment, but it may not grow as well as *S. pasteurii*, *B. sphaericus* #21776, or *B. sphaericus* #21787 due to its preference for higher temperatures.

$\underline{OD_{600}}$

The optical density at 600 nm (OD_{600}) is also measured over the course of the experiment. There is speculation that the calcium carbonate precipitate interferes with OD_{600} readings because there is a noticeable decrease in OD readings after CMM+ begins to appear in the effluent. The encapsulation of the cells by calcium carbonate would increase the optical density of the effluent; there would be more matter (cells and precipitate) in the sample placed in the 96 well plate. It is possible that the calcium carbonate precipitate is trapping the cells inside the column and not allowing them to detach, resulting in less matter in the effluent and therefore a lower OD_{600} reading.

Figure 13 shows that the OD_{600} for each *S. pasteurii* trial starts out very high and drops significantly over the first two to three days as the cells adjust to the column environment. Once the cells adjust, the OD_{600} measurements for the inoculated columns tend to level out. The OD_{600} measurements drop noticeably again after day 9, when CMM+ begins to appear in the effluent. Compared to the OD_{600} measurements for the control column, which remain static at a reading of about 0.038 throughout the course of the experiment, the higher OD_{600} readings for each *S. pasteurii* trial indicate that the organism is growing within the column.

Occasionally, there is a sudden increase in otherwise stable OD_{600} readings. Such increases could be due to a possible contamination within the column, a scratched or dirty 96 well plate, or a disruption within the plate reader. One of these sudden increases can be seen in the Trial 2 control data in Figure 13. Upon inspection of the raw data, the triplicate OD_{600} readings from day 16 are 0.127, 0.13, and 0.135. There is not a large

difference between these numbers, indicating that there probably was not a defect on the 96 well plate. Because a normal reading of 0.038 is observed on day 15 and day 17, a possible contaminant in the column is unlikely. There is also no noticeable difference in the appearance of the effluent from day 16 compared to the effluent from other days. The remaining possible explanation is a disturbance of the plate reader.

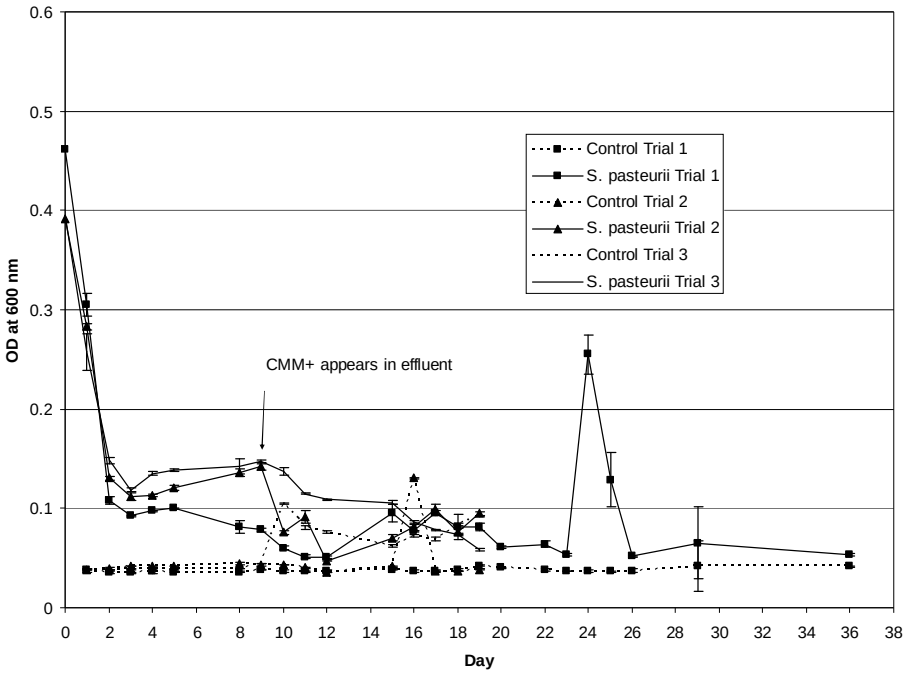

Figure 13: Change in OD_{600} over time for three replicate *S. pasteurii* experiments. The OD_{600} of each trial starts out high and decreases rapidly over the first three days as the cells adjust to the column environment. Error bars represent one standard deviation of triplicate measurements.

Another sudden increase in OD_{600} data can be seen on day 24 in the *S. pasteurii* Trial 1 data in Figure 13. This increase could also be due to a possible contamination within the column, a scratched or dirty 96 well plate, or a disruption within the plate reader. Upon inspection of the raw data, the triplicate OD_{600} readings from day 24 are

0.236, 0.253, and 0.276. There is not a large difference between these numbers, indicating that there probably was not a defect in the 96 well plate. A more consistent reading of 0.053 is observed on day 23, a higher reading of 0.128 is observed on day 25, and a more consistent reading of 0.052 is observed on day 26. The triplicate readings for each of these days are consistent among each other, indicating that there are probably no problems with the 96 well plate on those days. Because day 24 and 25 are the only days that exhibit unusual readings, it is possible that flushing the column dislodged some of the calcium carbonate precipitate from the column and into the column effluent. This would increase the amount of matter in the effluent sample and increase the OD_{600} reading. Because the readings become more consistent again on day 26 and remain so throughout the duration of the experiment, there is no indication of a contaminant in the system. If the system was contaminated, elevated readings would be expected from day 24 until the duration of the experiment. There was also no noticeable difference in the appearance of the effluent from days 24 and 25 compared to the effluent from other days. It is also unlikely that there would be a major disturbance within the plate reader two days in a row. Therefore, the presence of calcium crystals in the effluent is probably causing the difference in OD_{600} measurements on days 24 and 25.

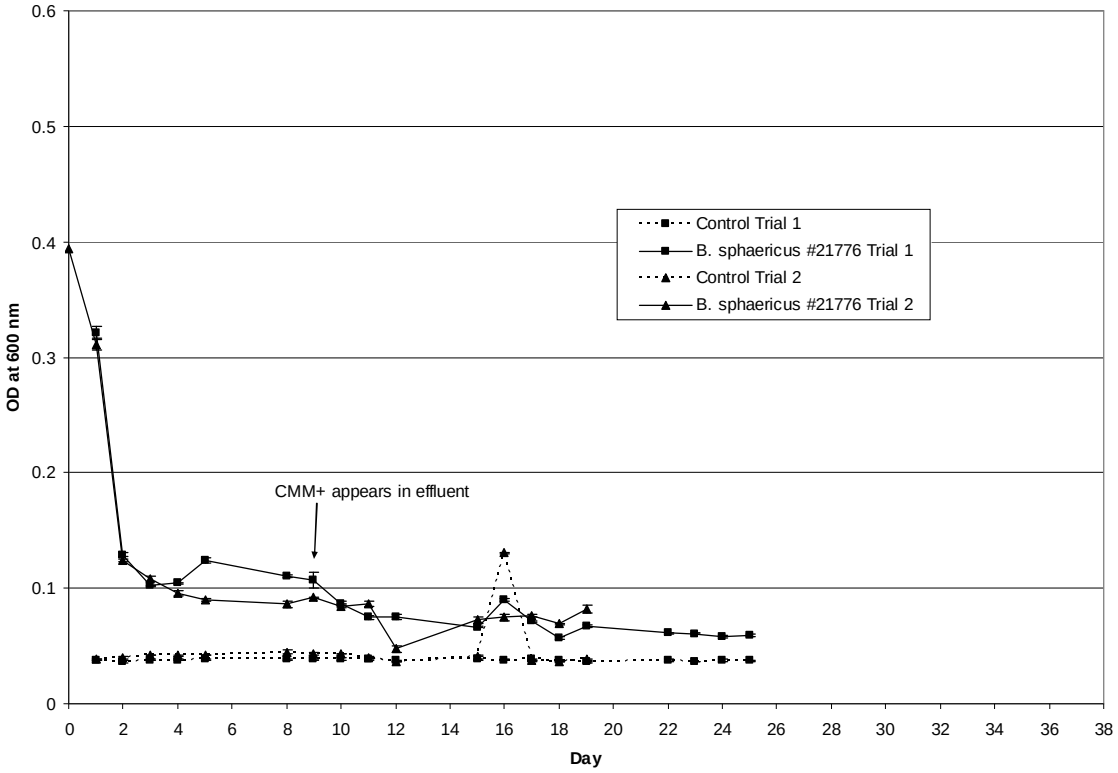

Figure 14: The change in OD_{600} over time for two replicate *B. sphaericus* #21776 experiments. Error bars represent one standard deviation of triplicate measurements.

Figure 14 shows that the OD_{600} for both *B. sphaericus* #21776 trials starts out very high and drops significantly over the first two to three days as the cells adjust to the column environment. Once the cells have adjusted, the OD_{600} measurements for the inoculated columns level out. The OD_{600} measurements drop again slightly after day 9, when CMM+ begins to appear in the effluent. This could be due to the encapsulation of the cells by calcium carbonate. It is possible that the calcium carbonate precipitate is trapping the cells inside the column and not allowing them to detach, resulting in less matter in the effluent and therefore a lower OD_{600} reading.

The OD_{600} measurements for the control columns remain static at a reading of about 0.038 throughout the course of the experiment except for a small disturbance in the Trial 2 control data in Figure 14. As discussed above, the most likely explanation for this increase in OD_{600} readings is a possible disturbance of the plate reader. The higher OD_{600} readings for each *B. sphaericus* #21776 trial relative to each control indicate that the organism is growing within the column.

Figure 15 shows that the OD_{600} measurements for both *B. sphaericus* #21787 trials start out high and drops significantly over the first two to three days as the cells adjust to the column environment. Once the cells adjust, the OD_{600} measurements for the inoculated columns level out. The OD_{600} measurements for Trial 1 drop dramatically in the first three days and parallel the control data almost exactly for the duration of the experiment. There are cells in the column that are capable of growth (see Figure 11), so the low OD_{600} measurements are not due to the absence of cells. The plate count values for Trial 2 are about an order of magnitude lower than those of Trial 1, but not low enough to indicate the absence of cells in the column. Because of this large difference, it is possible that a significant OD reading cannot be detected.

The OD_{600} measurements for Trial 2 drop again slightly after day 9, when CMM+ begins to appear in the effluent. This noticeable decrease could be due to the encapsulation of the cells by $CaCO_3$. It is possible that the calcium carbonate precipitate is trapping the cells inside the column and not allowing them to detach, resulting in less matter in the effluent and therefore a lower OD_{600} reading.

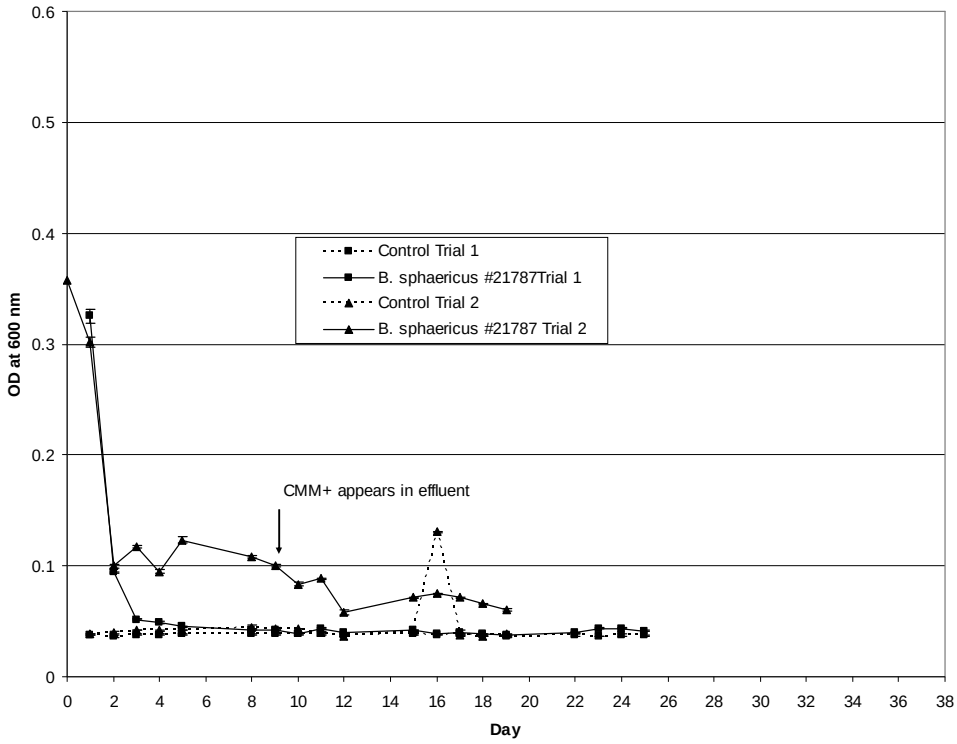

Figure 15: The change in OD_{600} over time for duplicate *B. sphaericus* #21787 experiments. The trend seen in the previous two bacterial experiments is seen here as well. Error bars represent one standard deviation of triplicate measurements.

The OD_{600} measurements for the control columns remain static at a reading of about 0.038 throughout the course of the experiment except for a small disturbance in the Trial 2 control data in Figure 15. As discussed above, the most likely explanation for this sudden increase in OD_{600} readings is a possible disturbance of the plate reader. The higher OD_{600} readings for each *B. sphaericus* #21787 trial relative to each control indicate that the organism is growing within the column.

Figure 16 shows the change in OD_{600} over time for the single *B. subtilis* trial. The same trend seen in many of the other trials is also seen here. The OD_{600} measurements start out very high at inoculation and decrease rapidly over the first three days as the cells

adjust to the column environment. Once the cells have adjusted, the OD_{600} readings parallel those of the control. The OD_{600} measurements for the control column remain static at a reading of about 0.038 throughout the course of the experiment. With the introduction of CMM+ (day 9), there is no decrease in the OD_{600} readings.

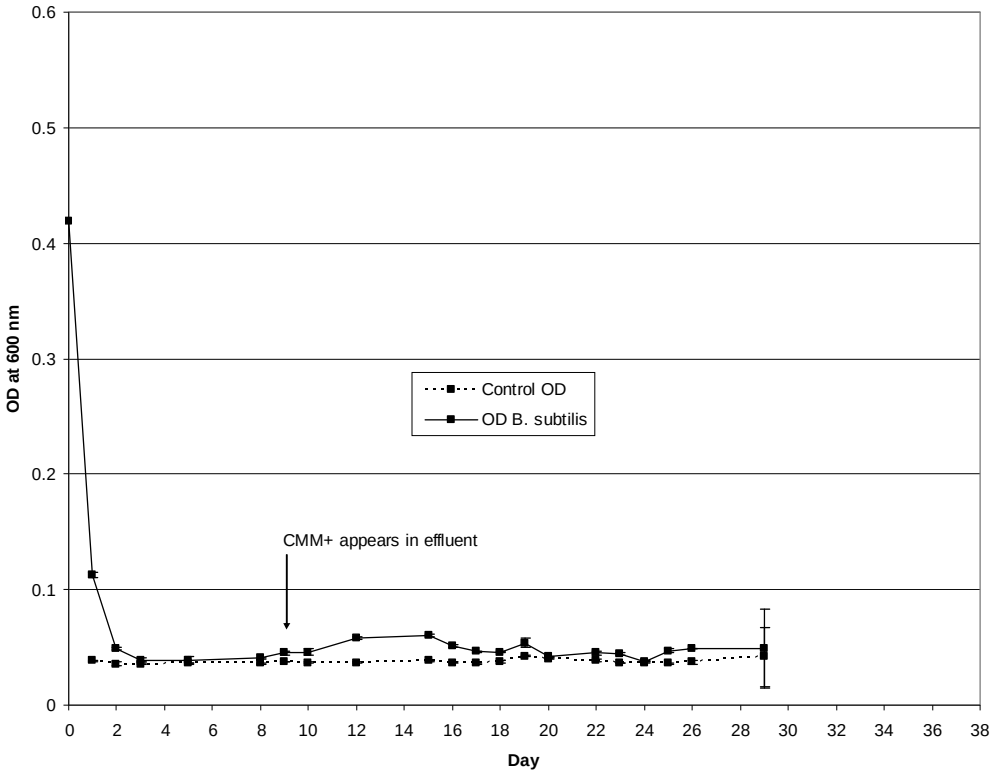

Figure 16: The change in OD_{600} over time for the only *B. subtilis* experiment. Error bars represent one standard deviation of triplicate measurements.

As was noted earlier, *B. subtilis* is not a ureolytic organism and therefore is not capable of utilizing urea or increasing the pH of the system and facilitating $CaCO_3$ precipitation. No $CaCO_3$ is precipitating in this system, so there is no precipitate present in the effluent to raise the OD_{600} readings. Because there is no precipitate, there is no

mechanism in the column to inhibit the cells from detaching, and there is no decrease in the OD_{600} readings. In fact, the OD_{600} measurements indicate that the cells have reached a steady state between cell growth and detachment. The OD_{600} readings support the hypothesis that *B. subtilis* is capable of growing in the column system.

Protein

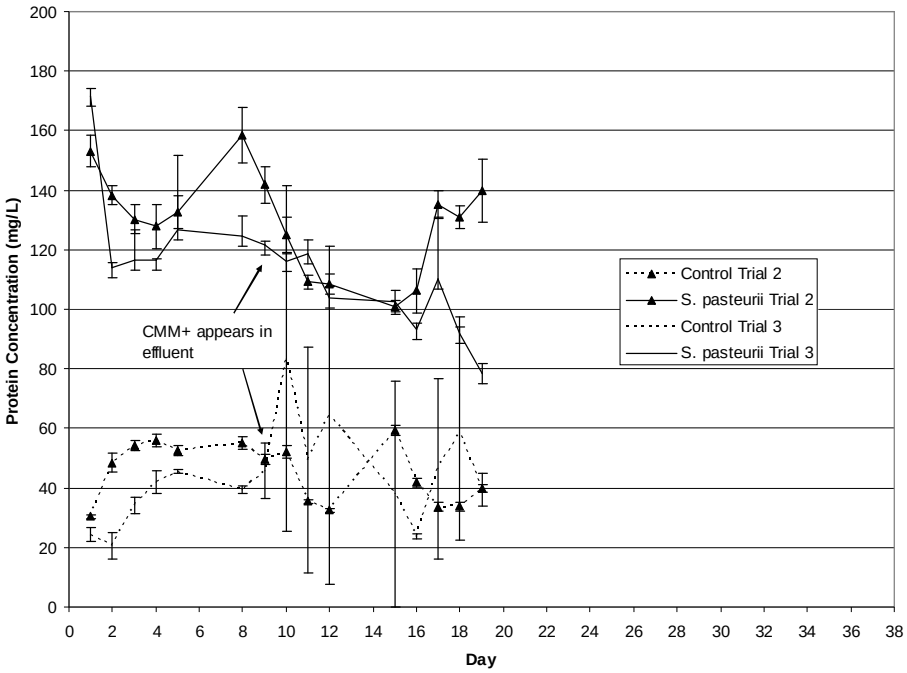

Figure 17: The change in protein concentration over time for duplicate *S. pasteurii* experiments. Error bars represent one standard deviation of triplicate measurements.

The amount of protein in the column effluent was also measured as a way of monitoring biomass. The protein protocol was not implemented until the second trial, so there is no protein data for the first *S. pasteurii* trial or the *B. subtilis* trial. Figure 17 shows the change in protein concentration over time for the second and third *S. pasteurii* trials.

It is easily seen that the protein concentration in both of the inoculated columns is much higher than that in both of the control columns, indicating the presence of cells in the *S. pasteurii* column systems. The only protein that should be present in the control columns is from the nutrient broth contained in the media. The control data and the *S. pasteurii* data from both Trial 2 and Trial 3 appear to be reproducible because they both exhibit a similar trend. What is interesting to note is that after CMM+ appears in the effluent (day 9), the protein concentration drops about 20 mg/L in both inoculated columns. This could be due to the fact that the cells are becoming encapsulated in $CaCO_3$. In the protein assay protocol, base is added to the sample before acid is added. If acid was added first, $CaCO_3$ that may have been encapsulating the cells would dissolve, freeing the cells and allowing that protein to be accounted for in the protein assay. Therefore, the inoculated columns that exhibit a decrease in protein concentration after CMM+ introduction probably have cells that are encapsulated in $CaCO_3$. The $CaCO_3$ fails to dissolve during digestion, and the trapped cells are not accounted for in the protein assay, causing the decrease in protein concentration that is seen over time. The protein concentrations in these trials are probably higher than what is reported.

In Trial 2, the protein concentration increases for the remaining days of the experiment, indicating a possible contamination in the column. There is no evidence when looking at pH or OD_{600} data, however, that there is contamination. In Figure 13, the OD_{600} for this trial is not unlike the data from the other two trials and the pH remains at a constant value of about 9.3. In Trial 3, the protein concentration decreases from

about 120 mg/L on day 9 to 80 mg/L on day 19, a drop of 40 mg/L. In the control column, especially in Trial 3, the error bars increase drastically after the addition of CMM+. Taken together, this disruptive data suggests that something is interfering with the measurements during the protein assay. It has already been hypothesized that the calcium carbonate is encapsulating cells and due to the way reagents are added, is not able to dissolve before protein concentration is measured. This explains why the protein concentration decreases after the addition of CMM+, but does not explain why there is so

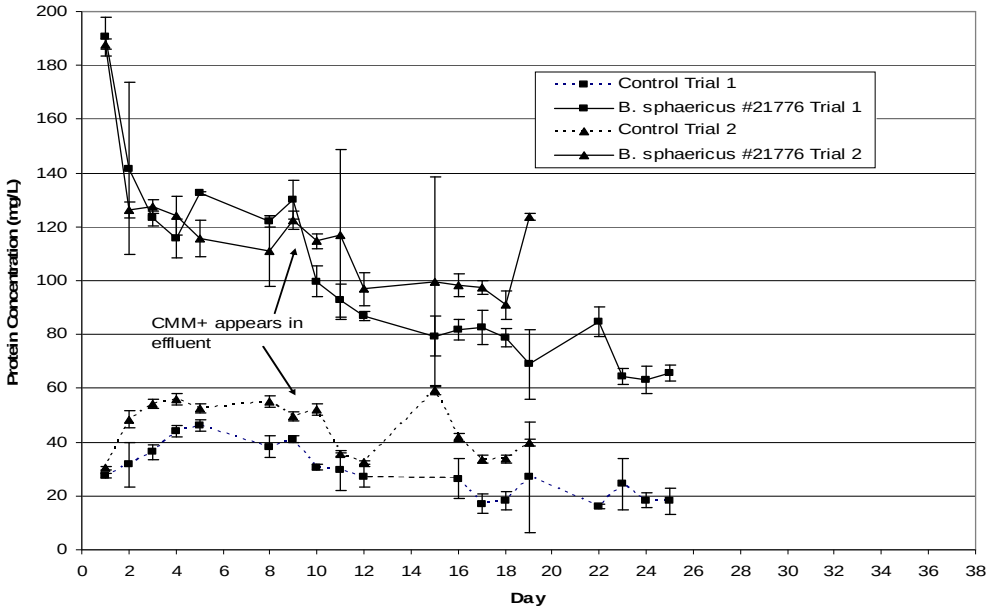

Figure 18: Change in protein concentration over time for duplicate *B. sphaericus* #21776 experiments. Error bars represent one standard deviation of triplicate measurements.

much error associated with the control column data. There should be no calcium carbonate precipitate due to biological processes in the control column, so the free calcium in the media should be passing through the column. However, the size of the error increases only after calcium starts to appear in the effluent. Therefore it is possible

that the free calcium is interfering with the protein assay protocol or with one of the reagents. If there is non-homogenous digestion, calcium carbonate precipitate is introduced. The addition of NaOH causes the pH of the system to rise and the free calcium in solution to precipitate out. If the calcium crystals are not removed before the protein assay is performed, then readings can be erratic.

Figure 18 shows the change in protein concentration over time for duplicate *B. sphaericus* #21776 trials and looks very similar to Figure 17. The protein concentration in both of the inoculated columns is much higher than that in both of the control columns, indicating the presence of cells in the inoculated column systems. The only protein that should be present in the control column is from the nutrient broth contained in the medium. The control data and the *B. sphaericus* #21776 data from both Trial 1 and Trial 2 appear to be reproducible because they both exhibit a similar trend. The protein concentration starts out high and decreases throughout the duration of the experiment. What is interesting to note is that after CMM+ appears in the effluent (day 9), the protein concentration drops significantly (about 60 mg/L) in both inoculated columns. This could be due to the fact that the cells are becoming encapsulated in $CaCO_3$. In the protein assay protocol, base is added to the sample before acid is added. If acid was added first, $CaCO_3$ that may have been encapsulating the cells would have dissolved, freeing the cells and allowing that protein to be accounted for in the protein assay. Therefore, the inoculated columns that exhibit a decrease in protein concentration after CMM+ introduction possibly have cells that are encapsulated in $CaCO_3$. The $CaCO_3$ fails to dissolve during digestion, and the trapped cells are not accounted for in the protein assay,

causing the decrease in protein concentration seen over time. The protein concentrations in these trials are probably higher than what is reported. For *B. sphaericus* #21776 Trial 2, the last point is much higher than the others. It is possible that a large number of cells detached from the column on that day and were detected in the column effluent.

Figure 19 shows the change in protein concentration over time for duplicate *B. sphaericus* #21787 trials. In Trial 1, the protein concentration of the inoculated column starts out very high, and then drops to a level that closely mirrors that of the control column.

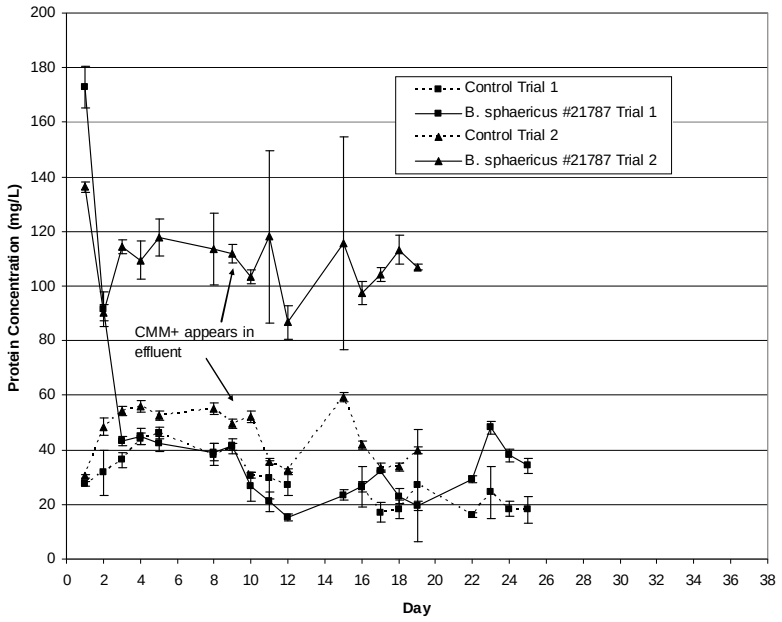

Figure 19: The change in protein concentration over time for duplicate *B. sphaericus* #21787 experiments. Error bars represent one standard deviation of triplicate measurements.

This trend of mirroring the control column has also been seen in the plate count and OD_{600} data for this trial. Because the reading for protein, plate counts and OD_{600} are much lower in Trial 2 than in Trial 1, it is possible that *B. sphaericus* #21787 inoculum

used in Trial 2 was contaminated or compromised in another way. The cells are still growing, but significant readings are not detected.

For Trial 2, the protein concentration starts out high and drops only slightly throughout the course of the experiment. It is much higher than the protein concentration in the corresponding control column. The error bars for each point increase with the appearance of CMM+ in the column effluent. This could be due to the fact that the cells are becoming encapsulated in $CaCO_3$ and either do not detach or are not accounted for in the protein assay. In the protein assay protocol, base is added to the sample before acid is added. If acid was added first, $CaCO_3$ that may have been encapsulating the cells would dissolve, freeing the cells and allowing that protein to be accounted for in the protein assay. It is possible that when aliquots are taken from the sample tube that one might contain more cells that were freed from calcium carbonate crystals than another sample. The presence of calcium in this column is affecting the readings from the protein assay.

After CMM+ appears in the effluent (day 9), the protein concentration does not change significantly as it did in the *S. pasteurii* and *B. sphaericus* #21776. It is possible that *B. sphaericus* #21787 is not able to convert urea as fast or as efficiently as *S. pasteurii* or *B. sphaericus* #21776. Not as much ammonium is being produced in the *B. sphaericus* #21787 columns, and therefore the pH does not increase as much. Not as much calcium carbonate is able to precipitate out and therefore not as many cells are becoming encapsulated in the calcium crystals. When acid is added during the assay, there is not as much calcium carbonate to dissolve, and then more cells accounted for in the assay.

The control data from Trial 1 and Trial 2 appear to be reproducible. The error bars do not increase as dramatically in the control columns as they did in the other control columns in the *S. pasteurii* trials. If it is the free calcium in the media that is causing interference in the protein assay, it is not seen in these trials.

The data obtained from plate counts and OD_{600}, suggest that *S. pasteurii*, *B. sphaericus* #21776, *B. sphaericus* #21787, and *B. subtilis* are capable of forming a biofilm and surviving in the pulse-flow porous media column system.

Ammonium-N Concentration and pH

If *S. pasteurii*, *B. sphaericus* #21776, *and B. sphaericus* #21787 are truly capable of carrying out the ureolytic process, urea in the medium will be broken down and ammonium produced. This production of ammonium results in a pH increase (see equation 4).

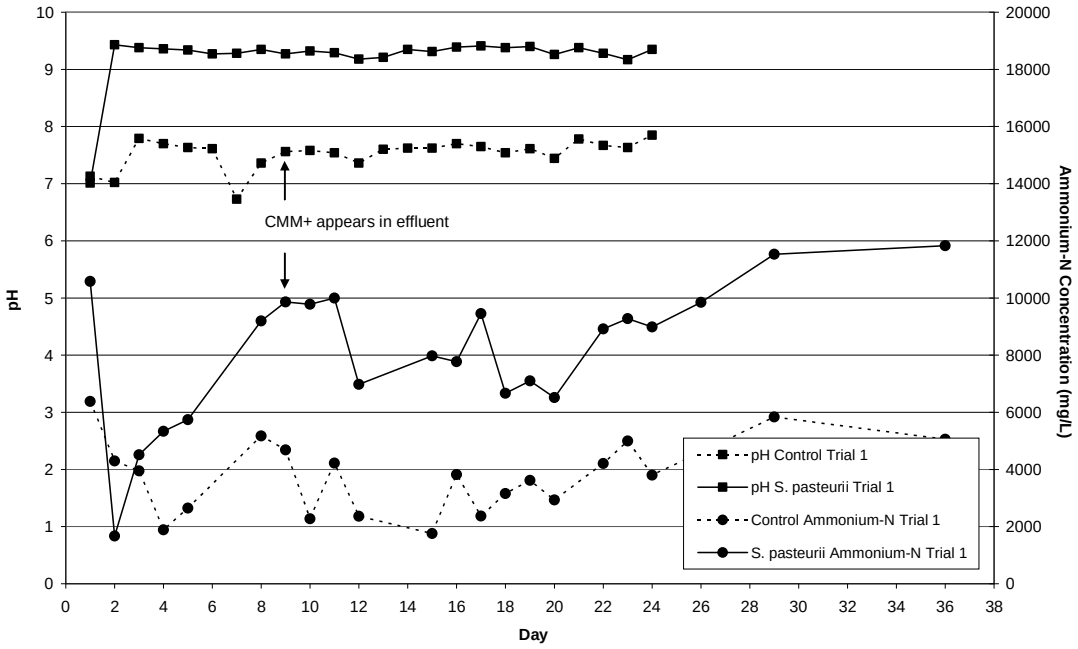

Figure 20: The relationship between pH and ammonium-N concentration for the first *S. pasteurii* trial. Error bars are very small, but represent one standard deviation of triplicate measurements

For this experiment, the Nessler Assay is used to monitor the amount of ammonium-N present in the column effluent and the pH of the column effluent is measured. Samples are not filtered before being analyzed with the Nessler Assay because they are tested immediately. Control experiments demonstrated that no statistically significant differences were detected between filtered and unfiltered samples, as long as samples are tested immediately (data not shown).

Figure 20 shows the relationship between pH and ammonium-N concentration for the first *S. pasteurii* trial. The pH increases from about 7 to about 9.5 in the first day, then remains constant throughout the duration of the experiment. The pH of the control column remains between 7 and 8 for the duration of the experiment. The pH of the

inoculated column and the control column does not change with the introduction of CMM+.

The ammonium-N concentration for the *S. pasteurii* inoculated column is higher than that of the control, indicating that urea is being hydrolyzed and ammonium being produced. Ammonium chloride is a component of the CMM medium, and that is accounted for in the readings from the control column. There is a sharp decrease in the ammonium-N values, from about 11000 mg/L to about 2000 mg/L from day 1 to day 2 in the inoculated column. After inoculation, the cells have about 72 hours to hydrolyze urea before the first feeding. After the first feeding, the cells only have about 24 hours to hydrolyze urea. While the data is a slightly noisy, the ammonium-N concentration generally increases for the rest of the experiment to a final reading of approximately 12000 mg/L.

While a relationship between pH and ammonium production can be inferred from this graph and the series of equations, a direct correlation between ammonium production and pH increase is not obvious. Because the pH increases in a matter of hours, a direct correlation between pH and ammonium-N concentration cannot be seen from any of the data collected from the column systems. Because an increase in pH does occur and the ammonium-N concentrations in the inoculated columns are significantly greater than in the control columns, it can be inferred that this rise in pH corresponds to the increased ammonium-N levels. However, a direct correlation between the two parameters would be better. Batch experiments using *S. pasteurii*, *B. sphaericus* #21776 and *B. sphaericus* #21787 conducted by Stacy Parks as part of her M.S. research project are sampled

hourly, not daily, and the relationship between pH and ammonium-N concentration is demonstrated in greater detail. In the *S. pasteurii* batch experiments, the pH reaches its highest value of about 9.3 at 30 hours post-inoculation. During this same time period, the ammonium-N concentration rises from about 2000 mg/L to a high of approximately 11000 mg/L. Conversely, in the control batch system, the pH remains at a constant value of about 7.3 for 30 hours post-inoculation and the ammonium-N concentration varies between 4500 mg/L and 6500 mg/L. Both the pH values and the ammonium-N values in the control systems are significantly lower than those in the inoculated batch systems.

Figure 21 shows the relationship between pH and ammonium-N concentration for the second *S. pasteurii* trial. Again the pH of the inoculated column increases within the

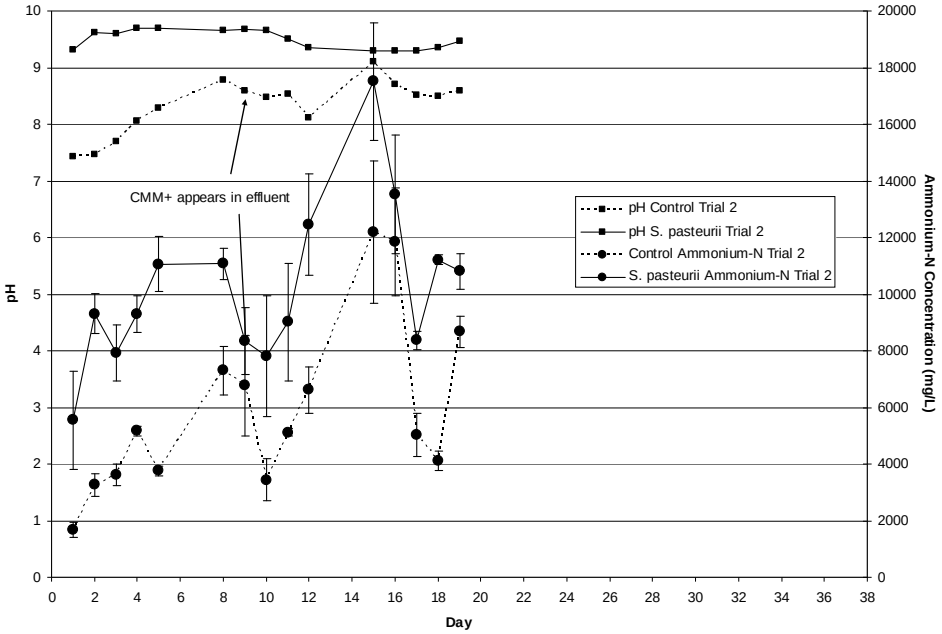

Figure 21: Relationship between pH and ammonium-N concentration for second *S. pasteurii* experiment. Error bars represent one standard deviation of triplicate measurements.

first day up to the normally seen high of about 9.3. The pH of the control column

increases as well, from 7.3 to a high of about 8.5. An increase of this magnitude is a strong indication that the control column has become contaminated.

The ammonium-N concentration of the inoculated column is higher than that of the control, indicating that a rise in pH correlates to increased levels of ammonium-N concentration. This is expected because *S. pasteurii* is a known ureolytic organism. Ammonium-N concentrations for the control column are generally about 4000 mg/L less than the concentrations observed in the inoculated column. After CMM+ appears in the effluent (day 9), the ammonium-N values increase from 8000 mg/L to almost 18000 mg/L, even though the same amount of urea is being delivered to the cells, so the same amount of ammonium is being produced. At this point in the trial, the cells are approaching a relative steady state between cell growth and detachment so there is not a sudden increase in cells that would account for greater urea utilization and ammonium production. The ammonium-N concentrations in the control column increase after the addition of CMM+ to the system. Calcium is important component for optimal cell growth, and has been denied to the cells until day 8. Once the cells have access to calcium, it is possible that there is a rapid increase in growth, resulting in more cells that are producing more ammonium-N. This would explain the increase seen after day 8. This increase is seen in *S. pasteurii* Trial 3 although the increase is not as drastic, and is not seen at all in Trial 1.

Figure 22 shows the relationship between pH and ammonium-N concentration for the third *S. pasteurii* trial. Once more, the pH of the inoculated column increases within

the first day up to the normally observed high of about 9.3. The pH of the control column remains relatively static at about 8 for the duration of the trial. The ammonium-N concentration of the inoculated column is higher than that of the control column. Ammonium-N concentrations for the control are 6000-8000 mg/L less than the concentration observed in the inoculated column. After CMM+ appears in the effluent (day 9), the ammonium-N values increase slightly from 8000 mg/L to 11000 mg/L, even though the same amount of urea is being delivered to the cells, so the same amount of ammonium can be produced.

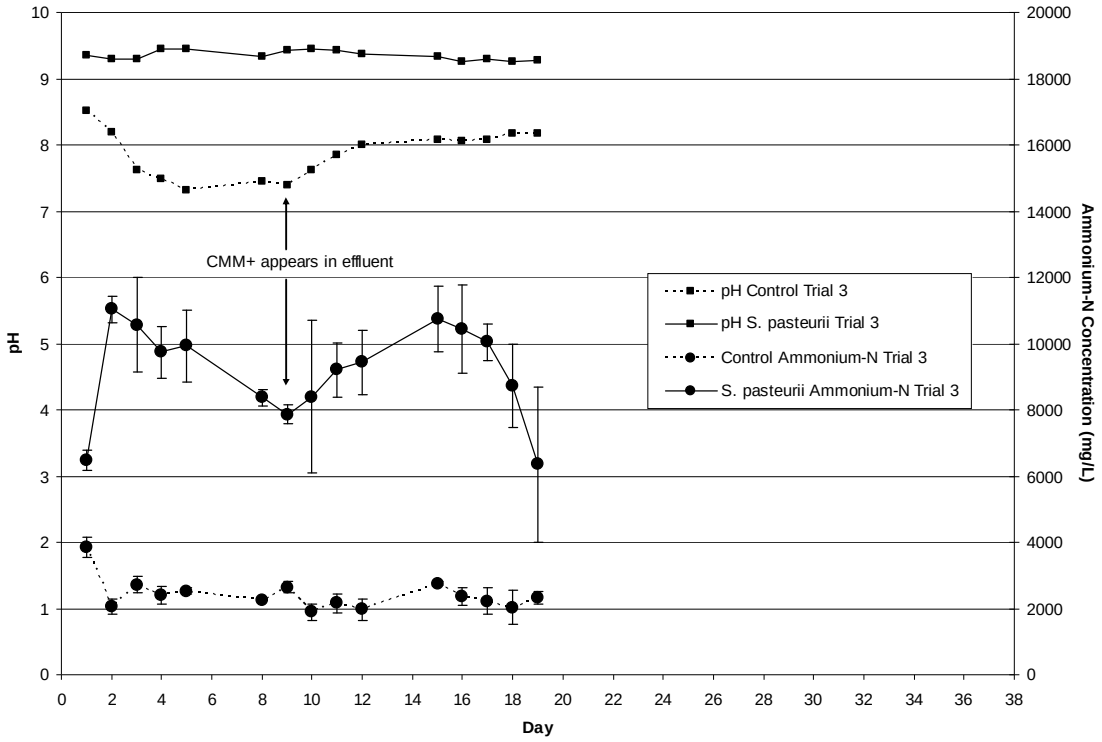

Figure 22: Relationship between pH and ammonium-N concentration for third *S. pasteurii* experiment. Error bars represent one standard deviation of triplicate measurements.

At this point in the trial, the cells are approaching a relatively steady state between cell growth and detachment, so there is not a sudden increase in cells that would account for greater urea utilization and ammonium production. Calcium is important component for optimal cell growth, and has been denied to the cells until day 8. Once the cells have access to calcium, it is possible that there is a rapid increase in growth, resulting in more cells that are producing more ammonium-N. This would explain the increase in ammonium-N concentration seen after day 8.

Figure 23 shows the relationship between pH and ammonium-N concentration for the first *B. sphaericus* #21776 trial. The pH of the system again increases within the first day to the normally seen high of about 9.3. This indicates that the bacteria are utilizing urea and producing ammonium. The ammonium-N concentration for the inoculated column is higher than the ammonium-N concentration of the control column, indicating that ammonium is being produced. There is no noticeable change in the system with the addition of CMM+; the ammonium-N concentration and pH remain relatively constant throughout the duration of the experiment. Unlike what was seen in the second and third *S. pasteurii* trials, there is no increase in ammonium-N concentration in the inoculated column after the appearance of CMM+ in the effluent. The urea concentration remains the same in CMM- and CMM+, so an increase in ammonium levels would be unusual after the medium was changed. However, since it was seen in two of the three *S. pasteurii* trials, this trend was checked for in subsequent trials. Even though this trend was not expected, the fact that it was *not* noticed in the first *B. sphaericus* #21776 trial could be due to the rate at which *B. sphaericus* #21776 converts urea. Slower conversion

of urea results in slower production of ammonium; hence no increase on the graph. It is also possible that the CMM- and CMM+ for this trial were made more consistently than for other trials. At day 10, when CMM+ regularly appears in the effluent, there is a sharp decrease in ammonium-N concentration, but it returns to normal the next day. This sharp decrease is probably due to the stress that occurs on the system when the medium is changed on day 8.

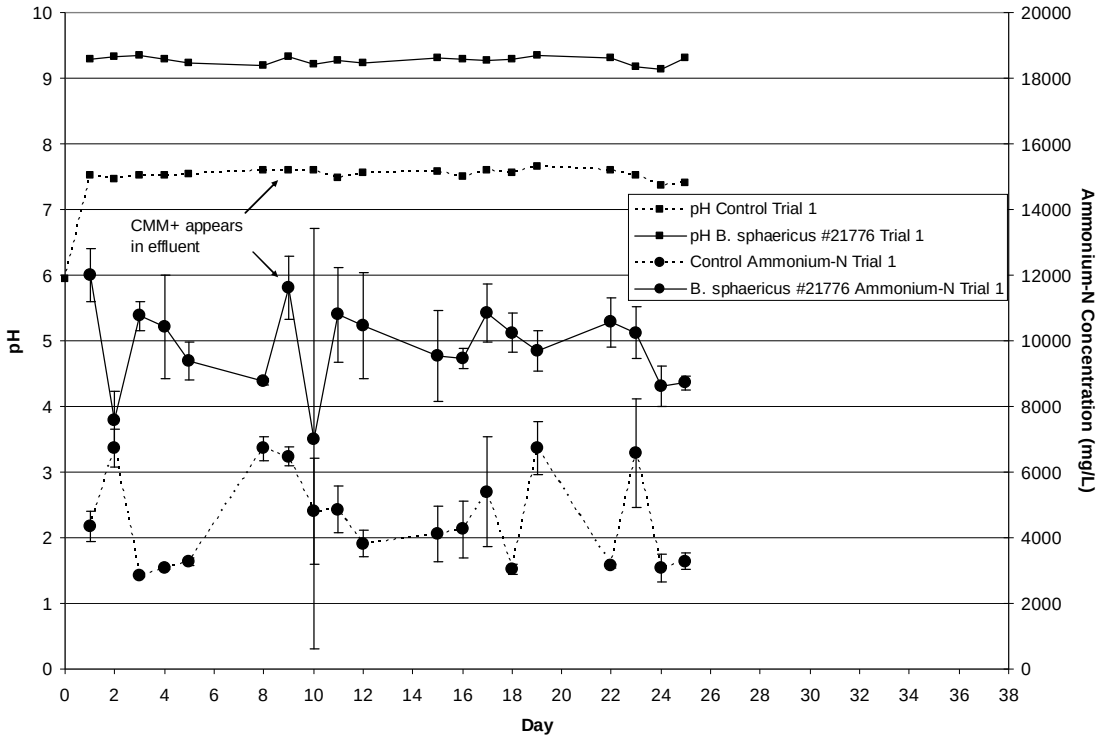

Figure 23: Relationship between pH and ammonium-N concentration for first *B. sphaericus* #21776 experiment. Error bars represent one standard deviation of triplicate measurements.

The trend seen in Figure 23 is carried over in Figure 24, which shows the relationship between pH and ammonium-N concentration for the second *B. sphaericus*

#21776 trial. The pH of the inoculated column increases to the normally observed high of about 9.3. This time, however, the pH of the control column starts increasing on day 3. This is a strong indication that the control column is contaminated. It is interesting to note that when this pH increases in the control column, the ammonium-N concentration increases in the control column as well. This is the first direct correlation between pH and ammonium-N concentration seen in the column systems.

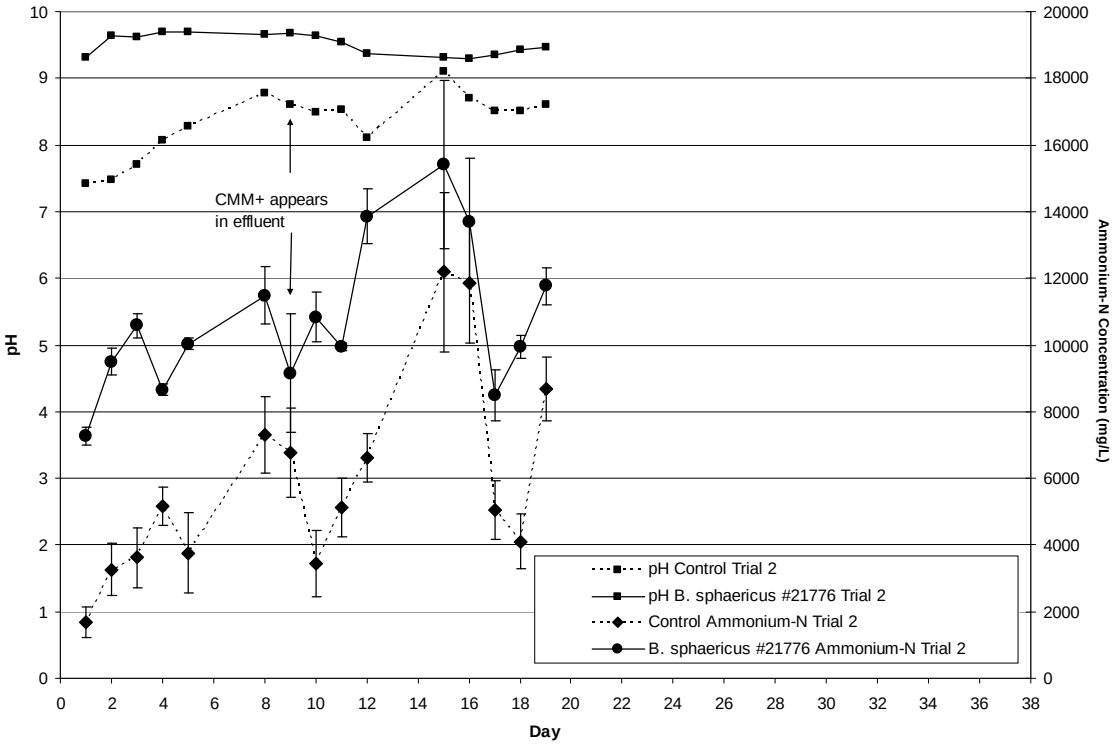

Figure 24: Relationship between pH and ammonium-N concentration for second *B. sphaericus* #21776 experiment. Error bars represent one standard deviation of triplicate measurements.

The ammonium-N concentration for the inoculated column still remains higher than that of the control throughout the duration of the experiment despite the contamination in the

control column. There is also an increase in ammonium-N concentration in the inoculated column with the introduction of the CMM+ medium. Calcium is important component for optimal cell growth, and has been denied to the cells until day 8. Once the cells have access to calcium, it is possible that there is a rapid increase in growth, resulting in more cells that are producing more ammonium-N. This would explain the increase in ammonium-N concentration seen after day 8. This trend is continually seen throughout the various column experiments.

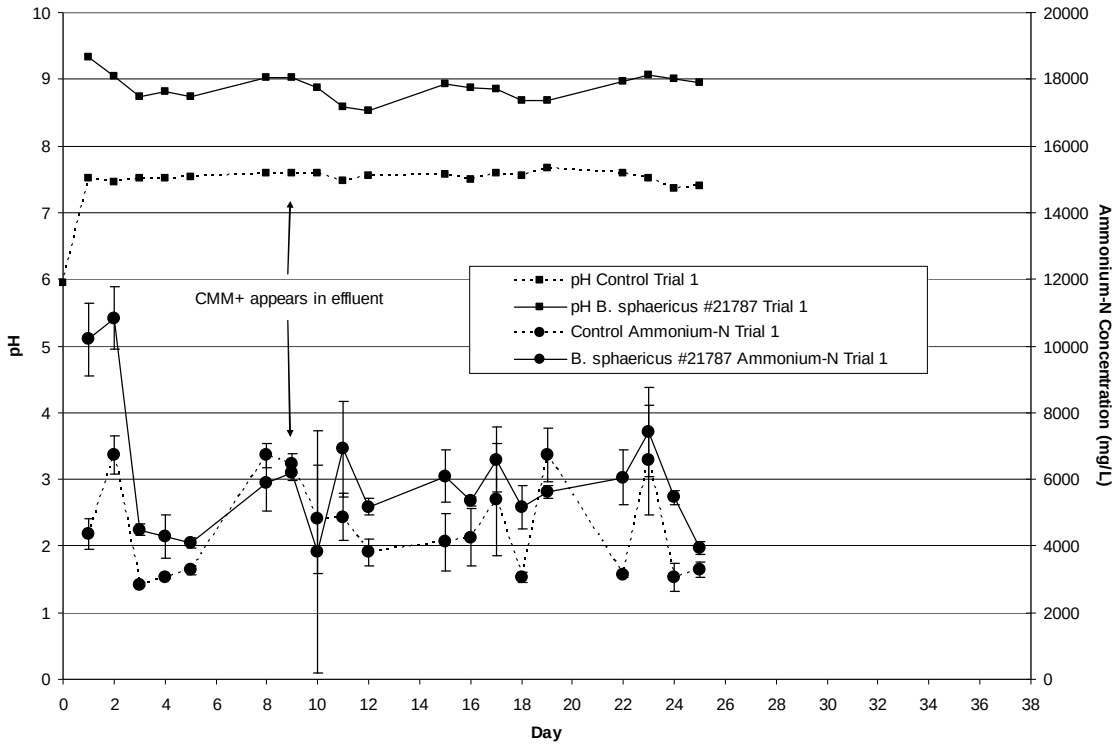

Figure 25: Relationship between pH and ammonium-N concentration for first *B. sphaericus* #21787 experiment. Error bars represent one standard deviation of triplicate measurements.

Figure 25 shows the relationship between pH and ammonium-N concentration for the first *B. sphaericus* #21787 trial. The pH of the inoculated column rises within the first day to the normally observed high of about 9.3. The control column rises from the initial pH of the media and reaches a high of about 7.5 throughout the duration of the experiment. The ammonium-N concentration of the inoculated column starts out high for the first two days and then drops to the ammonium-N concentration of the control column. The ammonium-N concentration of the inoculated column then follows the same trend as the control column. This unusual occurrence was also seen in the OD_{600} and protein data for this trial. Taken together, this data indicates that something unusual is happening in this system. The pH of the system is slightly lower than is typically observed, about 9 instead of 9.3, so it is possible that the inoculum prepared for this experiment may have been contaminated during the incubation or inocula preparation phase, and that could account for the unusual behavior exhibited in Trial 1.

Figure 26 shows the relationship between pH and ammonium-N concentration for the second *B. sphaericus* #21787 trial. The pH of the inoculated column rises within the first day to the normally observed pH of approximately 9.3. The control data is the same data described in Figure 24.

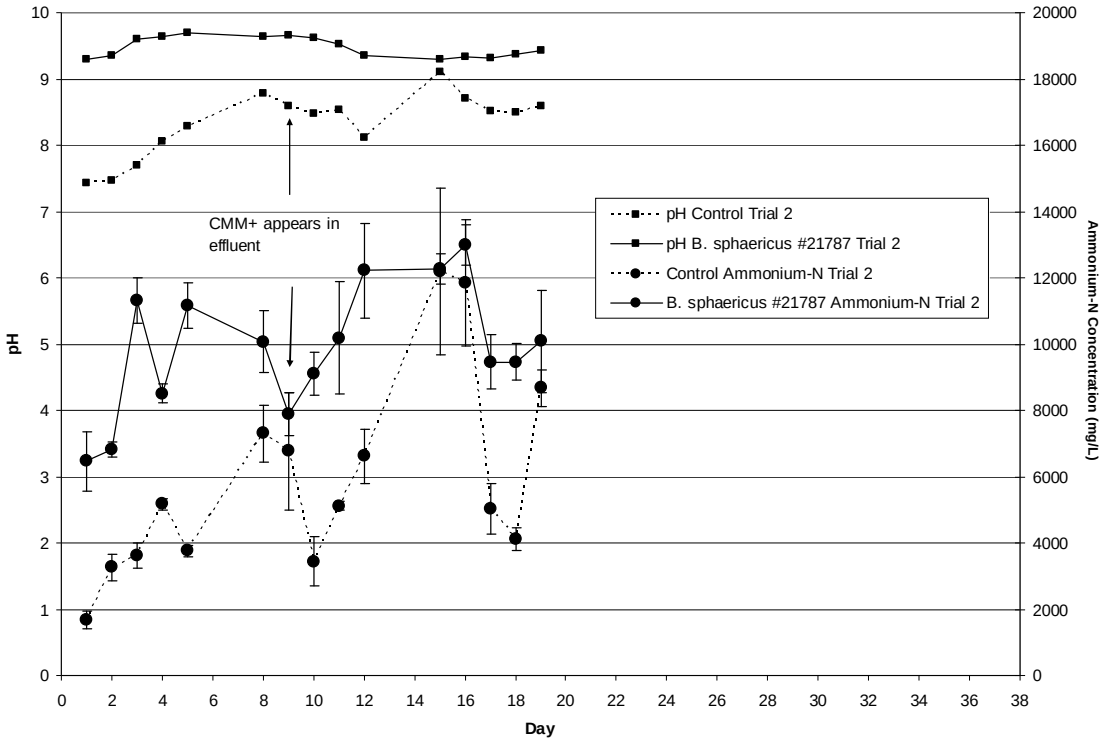

Figure 26: Relationship between pH and ammonium-N concentration for the second *B. sphaericus* #21787 experiment. Error bars represent one standard deviation of triplicate measurements.

The ammonium-N concentration for the inoculated column still remains higher than that of the control throughout the duration of the experiment despite the contamination observed in the control column. There is also an increase in ammonium-N concentration in the inoculated column with the introduction of the CMM+ medium. Calcium is important component for optimal cell growth, and has been denied to the cells until day 8. Once the cells have access to calcium, it is possible that there is a rapid increase in growth, resulting in more cells that are producing more ammonium-N. This would explain the increase in ammonium-N concentration seen after day 8.

Figure 27 shows the relationship between pH and ammonium-N concentration for the only *B. subtilis* trial. *B. subtilis* is not a ureolytic organism, and is unable to utilize urea, produce ammonium, and increase the pH of the system. In short, it should behave very similar to the control column, as Figure 27 shows. The pH values of both systems remain at about 7.6 for the entire experiment. The ammonium-N concentration for both systems parallels each other and remains between 2000 and 6000 mg/L throughout the course of the experiment.

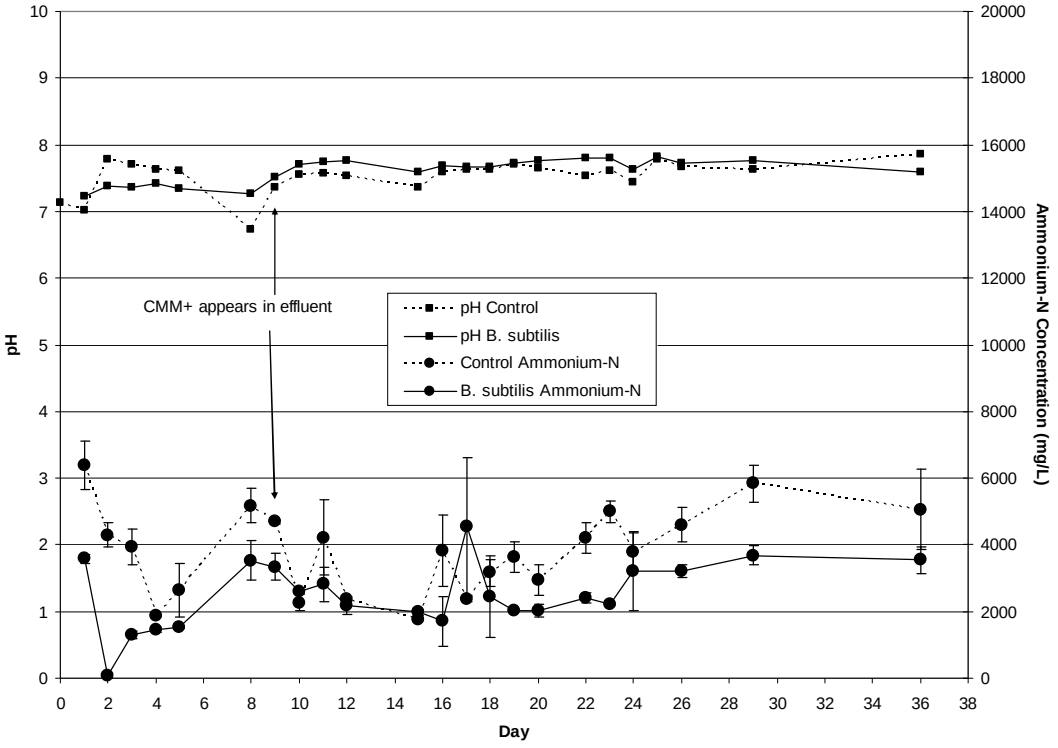

Figure 27: Relationship between pH an ammonium-N concentration for the only *B. subtilis* experiment. Error bars represent one standard deviation of triplicate measurements.

In summary, a direct correlation between ammonium production and pH increase can not be seen from the pulse-flow column data because the increase happens so rapidly.

However, a relationship between the two is inferred from the pH increase, and the fact that the ammonium-N concentration in the inoculated columns is higher than that in the control columns.

pH

Because each trial was presented separately for the ammonium-N data the pH values between identical trials were not compared. This data is would be a good indicator of reproducibility between experiments, and is therefore presented in this section. Figure 28 shows that the pH in each of the three *S. pasteurii* pulse-flow column trials increases from about 7.3 to a high of about 9.3 within the first day and remains that way throughout the duration of the experiment.

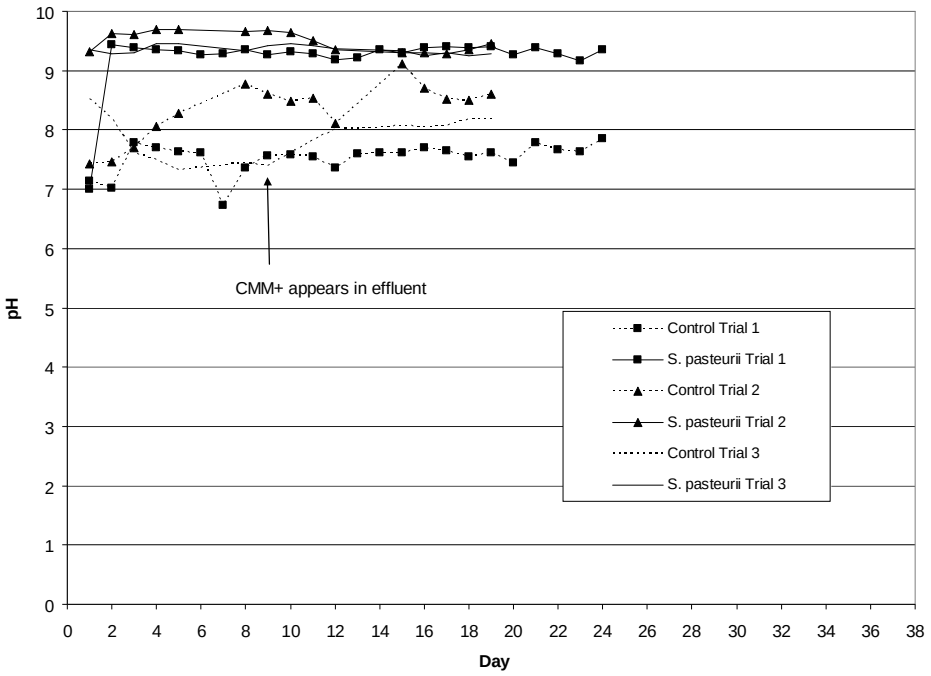

Figure 28: Change in pH over time for triplicate *S. pasteurii* experiments. pH increases within the first day to a high of 9.3 and remains at this level throughout the duration of the experiment.

The introduction of CMM+ does not cause the pH to change. The control columns remain at a pH of about 7.5 or 8 throughout the duration of the experiment, even with the introduction of CMM+. If there is an increase in pH seen after the introduction of CMM+, it is due to a contaminant that was introduced into the system when the media bottles were exchanged. For example, the control column for Trial 2 exhibits an increase in pH on day 9, and is due to a contaminant present in the column. This contamination is also evident through the OD_{600} measurements for this column (Figure 13). The measurements increase over time from the normally stable reading of 0.038. The highest pH level reached in the *S. pasteurii* batch experiments performed by Stacy Parks corresponds to the highest pH level reached in the column experiments.

The pH for both *B. sphaericus* #21776 trials exhibits the same trend (Figure 29). The pH rises within the first day and remains at the normally seen high of about 9.3

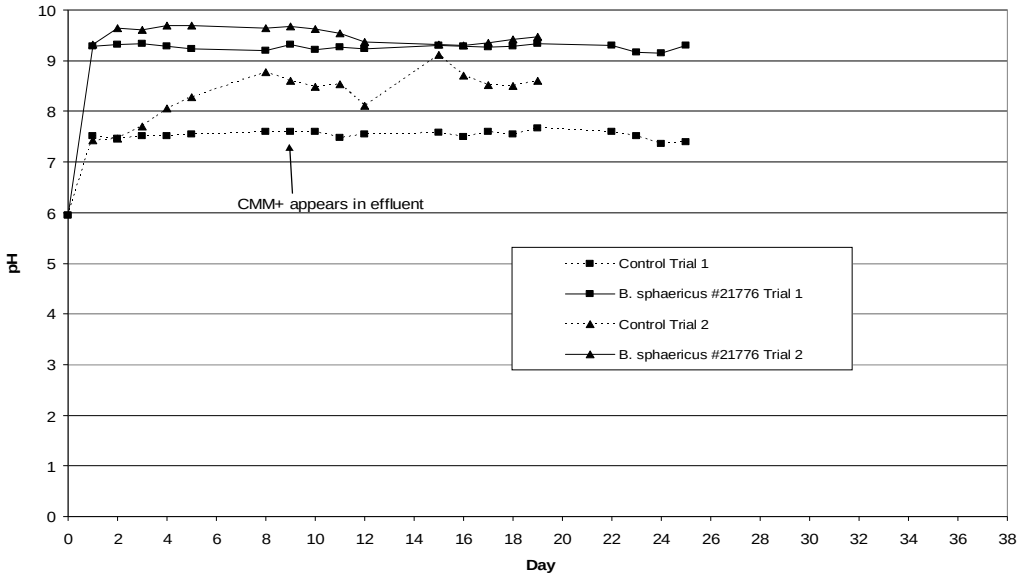

Figure 29: The change in pH over time for duplicate *B. sphaericus* #21776 experiments.

throughout the duration of the experiment. The control columns remain at a pH of about 7.5 or 8 throughout the duration of the experiment, even after the introduction of CMM+. If there is an increase in pH seen after the introduction of CMM+, it is likely due to a contaminant that was introduced into the system when the media bottles were exchanged.

For example, the control column for trial two exhibits an increase in pH on day 9, and is due to a contaminant present in the column. This contamination is also evident when looking at the OD_{600} measurements for this column (Figure 14). The measurements increase over time from the normally stable reading of 0.038. The highest pH level reached in the *B. sphaericus* #21776 batch experiments performed by Stacy Parks corresponds to the highest pH level reached in the column experiments.

Figure 30 shows the change in pH over time for both of the *B. sphaericus* #21787 trials. The pH of the first trial hovers at just less than pH 9 for most of the experiment. This trial was also the trial where the OD_{600} readings, the protein readings, and the ammonium-N readings were all very similar to that of the control. This low pH reading is another indication that there might be a potential problem with the inoculum. The control columns from the first trial remains at a pH of about 7.5 or 8 throughout the duration of the experiment, even with the introduction of CMM+. If there is an increase in pH seen after the introduction of CMM+, it is due to a contaminant that was introduced into the system when the media bottles were exchanged. For example, the control column for Trial 2 exhibits an increase in pH on day 9, and it is due to a contaminant present in the column. This contamination is also evident when looking at the OD_{600} measurements for this column (Figure 15). The measurements increase over time from the normally stable reading of 0.038. The highest pH level reached in the *B. sphaericus* #21787 batch experiments performed by Stacy Parks corresponds to the highest pH level reached in the column experiments.

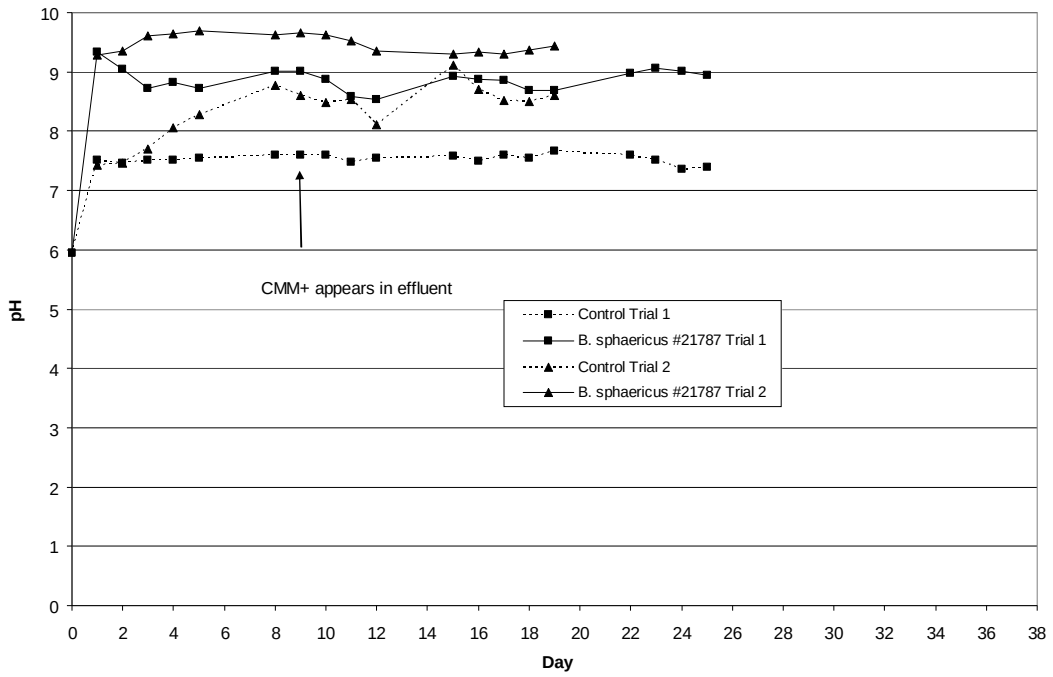

Figure 30: Change in pH over time for duplicate *B. sphaericus* #21787 experiments.

Figure 31 shows the change in pH over time for the only *B. subtilis* trial. Because *B. subtilis* is not ureolytic, it does not hydrolyze urea and ammonium is not produced. Therefore, it is unable to raise the pH of the system. The pH of the inoculated column should mirror that of the control column, and that is exactly what is seen in Figure 31.

When the CMM medium is made, the pH is adjusted to 5.95-6. The medium is left on the bench top before it is attached to the column, and during that time it readjusts itself to a pH of approximately 7.3 due to the shifting carbonate equilibrium (equations 4 and 5). While inconvenient, this inherent pH adjustment does not affect the daily monitoring of the pH, it is still low enough to see the pH increase to over 9 within the first day.

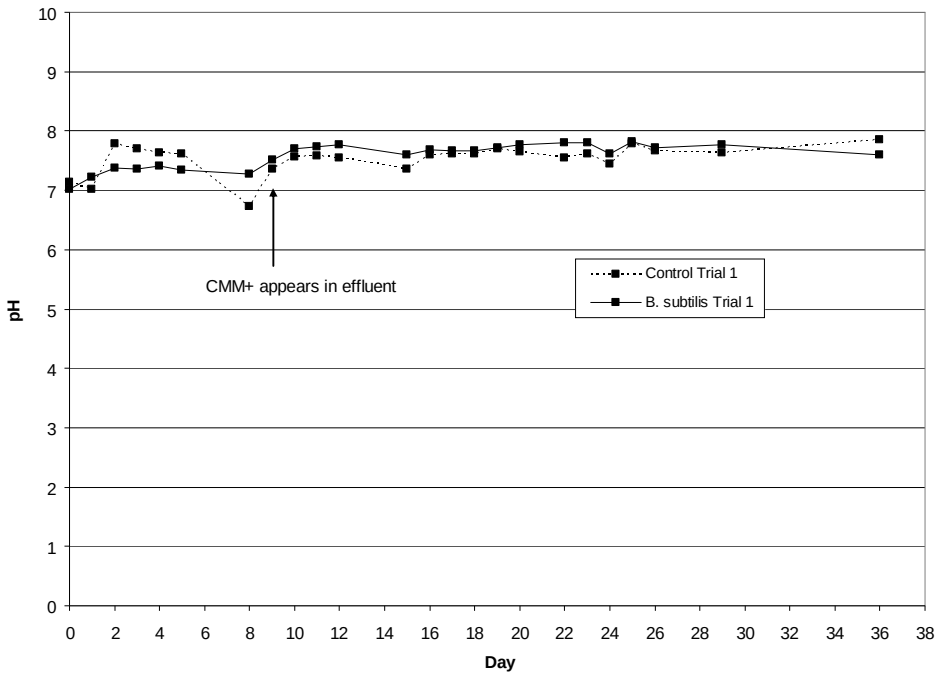

Figure 31: Change in pH over time for single *B. subtilis* trial.

Calcium and Flow Rate

The pH increase shifts the bicarbonate equilibrium and results in the formation of carbonate ions (equation 5). In the presence of soluble calcium ions, this can form the precipitate $CaCO_3$ (equation 6). Free calcium ions are introduced into the system via the CMM+ medium and the total and dissolved calcium in the column effluent are measured over time. Disappearance of calcium relative to a control indicates that the calcium is being consumed in the column system and possibly being precipitated out as calcium carbonate.

On day 8, CMM+ is pumped into the column system and CMM- is drained from the column system. From day 9 onward, only CMM+ is pumped daily into the system, so

only CMM+ should be draining from the system. Even though CMM+ is expected in the column effluent on day 9, it appears that calcium doesn't begin to appear in the effluent in measurable quantities until day 10 in some trials. For those trials, it is possible that day 9 is a transition period within the column and that there is some residual CMM- left, or, a full pore volume of medium was not exchanged during that time.

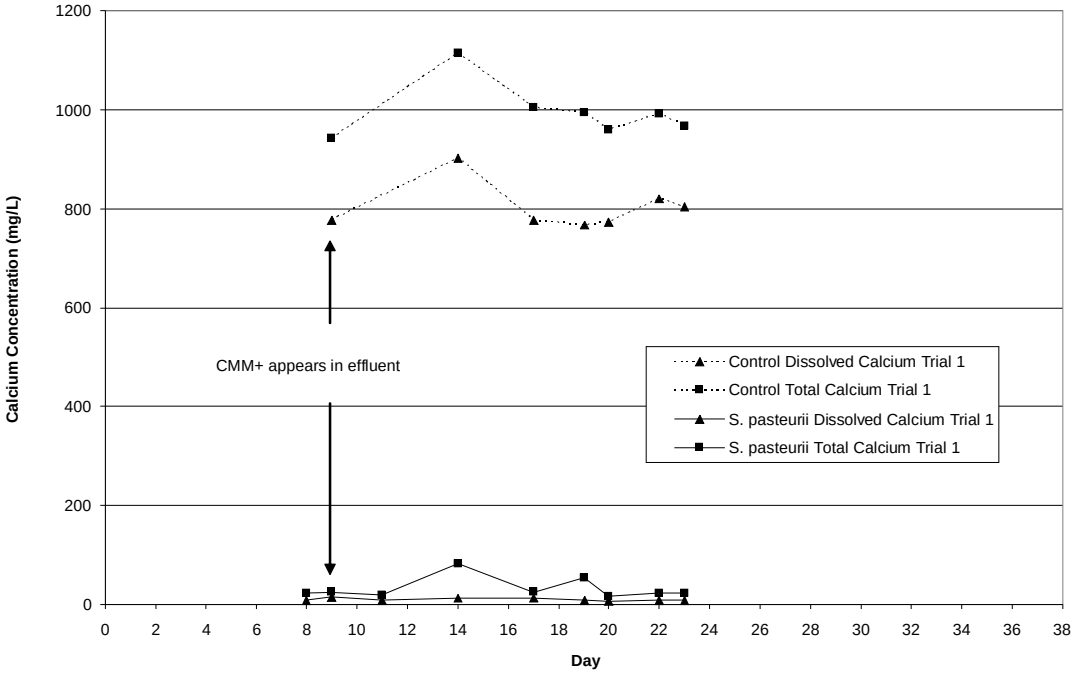

Figure 32: Change in calcium concentration over time for the first *S. pasteurii* trial.

For the first *S. pasteurii* trial (Figure 32), calcium begins appearing in the effluent on day 9. The total and dissolved calcium measurements for the inoculated column are much less than the total and dissolved calcium measurements for the control column, indicating that calcium is being consumed in the column system. The total calcium measurements for both the control and inoculated column are higher than the

dissolved calcium measurements throughout the whole experiment. This is expected because not all of the calcium present in the column is necessarily in solution (dissolved), some of the calcium might be in the form of $CaCO_3$, a solid. Total calcium measures how much calcium is present in the system, whether it is dissolved or solid.

Figure 33 shows the change in calcium concentration over time for the second *S. pasteurii* trial. Calcium begins appearing in the column effluent on or after day 10. Again, the total and dissolved calcium concentrations are higher for the control than for the inoculated column, indicating that calcium is being consumed in the column system. There is a drop in calcium concentration in the control column between days 12 and 16, indicating that there might be a ureolytic bacteria contaminant in the system that is utilizing calcium. The increase in calcium concentration on day 18 refutes this hypothesis, however. If there was a contaminant in the control system, more calcium would be consumed, and the decrease in calcium concentration would be seen for the remainder of the experiment. Another explanation for this decrease in calcium concentration is the cell's access to calcium. Calcium is important component for optimal cell growth, and has been denied to the cells until day 8. Once the cells have access to calcium, it is possible that there is a rapid increase in cell growth, resulting in a decrease in calcium concentration after day 10.

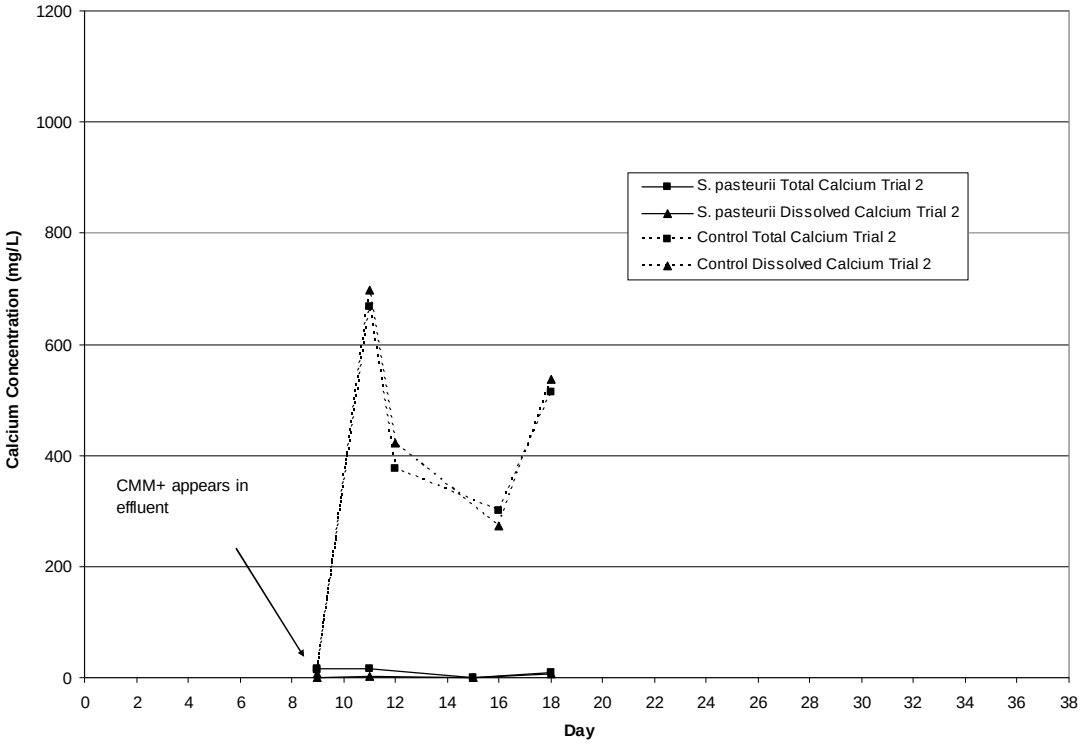

Figure 33: The change in calcium concentration over time for the second *S. pasteurii* experiment.

Figure 34 shows the change in calcium concentration over time for the third *S. pasteurii* trial. Calcium begins to appear in the column effluent on day 10. The total and dissolved calcium concentrations for the control column increase to almost 1000 mg/L. The concentrations stay relatively constant throughout the duration of the experiment. 1000 mg/L is the amount of calcium that should be present in the CMM+ media. Seeing this value in the control column indicates that the medium is being made consistently. Conversely, the total and dissolved calcium data for the *S. pasteurii* column is much lower, indicating that calcium is being consumed in the column system.

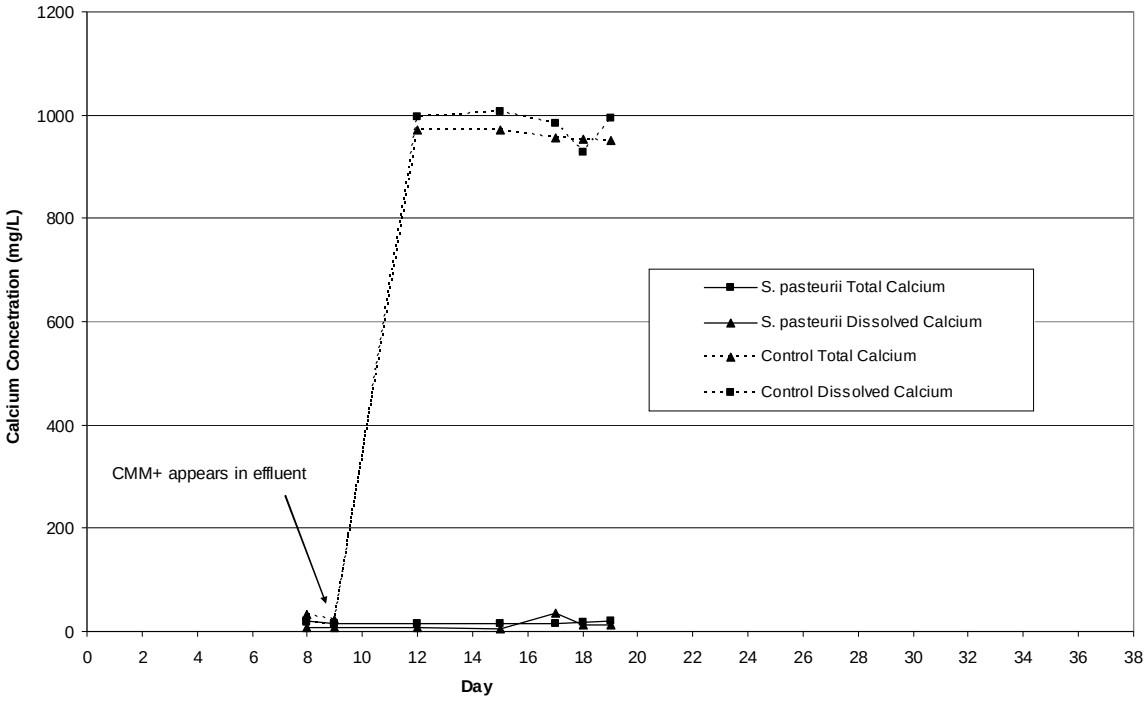

Figure 34: The change in calcium concentration over time for the third *S. pasteurii* trial.

While calcium carbonate is precipitating out over the course of the experiment, there is not enough precipitating out in the control columns or the *S. pasteurii* columns to significantly reduce the flow rate. Figure 35 shows the change in flow rates for all control columns and *S. pasteurii* columns over time. The only column that does not follow this trend is the third *S. pasteurii* column. This column did not have any more precipitate than any other column, but the flow rate does decrease from about 1.5 mL/s to about 0.9 mL/s, especially after day 9, when CMM+ appears in the effluent. It could be that there is more biomass in this column and that the increased biomass is reducing the flow rate. It is possible that not as many cells are detaching, leading to the increased biomass in the system. This was the first 1 mm bead column that showed this trend. See

the end of this section for a discussion on porosity, calcium carbonate precipitation, and their impact on flow rate.

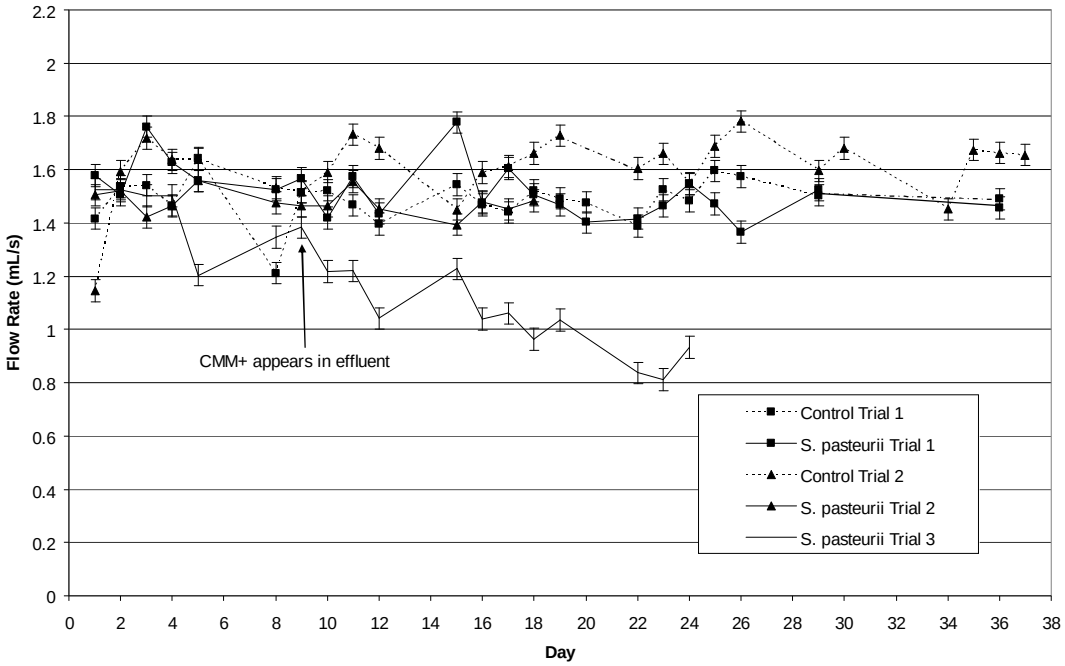

Figure 35: The change in flow rate over time for the three separate *S. pasteurii* experiments and corresponding control columns. Error bars represent one standard deviation of ten measurements obtained from an uninoculated column.

The accumulation of calcium in the inoculated column can be calculated over the course of the experiment (Figure 36). Calcium carbonate accumulates in a linear fashion over time in each of the three *S. pasteurii* trials. Calcium accumulation is calculated as per Appendix D.

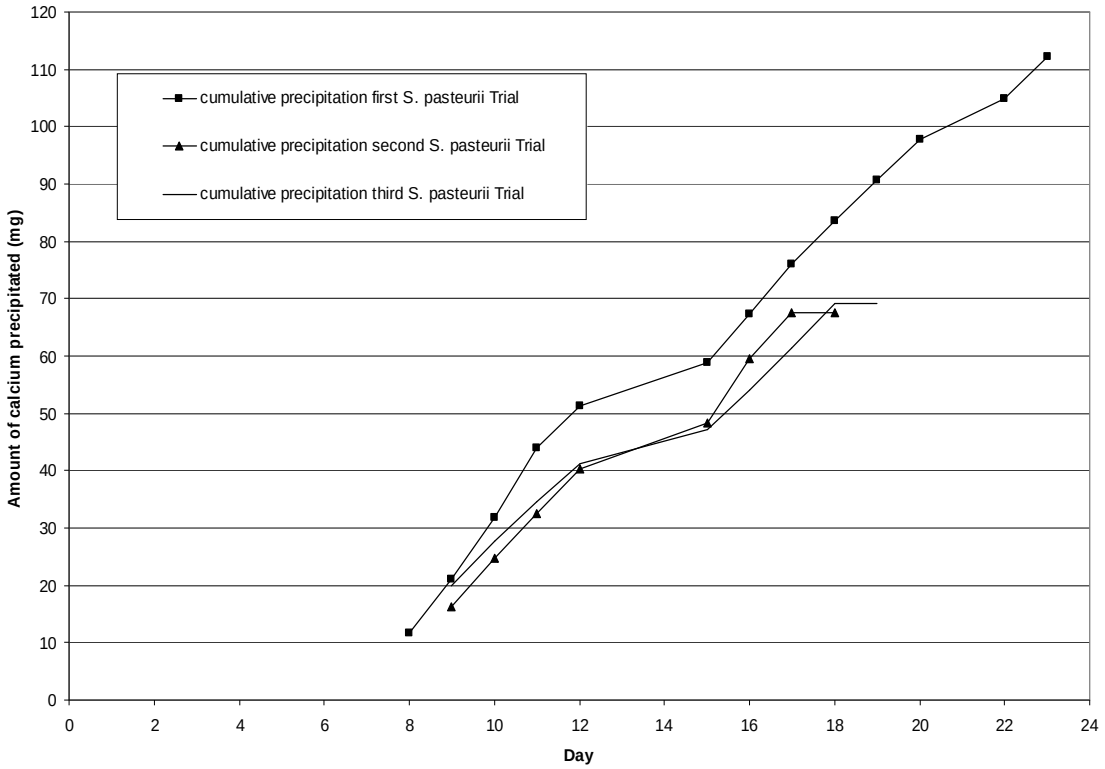

Figure 36: Accumulation of calcium for all *S. pasteurii* experiments.

For the first *B. sphaericus* #21776 trial (Figure 37), calcium begins appearing in the effluent on or after day 10. The total and dissolved calcium measurements for the inoculated column are much less than the total and dissolved calcium measurements for the control column, indicating that calcium is being consumed in the column system. The total calcium measurements for both the control and inoculated column are higher than the dissolved calcium measurements throughout the whole experiment. This is also expected because not all of the calcium present in the column is in solution (dissolved), some of the calcium is in the form of $CaCO_3$, a solid. Total calcium measures how much calcium is present in the system, whether it is dissolved or solid. The calcium

concentrations for the control are much greater than the 1000 mg/L that is what is introduced into the media. This indicates that the media was made inconsistently and more calcium chloride dihydrate was added than was supposed to be.

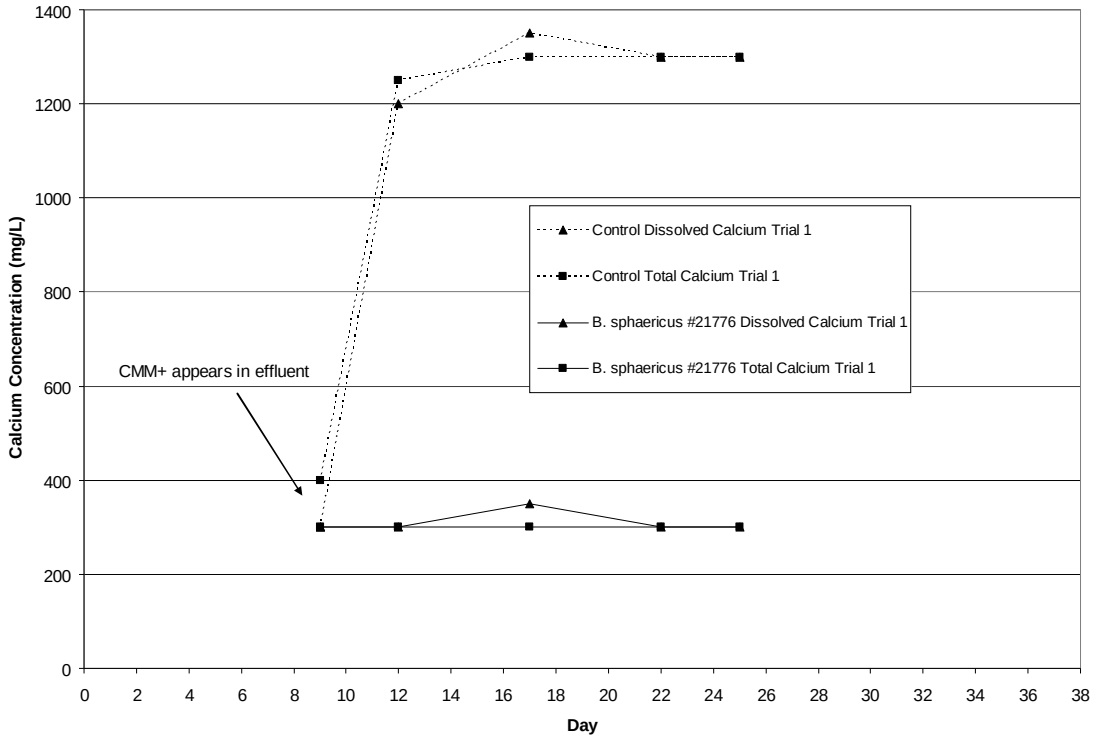

Figure 37: The change in calcium concentration over time for the first *B. sphaericus* #21776 experiment.

Figure 38 shows the change in calcium concentration over time for the second *B. sphaericus* #21776 trial. Again, the total and dissolved calcium concentrations are higher for the control than for the inoculated column, indicating that calcium is being consumed in the column system.

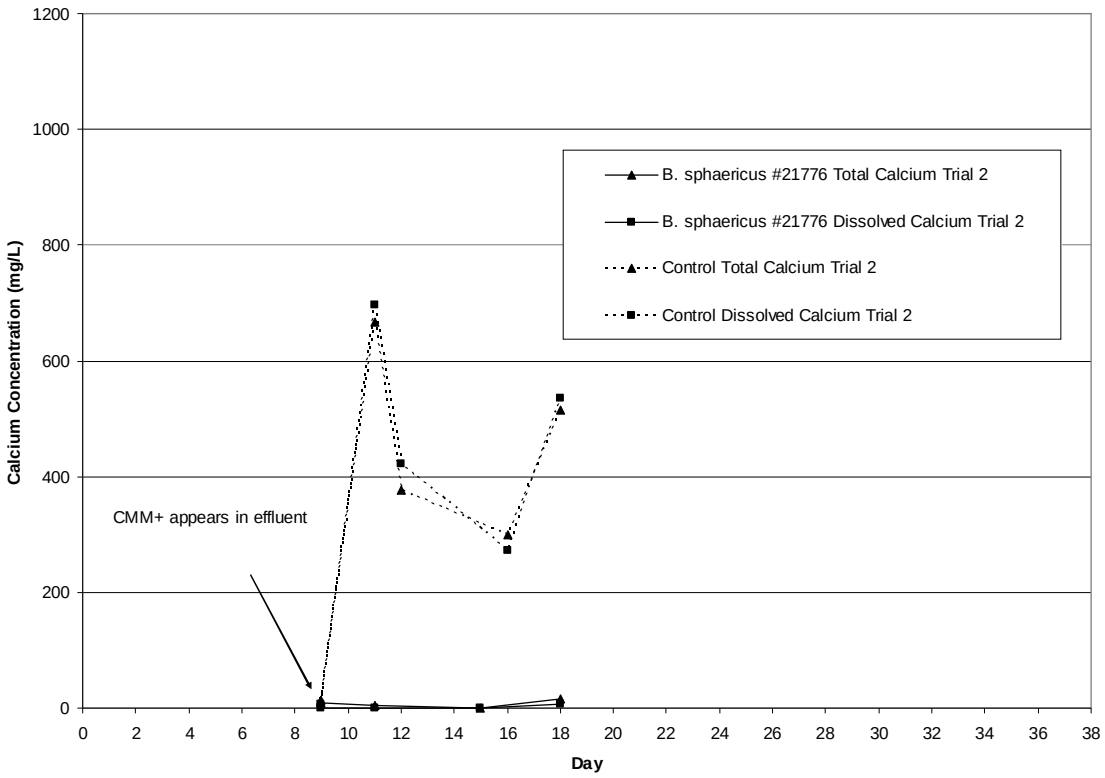

Figure 38: Change in calcium concentration over time for the second *B. sphaericus* #21776 experiment.

There is a drop in calcium concentration is the control column between days 12 and 16, indicating that there might be a contaminant in the system that is consuming calcium. The increase in calcium concentration on day 18 refutes this hypothesis, however. If there was a contaminant in the control system, more calcium would be utilized, and the decrease in calcium concentration would be seen for the remainder of the

experiment . Another explanation for this decrease in calcium concentration is the cell's access to calcium. Calcium is important component for optimal cell growth, and has been denied to the cells until day 8. Once the cells have access to calcium, it is possible that there is a rapid increase in cell growth, resulting in a decrease in calcium concentration after day 10.

Once again, while there is calcium carbonate precipitating out, it does not appear to be enough to decrease the flow rate within the columns. Figure 39 shows that the flow rate in the two inoculated columns increases slightly after the addition of CMM+. The increase is slight, but not significant. See the end of this section for a discussion on porosity, calcium carbonate precipitation, and their impact on flow rate.

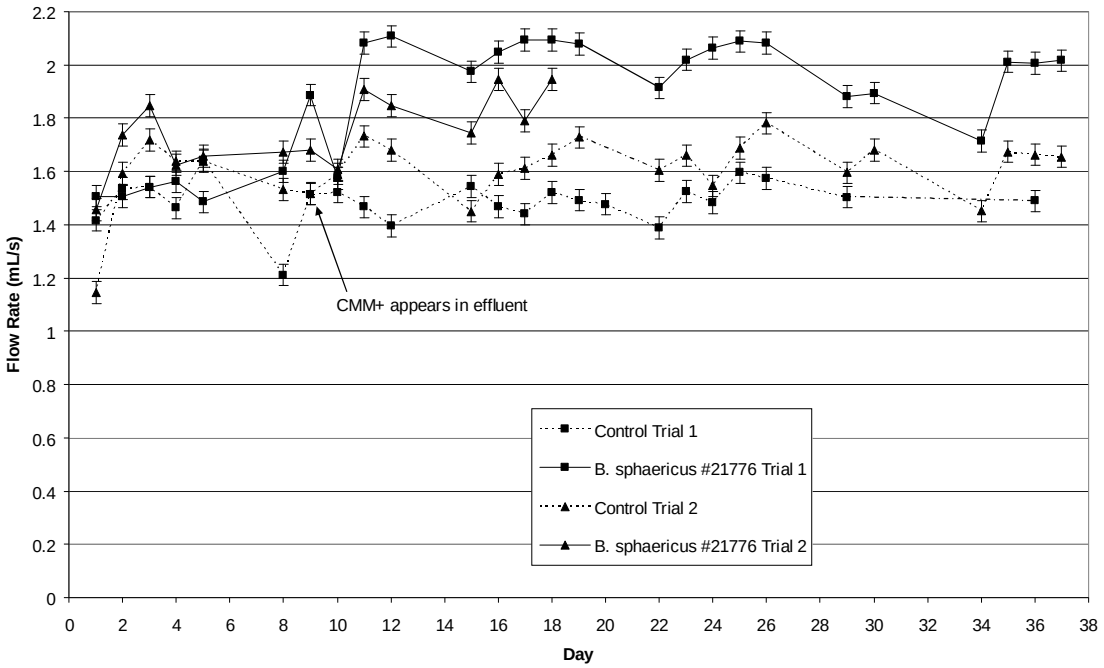

Figure 39: Change in flow rate over time for both *B. sphaericus* #21776 trials. Error bars represent one standard deviation of ten measurements obtained from an uninoculated column.

The accumulation of calcium in the inoculated columns is calculated over the course of the experiment (Figure 40). Calcium carbonate accumulates in a linear fashion over time for both of the *B. sphaericus* #21776 trials. Not as much calcium accumulates in either of the two *B. sphaericus* #21776 columns compared to the first *S. pasteurii* column However, 63 mg of calcium accumulated in the second *B. sphaericus* #21776 column which is comparable to the amount of calcium that accumulated in the second and third *S. pasteurii* columns; 68 and 69 mg, respectively.

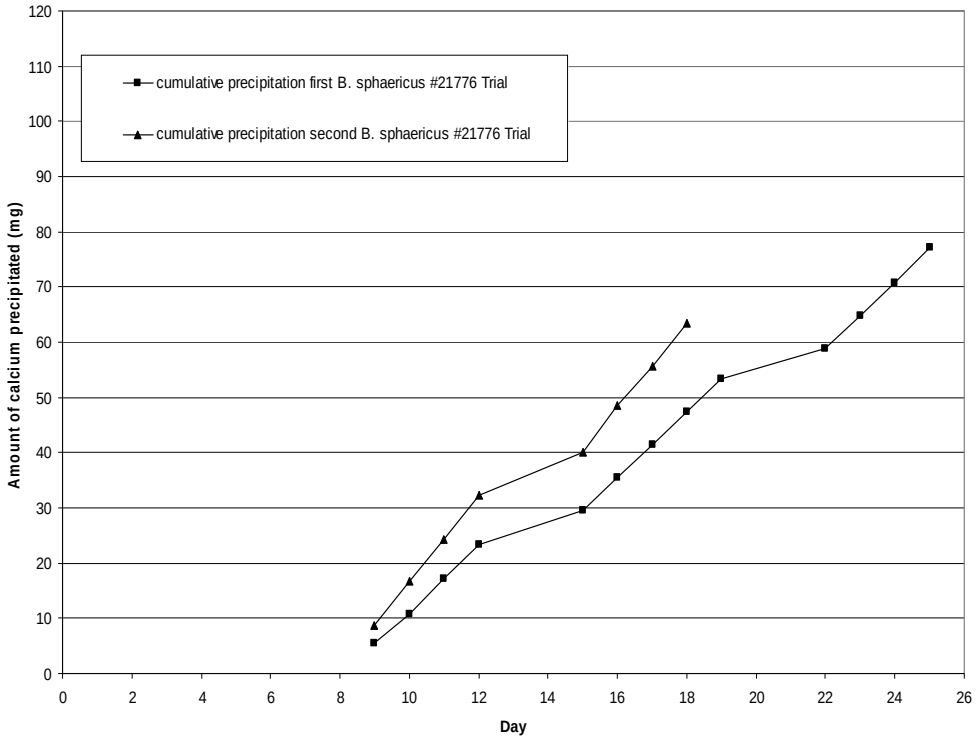

Figure 40: Accumulation of calcium in both *B. sphaericus* #21776 trials.

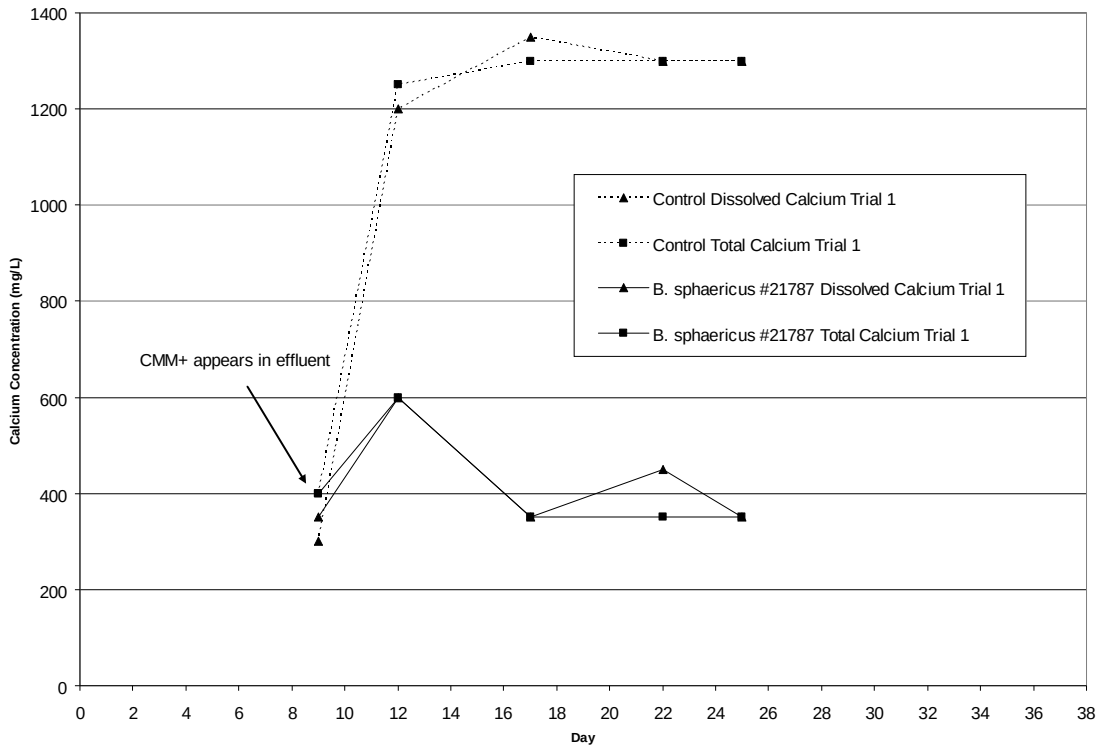

Figure 41: Calcium concentration over time for first *B. sphaericus* #21787 trial.

For the first *B. sphaericus* #21787 trial (Figure 41), calcium begins appearing in the column effluent on or after day 10. The total and dissolved calcium measurements for the inoculated column are much less than the total and dissolved calcium measurements for the control column, indicating that calcium is being consumed in the column system. The total calcium measurements for both the control and inoculated column are higher than the dissolved calcium measurements throughout the whole experiment. This is expected because not all of the calcium present in the column might be in solution (dissolved), some of the calcium is in the form of $CaCO_3$, a solid. Total calcium measures how much calcium is present in the system, whether it is dissolved or solid. The calcium concentrations for the control are much greater than the 1000 mg/L

that it should be. This indicates that the medium was made inconsistently and more calcium chloride dihydrate was added than was supposed to be.

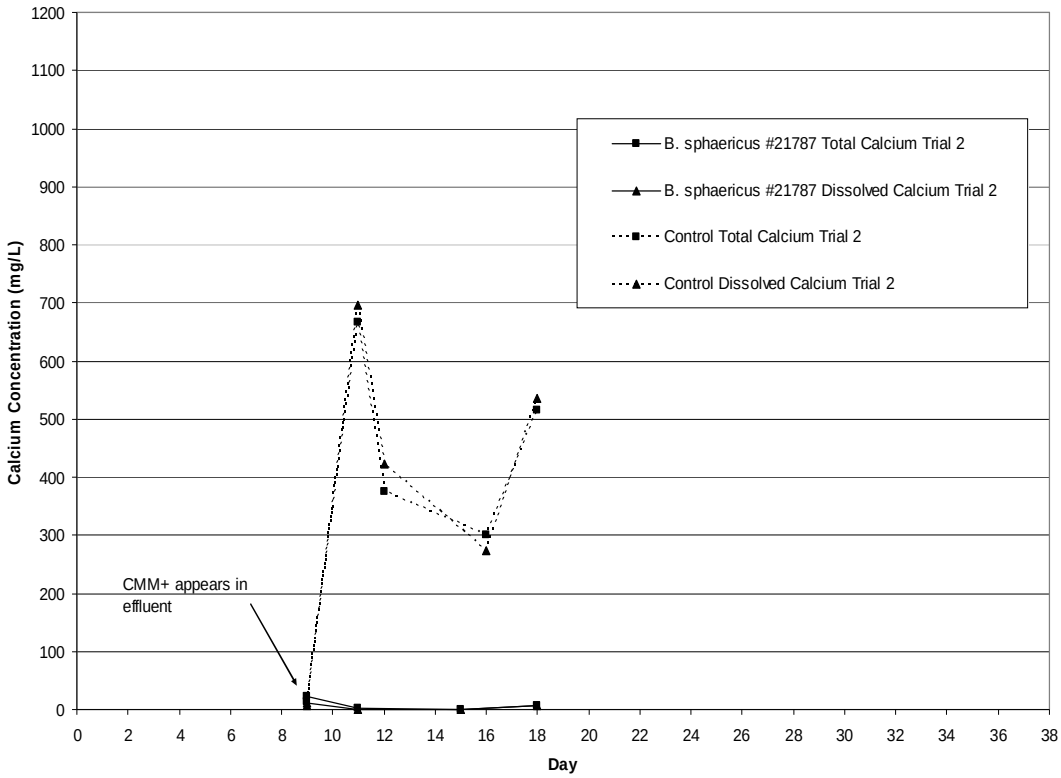

Figure 42: Calcium concentration over time for second *B. sphaericus* #21787 trial.

Figure 42 shows the change in calcium concentration over time for the second *B. sphaericus* #21787 trial. Calcium begins appearing in the column effluent on day 10. Again, the total and dissolved calcium concentrations are higher for the control than for the inoculated column, indicating that calcium is being consumed in the column system. There is a drop in calcium concentration is the control column between days 12 and 16, indicating that there might be a ureolytic bacteria contaminant in the system that is consuming calcium. The increase in calcium concentration on day 18 refutes this hypothesis, however. If there is a contaminant in the control system, more calcium

would be utilized, and the decrease in calcium concentration would be seen for the remainder of the experiment. Another explanation for this decrease in calcium concentration is the cell's access to calcium. Calcium is important component for optimal cell growth, and has been denied to the cells until day 8. Once the cells have access to calcium, it is possible that there is a rapid increase in cell growth, resulting in a decrease in calcium concentration after day 10.

Once again, while there is calcium carbonate precipitating out, it does not appear to be enough to decrease the flow rate within the columns. Figure 43 shows that the flow rate in the two inoculated columns does not change appreciably over time.

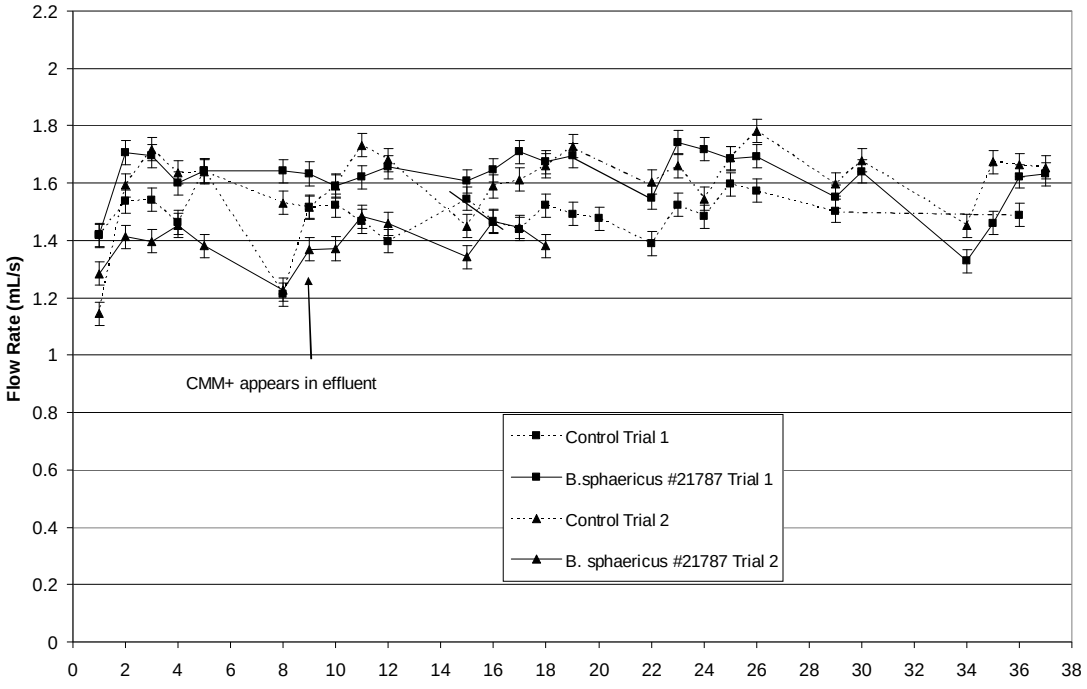

Figure 43: Change in flow rate over time for all *B. sphaericus* #21787 trials. Error bars represent one standard deviation of ten measurements obtained from an uninoculated column.

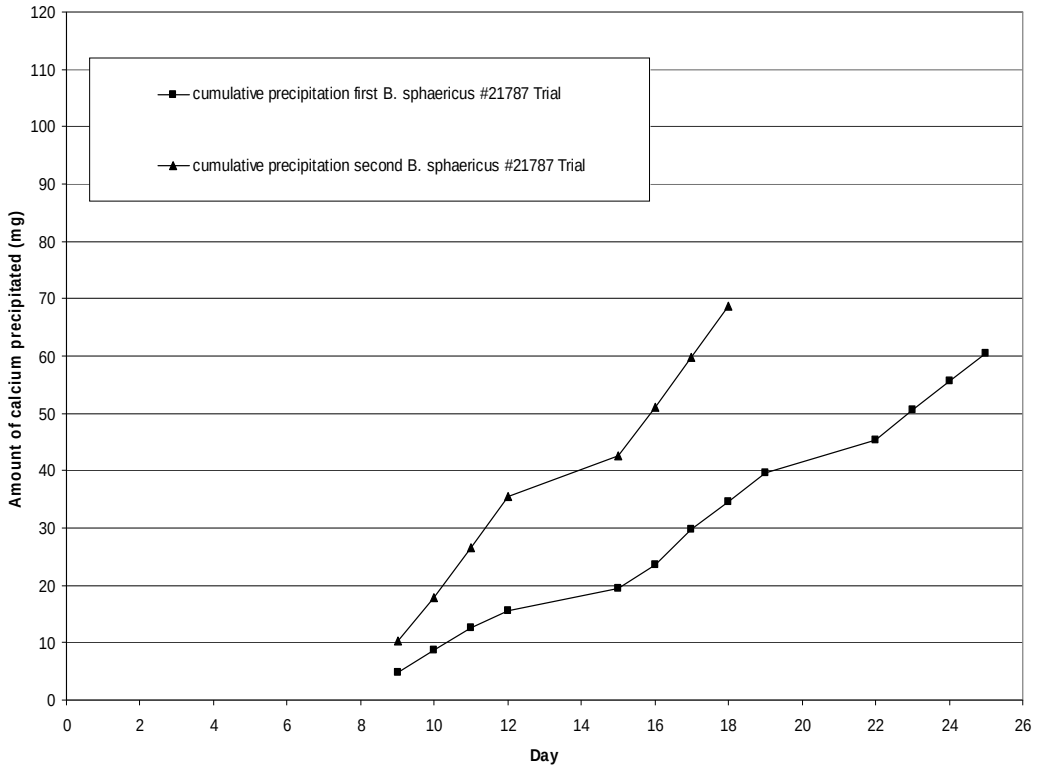

Figure 44: Amount of calcium carbonate precipitated for both *B. sphaericus* #21787 trials.

The accumulation of calcium in the inoculated columns is calculated over the course of the experiment (Figure 44). Calcium carbonate accumulates in a linear fashion over time for both of the *B. sphaericus* #21787 trials. For both *B. sphaericus* #21787 trials, the amount of calcium that accumulated is close to the amount of calcium that accumulated in the second and third *S. pasteurii* trials as well as both *B. sphaericus* #21776 trials.

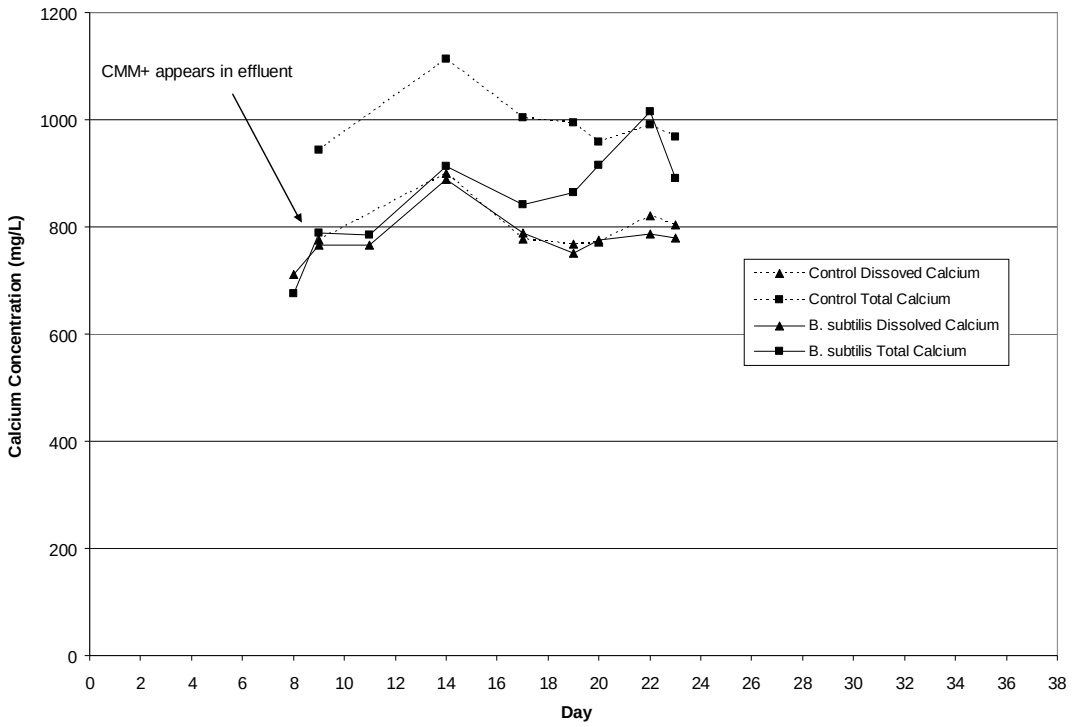

Figure 45: Calcium concentration over time for the single *B. subtilis* experiment.

Figure 45 shows the change in calcium concentration over time for the only *B. subtilis* experiment. The total calcium concentration for the control column is higher than that of the dissolved calcium concentration for the control column, which is what has been seen throughout the course of each experiment. The total calcium concentration for the *B. subtilis* inoculated column is also slightly higher than the dissolved calcium concentration of the inoculated column. Not all of the calcium present in the column is in solution (dissolved), some of the calcium might be in the form of $CaCO_3$, a solid. Total calcium measures how much calcium is present in the system, whether it is dissolved or

solid. *B. subtilis* is not a ureolytic organism and should not be converting free calcium to calcium carbonate. However, some calcium is necessary for optimal cell growth, so a slight difference between total and dissolved calcium would not be considered unusual. The dissolved calcium concentrations for the inoculated column and the control mirror each other throughout the duration of the experiment. This closeness of the control data and the *B. subtilis* data supports the fact that *B. subtilis* is not a ureolytic organism. There is significantly less precipitate present in the control column than in the inoculated

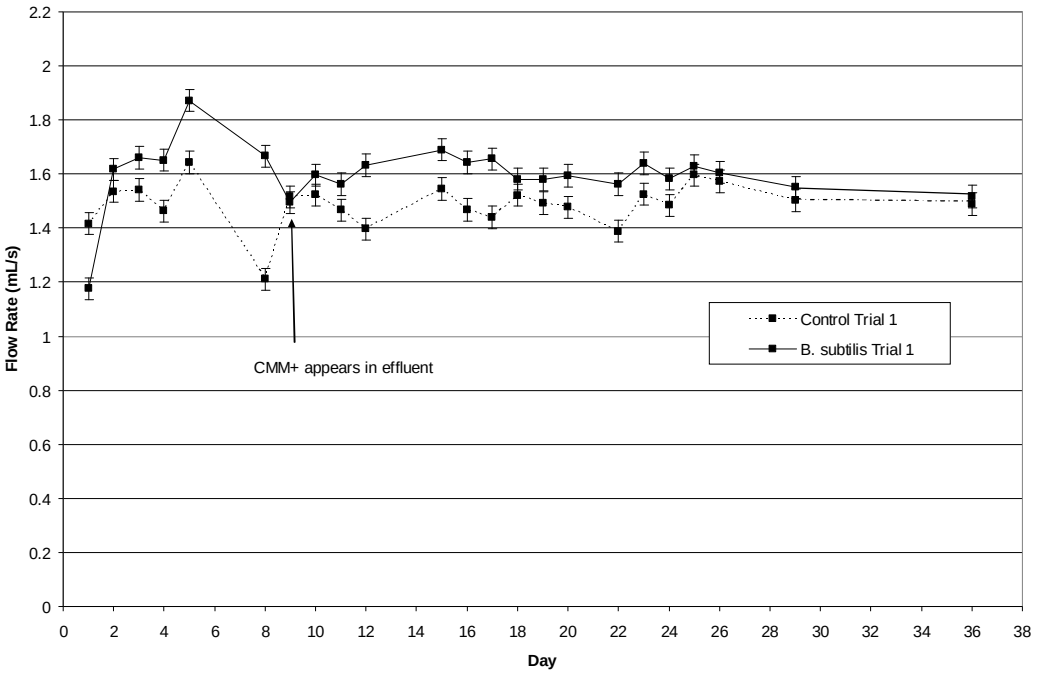

Figure 46: Change in flow rate over time for the only *B. subtilis* trial. Error bars represent one standard deviation of ten measurements obtained from an uninoculated column.

column, but neither column has enough precipitate to significantly reduce the pore space. Figure 46 shows the change in flow rate over time for the *B. subtilis* trial. The flow rate of either column does not significantly change over the duration of the experiment. See the end of this section for a discussion on porosity and calcium carbonate precipitation and its impact on flow rate.

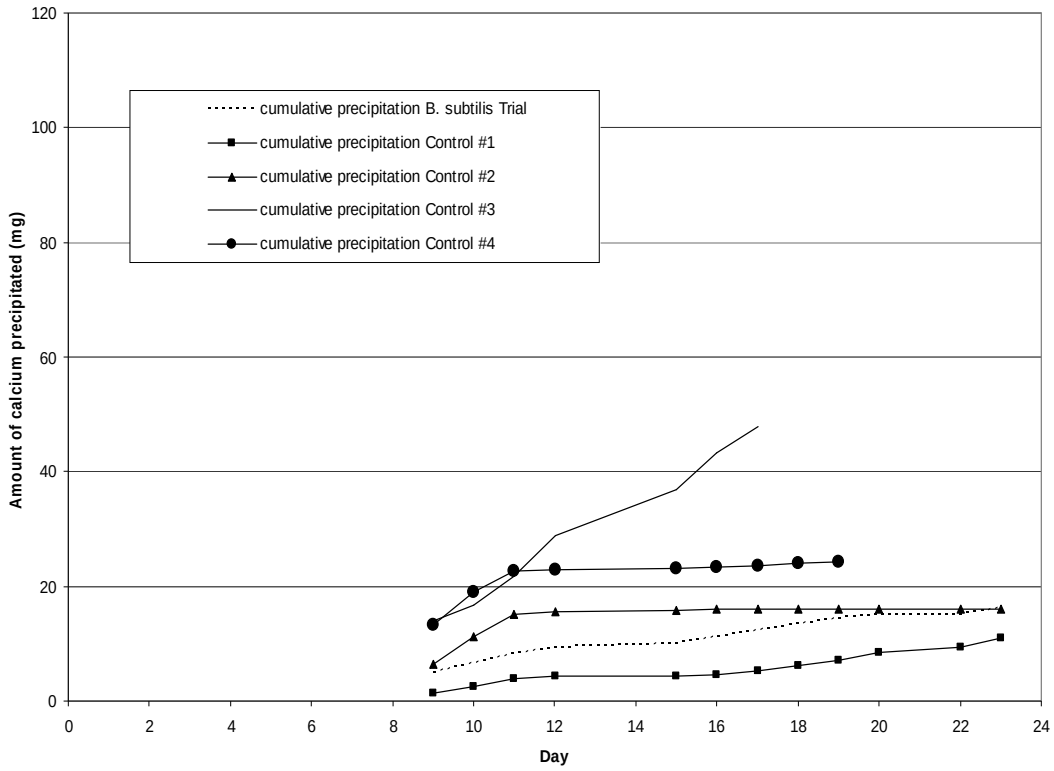

Figure 47: Accumulation of calcium precipitate in *B. subtilis* column.

The accumulation of calcium in the inoculated columns can be calculated over the course of the experiment (Figure 47). Calcium carbonate accumulates in a linear fashion over time for the *B. subtilis* trial just as it did for the ureolytic bacteria. However, because *B. subtilis* is not ureolytic and does not create the ideal environment for calcium

carbonate precipitation, the amount of calcium that precipitated out was considerably less than the amounts precipitated out in the ureolytic systems, in fact, it mirrors the amount of calcium accumulated in each of the four control columns. 16 mg of calcium accumulated in the *B. subtilis* column, compared to 11, 16, 48, and 24 mg of calcium that accumulated in the control columns.

In summary, the pH shifts the bicarbonate equilibrium, resulting in the formation of carbonate ions (equation 5), which in the presence of calcium ions precipitate as $CaCO_3$. The columns inoculated with ureolytic bacteria, especially *S. pasteurii*, accumulate more calcium carbonate precipitate than the control columns or the column inoculated with *B. subtilis*.

Imaging

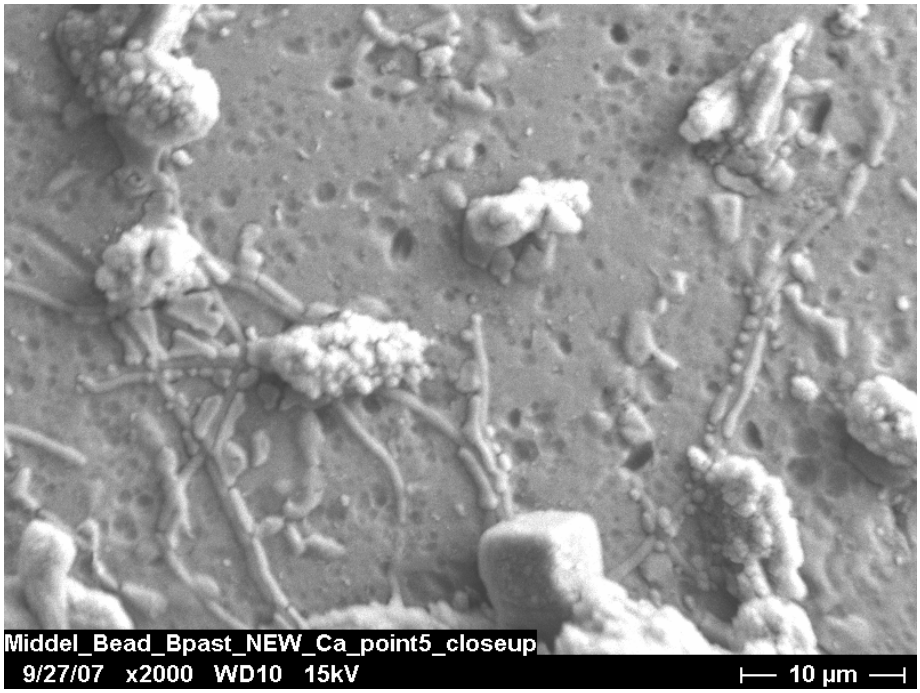

Figure 48: CryoSEM image of a bead from the middle of the first *S. pasteurii* column. This picture shows the interaction of cells and calcite crystals.

It has been demonstrated that the free calcium introduced into the ureolytic pulse-flow column systems is being utilized and is precipitating out as solid calcium carbonate. Because it is difficult to see any calcium deposits on the beads with the naked eye, beads from each section of the column are analyzed microscopically using a scanning electron microscope (SEM) and stereoscope. Interaction between cells and calcium carbonate crystals as well as the calcium deposits themselves were seen using both techniques (Figure 48).

Figure 49 is a CryoSEM picture of beads from the top of the first *S. pasteurii* column. As discussed in the destructive sampling section below, the top section of the column often has the highest concentration of cells, protein, and calcium. Several of these 1 mm beads are joined together by biofilm and EPS, the cloudy looking substance around and between some of the beads. Some of the beads appear to be joined together by biofilm but the fact that not all of them are may be the reason that a large reduction in permeability is not seen in the 1 mm bead pack columns. This figure also shows calcium deposits on the beads, which appear as the rough looking areas on the bead surface. From this picture, it is hard to determine how thick the deposits are on each individual bead, which is why stereoscope images are also taken. When SEM images are taken, the samples are sublimated in a vacuum, dehydrating the samples. Therefore, the amount of biofilm seen in the image might be less than the total amount of biofilm actually there.

Figure 49: 1 mm beads from the top of the first *S. pasteurii* column. The cloudy substance that joins some of the beads appears to be biofilm and EPS.

Figure 50 is a CryoSEM picture of beads from the middle of the first *S. pasteurii* column. The beads in this section are still connected to each other with biofilm and EPS, but there are not as many calcium deposit on the beads in this section. The middle of the column is probably more anaerobic than the top and bottom sections of the column, and therefore the bacterial cells in the middle did not grow as well. The lack of cell growth may result in less calcium deposit.

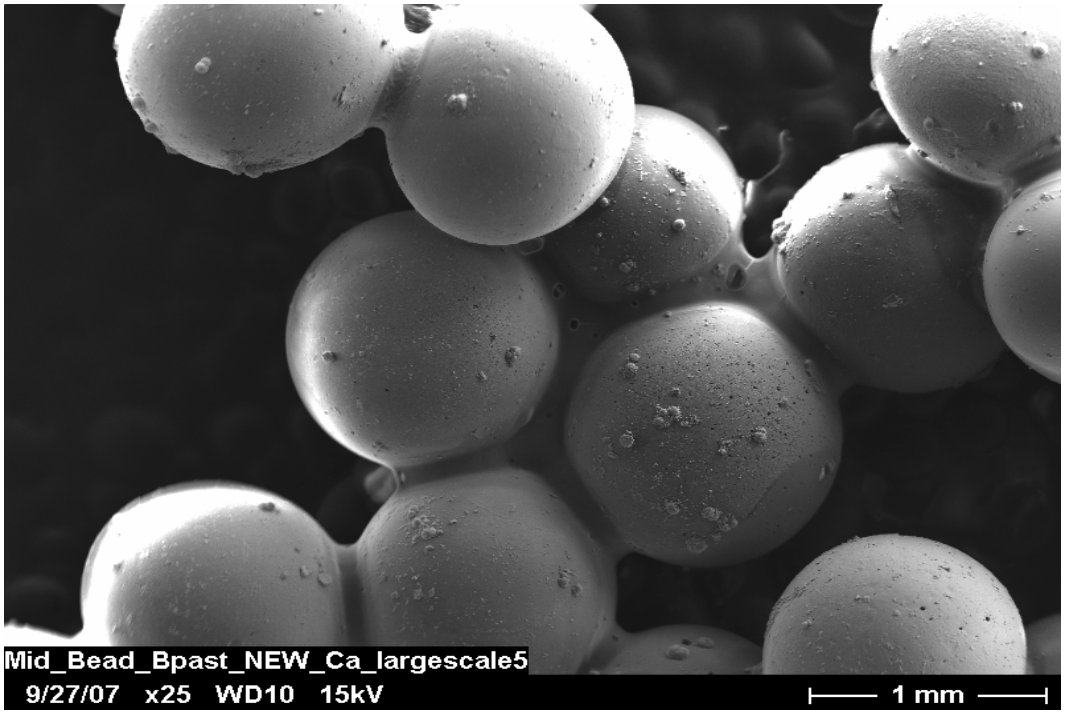

Figure 50: CryoSEM of beads from middle section of first *S. pasteurii* column.

Figure 51 is a CryoSEM image of beads from the bottom section of the first *S. pasteurii* column. The beads are very much connected by the biofilm and EPS, and there are more calcium deposits on the beads themselves. Because the silicon tubing near the bottom of the column is permeable to oxygen, the cells might have grown better at the bottom of the column than in the middle. The increased amount of calcium deposit on the beads compared to the middle section helps support that line of thought. More cells produce more ammonium and more calcium carbonate precipitates out, resulting in more deposits on the beads.

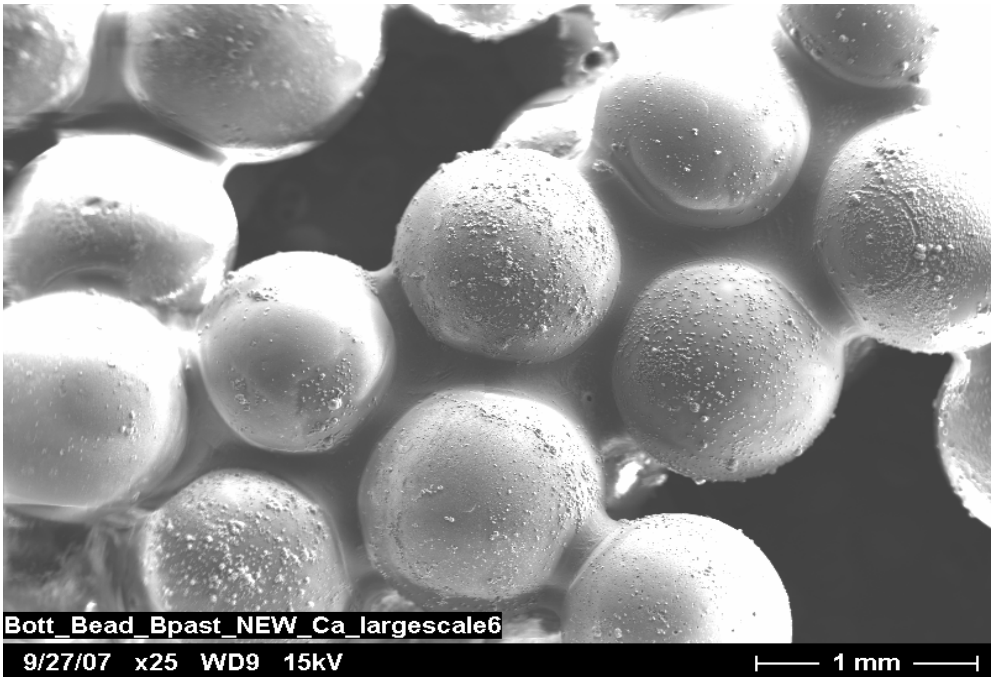

Figure 51: CryoSEM of beads from bottom section of first *S. pasteurii* column.

Figure 52: SEM image of a bead from the top (influent) section of the control column.

Figure 52 is a SEM image of a bead from the top section of the control column. This picture is at a much higher magnification than the others, but the difference to note here is the almost complete lack of calcium deposit and cells on the bead surface. This is what should be expected from the control column. There should be no cells, and therefore no precipitate.

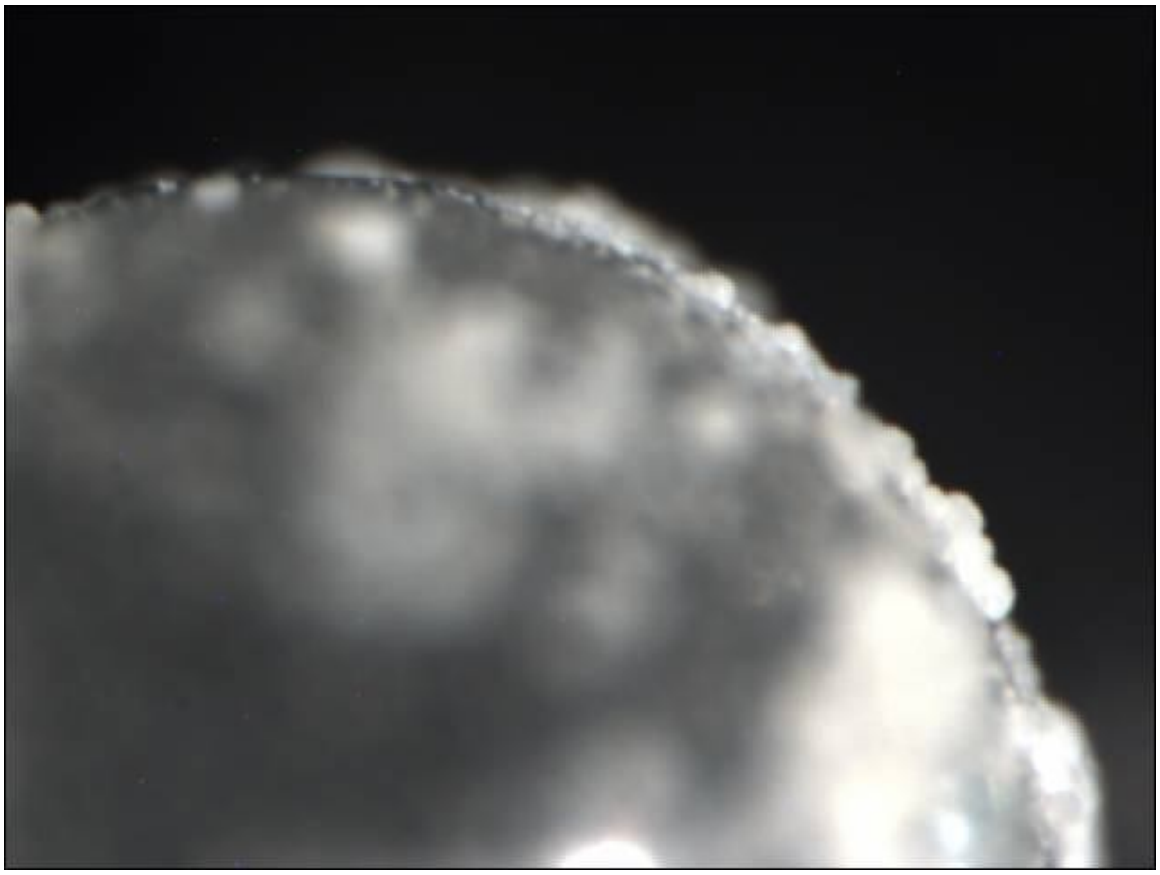

Figure 53: Stereoscope image of a single bead from the top of the first 1 mm *S. pasteurii* column. 100X magnification.

The stereoscope images of beads from the first *S. pasteurii* column allow for a close-up of the calcium deposits on the beads. Figure 53 is an image of a single bead from the top of the first *S. pasteurii* column at 100x magnification. This view of the bead shows the thickness of the calcium deposits. The deposits do not appear to be thick enough to plug the free pore space between the beads that is not already occupied by biomass. The deposits are just not thick enough to effectively reduce the permeability of the 1 mm bead packed column.

Figure 54 is a stereoscope image of a bead from the top section of the first *S. pasteurii* column at 80x magnification. This image was used for a rough calculation of biofilm thickness of the biofilm on the bead. For this picture 1 mm is roughly 6.315 inches. From the picture, the biofilm appears to be about 0.3725 inches, or about 59 μm thick.

$$\frac{1000\mu m}{6.315in} = \frac{X\mu m}{0.375in}$$

$$X = 59\mu m$$

Because there is no significant reduction in permeability with this biofilm thickness, the free pore space must be too large for the biofilm and calcium carbonate to completely plug the column.

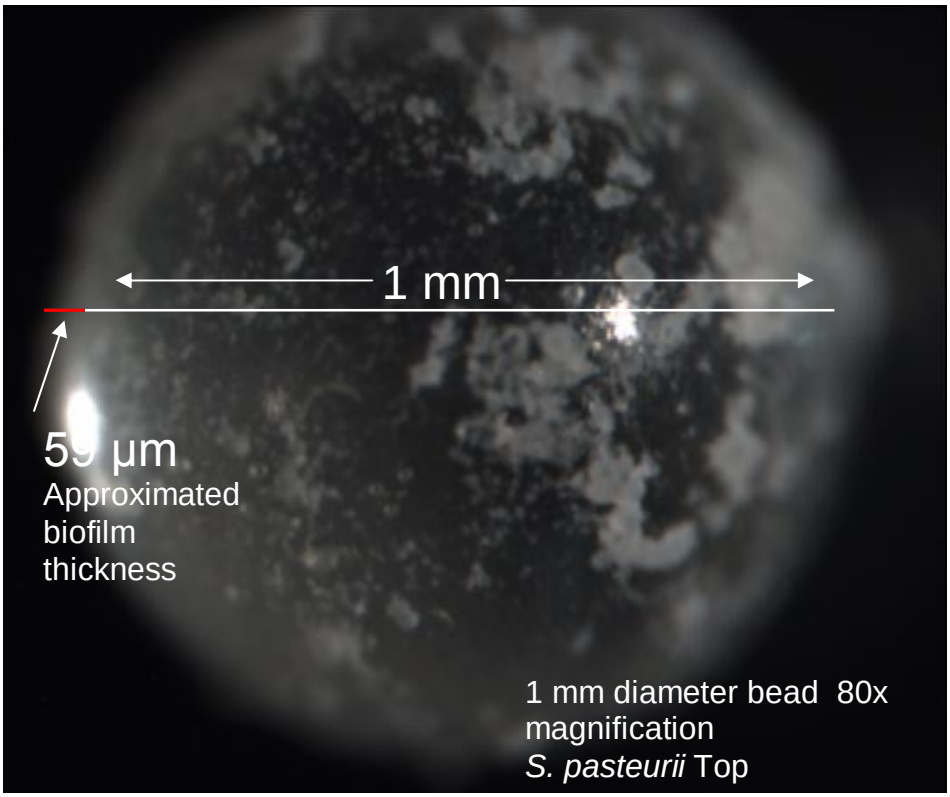

Figure 54: Stereoscope image of a single bead from the top section of the first *S. pasteurii* column at 80X magnification. This image was used to estimate biofilm thickness.

The porosity of the columns and the impact of calcium carbonate precipitate on the porosity of the columns are important to know because of the potential long-range applications of this research. It has been shown that calcium carbonate will precipitate in the pulse-flow column system, but it is important to know where it is being deposited in the system and what impacts that may have. The following is a discussion on the porosity of the

columns filled with 1 mm diameter glass beads and the effect of calcium carbonate precipitation on the porosity.

The empty bed volume of the column section that was filled with beads 11.78 mL.

$$V=\pi\cdot r^2\cdot h=\pi(0.5\text{ cm})^2(15\text{ cm})=11.78\text{ cm}^3=11.78\text{ mL}$$

Twenty 1 mm beads were weighed and an average weight of 0.0383 grams per 20 beads was calculated. The intrinsic density of beads was calculated using this average weight, and the average volume of 20 beads:

$$V_{20\text{ beads}} = (4/3)\cdot\pi\cdot r^3=(4/3)\pi(0.05\text{ cm})^3=5.25\text{x}10^{-4}(20\text{ beads})=0.0105\text{ mL}$$

Intrinsic Density=0.0383g/0.0105 mL = 3.65 g/mL

The average weight of 1 mm beads that was used to fill a column to the 15 cm mark was approximately 29.5 grams of beads. Using the average weight of twenty 1 mm beads, the volume of space that the beads take up in the column can be calculated:

$$V_{\text{beads}} = \frac{20\text{ beads}}{0.0383\text{ gr}}\text{x}\frac{29.5\text{ gr beads}}{1\text{ column}}\text{x}\frac{5.25\text{x}10^{-4}\text{ mL}}{\text{bead}} = 8.09\text{ mL}$$

The free pore space in the column can be calculated to be: 11.78 mL-8.09 mL= 3.69 mL. The porosity of this bead pack can be calculated to be:

$$\text{Porosity} = \frac{\text{pore space}}{\text{total space}} = \frac{3.69\text{ mL}}{11.78\text{ mL}} = 31\%$$

The total mass of Ca^{2+} precipitated out is obtained from the ICP-MS results. Total, not dissolved, calcium measurements were used for these calculations. Milligrams is converted to grams of Ca^{2+} and then converted to grams of $CaCO_3$. Using an estimated density of 2.71 g/mL (37), grams of $CaCO_3$ is converted to milliliters.

$$\text{X mg Ca}^{2+}\text{x}\frac{1\text{ gr}}{1000\text{ mg}}\text{x}\frac{100\text{ gr CaCO}_3}{40\text{ gr Ca}^{2+}}\text{x}\frac{1\text{ mL}}{2.71\text{ g CaCO}_3} = \text{mL of CaCO}_3\text{ precipitated out}$$

The amount of calcium precipitated out for each 1 mm experiment is tabulated in Table 6.

Table 6: Volume of calcium carbonate precipitated out in each column filled with 1 mm diameter glass beads.

Column Name	**mg Ca^{2+} precipitated out**	**gr Ca^{2+} precipitated out**	**gr $CaCO_3$ precipitated out**	**mL of $CaCO_3$ precipitated out**
1 mm *S. pasteurii* #1	112	0.112	0.280	0.10
1 mm *S. pasteurii* #2	68	0.068	0.169	0.06
1 mm *S. pasteurii* #3	69	0.069	0.173	0.06
1 mm *B. subtilis*	16	0.016	0.040	0.01
1 mm *B. sphaericus* #21776 #1	77	0.077	0.193	0.07
1 mm *B. sphaericus* #21776 #2	63	0.063	0.158	0.06
1 mm *B. sphaericus* #21787 #1	61	0.061	0.151	0.06
1 mm *B. sphaericus* #21787 #2	69	0.069	0.172	0.06
1 mm Control #1	11	0.011	0.028	0.01
1 mm Control #2	16	0.016	0.040	0.01
1 mm Control #3	48	0.048	0.119	0.04

Assuming that the calcium carbonate precipitates out throughout the entire bead pack in the column and not just in the top 1 cm, a new set of calculations is performed. Using the same equations from above, the volume of the empty column is 11.78 mL, the volume of the 1mm beads in column space is 8.09 mL, and the free space leftover is 3.69 mL. The porosity of the whole column is 31%. Subtracting the volume of $CaCO_3$ that precipitated out from the free space available gives the remaining free space available. The “new” porosity of this section is then calculated. Comparing this new value to the initial porosity of this section, it is seen that the precipitation of the calcium carbonate does not significantly reduce the porosity of the column as a whole.

Table 7: Percent porosity reduction in the columns filled with 1 mm diameter beads, assuming that the calcium carbonate precipitate is distributed evenly throughout the column.

Column Name	mg Ca^{2+} precipitated out	mL of free space remaining after precipitation	Initial porosity of entire bead pack (%)	Porosity of entire bead pack after precipitation (%)	Percent porosity reduction (%)
1 mm *S. pasteurii* #1	112	3.6	31.3	30.4	2.8
1 mm *S. pasteurii* #2	68	3.6	31.3	30.8	1.7
1 mm *S. pasteurii* #3	69	3.6	31.3	30.8	1.7
1 mm *B. subtilis*	16	3.7	31.3	31.2	0.4
1 mm *B. sphaericus* #21776 #1	77	3.6	31.3	30.7	1.9
1 mm *B. sphaericus* #21776 #2	63	3.6	31.3	30.8	1.6
1 mm *B. sphaericus* #21787 #1	61	3.6	31.3	30.9	1.5
1 mm *B. sphaericus* #21787 #2	69	3.6	31.3	30.8	1.7
1 mm Control #1	11	3.7	31.3	31.2	0.3
1mm Control #2	16	3.7	31.3	31.2	0.4
1 mm Control #3	48	3.6	31.3	31.0	1.2

Table 7 shows the reduction in porosity that occurs if calcium carbonate precipitates out in the whole column. For the three *S. pasteurii* columns, the precipitation of calcium carbonate in the whole column reduces the porosity of the whole column by 2.8, 1.7, and 1.7 % for an average reduction of about 2.1%. For both *B. sphaericus* #21776 columns, the precipitation of calcium carbonate in the whole column reduces the porosity of the whole column by 1.9% and 1.6% for an average of 1.8%. For both *B. sphaericus* #21787 columns, the precipitation of calcium carbonate in the top 1 cm of the column reduces the porosity of that 1 cm by 1.5% and 1.7% for an average of 1.6%.

Both *B. sphaericus* strains are able to reduce the porosity of the columns, but not as effectively as *S. pasteurii*. *B. subtilis* is used as a control organism in these experiments because it is not a ureolytic organism and is not able to maintain an environment that facilitates calcium carbonate precipitation. For the *B. subtilis* column, the precipitation of calcium carbonate in whole column reduces the porosity of the whole column by 0.4%. For the three control columns, the precipitation of calcium carbonate in the whole column reduces the porosity of the whole column by 0.3, 0.4, and 1.2 % for an average reduction of about 0.6%. Because *B. subtilis* is not a ureolytic organism and does not facilitate calcium carbonate precipitation, it was expected that the reduction is porosity between it and the control columns would be similar. Both the *B. subtilis* and the control columns had enough calcium carbonate precipitate out to reduce the porosity of the whole column system. However, the reduction in porosity is much less than what was observed in the columns inoculated with a ureolytic bacteria. From the destructive sampling data in the next section, it is shown that calcium does precipitate throughout the whole length of the bead pack. However, there is usually more calcium present in the top sections of the columns. In the case where the column is filled with 1 mm beads, there is a reduction in porosity but it is not enough of a reduction to make an impact on flow rate. In short, calcium carbonate is precipitating out of solution, and the porosity of the column is reduced by this precipitation but not enough to impact the flow rate.

From observations of the column during operation, it is known that there is calcium carbonate residue on the glass near the top of the bead pack, indicating that calcium carbonate is precipitating out near the top of the column. Assuming that 100%

of the $CaCO_3$ precipitates in the top 1 cm of the column, the affect of the precipitate on the porosity of the columns can be visualized. The porosity of this 1 cm section is 31%. Subtracting the volume of $CaCO_3$ that precipitated out from the free space available gives the remaining free space available after the precipitation has occurred. The "new" porosity of this section is then calculated. Comparing this new value to the initial porosity of this section, it is seen that the precipitation of the calcium does reduce the porosity of the system.

Table 8 shows the reduction is porosity that would occur in the top (influent) 1 cm of the columns packed with 1 mm diameter glass beads if all the calcium carbonate had precipitated out in the top 1 cm of the column. For the three *S. pasteurii* columns, the precipitation of calcium carbonate in the top 1 cm of the column would have reduced the porosity of that 1 cm by 81.2, 64.6, and 65.1 % for an average reduction of 70.3%. For both *B. sphaericus* #21776 columns, the precipitation of calcium carbonate in the top 1 cm of the column reduces the porosity of that 1 cm by 68.1% and 63% for an average of 66%. For both *B. sphaericus* #21787 columns, the precipitation of calcium carbonate in the top 1 cm of the column would have reduced the porosity of that 1 cm by 61.9% and 65% for an average of 63%. Both *B. sphaericus* strains are able to reduce the porosity of the columns, but not as effectively as *S. pasteurii*. *S. pasteurii* seems to convert urea faster than any of the bacteria used in this project, followed by *B. sphaericus* #21776. *B. sphaericus* #21787 does not appear to convert urea as fast as *S. pasteurii* and based on this analysis is not as effective as precipitating out calcium carbonate and reducing the porosity of the system. *B. subtilis* was used as a control organism in these experiments

because it is not a ureolytic organism and is not able to maintain an environment that facilitates calcium carbonate precipitation.

Table 8: Percent porosity reduction in each column filled with 1 mm beads.

Column Name	mL of $CaCO_3$ precipitated out	mL of free space remaining after precipitation	Initial porosity of 1 cm space (%)	Porosity of 1 cm space after precipitation (%)	Percent porosity reduction (%)
1 mm *S. pasteurii* #1	0.10	0.047	31.3	5.9	81.2
1 mm *S. pasteurii* #2	0.06	0.088	31.3	11.1	64.6
1 mm *S. pasteurii* #3	0.06	0.086	31.3	10.9	65.1
1 mm *B. subtilis*	0.01	0.135	31.3	17.1	45.4
1 mm *B. sphaericus* #21776 #1	0.07	0.079	31.3	10.0	68.1
1 mm *B. sphaericus* #21776 #2	0.06	0.092	31.3	11.6	63.0
1 mm *B. sphaericus* #21787 #1	0.06	0.094	31.3	11.9	61.9
1 mm *B. sphaericus* #21787 #2	0.06	0.087	31.3	11.0	65.0
1 mm Control #1	0.01	0.140	31.3	17.7	43.5
1 mm Control #2	0.01	0.135	31.3	17.1	45.3
1 mm Control #3	0.04	0.106	31.3	13.4	57.2

For the *B. subtilis* column, the precipitation of calcium carbonate in the top 1 cm of the column reduces the porosity of that 1 cm by 45%. For the three control columns, the precipitation of calcium carbonate in the top 1 cm of the column would have reduced the porosity of that 1 cm by 43.5, 45.3, and 57.2 % for an average reduction of 49%. Both the *B. subtilis* and the control columns had enough calcium carbonate precipitate out to reduce the porosity of the system assuming that all the calcium carbonate precipitated in

the top 1 cm of the column. However, the reduction in porosity is less than what is observed in the columns inoculated with ureolytic bacteria.

Carbon sequestration sites contain many different soil and rock types including shale, basalt, sandstone, and clay (35). These soil types have many different properties including diameter and porosity and Table 9 details the varying range soil particle diameters. The 1 mm beads used in this research project represent a coarse sandy soil, and the 0.1 mm beads represent a sandy soil. Table 10 details the ranges of porosity for various types of rocks that are present in geologic sequestration sites. The 1 mm bead filled columns used in this experiment have a porosity of about 31%, which falls in the range of gravel and sand, sandstone, limestone, and igneous rocks (39). The 0.1 mm bead filled columns have a porosity of about 32%, which falls in the range of igneous rocks.

Table 9: Diameters of common soil components (36).

Name	**Diameter Size Range (mm)**
gravel	>2.0
very coarse sand	1.0-1.999
coarse sand	0.500-0.999
medium sand	0.250-0.499
fine sand	0.100-0.249
very fine sand	0.050-0.099
silt	0.002-0.049
clay	< 0.002

Table 10: Porosity of certain soil components (38).

Name	Porosity
Soil	55%
Gravel and Sand	20-50%
Clay	50-70%
Sandstone	5-30%
Limestone	10-30%
Igneous Rocks	10-40%
Basalt	7-26%

1 mm Columns Destructive Sampling Data

After the termination of each column experiment, the columns are taken down and destructively sampled. Beads are taken from each section of the column and tested for plate counts, direct counts, protein, and calcium. Based on the method of column inoculation and operation, it is expected that there will be more cells, protein, and calcium at the top (influent) section of the column. It is also expected that there will be more cells at the top of the column because that is where the greatest amount of oxygen was available. Bacilli cells need oxygen to grow and do not grow as well without it. Plate counts are performed for the control columns as well. Nothing grew on the agar plates, however, which was expected because the control columns should not contain any cells.

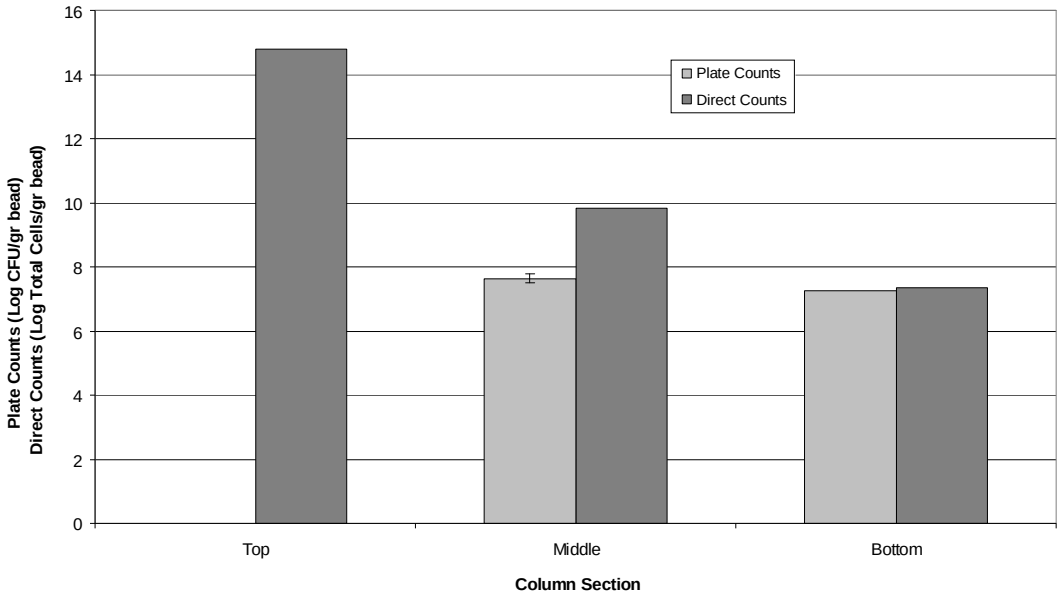

Figure 55: Plate counts and direct counts for the first *S. pasteurii* trial. Error bars represent one standard deviation. There is no plate count data for the top section due to an uncountable agar plate.

Plate Counts and Direct Counts

Direct counts measure the amount of live and dead cells, and should always be higher than plate counts, which only measure the amount of viable cells in the system.

Figure 55 represents the direct counts and plate counts for the first *S. pasteurii* trial. Here, the direct counts are higher than the plate count data, which is expected, and are higher in the top of the column than at the middle or bottom section of the column. This trend is also expected. There are no plate count data for the top section of the column because the agar plate was wet, the drops ran together, and the plate became uncountable.

Figure 56 shows the direct counts and plate counts for the second *S. pasteurii* trial. The direct counts are once again higher than the plate counts, and are higher at the top of the column than in the middle or the bottom. Both of these observations are

expected. The plate counts are slightly higher in the middle section of the column, but the difference between each section is not significant.

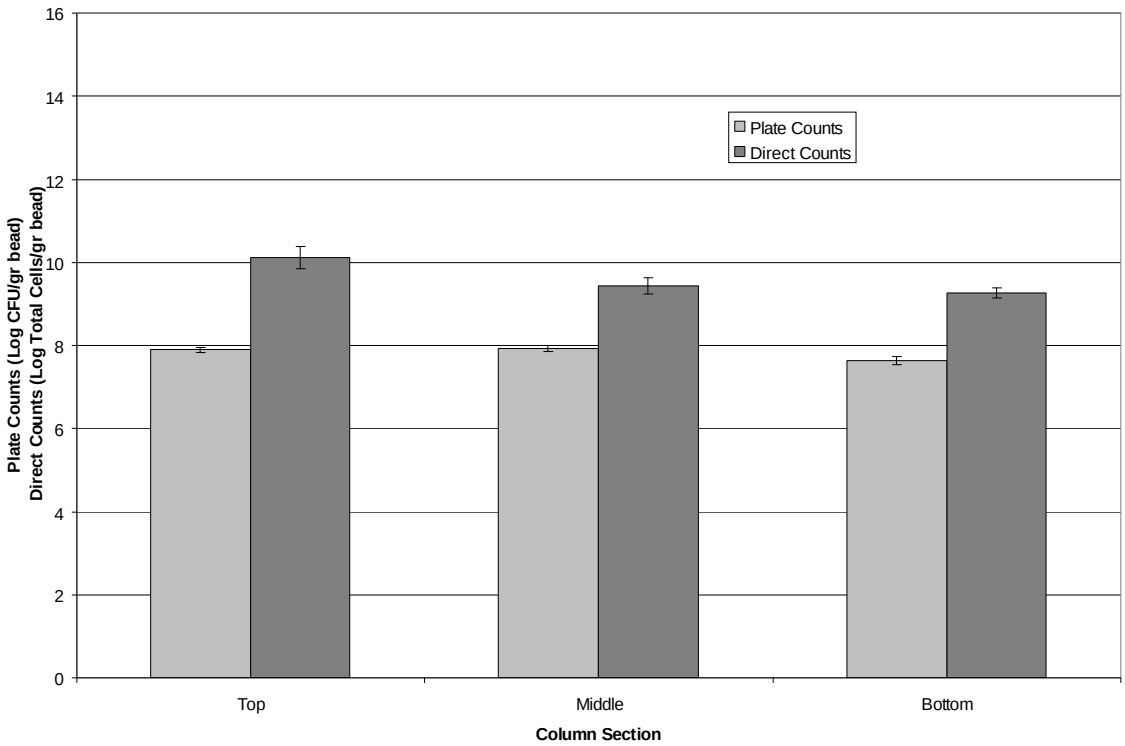

Figure 56: Plate counts and direct counts for second *S. pasteurii* trial. Error bars represent one standard deviation.

Figure 57 shows the direct counts and plate counts for the third *S. pasteurii* trial. The direct counts are once again higher than the plate counts, and are higher at the top of the column than in the middle or the bottom. Both of these observations were expected. The plate counts are slightly higher in the top and bottom of the column, but the difference between each section is not significant.

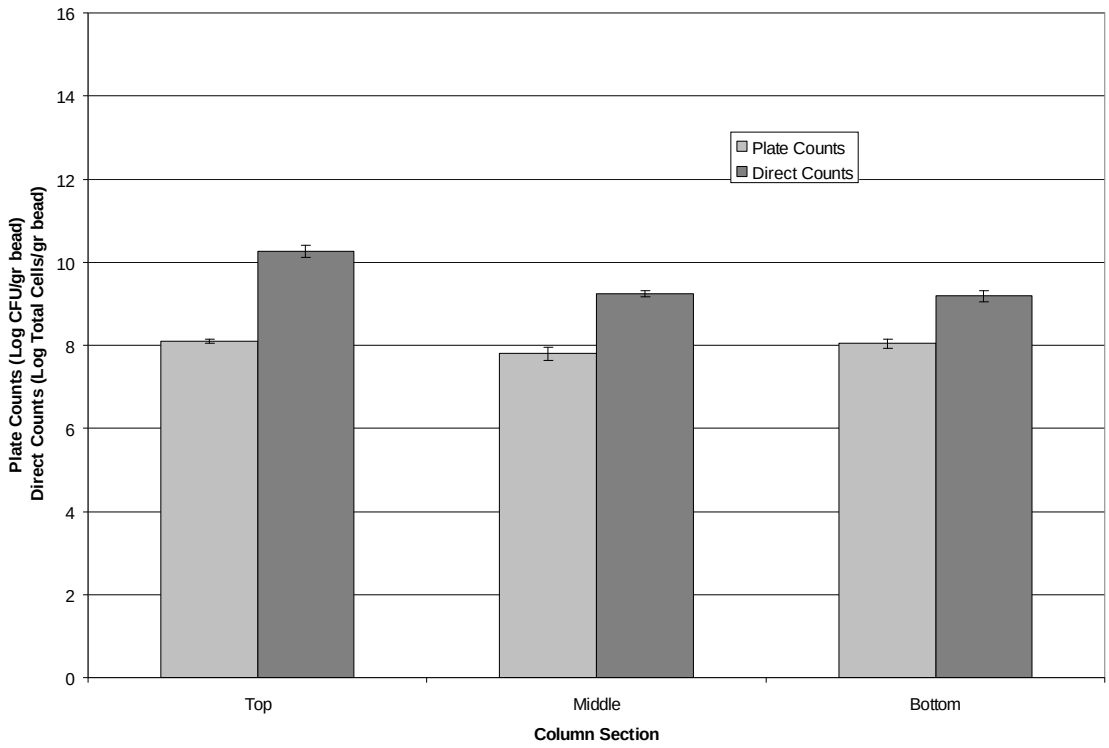

Figure 57: Plate counts and direct counts for third *S. pasteurii* trial. Error bars represent one standard deviation.

For each *S. pasteurii* trial, the direct counts for every column section are higher the plate counts for every column section. This is expected because direct counts measure the amount of live and dead cells in the system while plate counts just measure the amount of viable cells in the system. For each trial, there are more cells in the top section of the column than in the middle and bottom sections. This is also an expected trend because the cells in the top section of the column are exposed to more oxygen than the cells in the middle and bottom sections of the column. However, the difference in cell numbers between each column section was expected to be significant. Instead, the cells are almost homogeneously distributed throughout the sections.

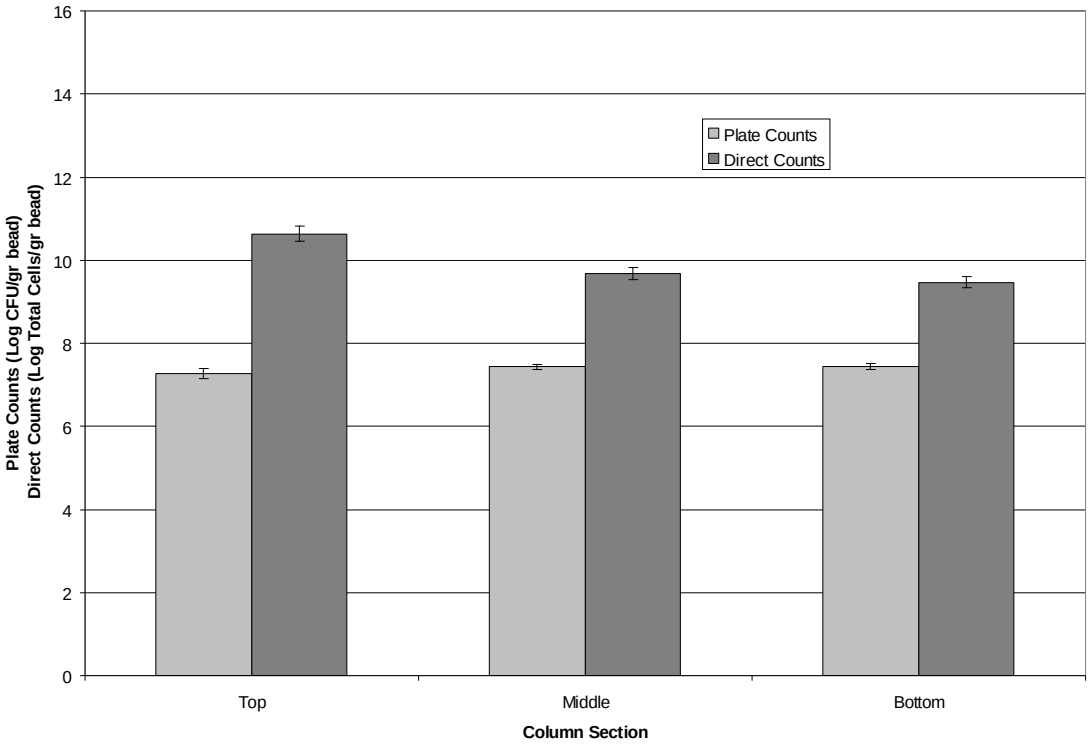

Figure 58: Plate counts and direct counts for the first *B. sphaericus* #21776 trial. Error bars represent one standard deviation.

Figure 58 shows the direct counts and plate counts for the first *B. sphaericus* #21776 trial. The direct counts are once again higher than the plate counts, and are higher in the top section of the column than in the middle or the bottom. Both of these observations are expected. The plate counts are slightly higher in the middle and bottom sections of the column, but the difference between each section is not significant.

Figure 59 shows the direct counts and plate counts for the second *B. sphaericus* #21776 trial. The direct counts are once again higher than the plate counts, and have almost same value across the column sections. The plate counts are highest in the middle and the bottom sections of the column. The difference between each section is

significant here; there are more culturable cells in the middle section of the column. There are several explanations for differences seen between the first and second *B. sphaericus* #21776 trials. One explanation is the fact that the cells are becoming encapsulated in $CaCO_3$ and are no longer culturable.

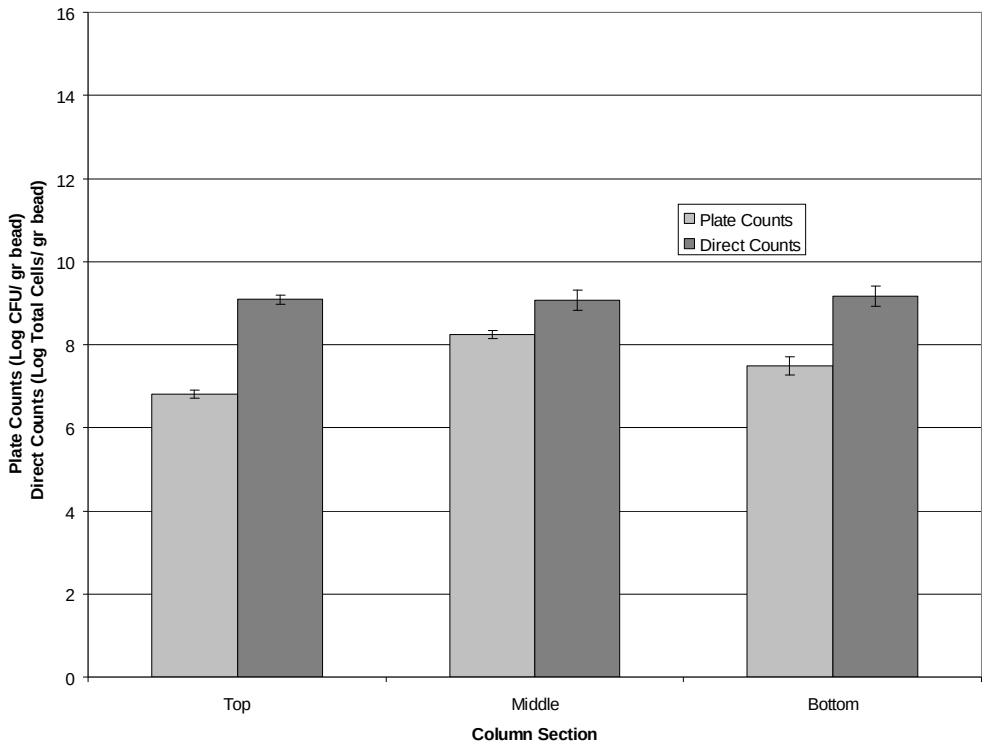

Figure 59: Plate counts and direct counts for the second *B. sphaericus* #21776 trial. Error bars represent one standard deviation.

The section on ammonium-N concentration and pH demonstrated that *S. pasteurii* (and the two *B. sphaericus* strains) can significantly raise the pH of the system so calcite precipitation is favored. It has also been hypothesized that there are more cells near the top of the column because more oxygen is available. The cells at the top section of the column are in contact with the medium first and immediately begin utilizing the nutrients

and creating an environment suitable for precipitation, so those cells would be among the first to become encapsulated. That could account for the lower plate count numbers seen in the top section of the column. Silicon tubing, which is permeable to O_2 (34), is used to connect the rubber stopper at the bottom of the column to the effluent collector. In this manner, more oxygen is reaching the cells in bottom section of the column and promoting greater cell growth. Cells in the middle section of the column would therefore be the most oxygen deprived and consequently might not grow as well nor promote a lot of calcite precipitation. This would account for the higher plate counts seen in that section of the column in the second trial.

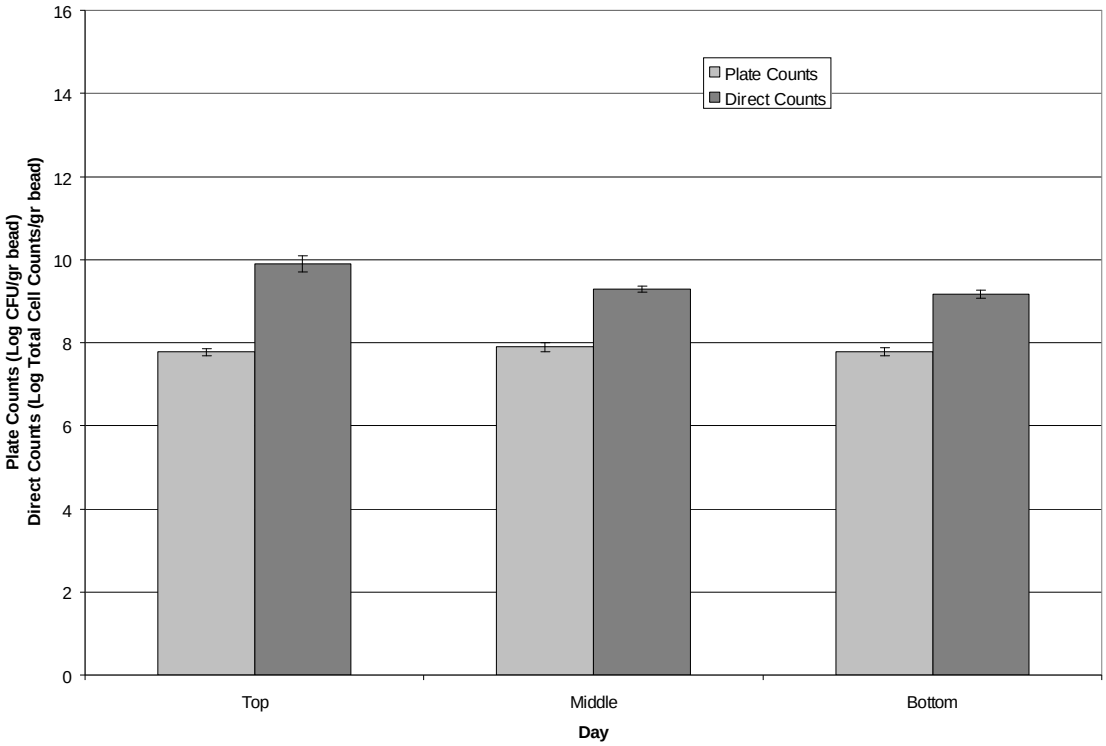

Figure 60: Plate counts and direct counts for the first *B. sphaericus* #21787 trial. Error bars represent one standard deviation.

Figure 60 shows the direct counts and plate counts for the first *B. sphaericus* #21787 trial. The direct counts are once again higher than the plate counts, and are higher at the top of the column than in the middle or the bottom. Both of these observations are expected. The plate counts are slightly higher in the middle and bottom of the column, but the difference between each section is not significant.

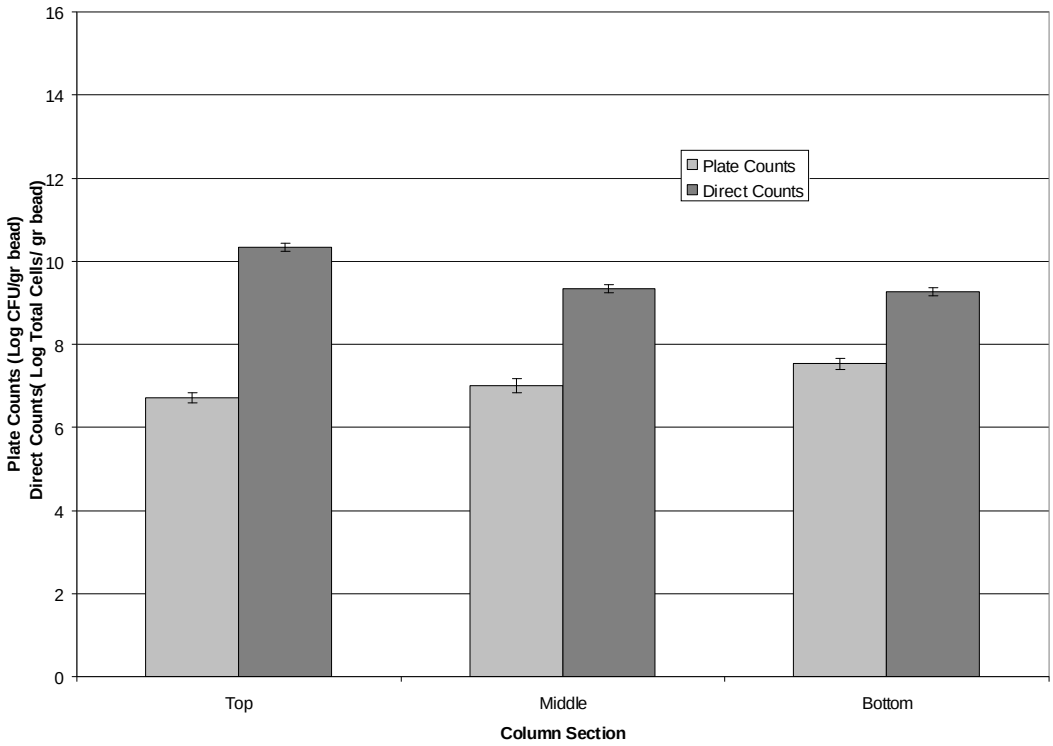

Figure 61: Plate counts and direct counts for the second *B. sphaericus* #21787 trial. Error bars represent one standard deviation.

Figure 61 shows the direct counts and plate counts for the second *B. sphaericus* #21787 trial. The direct counts are once again higher than the plate counts, and are higher at the top of the column than in the middle or the bottom. Both of these observations are expected. The plate counts are higher towards the middle and bottom of the column and lower at the top.

There are several explanations for differences seen between the first and second *B. sphaericus* #21787 trials. One explanation is the fact that the cells are becoming encapsulated in $CaCO_3$ and are no longer viable. If they are no longer viable, they will not be accounted in plate counts. It has already been shown that *S. pasteurii* can significantly raise the pH of the system so calcite precipitation is favored, and it may be the same case with *B. sphaericus* #21787. It has also been hypothesized that there are more cells near the top of the column because oxygen is more available. The cells at the top section of the column are in contact with the medium first and immediately begin utilizing the nutrients and creating the right environment for precipitation, so those cells would be among the first to become encapsulated. That could account for the lower plate count numbers seen in the top section of the column, even though there might really be more cells. Silicon tubing, which is permeable to O_2 (34), is used to connect the rubber stopper at the bottom of the column to the effluent collector. In this manner, more oxygen might be available to the cells in the bottom section of the column and promoting greater cell growth. For the second trial, the bottom section may have achieved the perfect balance between oxygen availability and calcite precipitation. The cells have sufficient oxygen for growth and calcite is precipitating out at a slow enough rate that the cells are not becoming encapsulated.

Figure 62 shows the direct counts and plate counts for the only *B. subtilis* trial. The direct counts are once again higher than the plate counts, and are higher at the top of the column than in the middle or the bottom. The plate counts are slightly higher towards top of the column. As mentioned earlier, *B. subtilis* is not a ureolytic organism and

cannot raise the pH of the system. The environment is not right for calcium carbonate precipitation, and therefore the cells cannot become encapsulated; that is why the plate counts are higher towards the top of the column.

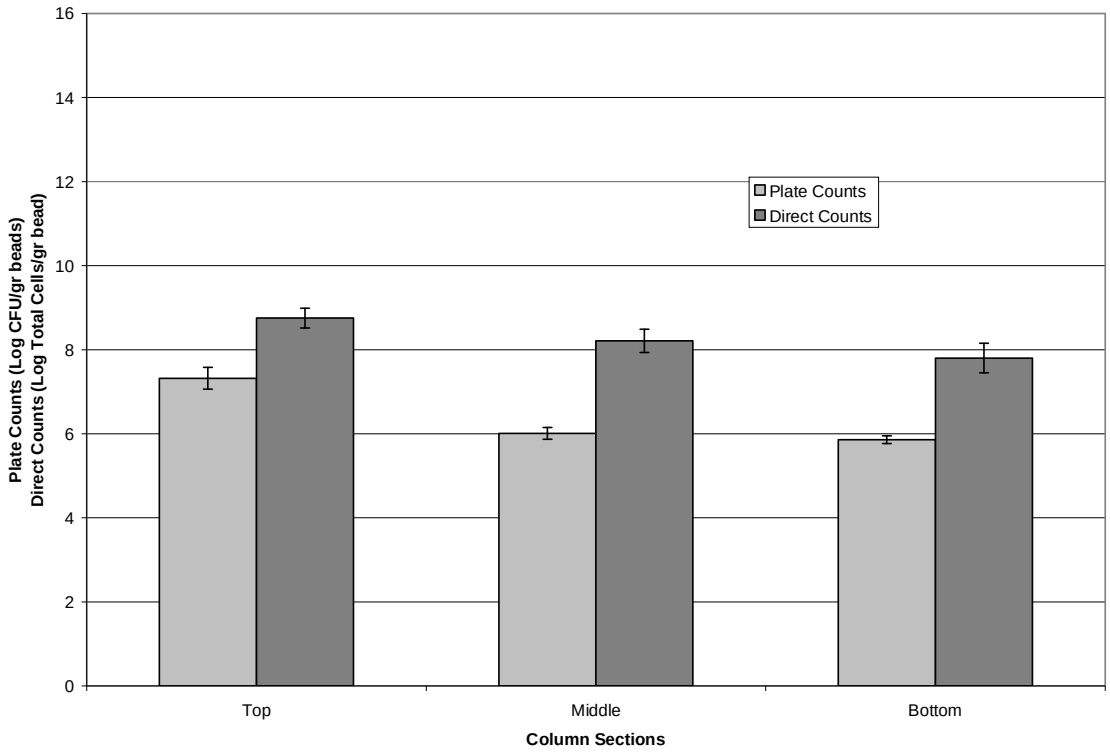

Figure 62: Plate counts and direct counts for *B. subtilis* trial. Error bars represent one standard deviation.

Protein

Protein concentration is another way to assess how much biomass is in each column section. However, looking at the protein data, it appears that the protein assay reagents and calcium carbonate may interfere with the assay. If cells are indeed encapsulated by calcium carbonate, then it is possible that the protein from those cells are

not being counted in the assay. In the protein assay protocol, base is added to the beads before acid is added. If acid had been added first, $CaCO_3$ that may have been encapsulating the cells could have dissolved, freeing the cells and allowing that protein to be accounted for in the protein assay. The large error bars associated with the protein data also indicate that either calcium or a protein assay reagent may be interfering with the assay.

Figure 63 shows protein concentration per column section for the first *S. pasteurii* trial. There is much more protein in the middle section of the column section, and there is large error associated with this data. Looking back at the raw data, the three triplicate measurements from this column section are 0.294, 0.319, and 1.016. The first two numbers are more in keeping with the other data from the experiment. The fact that one number is much larger than the other could be due to an imperfection in the 96 well plate, or an error in how much Pierce-Coomassie reagent was added to the well. Not much protein was detected in the top section, probably due to the encapsulation of the cells in the calcium carbonate. There is not much protein in the bottom of the column either, but that is probably due to the fact that the cells in that section may be oxygen deprived and not growing as well. Comparing the protein data to the plate count data for the first *S. pasteurii* trial, we can see that there is more protein in the middle section of the column just as there were more viable cells in that section of the column. This is expected because more cells would correspond to more protein.

The only protein that should be present in the control column is the protein that is contained within the CMM medium. Unless the control column was contaminated, there are no cells that contribute toward final protein concentration readings. When control data is compared to data from an inoculated column, the inoculated column should always have more protein per column section due to the presence of cells. Looking at the protein data for the control column that was run simultaneously with the first *S. pasteurii* column, this is the case for the middle section of the columns, but not for the top and the bottom sections. This data could be understandable if the control column had become contaminated, but a check of the OD_{600} and pH data for the control column do not indicate the presence of any contamination.

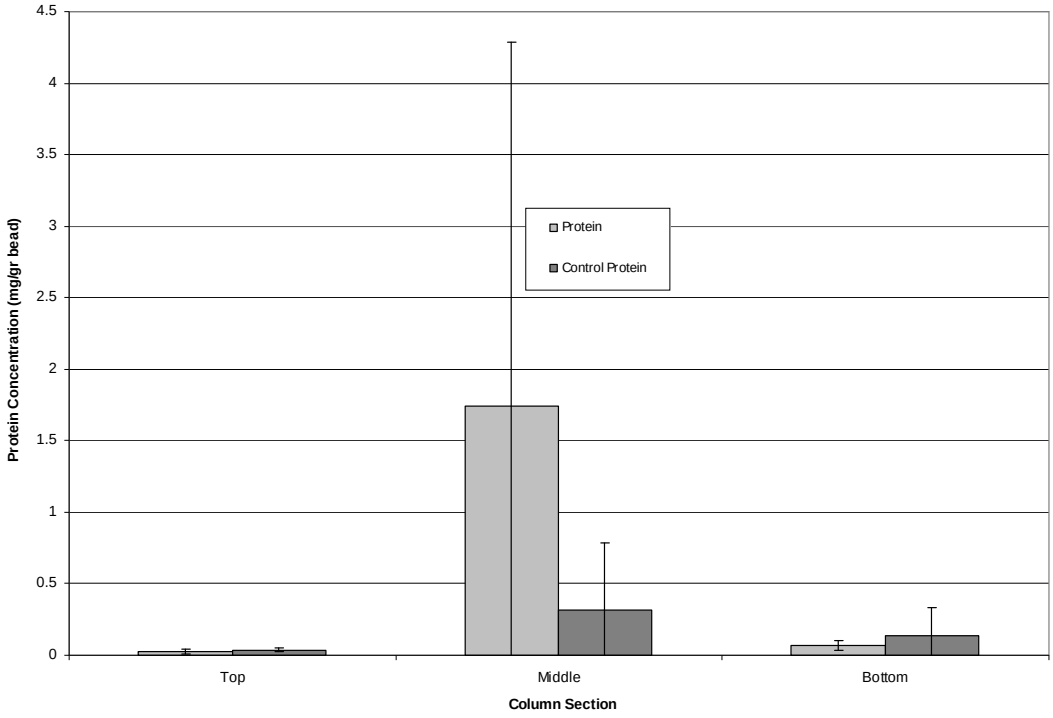

Figure 63: Protein concentration per column section for first *S. pasteurii* trial. Error bars represent one standard deviation.

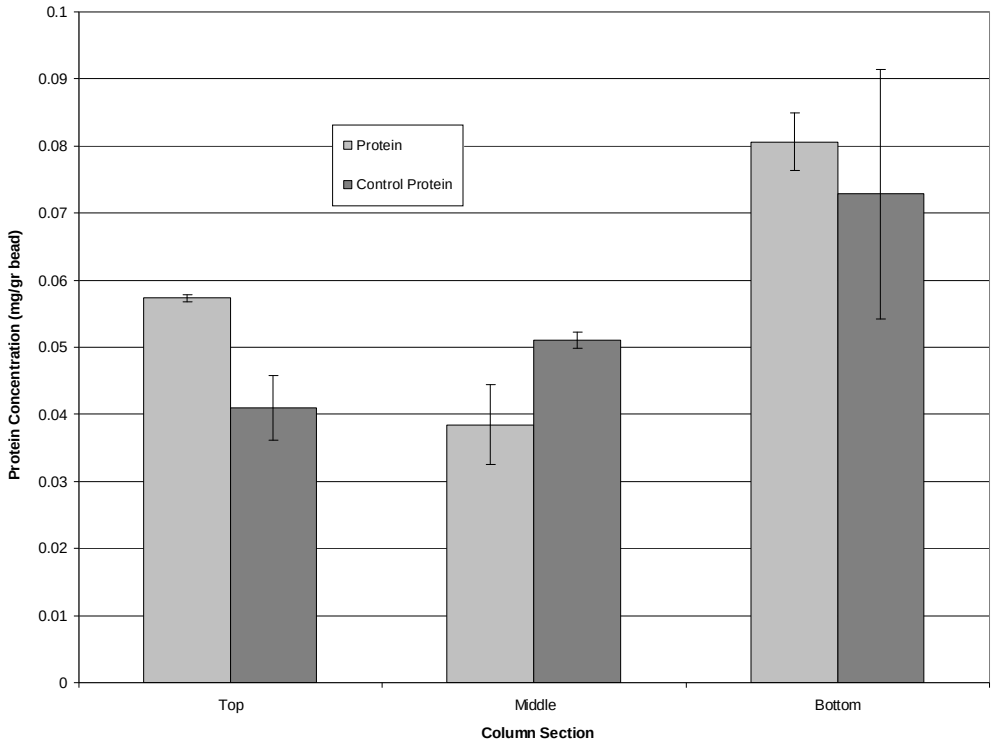

Figure 64: Protein concentration for second *S. pasteurii* trial. Error bars represent one standard deviation.

Figure 64 shows the protein concentration for the second *S. pasteurii* trial. There is more protein in the bottom section of the inoculated column, and more protein in the top of the inoculated column than in the middle. That there is more protein in the top and bottom sections of the inoculated column is probably due to the fact that these sections have ready access to oxygen. The silicon tubing near the bottom section of the column is very permeable to oxygen, and the beads at the top of the column are exposed to the air on top of the bead pack. Oxygen is necessary for cell growth and aerobic cells will grow better in an environment with plenty of oxygen. The middle section of the column does not have direct access to oxygen like the top and bottom sections do, and as a consequence may not grow as well. If there are less cells, there will be less protein. This

is one explanation for the lower protein concentration seen in the middle section of the inoculated column. Looking at the plate counts per column section for the second *S. pasteurii* trial, there appear to be more viable cells in the top and middle sections of the inoculated column. It would be expected that there would be more protein in these sections then, too, but that is not the case. It is possible that the cells have become encapsulated in the calcium carbonate precipitate and are not being accounted for in the protein assay. This would account for the lower protein concentrations seen in the top and middle sections.

For the control column, there is much more protein in the bottom section of the column than in the middle or the top. The only protein that should be present in the control column is the protein that is introduced within the CMM medium. Unless the control column was contaminated, there are no cells that contribute toward final protein concentration readings. When control data is compared to data from an inoculated column, the inoculated column should always have more protein per column section due to the presence of cells. Looking at the protein data for the control column that was run simultaneously with the first *S. pasteurii* column, this is the case for the middle section of the columns, but not for the top and the bottom sections. This data could be understandable if the control column had become contaminated, but a check of the OD_{600} and pH data for the control column do not indicate the presence of any contamination. In this case, it is possible that beads from the different sections could have been mixed together due to sampling methods, or that there was interference with the reagents used during the protein assay.

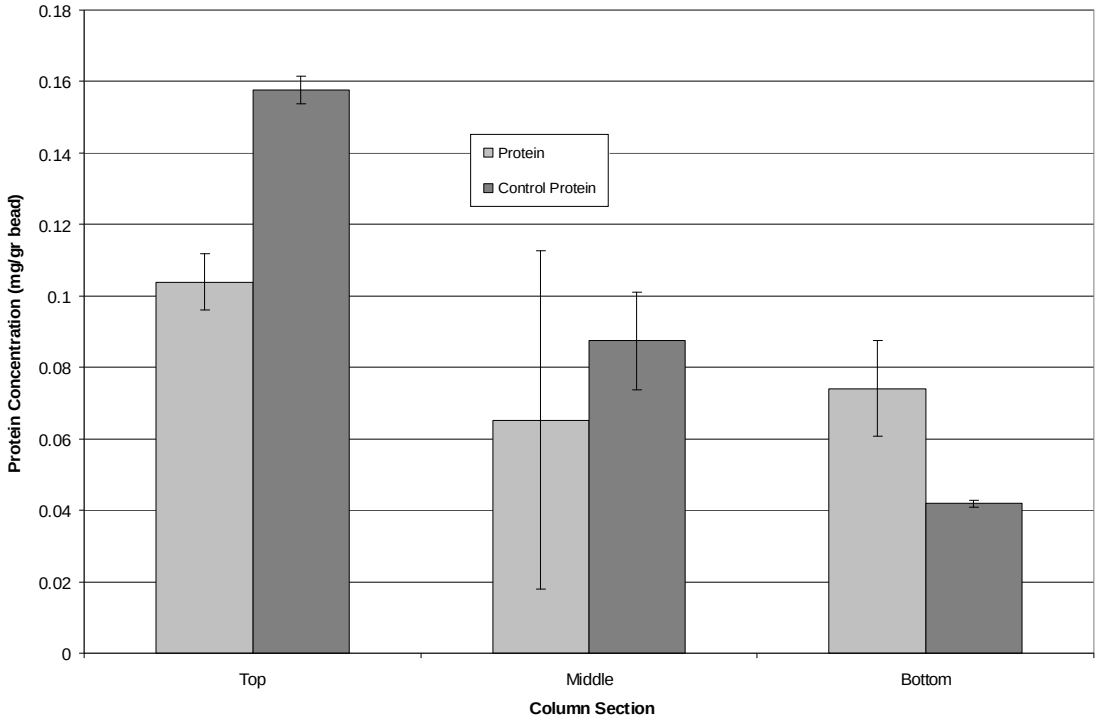

Figure 65: Protein concentration for the third *S. pasteurii* column. Error bars represent one standard deviation.

Figure 65 shows the protein concentration per column section for the third *S. pasteurii* column. More protein was detected in the top section of the inoculated column than in the bottom and the middle. This was an expected trend because of the method of inoculation and the availability of oxygen to the cells. Because of this easy access to oxygen, the cells are in a prime growing environment, and there should be more cells in this area. Looking at the plate count data for this section, there are more cells. More cells would therefore mean more protein, and that is what is seen in Figure 65. Because the silicon tubing near the bottom (effluent) section of the column is very permeable to oxygen, the cells in the bottom section of the column have greater access to the oxygen and should be growing much faster than cells in the middle section, which is the most

anaerobic. The plate count data shows that there are more cells in the bottom section of the column than the middle section, and the protein data shows that there is more protein in the bottom section of the column than the middle section. This makes sense because more cells should equal more protein.

Looking at Figure 65, it appears that there is more protein in the top and middle sections control column than in the inoculated column, which is not expected. The only protein that should be in the control column is introduced in the CMM media. Unless the control column was contaminated, there should be no cells present in the column. Looking at the OD_{600} and pH readings for the third control column, there is nothing to indicate that the control column was contaminated. No viable cells were present in the plate counts performed for each control column section. There should be more protein in the inoculated columns because there are cells present. One explanation for the low protein readings in the inoculated column is the encapsulation of the cells by calcium carbonate. The cells at the top of the column are growing well because they have a steady supply of oxygen. Because there are more cells that are raising the pH and producing ammonium, there is more calcium carbonate precipitating out. The cells are becoming encapsulated in the calcium carbonate and are not being accounted for in the protein assay, resulting in the lower numbers. The only section of the control column that has protein readings below that of the inoculated column is the bottom section. It is possible that the calcium carbonate precipitate and the cells are washed from the column during fluid exchanges and the acid in the protein assay dissolved the rest of the precipitate. This allows for the cells to be counted during the protein assay.

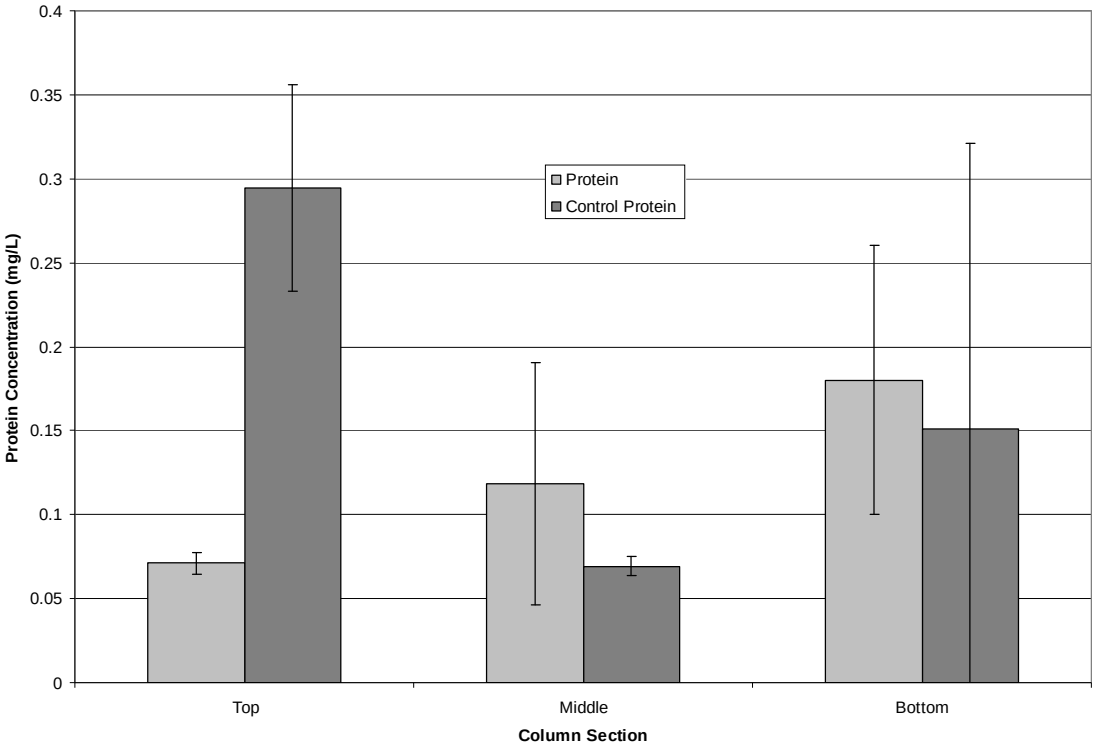

Figure 66: Protein concentration for the first *B. sphaericus* #21776 column. Error bars represent one standard deviation.

Figure 66 shows the protein concentration per column section for the first *B. sphaericus* #21776 trial. Here, there is much more protein in the bottom section of the column than in the other sections of the inoculated columns. There is also much more protein in the top section of the control section. Another possible explanation for having higher concentrations of protein in the bottom sections of the column is the use of silicon tubing when building the column system. Silicon tubing is highly permeable to oxygen (34) and silicon tubing near the effluent (bottom) end of the column allows oxygen to reach the cells at the bottom of the column. Therefore, the middle section of the column

could be the most anaerobic section of the column. If the cells at the bottom of the column are receiving oxygen, then that could account for better growth. More cells would then be represented by more protein.

Figure 67 shows the protein concentration per column section for the second *B. sphaericus* #21776 trial. There is more protein in the bottom section of the inoculated column, possibly because the silicon tubing allows oxygen to pass through, as discussed previously. There is also more protein in the bottom section of the control column. For the middle and bottom sections there is more protein in the control column than in the inoculated column. This could be due to the encapsulation of the inoculated column cells by calcium carbonate.

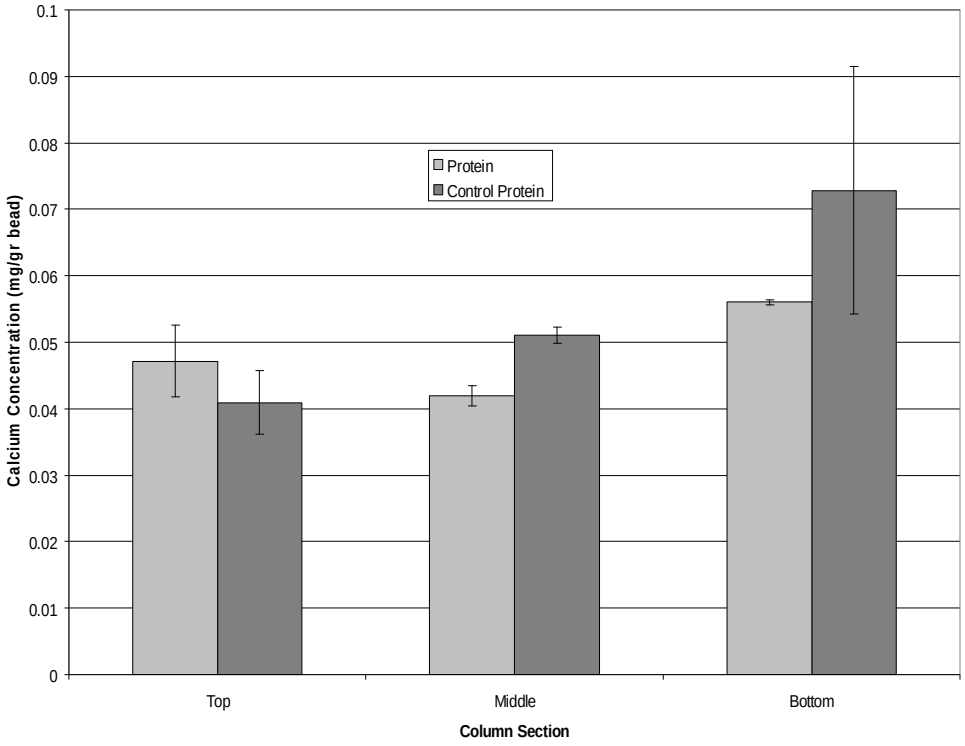

Figure 67: Protein concentration per column section for the second *B. sphaericus* #21776 column.

Figure 68 shows the protein concentration per column section for the first *B. sphaericus* #21787 column. There is more protein in the middle section of the inoculated column than in the top or the bottom. In the control column there is more protein in the top section than in the middle or the bottom sections.

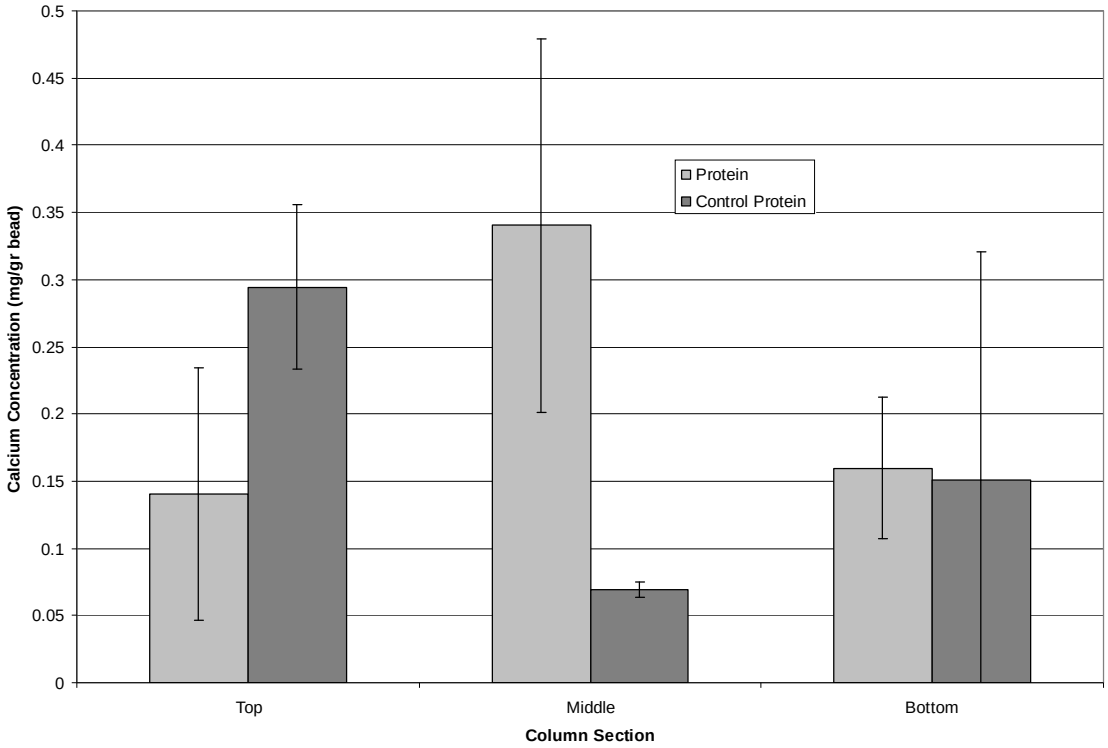

Figure 68: Protein concentration for the first *B. sphaericus* #21787 column. Error bars represent one standard deviation.

Figure 69 shows the protein concentration per column section for the second *B. sphaericus* #21787 trial. The protein concentration is higher in the bottom section for both the inoculated column and the control. In all sections, the protein concentrations in the control are higher than in the inoculated columns. This could be due to the encapsulation of the cells by calcium carbonate. Even though *B. sphaericus* #21787 does

not seem to exhibit the same degree of ureolytic behavior as *S. pasteurii* or *B. sphaericus* #21776, it is still capable of creating an environment that favors calcite precipitation.

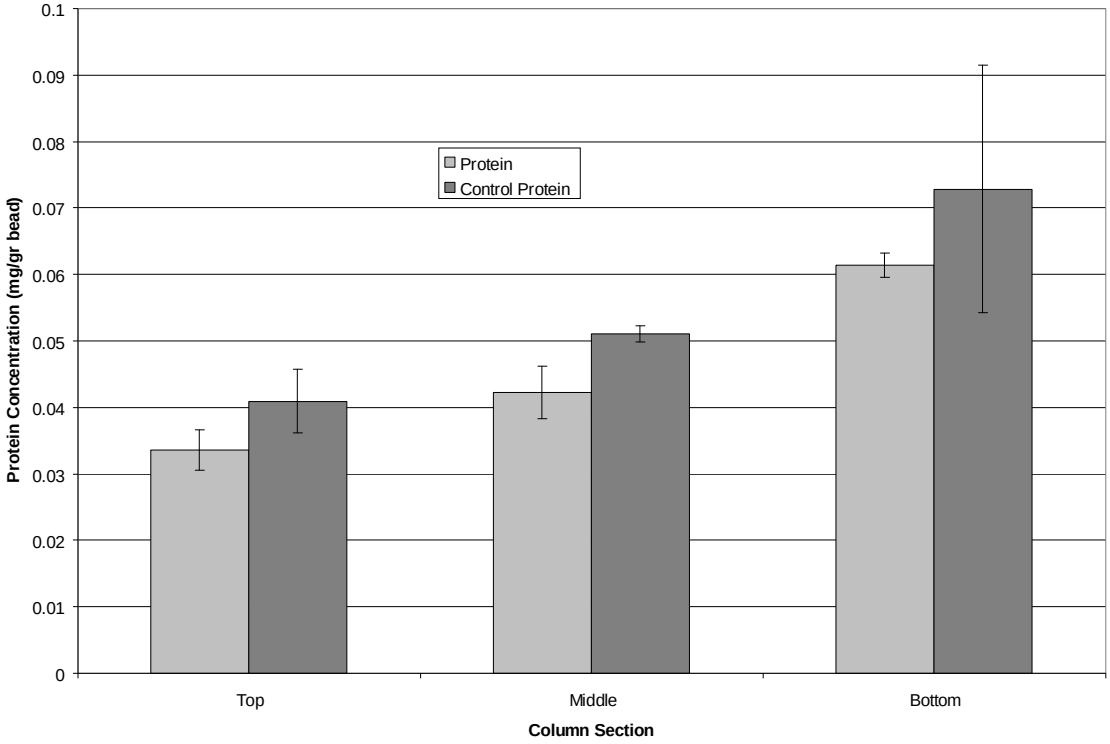

Figure 69: Protein concentration per column section for the second *B. sphaericus* #21787 column. Error bars represent one standard deviation.

Figure 70 shows the protein concentration per column section for the only *B. subtilis* trial. Here, the protein concentration is much higher in the middle section of the column than the top or the middle. Looking at the raw data for the middle section, the triplicate readings are 0.44, 0.922, and 0.266. The first two numbers are more in keeping with the other data from the experiment. The fact that one number is much larger than the other could be due to an imperfection in the 96 well plate, or an error in how much Pierce-Coomassie reagent was added to the well.

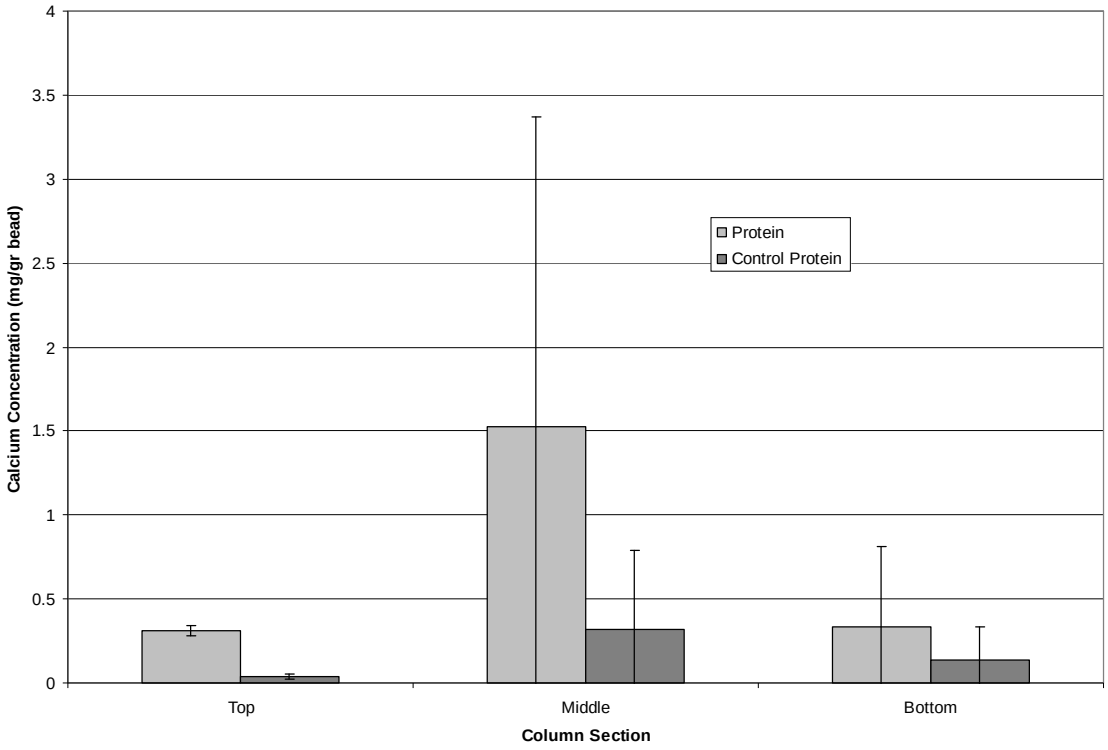

Figure 70: Protein concentration per column section for the only *B. subtilis* trial. Error bars represent one standard deviation.

Based on the protein data, it was expected that there would be a significant difference in cell concentrations in each section (top, middle, bottom) of the column. It was also noticed that the amount of protein in each section varied greatly between replicated columns. For example, between the three *S. pasteurii* trials, the amount of protein in the top section of the column varies from almost zero mg/gr bead, to 0.06 mg/gr bead, to over 0.1 mg/gr bead. The plate count data, however, indicate that the cells are homogeneously distributed throughout the column systems, maintaining an average cell concentration of about 7 log CFU/gr bead over each column section and replicate trials.

In order to compare the results from plate counts, direct counts, and protein for each column section, plate counts were converted to grams of protein using the following equation (47):

$$\text{CFU x } \frac{1.5\text{x}10^{-13} \text{ gr protein}}{\text{cell}} = \text{grams of protein}$$

Direct counts were converted to grams of protein using a similar equation:

$$\text{total cells x } \frac{1.5\text{x}10^{-13} \text{ gr protein}}{\text{cell}} = \text{grams of protein}$$

As was discussed previously, plate counts measure the amount of culturable cells in the system while direct counts measure both live and dead cells in the system. The protein assay also measures the amount of total amount of protein in the system, whether it comes from live or dead cells.

Figure 71 shows the amount of protein estimated from plate counts, direct counts, and measured using the protein assay for all three *S. pasteurii* trials. For each column section, the equivalent protein concentration based on direct counts is higher than for the plate counts or the protein assay itself. This supports the hypothesis that the protein assay suffered interferences due to the presence of high concentrations of calcium in the experimental systems. There also appears to be more protein measured from the protein assay than the equivalent protein concentration expected from plate counts. This is not unusual because plate counts are only measuring viable cells, and not every cell in the system is a viable cell.

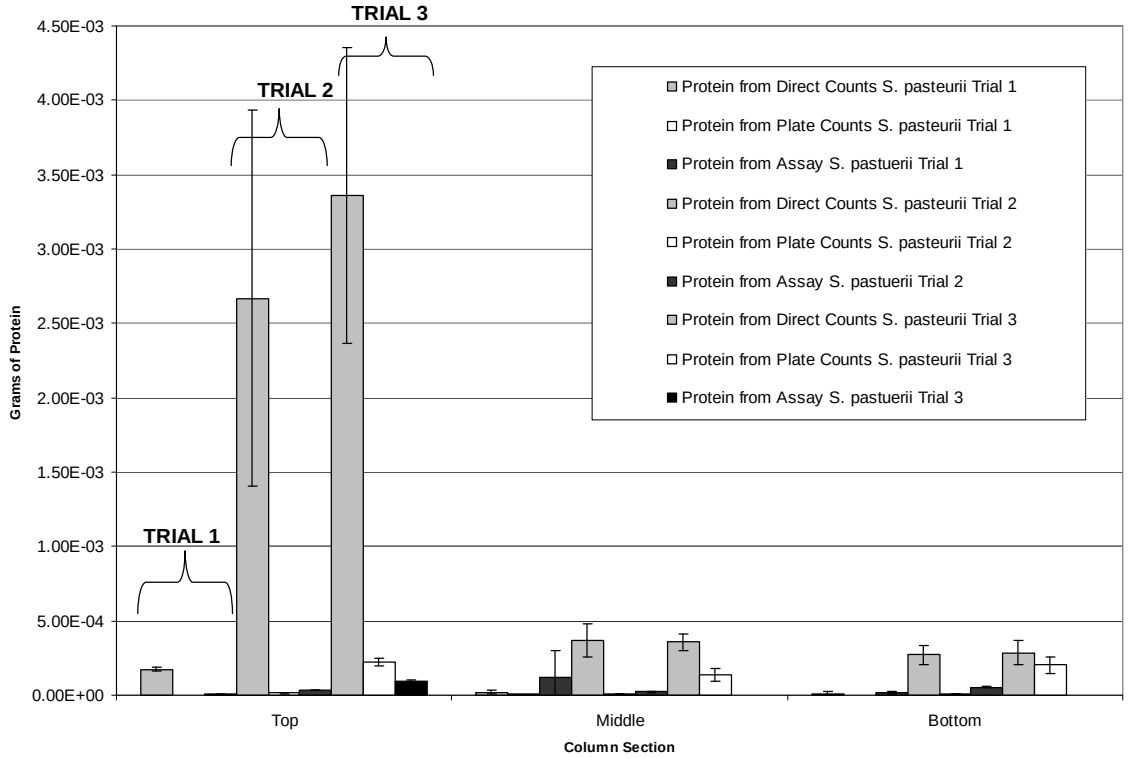

Figure 71: Estimated mass of protein based on plate counts, direct counts, and the Coomassie protein assay for all *S. pasteurii* trials. Error bars represent one standard deviation.

It was initially hypothesized that there would be more cells in the top sections of the columns based on the method of inoculation and the environment. Looking at the estimated mass of protein obtained from direct counts, there is more protein in the top section of each column for almost each bacterium across multiple trials. Also, there is generally more protein obtained from the protein assay than from plate counts across each column. However, as measured by the protein assay, there is not consistently more protein in one section of the column versus another section of the column, even across multiple trials.

Based on this comparison, direct counts yield the most cells. The protein assay might not be a good measure for biomass in these calcite precipitating columns since

$CaCO_3$ might interfere with the digestion of cells in the spectrophotometric assay. The protein assay could potentially be improved by adding a strong acid to the samples first in order to dissolve the $CaCO_3$ before digestion at 90ºC. The Coomassie assay may also not be as sensitive as other protein assays, such as the NanoOrange assay (Molecular Probes, Eugene, OR). The protein assay can yield useful information when used in conjunction with other methods of monitoring biomass. Graphs comparing amounts of protein from plate counts, direct counts, and the protein assay can be seen in Appendix C. Figure 105 in Appendix C compares the amount of protein from plate counts direct counts and the protein assay for the only *B. subtilis* trial. *B. subtilis* is not a ureolytic organism and will not create the right environment for calcium carbonate precipitation. When no $CaCO_3$ precipitates, such as in the *B. subtilis* column, the Coomassie protein assay estimates a larger amount of biomass than the direct counts. Together with the fact that measured protein concentrations in the calcite precipitating columns are lower than the protein concentration measurements in the uninoculated columns, this data makes it clear that the Coomassie protein assay is not appropriate for assessing biomass in this column system.

Calcium

Figure 72 shows the calcium concentration per column section for all *S. pasteurii* trials. Each *S. pasteurii* column (#1-#3) is light gray, and the corresponding control is dark gray and to the right. For the first *S. pasteurii* trial, there is much more calcium in each column section for the inoculated column than for the control. This is expected; the cells in the inoculated column have created an ideal environment for calcite precipitation

and there should be deposits on the beads. There is more calcium in the middle of the first *S. pasteurii* column. There are more cells in the middle portion of the column than the bottom, but the middle section of the column is probably the most anaerobic section, and while cells may not be growing as well here, they are still ureolytically active.

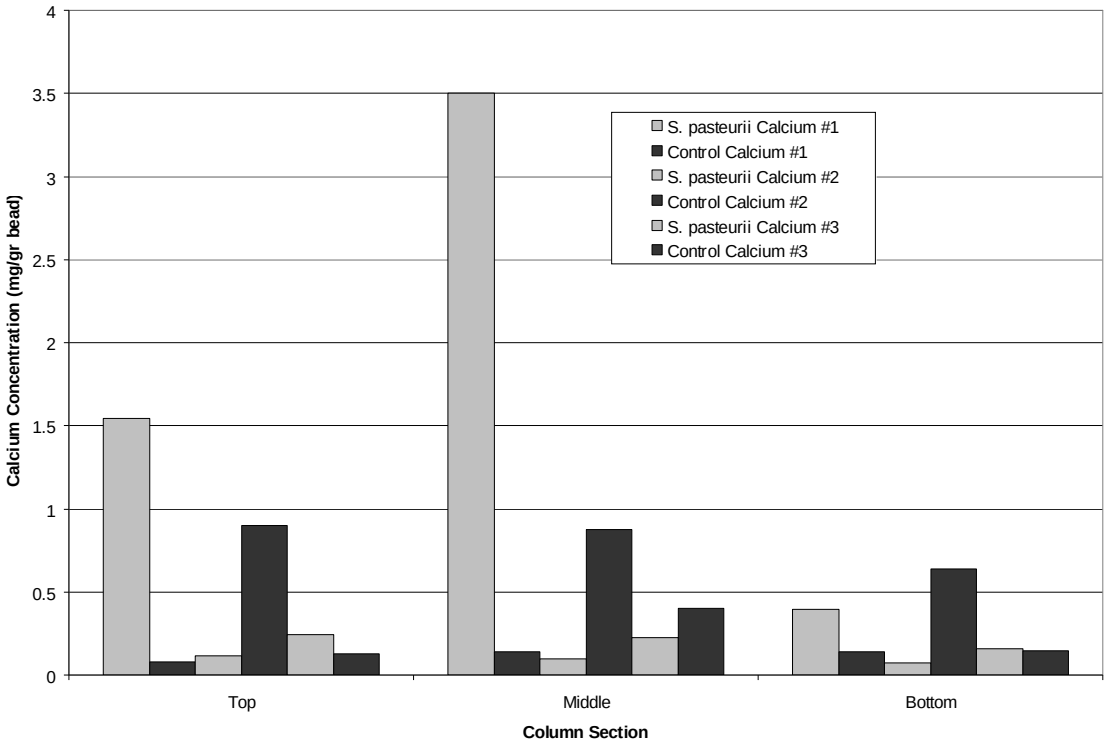

Figure 72: Calcium concentration per column section for the triplicate *S. pasteurii* experiments.

Since the cells are not growing as well, there may not be as many and therefore not as much calcium carbonate will precipitate out. However, whatever cells are there are still able to serve as nucleation points for calcium carbonate precipitation, and that could explain the increased amounts seen in the middle section. For the second *S. pasteurii* column there is about 1.5 mg/gr bead less calcium per column section than in the first *S. pasteurii* trial. There is more calcium in the top section of this column, which

is expected. More cells in an area of the column should be converting urea faster and increasing the pH and ammonium concentration, and therefore more calcium carbonate should be precipitating out. Calcium carbonate should not be precipitating out in the control column because there are no cells in the control columns. There is slightly less calcium in the bottom section of the control column than in the top or the middle. However, there is more calcium in the control column than in the inoculated column, and that was not expected. This trend also carries over into the third *S. pasteurii* trial. There is more calcium in the top and middle sections of the inoculated column than in the bottom. For the third *S. pasteurii* column there is about 1 mg/gr bead less calcium per column section than in the first *S. pasteurii* trial. There is also more calcium in the middle section of the control column than in the inoculated column, but not in the top and bottom sections.

This data can be used in conjunction with the accumulation of calcium carbonate from effluent measurements (Figure 36) in order to close the calcium mass balance. The mass of calcium deposited on the beads was subtracted from accumulated mass of calcium to find the mass of calcium that was retained on in the column and on the other system parts such as silicon tubing, stoppers, and glass pieces. This data is tabulated in Appendix D.

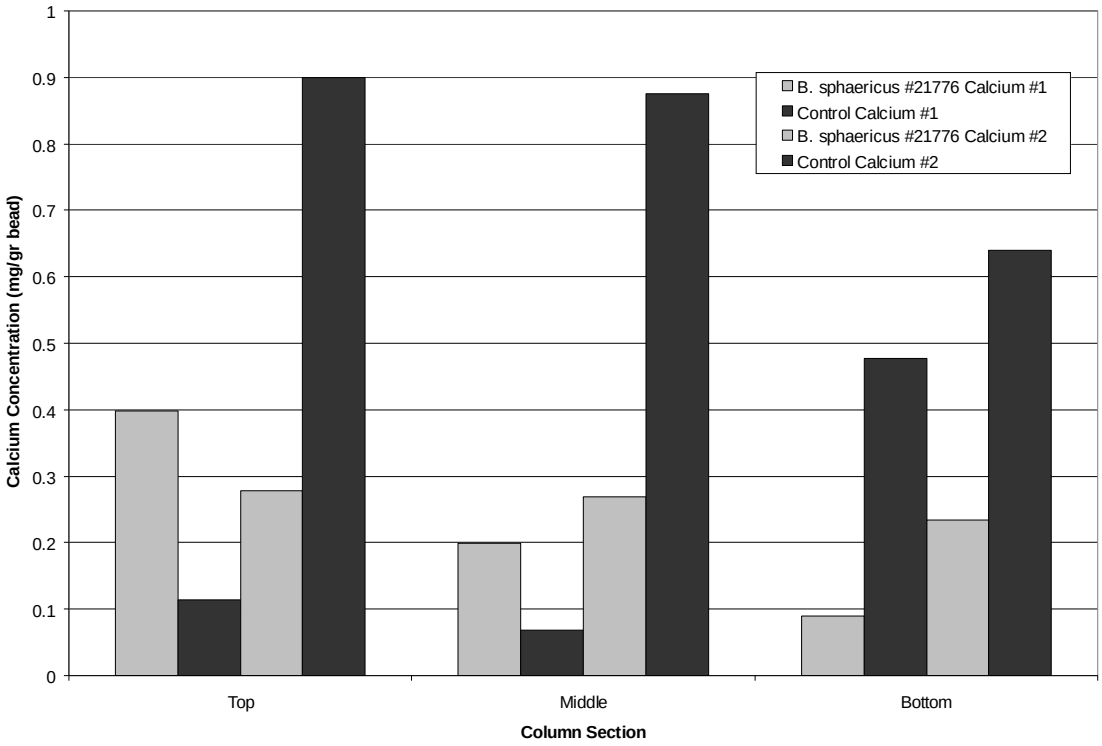

Figure 73: Calcium concentration per column section for duplicate *B. sphaericus* #21776 experiments

Figure 73 shows the calcium concentration per column section for both *B. sphaericus* #21776 trials. Each *B. sphaericus* #21776 column is light gray, and the corresponding control is dark gray and to the right. For the first trial there is more calcium in the top and middle section of the inoculated column than in the bottom, which is an expected trend. For the corresponding control column, there is less calcium in the top and middle section than in the inoculated column, which is what is expected, but there is more calcium in the bottom section of the control column than in the bottom section of the inoculated column. This is unexpected, but not out of the ordinary because this was also seen the *S. pasteurii* columns.

For the second *B. sphaericus* #21776 trial, there is more calcium in the top and middle section than in the bottom section, which is expected. The amount of calcium present in the first inoculated *B. sphaericus* #21776 trial is also similar to that in the second *B. sphaericus* #21776 trial. The second control column has much more calcium per column section than the second inoculated column. This is possibly due to a contaminant in the control column. Figure 29 shows an increase in the pH in control column for Trial 2, which is a strong indication of contamination. Therefore, the comparison between the inoculated and control column for the second trial is not very accurate. There should not be any calcium deposits on the beads because there are no cells in the control column to create an environment for calcite precipitation. The fluid is drained from the column on the days the columns are destructively sampled, and the only calcium that should be present on the beads should be from residual media on the beads. However, that amount of media is probably not enough to cause elevated calcium readings.

This data can be used in conjunction with the accumulation of calcium carbonate from effluent measurements in order to close the calcium mass balance. The mass of calcium deposited on the beads was subtracted from accumulated mass of calcium to find the mass of calcium that was retained on in the column and on the other system parts such as silicon tubing, stoppers, and glass pieces. This data is tabulated in Appendix D.

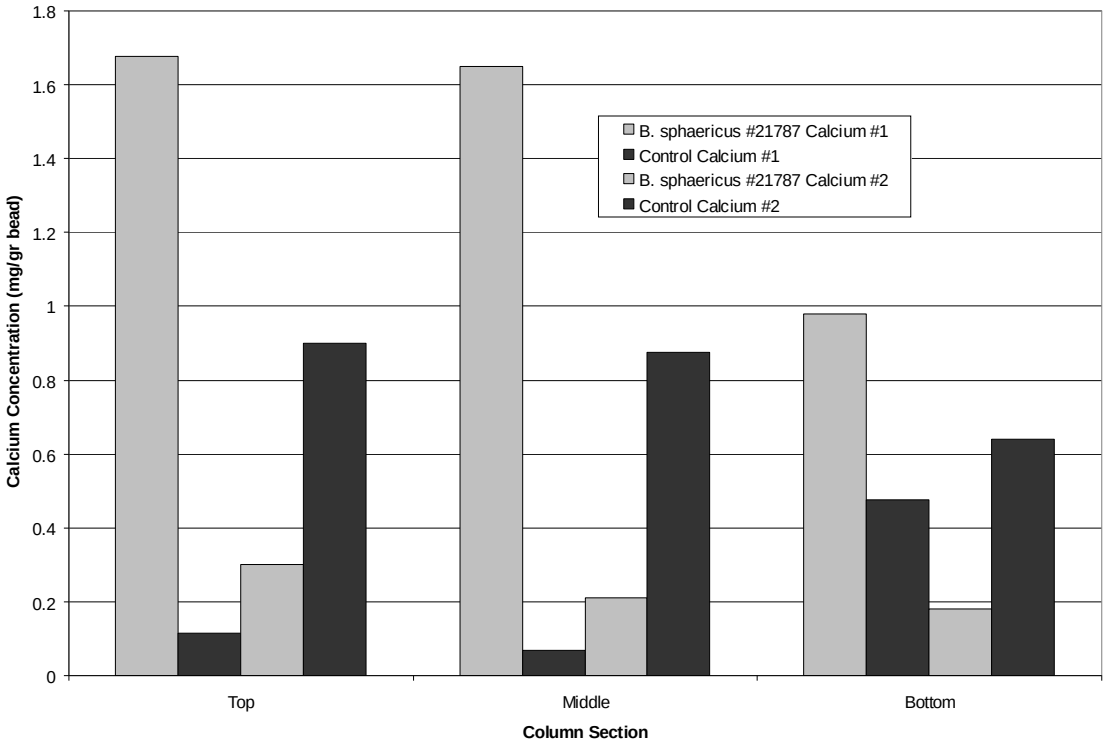

Figure 74: Calcium concentration per column section for both *B. sphaericus* #21787 trials.

Figure 74 is the calcium concentration per column section for both *B. sphaericus* #21787 trials. Each *B. sphaericus* #21787 column is light gray, and the corresponding control is dark gray and to the right. For the first trial there is more calcium in the top and middle section of the inoculated column than in the bottom. There is much less calcium in the control column for each section than in the inoculated column. For each control column, there is more calcium in the bottom section of the column than in the top and middle sections. This could be due to the fact that when all the remaining fluid is drained from the column, the most residual fluid pools into the bottom of the column. However, there is probably not enough residual fluid to raise the calcium levels very high. For the second trial, there is still more calcium in the top and middle sections of the

inoculated columns, but there is much more calcium in the each section of the control column. This is the same control column that was discussed above.

This data can be used in conjunction with the accumulation of calcium carbonate from effluent measurements in order to close the calcium mass balance. The mass of calcium deposited on the beads was subtracted from accumulated mass of calcium to find the mass of calcium that was retained on in the column and on the other system parts such as silicon tubing, stoppers, and glass pieces. This data is tabulated in Appendix D.

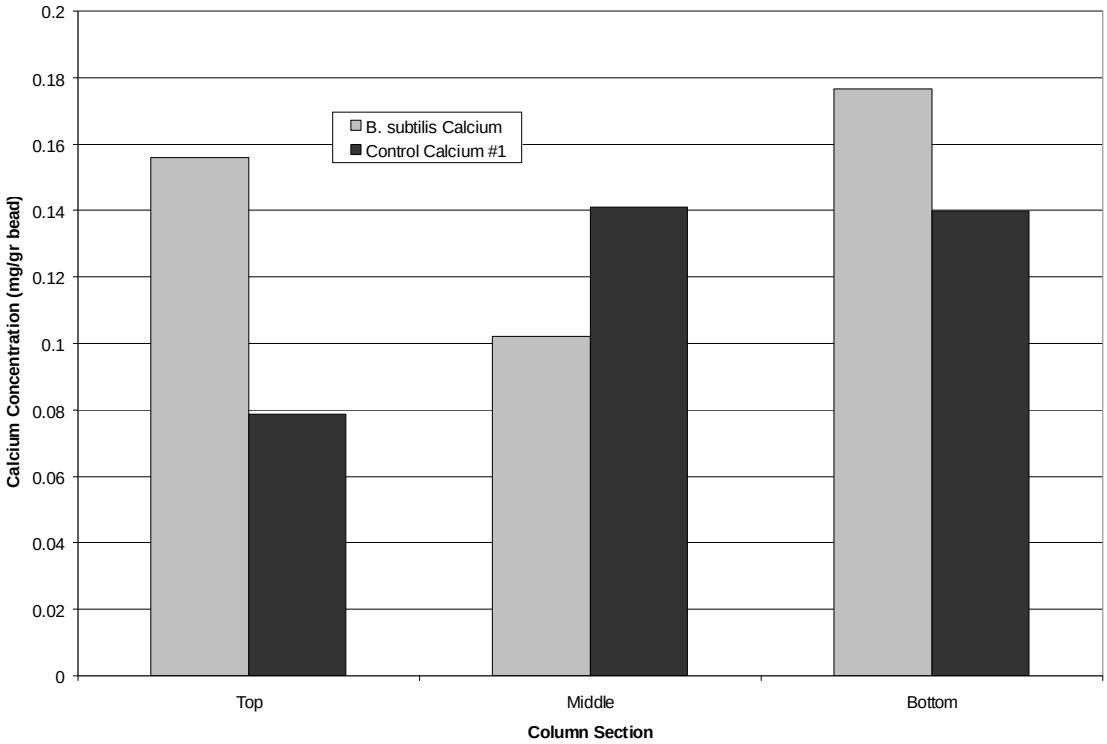

Figure 75: Calcium concentration per column section for the single *B. subtilis* experiment.

Figure 75 shows the calcium concentration per column section for the only *B. subtilis* trial. There is more slightly more calcium in the bottom section of the inoculated column than the top of the column. The middle and bottom sections of the control column have the most calcium, but only 0.06 mg/gr bead more than the top. The inoculated column has more calcium in each column section than the control.

This data can be used in conjunction with the accumulation of calcium carbonate from effluent measurements in order to close the calcium mass balance. The mass of calcium deposited on the beads was subtracted from accumulated mass of calcium to find the mass of calcium that was retained on in the column and on the other system parts such as silicon tubing, stoppers, and glass pieces. This data is tabulated in Appendix D. The calcium results per column section show some unusual trends. It was expected that the column sections of the inoculated columns would have more calcium present because the ureolytic cells would be creating an ideal environment for calcium carbonate precipitation. This was not always the case, however. Certain sections of the control column contained more calcium than the same sections of the inoculated columns, probably due to a contaminant in the system. Beads from each column (inoculated and control) and each section were treated the same way.

Thus far, is has been shown that the three chosen ureolytic bacteria, *S. pasteurii*, *B. sphaericus* #21776, and *B. sphaericus* #21787 are capable of establishing a biofilm community within the column through plate counts, OD_{600}, and protein data. It has been

shown that they are also capable of utilizing urea by monitoring the change in pH over time and the increase in ammonium production over time. It has also been shown that these bacteria are capable of creating an environment that facilitates calcium carbonate precipitation. The use of *B. subtilis* as a control organism indicated that ureolytic activity is necessary to promote $CaCO_3$ precipitation in the column systems. *B. subtilis* is capable of growing within the column system, but does not increase the pH or create an environment that facilitates calcite precipitation.

There does not seem to be a consistent trend throughout each trial in which column section has the highest concentration of each parameter. It was expected that the top section of each column would have the most cells, protein, and calcium, but this was not always the case. This could be due to the inoculation method, sampling method, or the column system design.

0.1 mm Column Effluent Data

The first objective in this research project was to establish viable communities of microorganisms using *B. pasteurii*, *B. sphaericus* #21776, and *B. sphaericus* #21787 capable of ureolysis that in turn promotes $CaCO_3$ precipitation. The second objective was to reduce the permeability in porous media using the individual microorganism communities. It has already been shown that a viable ureolytic biofilm community is capable of being established, but that it is not thick enough nor is there enough calcium carbonate precipitated out to sufficiently reduce the permeability of a column filled with 1 mm diameter beads. The pore size in the 1 mm bead pack is just too large. In order to reduce the average pore size in the columns, a new experiment was designed using columns filled with 0.1 mm diameter beads.

It is still important to monitor the bacteria in the columns and make sure that the cells are surviving and able to carry out the ureolytic process. Plate counts, OD_{600}, protein concentration, ammonium-N concentration, pH and calcium concentration are monitored over time. *S. pasteurii* was the only bacterium tested within the 0.1 mm columns.

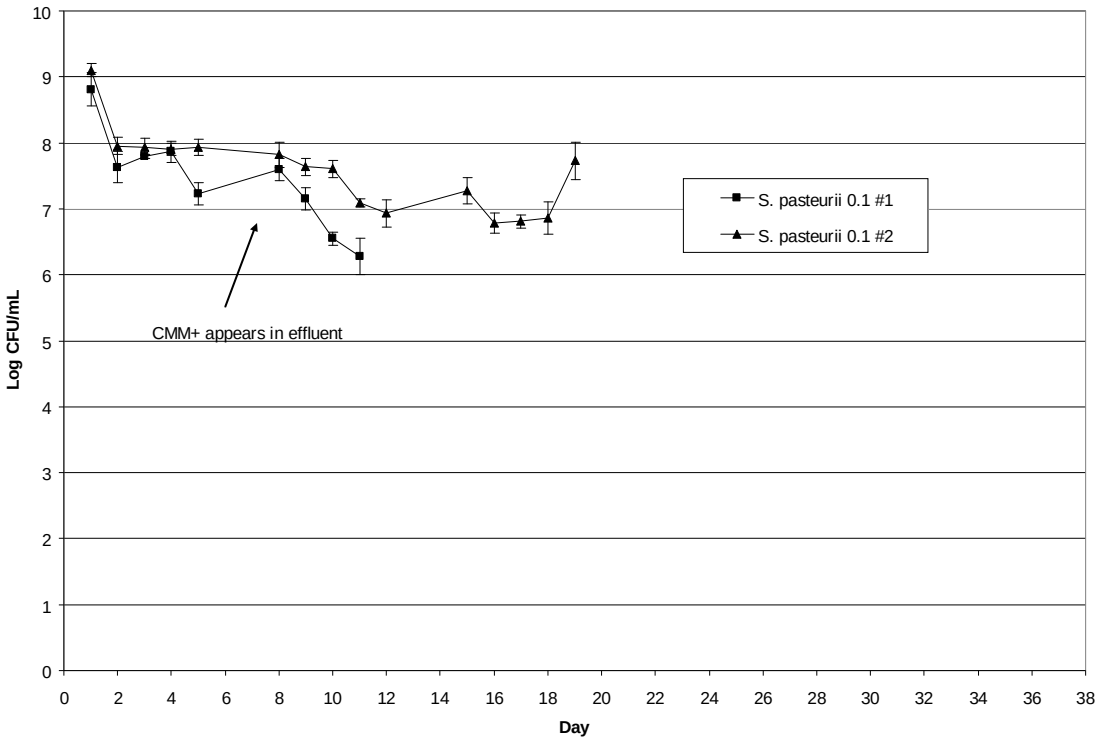

Figure 76: The change in plate counts over time for duplicate 0.1 mm columns inoculated with *S. pasteurii*. Error bars represent one standard deviation.

Plate Counts

The trend seen in Figure 76 is similar to the trend seen in the plate count data from the 1 mm columns. The plate counts start out high and decrease throughout the course of the experiment. The plate counts decrease once calcium is introduced into the system. This is probably due to the encapsulation of the cells by calcium carbonate. Plate counts end earlier for the first *S. pasteurii* trial than the second because the column was completely plugged and no media was able to pass through. The plate counts for the second column continue for another week, but do not decrease anymore throughout the rest of the trial.

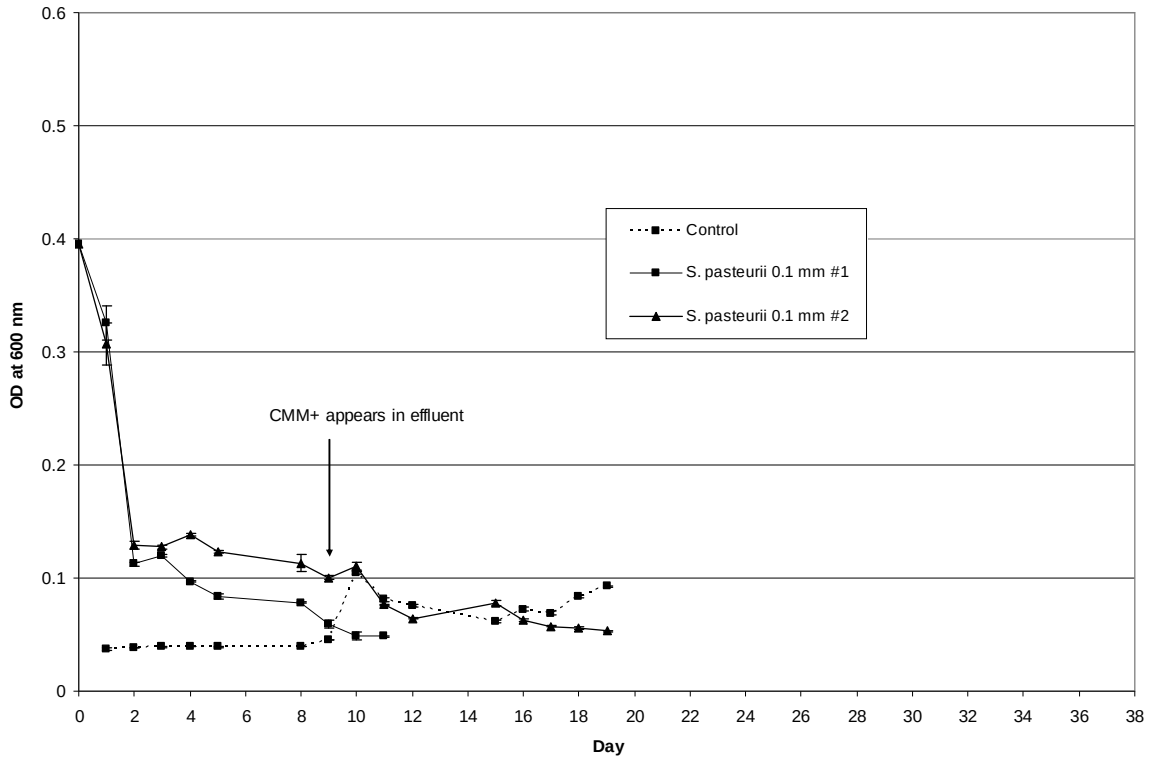

Figure 77: Change in OD_{600} over time for both 0.1 mm columns. Error bars represent one standard deviation of triplicate measurements.

<u>OD_{600}</u>

Figure 77 shows the change in OD_{600} over time for the 0.1 mm column experiments. Both inoculated columns have a higher OD than the control column until day 9. On day 9, the OD of the control column increases. This is a strong indication that the control column is contaminated. The media bottles are switched from CMM- to CMM+ on day 8, and this is a time when a contaminant could be introduced into the system. The increase in OD_{600} could also be due to the non-biological induced precipitation of $CaCO_3$. However, since the OD of the inoculated columns is higher, this indicates that the cells are growing in the pulse-flow column system.

Protein

Figure 78 shows the change in protein concentration over time for the 0.1 mm column experiments. There is more protein in both of the inoculated columns than in the control column throughout the course of the experiment. There is a slight increase in the control protein concentration on day 9 when the control column became contaminated.

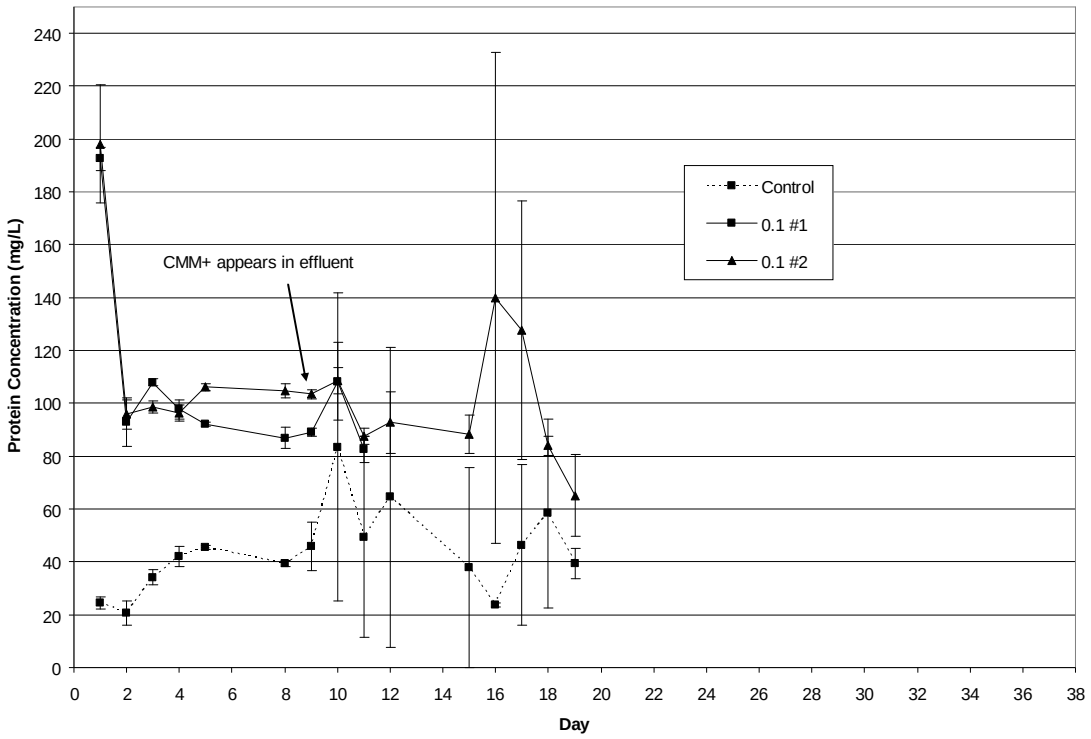

Figure 78: Change in protein concentration over time for both 0.1 mm columns. Error bars represent one standard deviation of triplicate measurements.

As soon as CMM+ appears in the effluent, there is a dramatic increase in the size of the error bars associated with each data point, indicating that the presence of calcium or calcium carbonate is interfering with the assay. This trend was also noted in other protein data from the 1 mm columns.

Based on these data, *S. pasteurii* is still capable of surviving within the 0.1 mm bead pack.

Ammonium-N and pH

Figure 79 shows the change in ammonium-N concentration over time for both of the 0.1 mm columns. There is about a 4000-5000 mg/L difference between the inoculated columns and the control. This difference indicates that ammonium-N concentration has increased, and is probably due to bacterial activity. Once again this increase happens very quickly. The error bars for the inoculated column and the control column increase with the addition of CMM+ into the system. This increase in variability in the measurements was also observed in the protein assay for other columns. It is possible that the calcium is interfering with the Nessler assay reagents or with the readings from the plate reader.

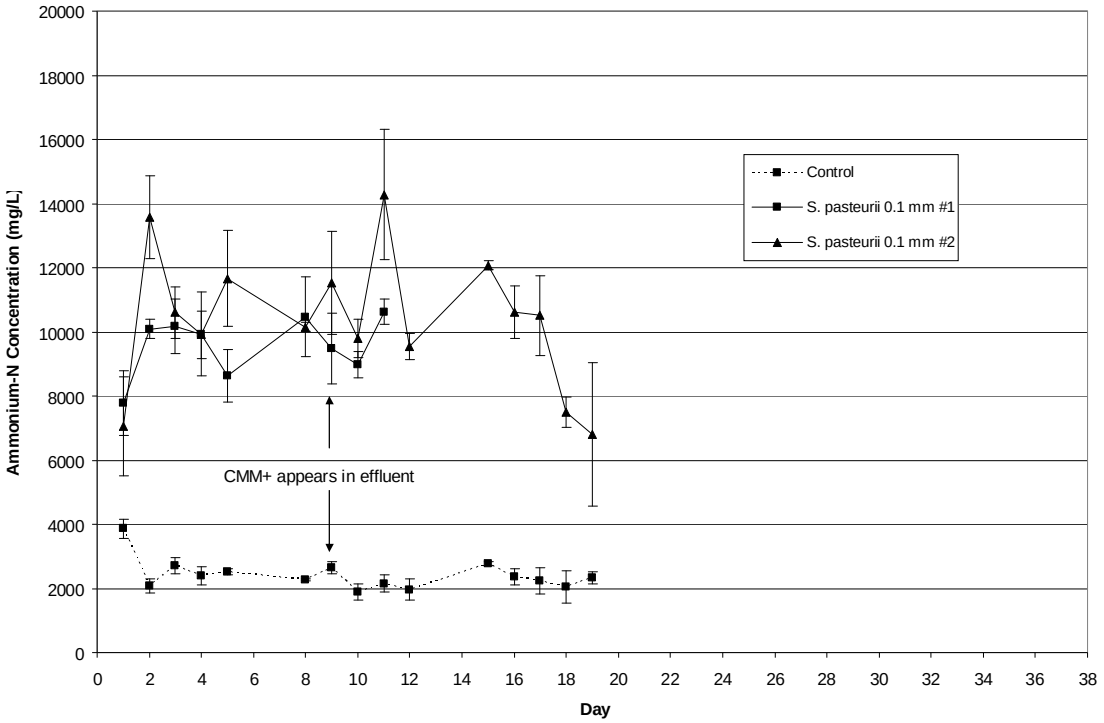

Figure 79: Change in ammonium-N concentration over time for both 0.1 mm columns. Error bars represent one standard deviation.

pH

The pH of both inoculated columns rises to the typically seen high of about 9.3 (Figure 80). Taken with the ammonium-N data, the rise in pH is a good indicator that the bacteria are capable of utilizing urea, producing ammonium, and raising the pH of the system. Looking at Figure 80, the pH of the control column and the media itself increases when CMM+ is introduced into the system. Because the CMM is adjusted to pH 6 before the bottle is hooked up to the system, this pH increase is another indication that the control column might be contaminated.

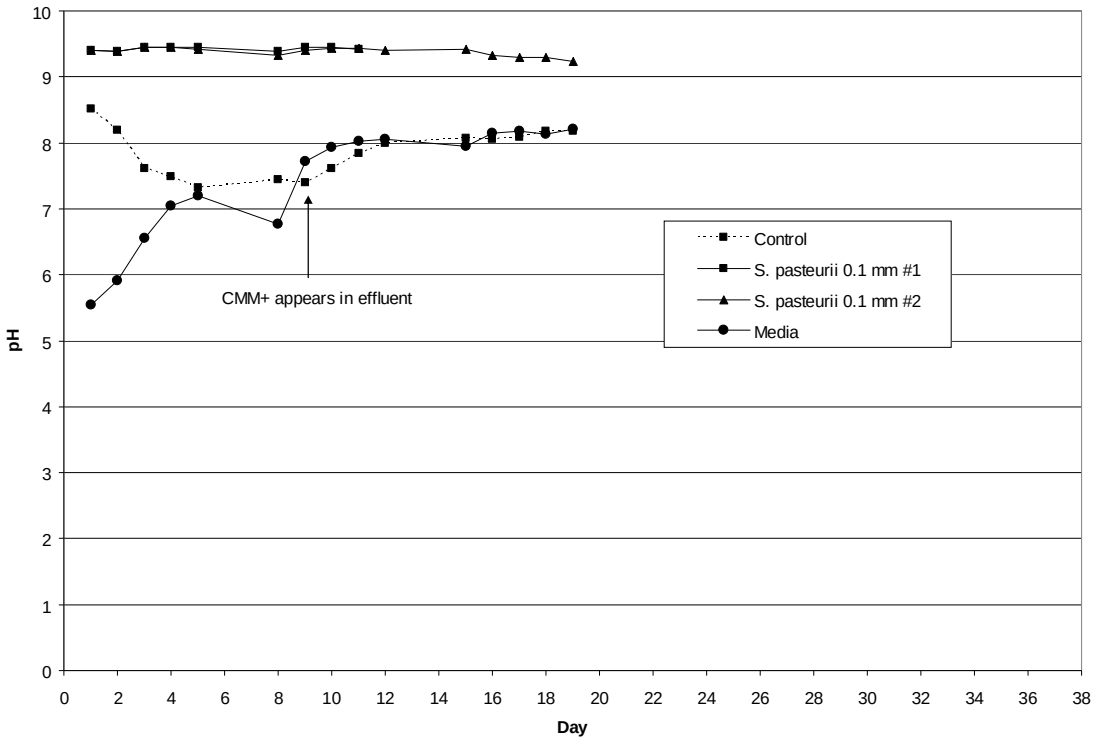

Figure 80: Change in pH over time for both 0.1 mm columns.

Calcium and Flow Rate

Looking at Figure 81, which shows the change in calcium concentration over time for the *S. pasteurii* 0.1 #1 column, it is seen that the total and dissolved calcium concentrations for the inoculated column are much lower than those of the control. The control calcium concentration is at about 1000 mg/L, which is how much calcium is added to the CMM+ medium when it is made.

There is already a 10x reduction in flow rate with the 10x reduction in bead size (Figure 82), but the flow rate of the 0.1 mm columns decreases even more with the introduction of CMM+ into the system (Figure 83).

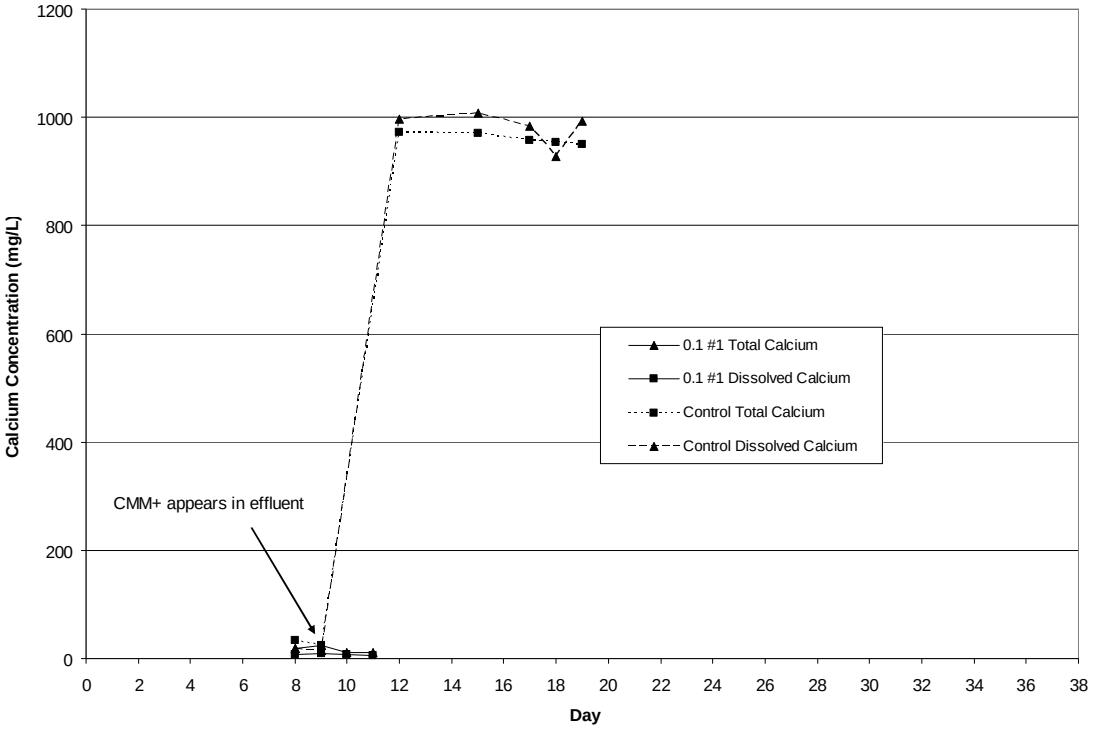

Figure 81: The change in calcium concentration over time for 0.1 mm #1 *S. pasteurii* column.

Figure 83 shows that the flow rate of the 0.1 mm column goes to zero within four days of CMM+ being introduced to the system. The flow rate of the control column also decreases slightly after the introduction of CMM+, but not to the degree that the 0.1 mm column does. Several days later, another attempt was made to drain fluid from the column. The column was completely plugged, and there was a thick film and deposit on top of the bead pack.

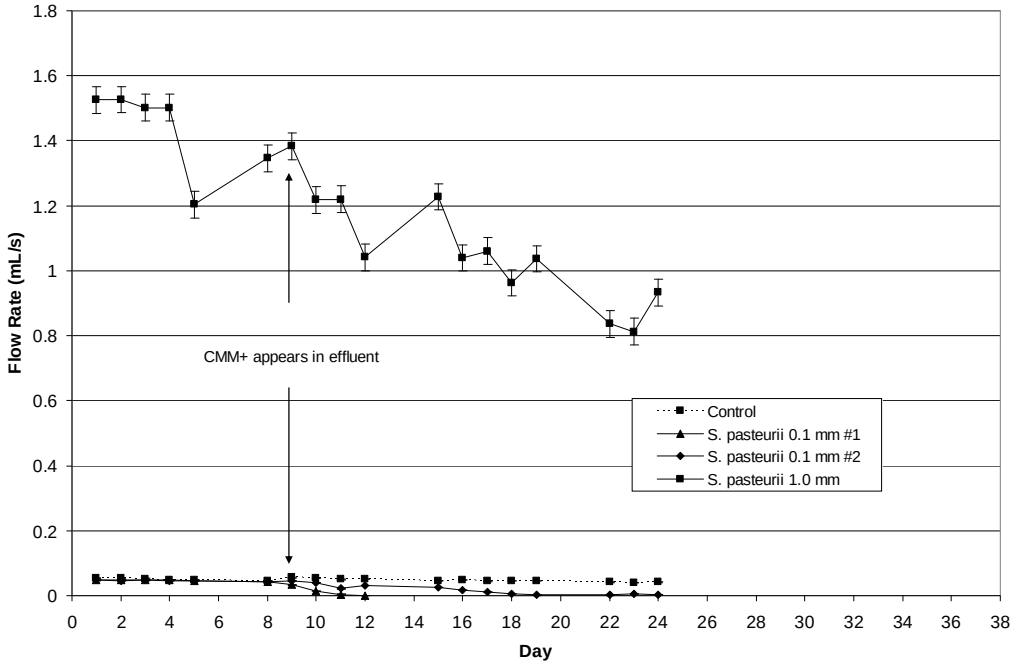

Figure 82: The change in flow rates between the 1 mm and 0.1 mm diameter bead columns. Error bars represent one standard deviation of ten measurements obtained from an uninoculated column.

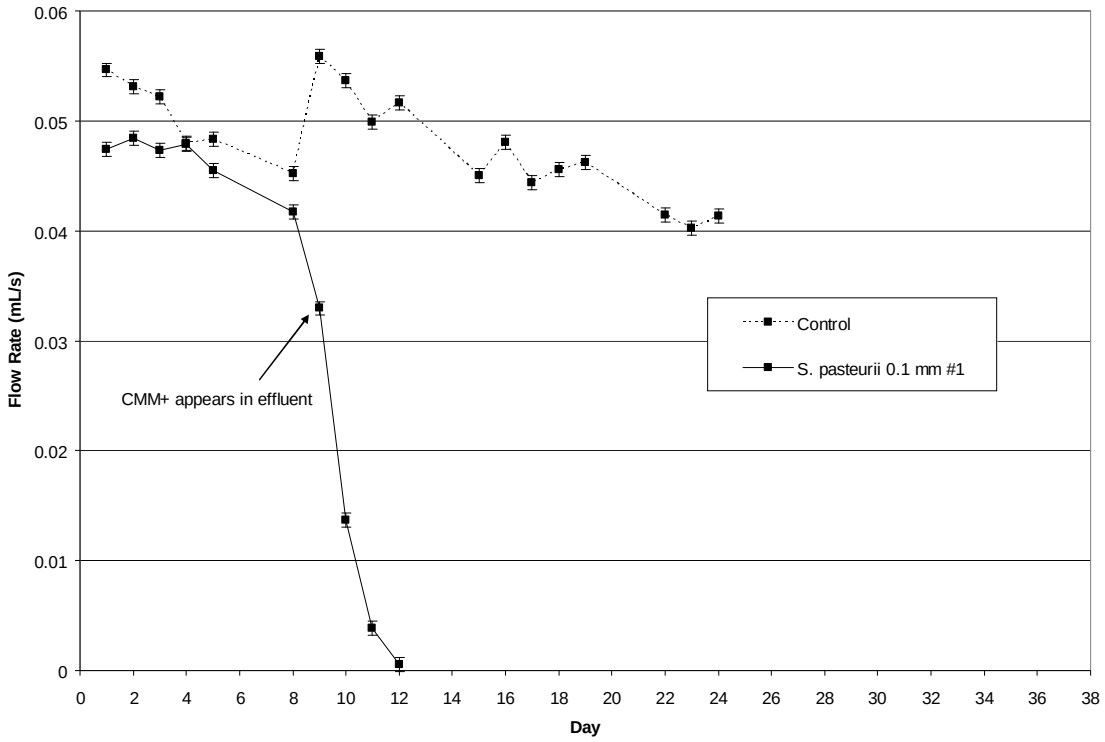

Figure 83: The change in flow rate over time for 0.1 mm #1 *S. pasteurii* column. Error bars represent one standard deviation of ten measurements obtained from an uninoculated column.

Looking at Figure 84, which shows the change in calcium concentration over time for the *S. pasteurii* 0.1 #2 column, it is seen that the total and dissolved calcium concentrations for the inoculated column in much less than that of the control. The control calcium concentration is at about 1000 mg/L, which is how much calcium is added to the CMM+ medium when it is made.

There is already a 10x reduction in flow rate with the 10x reduction in bead size (Figure 81), but the flow rate of the 0.1 mm column decreases even more with the introduction of CMM+ into the system (Figure 84).

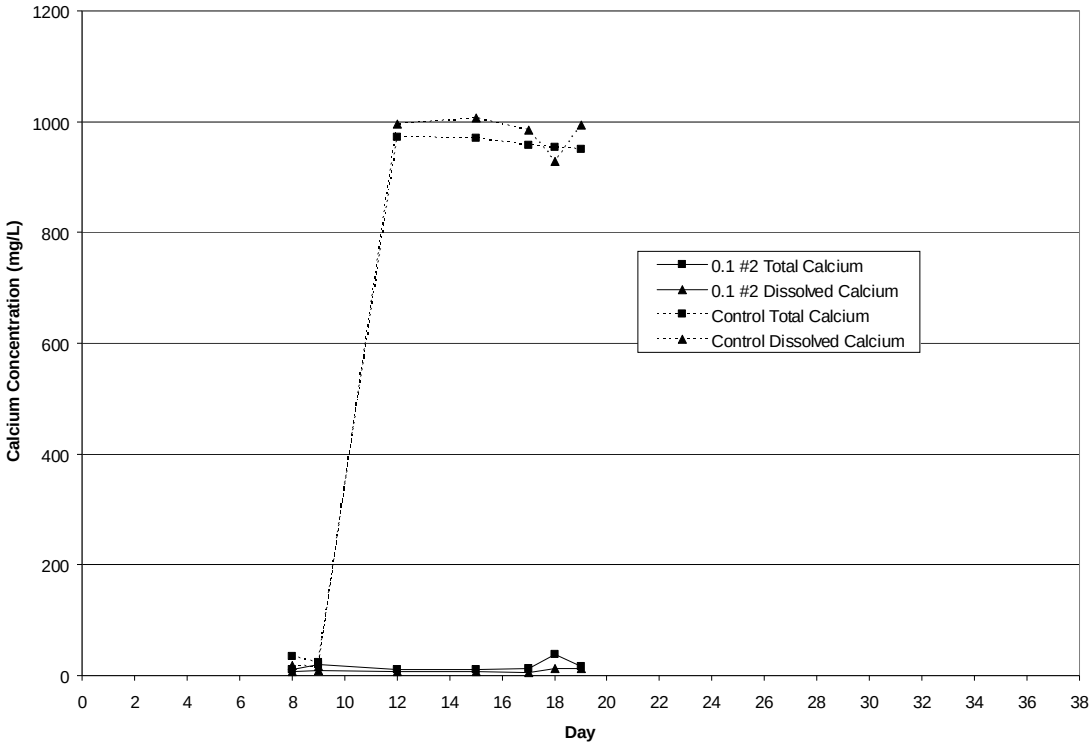

Figure 84: The change in calcium concentration over time for the 0.1 mm #2 *S. pasteurii* column.

Figure 85 shows the flow rate for the second 0.1 mm column. The flow rate does not decrease as fast as in the first 0.1 mm column, but it does essentially reach zero at day 19. This discrepancy between two columns that were inoculated at the same time with the same inoculum could be due to packing differences. The beads in each column were the same, but could have been situated in the column differently, causing the biofilm to develop differently and calcium carbonate to precipitate out differently. This is one reason that the columns might have behaved differently.

Figure 86 shows the cumulative amount of calcium precipitated in both of the 0.1 mm columns. The calcium increases linearly, just like it has in the other cumulative

calcium graphs. The 0.1 #1 column terminates early because it plugged very fast. The amount of precipitate in the other column continues to increase throughout the duration of the experiment.

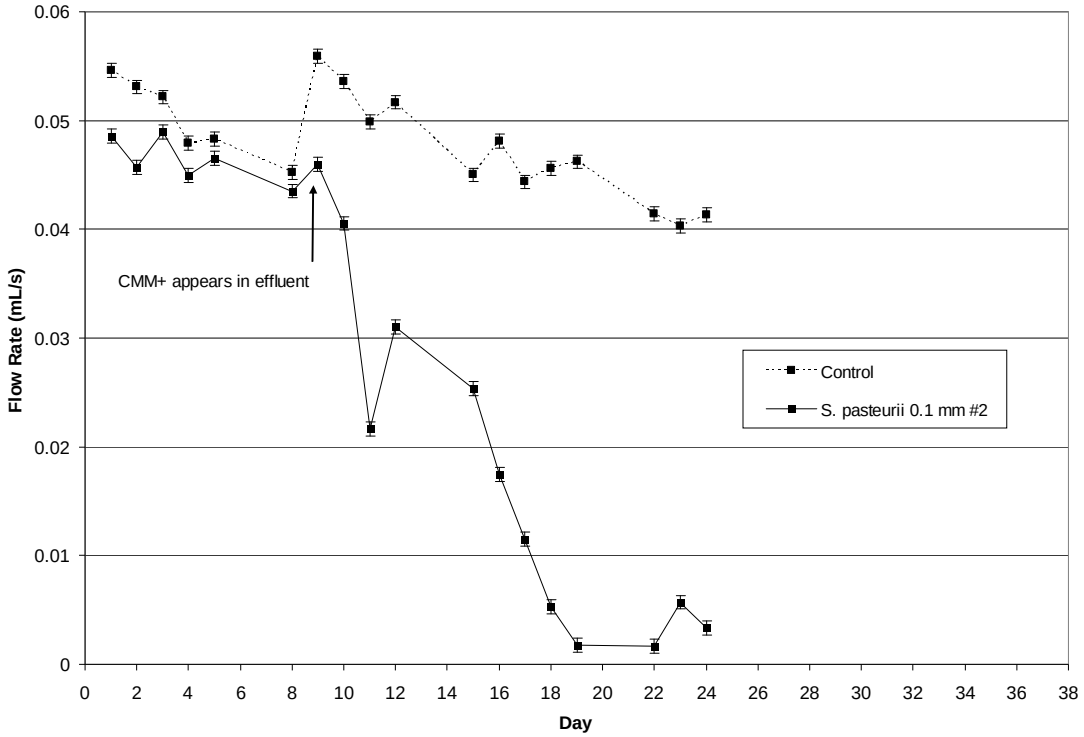

Figure 85: The change in flow rate for the 0.1 mm #2 *S. pasteurii* column. Error bars represent one standard deviation of ten measurements obtained from an uninoculated column.

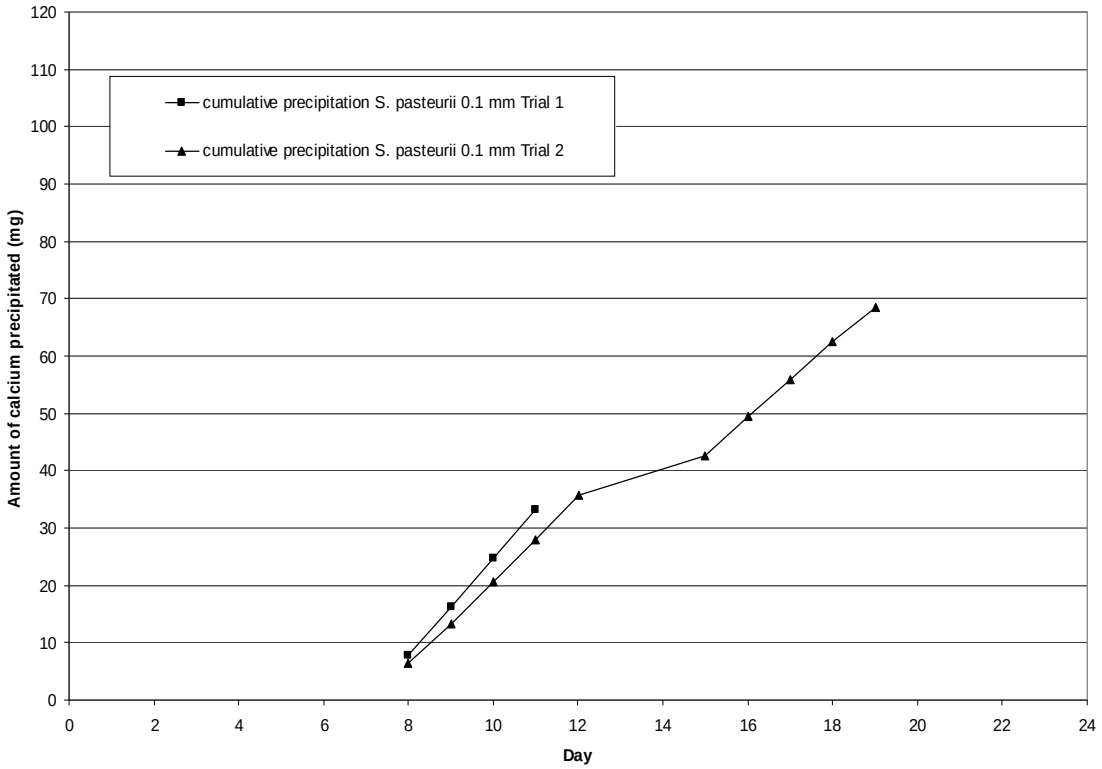

Figure 86: Accumulation of calcium carbonate precipitated for both 0.1 mm *S. pasteurii* columns.

Imaging

No SEM pictures were taken of the 0.1 mm columns. Figure 88 is a stereoscope image from the top of the column. This column had a large biofilm and calcium deposit on the top of the column (Figure 87). Figure 87 shows the interaction of the large crystal deposit with the beads.

Figure 87: Picture of large biofilm and calcium deposit on top of the 0.1 mm column.

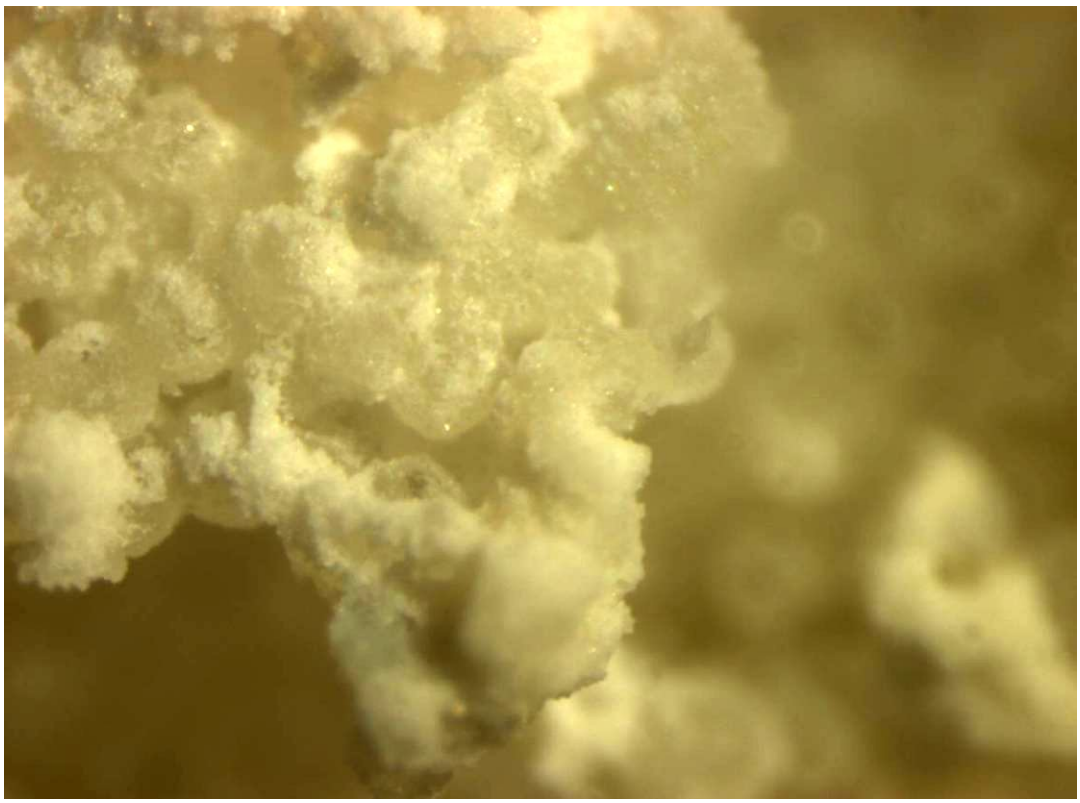

Figure 88: Stereoscope image of calcium deposit on top of 0.1 mm *S. pasteurii* column.

In Figure 88, the 0.1 mm beads are completely cemented together by the calcium deposits. When the column was destructively sampled, this section was difficult to extrude from the column. The top 2 cm of the columns were completely cemented together and to the sides of the column. In the 0.1 mm columns, there are more beads per gram and more surface area for deposits to adhere to. The 0.1 mm beads also have a smaller average pore size, so a smaller amount of deposit can completely block the area between the beads. The fact that the first 2 cm of the column are completely plugged was enough to reduce the flow rate of the column to zero.

Figure 89 was used to calculate the thickness of the biofilm in the 0.1 mm column. Here the biofilm thickness is about 18 µm. This is thinner than in the 1 mm columns, but it appears to be thick enough to reduce the flow rate in the 0.1 mm columns. This image was used for a rough calculation of biofilm thickness of the biofilm on the bead. For this picture 1mm is roughly 1.375 inches. From the picture, the biofilm appears to be about 0.35 inches, or about 18 µm.

$$\frac{100\ \mu m}{1.375\ in} = \frac{X\ \mu m}{0.25\ in}$$

$$X = 18\ \mu m$$

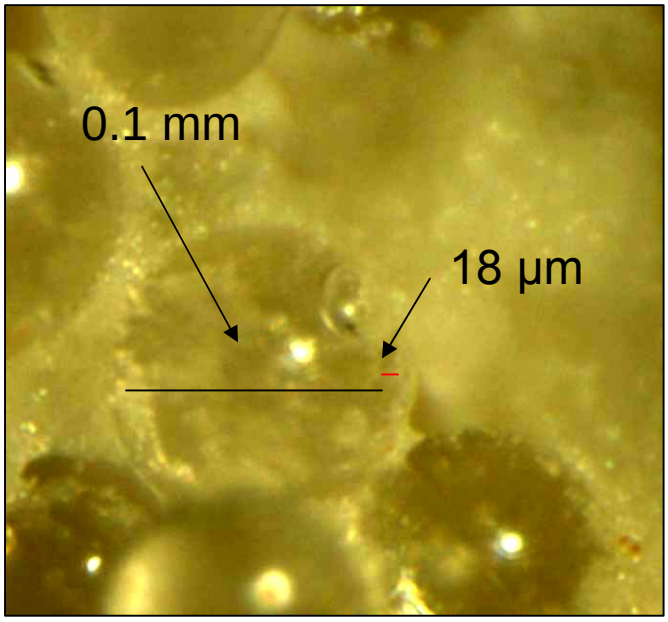

Figure 89: Stereoscope image of beads from the 0.1 mm *S. pasteurii* columns that was used to calculate biofilm thickness.

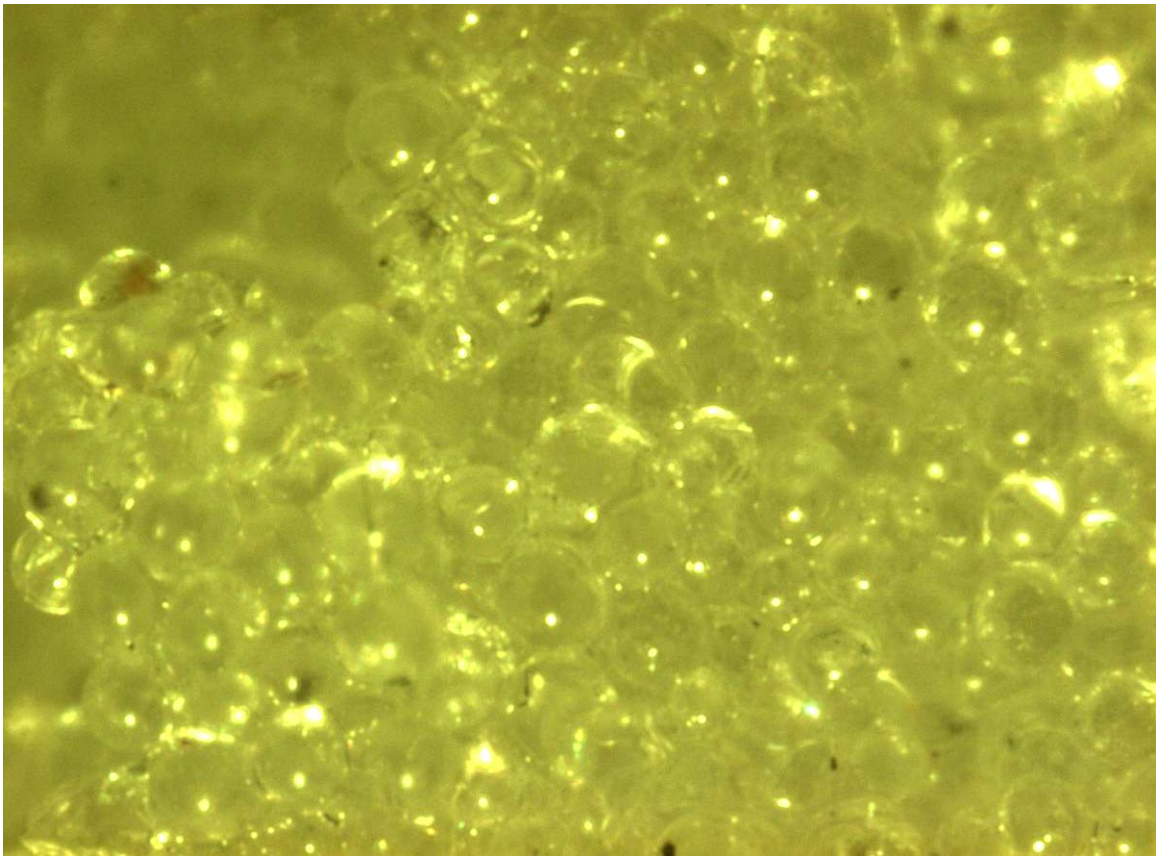

Figure 90: Stereoscope image of beads from the 0.1 mm control column

Figure 90 is a stereoscope image of the top section of the 0.1 mm control column. There is clearly no calcium deposit here, and the beads are not noticeably stuck together. They appear to be tightly packed with less pore space between the beads than in the 1 mm columns.

The porosity of the columns and the impact of calcium carbonate precipitate on the porosity of the columns are important to know because of the long-range applications of this research. It has been shown that calcium carbonate will precipitate in the pulse-flow column system, but it is important to know where it is being deposited in the system and what impacts that may have. The following is a discussion of the porosity of the

columns filled with 0.1 mm beads and the impact of calcium carbonate precipitation on the porosity.

The empty bed volume of the column is 11.78 mL.

$$V=\pi\cdot r^2\cdot h=\pi(0.5\text{ cm})^2(15\text{ cm})=11.78\text{ cm}^3=11.78\text{ mL}$$

20 1 mm beads were weighed, and an average weight of 0.0383 grams per 20 beads was calculated. The intrinsic density of beads was calculated using this average weight, and the average volume of 20 beads:

$$V=(4/3)\cdot\pi\cdot r^3=(4/3)\pi(0.05\text{ cm})^3=5.25\text{x}10^{-4}\text{ cm (20 beads)}=0.0105\text{ mL}$$

Intrinsic Density=0.0383g/0.0105 mL = 3.65 g/mL

The columns used in the 0.1 mm experiments are packed in three layers: a 1 cm bottom layer of 1 mm beads, a 1 cm layer of 0.5 mm beads, and a top layer of 13 cm 0.1 mm beads. The individual porosities of each layer as well as for the total column are calculated.

For the first 1 cm section filled with 1 mm beads, a porosity of 31% had previously been calculated.

For the second 1 cm section filled with 0.5 mm beads, an average weight of 2.33 grams of beads is used to fill the section. Using the intrinsic density, the volume of beads in that 1 cm can be calculated:

$$2.33\text{ grx}\frac{1\text{ mL}}{3.65\text{ gr}}=0.64\text{ mL}$$

The empty volume of the 1 cm is:

$$V=\pi(0.5\text{ cm})^2(1\text{ cm})=0.79\text{ cm}^3=0.79\text{ mL}$$

This means that there is 0.79-0.64=0.15 mL of free space available in the 1 cm section of column. The porosity of this 1 cm section of the column is:

$$\text{Porosity} = \frac{0.15\ \text{mL}}{0.79\ \text{mL}} = 19\%$$

For the remaining 13 cm of column that is filled with 0.1 mm beads, an average weight of 24.6 grams of beads is used to fill the section. Using the intrinsic density, the volume of beads in the 13 cm can be calculated:

$$2.46\ \text{grx}\frac{1\ \text{mL}}{3.65\ \text{gr}} = 6.74\ \text{mL}$$

The empty volume of the 13 cm is:

$$V = \pi(0.5\ \text{cm})^2(13\ \text{cm}) = 0.79\ \text{cm}^3 = 10.21\ \text{mL}$$

This means that there is 10.21-6.74=3.47 mL of free space available in the 13 cm section of column. The porosity of this 13 cm section of the column is:

$$\text{Porosity} = \frac{3.47\ \text{mL}}{10.21\ \text{mL}} = 34\%$$

For the final column that is packed with the three different layers of beads, the empty volume is 11.78 mL, and the volume filled with beads is 0.64 mL+ 0.64 mL+6.74 mL= 8.02 mL. This means that the remaining free space is 11.78 mL-8.02 mL=3.76 mL. The porosity of this bead pack can be calculated: The porosity of this column is:

$$\text{Porosity} = \frac{3.76\ \text{mL}}{11.78\ \text{mL}} = 32\%$$

The amount of calcium carbonate precipitated out for each 0.1 mm experiment has been tabulated in Table 11:

Table 11: Volume of calcium carbonate precipitated in each column filled with 0.1 mm beads.

Column Name	**mg Ca^{2+} precipitated out**	**gr Ca^{2+} precipitated out**	**gr $CaCO_3$ precipitated out**	**mL of $CaCO_3$ precipitated out**
0.1 mm Control	24	0.024	0.061	0.02
0.1 mm *S. pasteurii* #1	33	0.033	0.083	0.03
0.1 mm *S. pasteurii* #2	69	0.069	0.171	0.06

The total mass of Ca^{2+} precipitated out is obtained from the ICP-MS measurements. Milligrams is converted to grams of Ca^{2+} and then converted to grams of $CaCO_3$. Using an estimated density of 2.71 g/mL (37), grams of $CaCO_3$ is converted to milliliters. Total, not dissolved, calcium measurements were used for these calculations.

Assuming that the calcium carbonate precipitates out throughout the entire bead pack in the column, a new set of calculations is performed. The unoccupied volume of the column is 0.27 mL and the porosity of the whole column is about 32%. Subtracting the volume of $CaCO_3$ that precipitated out from the free space available gives the remaining free space available after the precipitation has occurred. The “new” porosity of this section can then be calculated.

Table 12: Percent reduction in porosity that occurs if all the calcium carbonate precipitates homogeneously throughout in the whole column instead of the first centimeter. This data is for the 0.1 mm diameter bead columns.

Column Name	mL of $CaCO_3$ precipitated out	mL of free space remaining after precipitation	Initial porosity of 1 cm space (%)	porosity of 1 cm space after precipitation (%)	Percent porosity reduction (%)
0.1 mm control	0.02	3.7	31.9	31.7	0.6
0.1 mm *S. pasteurii* #1	0.03	3.7	31.9	31.7	0.8
0.1 mm *S. pasteurii* #2	0.06	3.7	31.9	31.4	1.7

Table 12 shows the reduction in porosity that occurs if calcium carbonate precipitates out in the whole column. For the two *S. pasteurii* columns, the precipitation of calcium carbonate in the whole column reduces the porosity of the whole column by 0.6 and 0.8% for an average reduction of about 0.7%. For the control column, the precipitation of calcium carbonate throughout the whole column reduces the porosity of the column by 0.6%. From the destructive sampling data in the next section, it is shown that calcium does precipitate throughout the whole length of the bead pack. However, there is usually more calcium in the top sections of the columns. The 0.1 mm *S. pasteurii* #1 column became plugged first, within the first three days after the introduction of CMM+. This column had clear calcium and biofilm deposit at the top of the bead pack; the stereoscope images (Figure 88) show a close-up view of this deposit and its interaction with the 0.1 mm beads. It is possible that the majority of the calcium carbonate did precipitate out in the top 0.5 cm instead of the top 1 cm. Even though the reduction in porosity is only about 0.7% it appears to be enough to plug the column sufficiently.

Assuming that 100% of the $CaCO_3$ precipitates in the top 1 cm of the column, the affect of the precipitate on the porosity of the columns can be visualized. There is 0.27 mL of unoccupied space in this 1 cm section and the porosity of the section is 34%. Subtracting the volume of $CaCO_3$ that precipitated out from the free space available gives the remaining free space available after the precipitation has occurred. The "new" porosity of this section can then be calculated.

Table 13: Percent reduction in porosity if all the calcium carbonate precipitates out in the first top centimeter of the 0.1 mm diameter bead columns.

Column Name	**mL of $CaCO_3$ precipitated out**	**mL of free space remaining after precipitation**	**Initial porosity of 1 cm space (%)**	**Porosity of 1 cm space after precipitation (%)**	**Percent porosity reduction (%)**
0.1 mm Control	0.02	0.248	31.9	31.3	1.8
0.1 mm *S. pasteurii* #1	0.03	0.239	31.9	30.3	5.1
0.1 mm *S. pasteurii* #2	0.06	0.207	31.9	26.2	18.0

Table 13 shows the reduction in porosity that occurs in the top (influent) 1 cm of the columns packed with 0.1 mm diameter glass beads. For the two *S. pasteurii* columns, the precipitation of calcium carbonate in the top 1 cm of the column reduces the porosity of that 1 cm by 5.1 and 18 % for an average reduction of about 12%. For the single control column, the precipitation of calcium carbonate in the top 1cm of the column reduces the porosity of that 1 cm by 1.8%. The control column had enough calcium carbonate precipitate out to reduce the porosity of the system assuming that all the calcium carbonate precipitated in the top 1 cm of the column. However, the reduction in porosity is much less than what was observed in the columns inoculated with *S. pasteurii*.

0.1 mm Columns Destructive Sampling Data

After the termination of each column experiment, the columns are taken down and destructively sampled. Beads are taken from each section of the column and tested for plate counts, direct counts, protein, and calcium. Based on the method of inoculation, it was expected that there would be more cells, more protein, and more calcium at the top section of

the column. It was also expected that there would be more cells at the top of the column because that is where the greatest amount of oxygen is concentrated. Plate counts were performed for the control columns as well, but nothing grew on the agar plates, which is what was expected because the columns should not have had any cells.

Plate Counts and Direct Counts

Direct counts measure the amount of live and dead cells, and should always be higher than plate counts, which only measure the amount of culturable cells in the system. Figure 90 represents the direct counts and plate counts for the both *S. pasteurii* 0.1 mm columns. For the first trial, the direct counts are higher than the plate count data for each column section, and are higher in the top than in the middle of the bottom. This trend was expected. The plate counts data also follows this trend. The counts are higher in the top of the column than in the middle. There are no plate count data for the bottom section of the column because the agar plate was wet and the drops ran together.

For the second 0.1 mm column the plate counts are higher in the top section than the middle or the bottom section (Figure 91), but the plate counts for the bottom are higher than in the middle. This could be due to oxygen diffusion into the effluent silicon tubing (34) and the cells might have been able to grow better in this column section. The direct counts are higher in the top of the column and decrease in magnitude towards the bottom of the column.

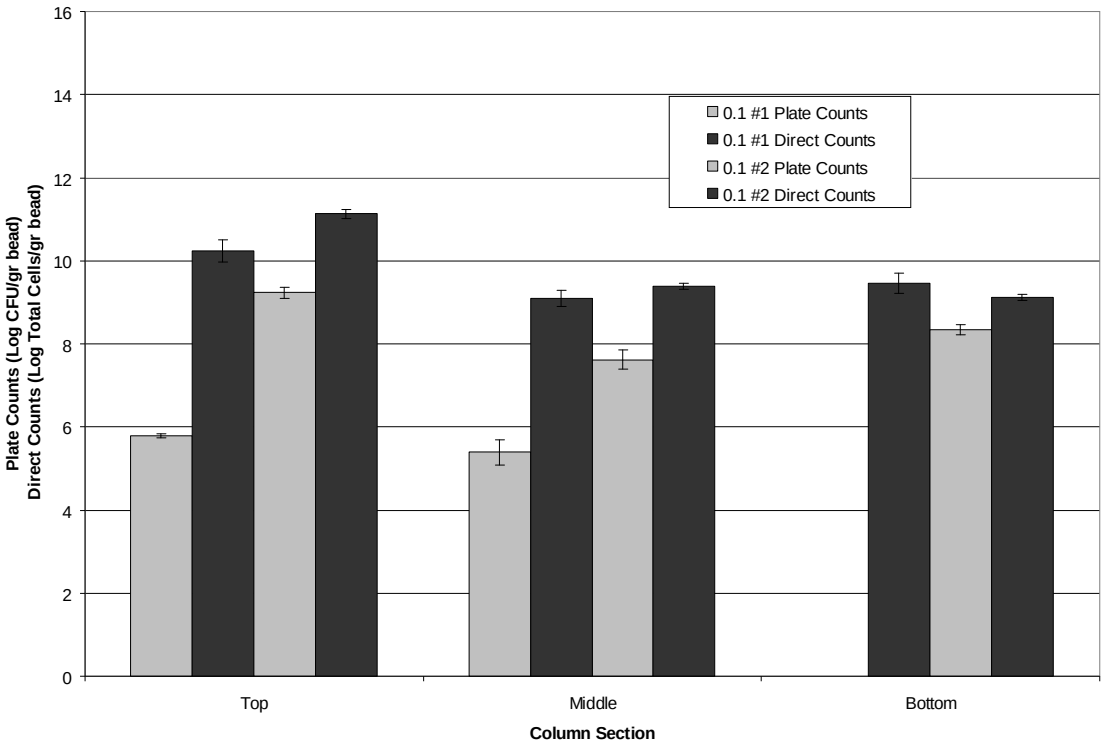

Figure 91: Plate counts and direct counts per column section for both 0.1 mm *S. pasteurii* columns.

Protein

Figure 92 shows the protein concentration per column section for both the 0.1 mm columns. For the control column, there is more protein near the top of the column than in

the middle or the bottom. The opposite is true for the 0.1 #1 column; there is less protein in the top of the column and the concentration increases in magnitude towards the bottom of the column. However, the error bars overlap, so the difference between this data is not significant. This matches with the plate count data except for the bottom section. The protein concentration for the top control section is more than the protein concentration for the first inoculated column, but the protein concentrations for the other sections of the control are less than those for the inoculated column.

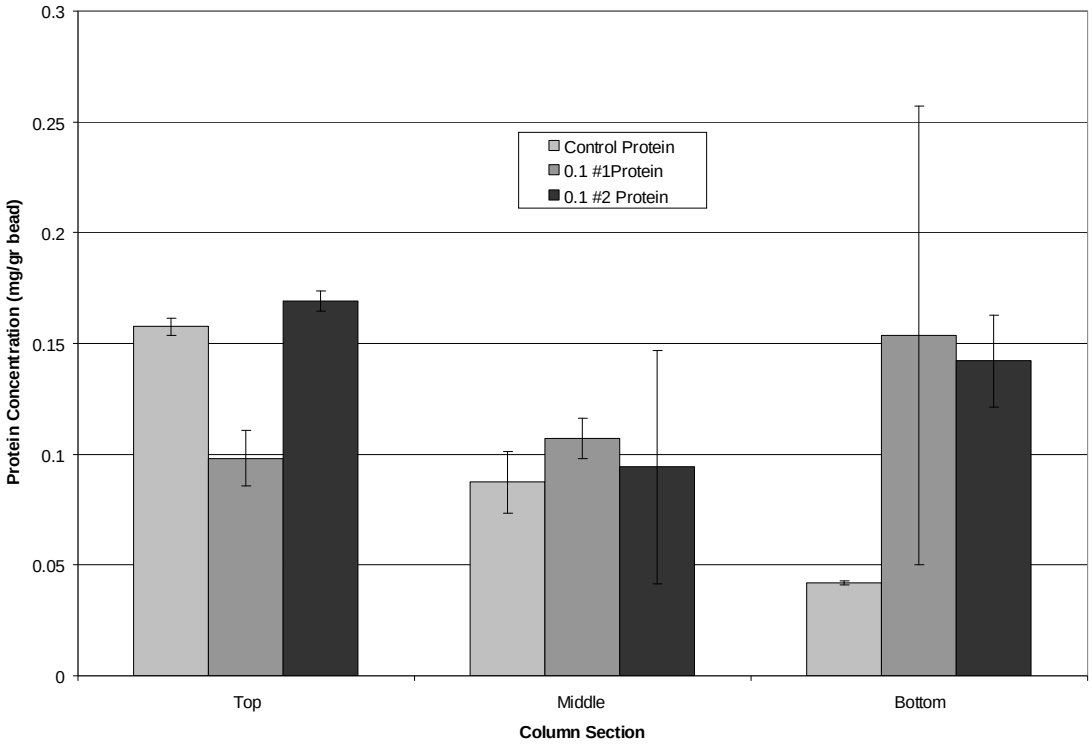

Figure 92: Protein concentration per column section for both 0.1 mm columns. Error bars represent one standard deviation.

For the second 0.1 mm column, the protein concentration is higher in the top of the column, then the bottom, then the middle. This also matches the plate count data (Figure 90) for concentration per column section.

The plate count and direct count data support the fact that *S. pasteurii* is capable of growing in the 0.1 mm column. The interference seen in the 1 mm columns is repeated in the data from the 0.1 mm columns. This interference makes the protein data less reliable.

Calcium

Figure 93 shows the calcium concentration per column section for both 0.1 mm columns relative to a control. The control column shows a much higher calcium concentration in the middle section of the column, and the top and the bottom sections of the column have almost the same calcium concentration. The inoculated columns should have a higher concentration of calcium in each column section relative to the control and this is true for the 0.1 mm #1 column.

This data can be used in conjunction with the accumulation of calcium carbonate from effluent measurements in order to close the calcium mass balance. The mass of calcium deposited on the beads was subtracted from accumulated mass of calcium to find the mass of calcium that was retained on in the column and on the other system parts such as silicon tubing, stoppers, and glass pieces. This data is tabulated in Appendix D.

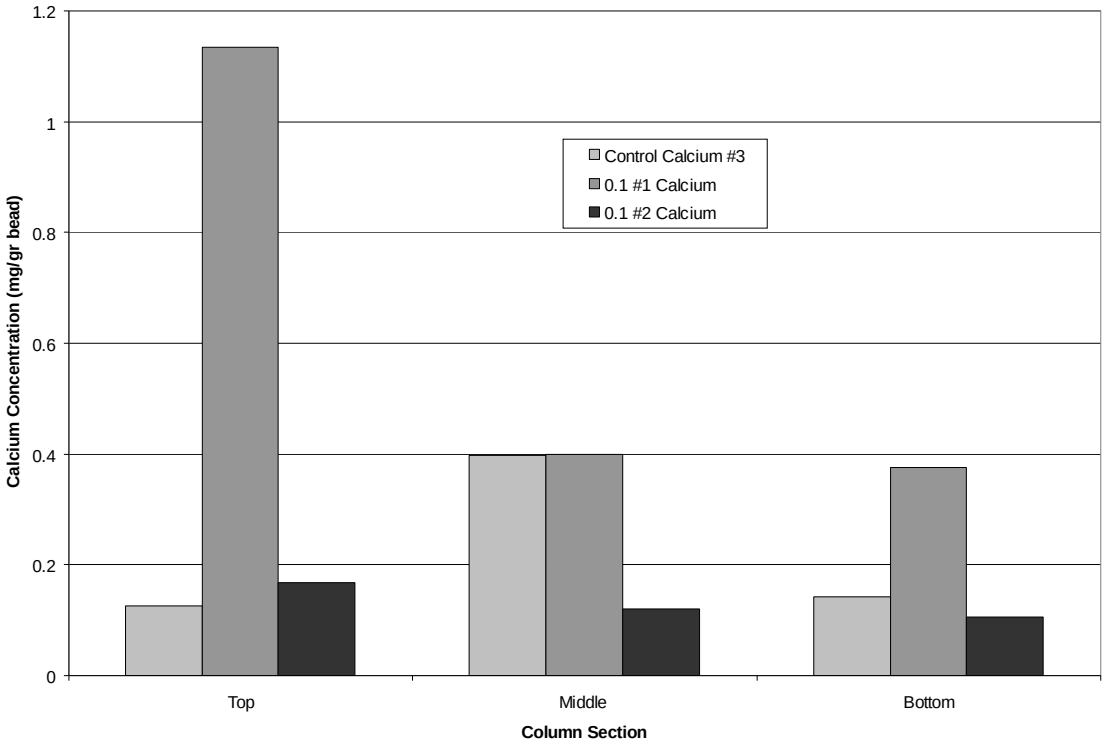

Figure 93: Calcium concentration per column section for both 0.1 mm *S. pasteurii* columns.

This is the column that plugged the quickest, and it is the one exhibits the most calcium in the top section. There was a large film and a large deposit on the top of the bead back, so a large amount of calcium in this section was expected. For the 0.1 mm #2 column, there is also more calcium in the top section of the column, which was expected. However, the calcium concentration per column section for the control is higher for the middle and bottom sections, which is not expected.

CONCLUSIONS

It was seen from the 1 mm column results that the chosen bacteria, *S. pasteurii*, *B. sphaericus* #21776, *B. sphaericus* #21787, and *B. subtilis* are capable of establishing a viable biofilm community within the pulse-flow column system. The ureolytic bacteria, *S. pasteurii*, *B. sphaericus* #21776, and *B. sphaericus* #21787, are also capable of creating an environment that facilitates calcium carbonate precipitation through the hydrolysis of urea, which results in the production of ammonium and an increase in pH. While each ureolytic bacterial strain is capable of creating this environment, *S. pasteurii* shows the greatest ureolytic activity. *B. subtilis* is not capable of increasing the pH of the system.

Stereoscope and SEM images confirm the presence of cells and calcite mineral together in the pulse-flow column system and show that the cells can be encased within the calcite precipitate. Though there are calcium deposits on the beads, they are not large enough to effectively reduce the porosity of the 1 mm bead pack.

Destructively sampling the columns yields information about which section of the column has the highest concentration of cells, protein, and calcium. This provides information on whether or not gradients are forming in the column and how the reduction in permeability is occurring. The information obtained here is important for assessing the feasibility of biomineralization as a viable solution for the sequestration of carbon dioxide.

A simple way to reduce the free pore space in the column is to reduce the bead size. A 10 fold reduction in bead size from 1 mm to 0.1 mm results in a bead pack with

more surface area, but smaller average pore size. *S. pasteurii*, the most ureolytic bacterium used in the research was used to inoculate the columns. In this case, the amount of precipitated calcium carbonate was sufficient to reduce the flow rate to essentially zero and completely reduce the permeability of the columns presumably due to rapid precipitation of calcium carbonate in the topmost influent section of the columns.

Research projects such as this are the building blocks for further studies on the viability of biomineralization for carbon sequestration purposes as well as other environmental applications.

FUTURE STUDIES

This research was focused on establishing viable, ureolytic biofilm communities in a pulse-flow column system, and using those viable communities to reduce the permeability of the porous media. Other avenues of biomineralization research are currently being pursued and with those in mind, these are some recommendations for future work.

1. A third trial involving *B. sphaericus* #21787 should be run in a 1 mm bead pack to determine if the data from the first trial was an anomaly.

2. Experiments involving *B. sphaericus* #21776, *B. sphaericus* #21787, and *B. subtilis* should be run, at least in duplicate, in the 0.1 mm column systems in order to compare the 1 mm and 0.1 mm results.

3. It has been hypothesized that running the current system as a continuous flow system and not a pulse flow system would allow for faster precipitation of calcium carbonate. Such a system was modeled using the Biofilm Accumulation Model and the output data can be seen in Appendix A. Preliminary results from the model indicate that maximum calcium utilization and precipitate formation occur at low flow rates, indicating that a continuous flow system might be more effective at reducing the permeability of a 1 mm beadpack.

APPENDICES

APPENDIX A

BAM MODELING PROJECT

Introduction

In the laboratory, 1 mm diameter glass beads are being used. However, there has been no noticeable decrease in flow rate, such as was seen in Jeff Ashe's previous column experiment that was inoculated with a ureolytic strain of *E. coli*. Because the goal of this project is to plug up the bead pack with biomass and calcium carbonate, there were several different routes that were proposed so that this plugging would be able to be seen. The suggestions included, using a smaller diameter bead pack, changing the pulse-flow system to a continuous flow system, and using a smaller diameter/shorter column. Of these options, using a smaller diameter bead pack seemed the quickest and cheapest way to lessen the pore space within the column. Because it is known that a continuous flow system is capable of becoming plugged, a continuous flow column system was strongly discussed. This was too detailed to install in the lab, a computer modeling system, the Biofilm Accumulation Model (BAM), was used to simulate what would happen if the columns were run as a continuous flow system.

Goals and Objectives

The purpose of this project was to model a continuous flow reactor system and determine the effect of flow rate on pH, calcium carbonate precipitation and the effect of surface area to volume ratio on carbonate precipitation for a ureolytic biofilm system.

Materials and Methods

Conceptual Model

It was assumed that a glucose and calcium containing media flowed continuously through a column inoculated with ureolytic bacteria. The media flowed at varying flow rates. The glucose and calcium was assumed to diffuse into the biofilm, where they were assumed to be utilized through the governing series of reactions listed in the introduction. The OH^- ions produced diffused out of the biofilm into the bulk fluid. The concentration of OH^- ions in the center of the biofilm and in the bulk fluid was monitored at the different flow rates and eventually converted to the concentration of H^+ ions, or pH (41). The increase in pH and the presence of free calcium ions lead to carbonate precipitation and the concentration of precipitate in the bulk fluid was also be monitored as the flow rate changes. The above scenario was repeated, only changing the surface area to volume ratio to those of the flat plate reactor, another continuous flow system currently in use in the lab. The concentration of precipitate in the bulk fluid for the flat plate reactor system was monitored as flow rate changes.

Modeling Approach

In the model, glucose was designated as the first substrate and live cells were designated as the first particulate. The production of OH^- ions was modeled as a second substrate that was produced from the first substrate. Free calcium ions were introduced as the third substrate, and calcium carbonate was introduced as a second particulate that was formed from the third substrate. Other parameters, such as surface area, volume,

diffusion concentrations and substrate concentrations were either estimate, calculated, or retrieved from literature.

To establish a "base case" for modeling the column system, all the geometric parameters for the column were entered into the model, glucose was entered in as the first substrate, and live cells were entered in as the first particulate. A flow rate of 0.15 mL/min was used, and the detachment rate (L_f^2) was varied until the system reached a steady state biofilm thickness of 59 µm, the biofilm thickness previously calculated.

Table 14: BAM parameters at steady state.

Parameter	**Input Value**	**Reference**
Column and Bead Surface Area	0.04902 m^2	From Experimental Data
Column Volume	1.178×10^{-5} m^3	From Experimental Data
Initial Flow Rate (Q)	0.000216 m^3/day	From Experimental Data
Liquid Layer Film Thickness L_L	10 µm	Estimated
Liquid Volume Fraction (ε_L)	0.3	Calculated
D_e/D_{aq}	0.3	[42,43]
S_i Glucose	36000 g/m^3	From Experimental Data
X_b	20000 g/m^3	Estimated
μ_{max}	10.37 day^{-1}	From Experimental Data
D_{aq} of Glucose	5.962×10^{-5} m^2/day	[42]
K_s	1 mg/L	Estimated
Y_{xs}	0.5085 g/g	Estimated
L_{ss}	59 µm	From Experimental Data
Lf^2	175000	Calculated
Initial Biofilm Thickness	5 µm	Estimated

Table 15: Other BAM parameters.

Parameter	**Input Value**	**Reference**
Flat Plate Reactor Surface Area	0.006499 m^2	From Experimental Data
Flat Plate Reactor Volume	2.517x10-6 m^3	From Experimental Data
S_i Calcium	3700 g/m^3	From Experimental Data
X_b Calcium	100000 g/m^3	Estimated
D_{aq} Calcium and OH^- *	2.03×10^{-9} m^2/s	[42]

* Diffusion coefficients for Ca^{2+} and OH^- were assumed to be the same as the diffusion coefficient for Cl^-.

Working from this base case model, substrate flow rate was varied and its effect on pH and calcium carbonate precipitation in the column system was monitored. Next, the surface area was changed to that of the flat plate reactor. The flow rate was varied in the same way and its effect on calcium carbonate precipitation was monitored.

Table 16: Reaction matrix at steady state

Reaction: Growth	Stoichiometric Coefficient	Rate Law	Rate Law Coefficient
PO1	1	First Order	10.37
SO2	-1.96	Monod Order	1

Table 17: Reaction Matrix including OH^- production

Reaction: Growth	Stoichiometric Coefficient	Rate Law	Rate Law Coefficient
PO1	1	First Order	10.37
SO1	-1.96	Monod Order	1
SO2	3.92	Zero Order	1

Table 18: Reaction Matrix including OH^- production and $CaCO_3$ precipitation

Reaction: Growth	Stoichiometric Coefficient	Rate Law	Rate Law Coefficient
PO1	1	First Order	10.37
PO2	0	Zero Order	1
SO1	-1.96	Monod Order	1
SO2	0	Zero Order	0
SO3	0	Zero Order	1
Reaction: Precipitate			
PO1	0	Zero Order	1
PO2	1	Zero Order	1
SO1	0	Zero Order	1
SO2	-1	Zero Order	1440
SO3	-1	Zero Order	1

BAM Parameters

The geometric parameters for the column and flat plate reactors were determined by actual experimental measurements. The surface area for the column reactor was high because it included the total surface areas for the beads, but did not account for the areas not available to biofilm growth because the beads were touching. The initial flow rate was chosen to be 0.15 mL/min because that was the flow rate used in the flat plate reactor currently operating in the lab. The first substrate was approximated as glucose because there was no data available to calculate the other parameters needed. The inlet and bulk concentrations of the two substrate components, glucose and calcium, were taken from the media recipe used in the column experiments. The cell density in the biofilm was an estimate, as there was no published value found. μ_{max} was calculated from protein assay data collected from steady state batch experiments with *S. pasteurii* performed in the lab by Stacy Parks. Y_{xs} was calculated from stoichiometric methods. The initial biofilm thickness was chosen to be 5 µm. The biofilm thickness at steady state was calculated from looking at a stereoscope image of a bead taken from the top of a column inoculated with *S. pasteurii*. The image shows deposits on the bead surface. Approximating these deposits as "biofilm thickness", a thickness could be calculated. D_{aq} for glucose was approximated at 6.9 x 10^{-10} m^2/s (5) D_e/D_{aq} was estimated to be 0.3 (42, 43). D_{aq} for calcium was approximated as that of chlorine (42). K_s was estimated at 1 mg/L and the liquid layer thickness estimated at 10 µm in the absence of published values. The fraction of liquid in the biofilm, ε_L, was estimated from looking at pictures and from the literature (44).

Results

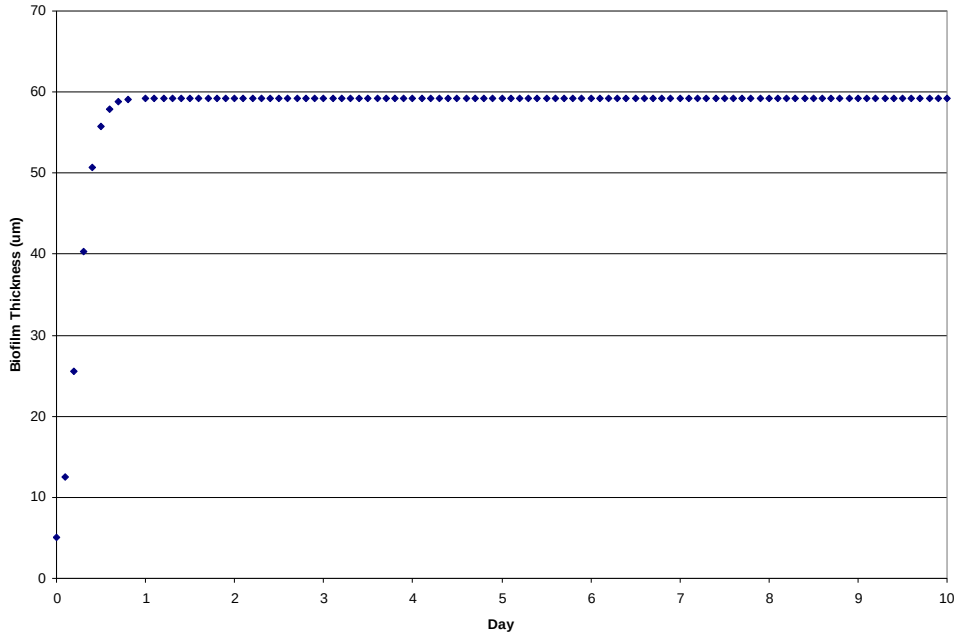

Figure 94: The change in biofilm thickness over time at steady state parameters. The steady state thickness is reached by the first day.

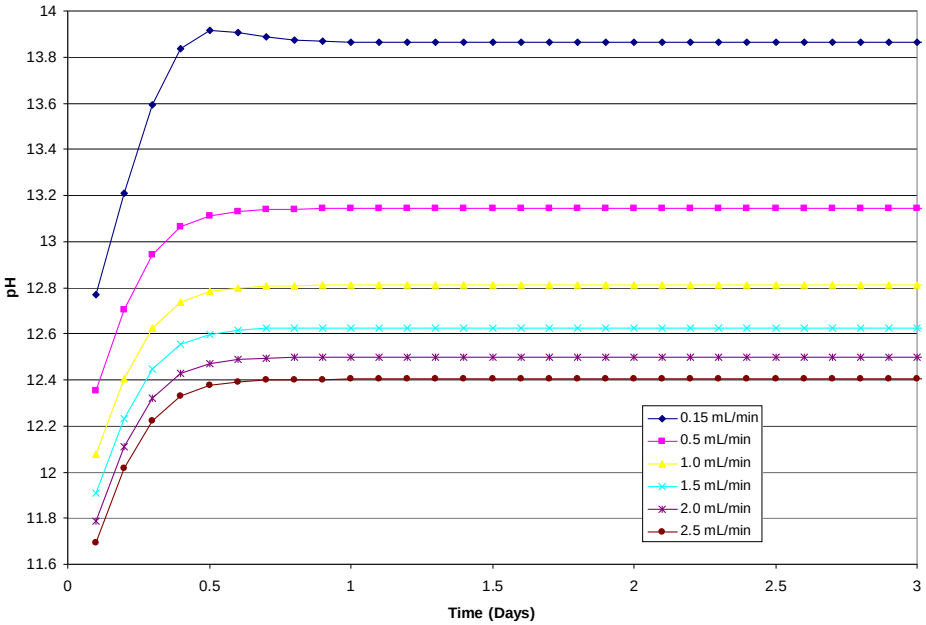

Figure 95: Change in pH in the center of the biofilm (grid 3) with varying flow rate. This is for the continuous flow column system

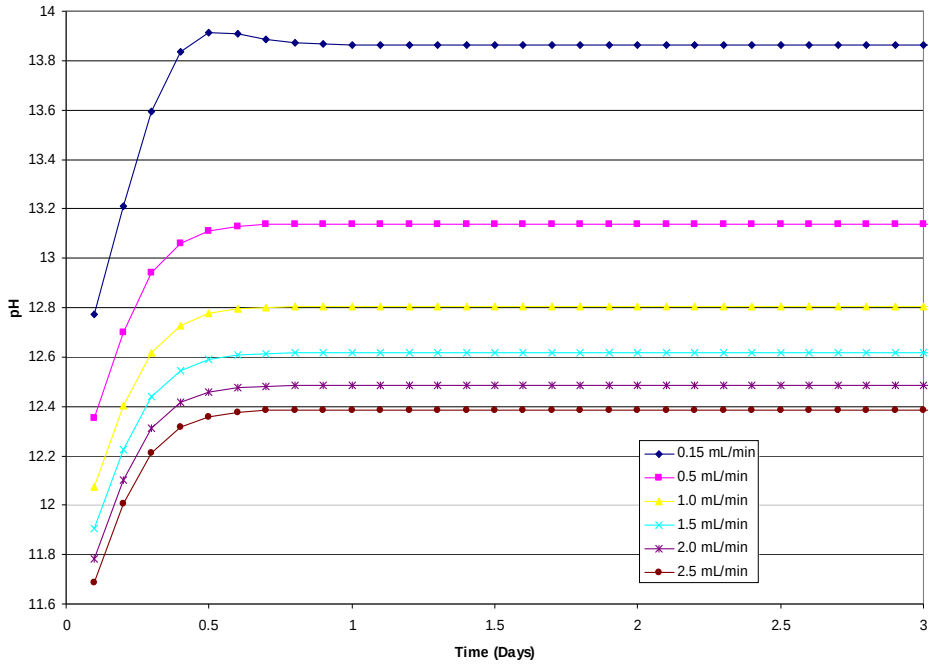

Figure 96: Change in pH in bulk fluid with vary flow rate. This is for the continuous flow column system.

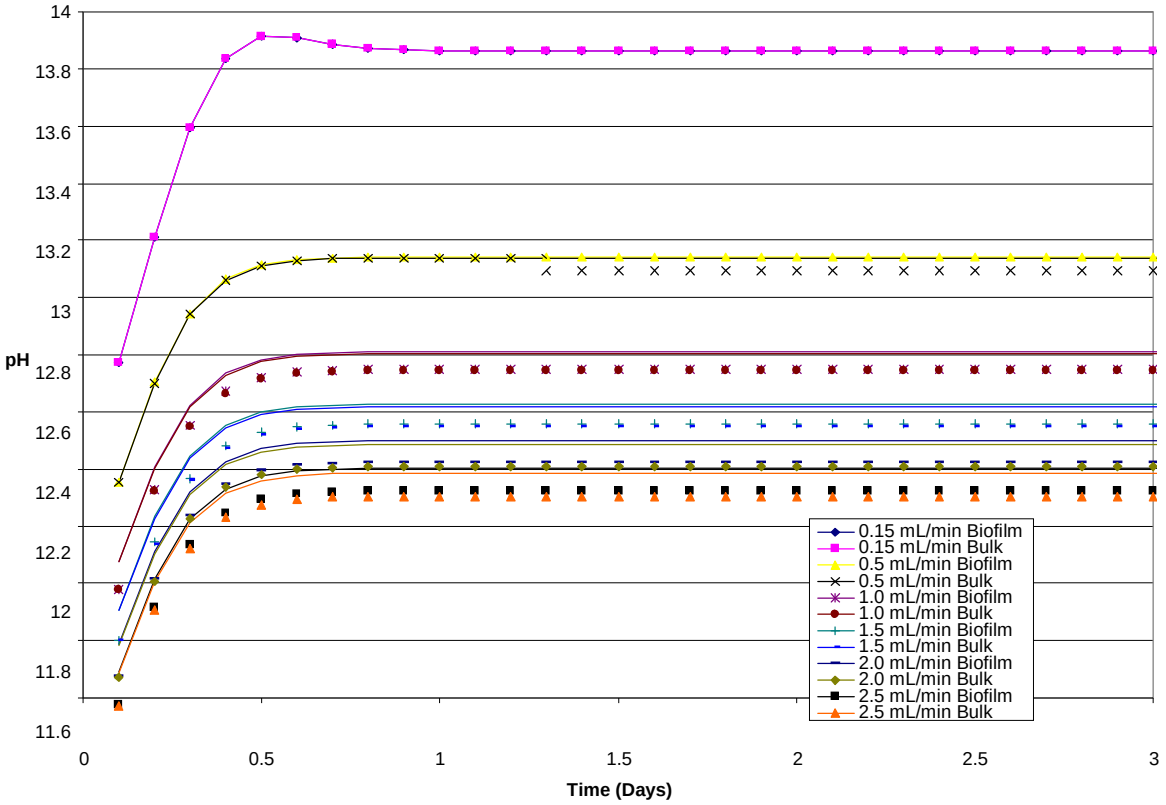

Figure 97: Overlay of pH changes in center of biofilm and bulk fluid for continuous flow column system.

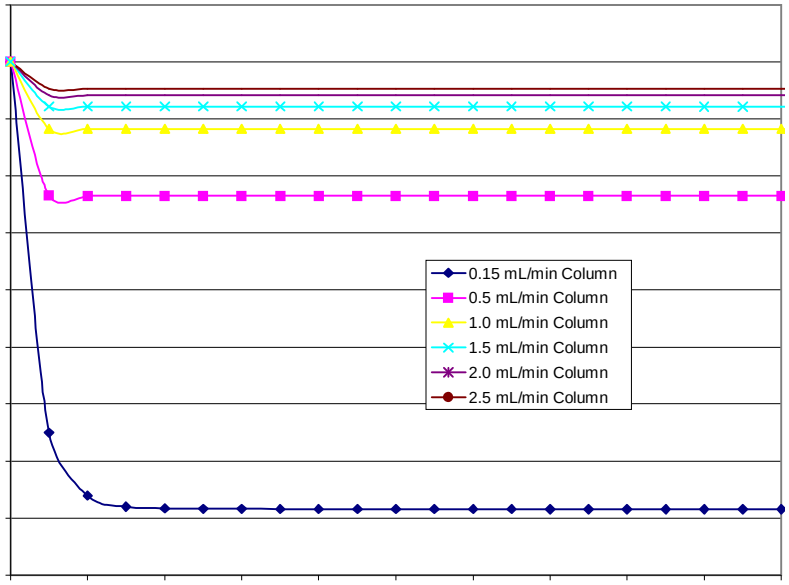

Figure 98: Free Calcium ion utilization in bulk fluid for column reactor system

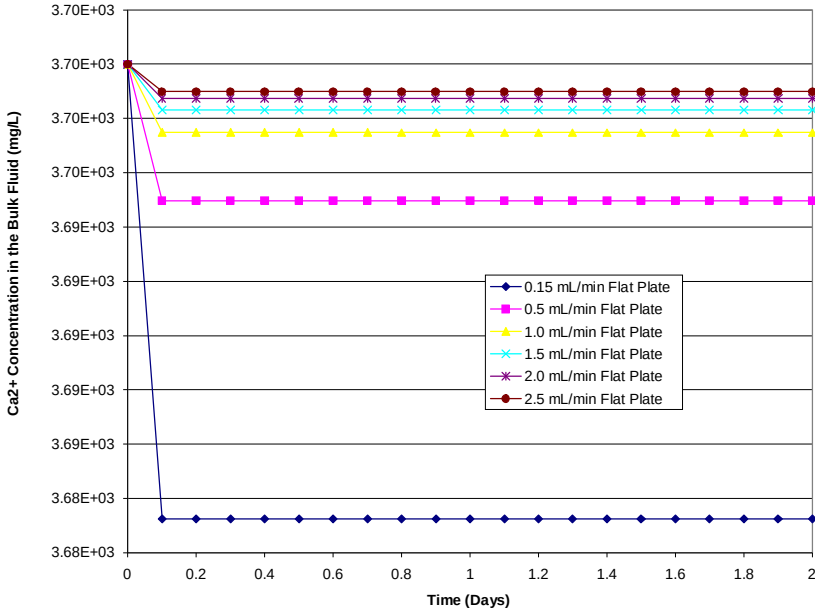

Figure 99: Free Calcium ion utilization in bulk fluid for flat plate reactor system

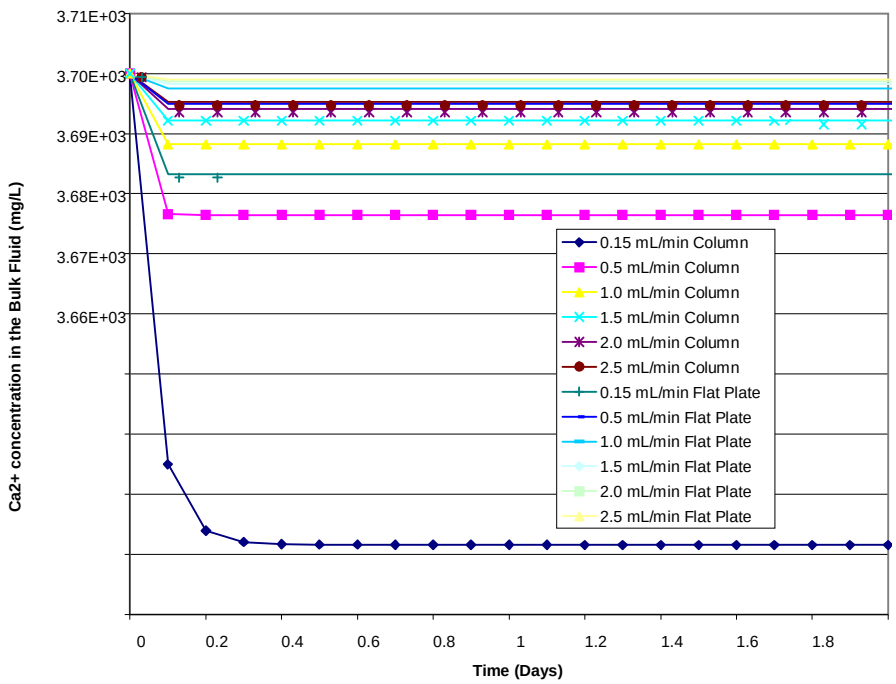

Figure 100: Overlay of free calcium ion utilization in bulk fluid for both systems.

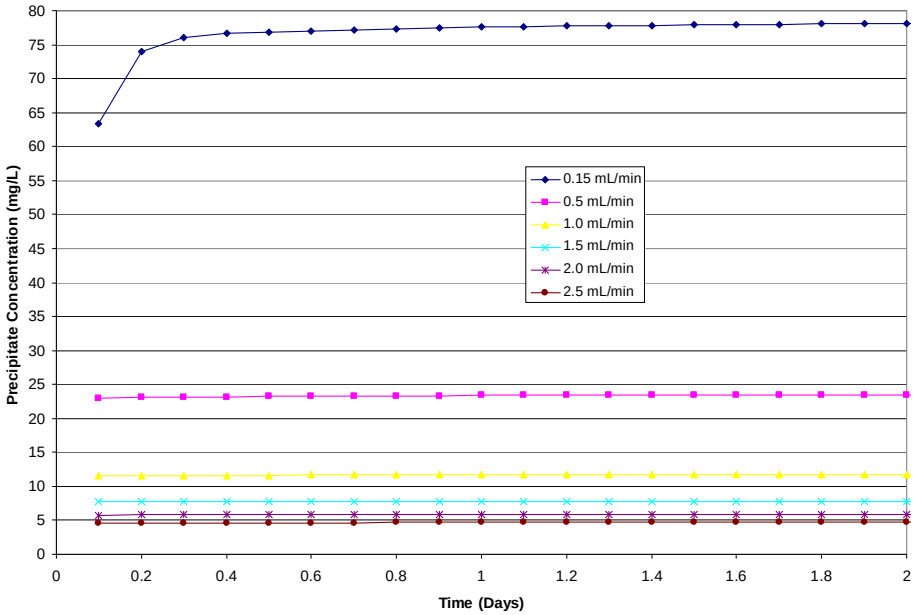

Figure 101: Precipitate concentration in the bulk fluid for column reactor system

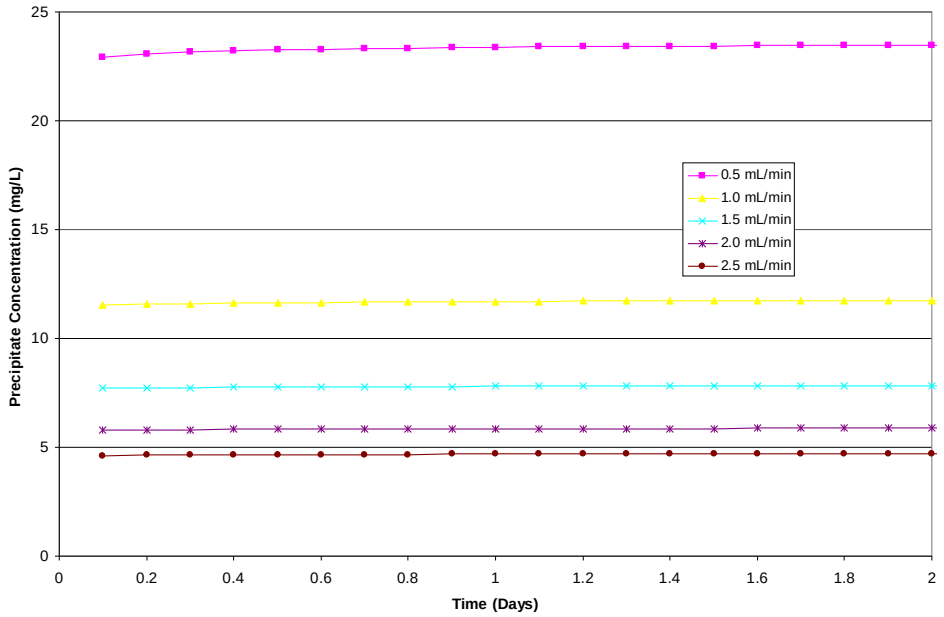

Figure 102: Precipitate concentration in the bulk fluid for flat plate reactor system

A steady state biofilm 59 µm thick was reached under the conditions described above in 1.2 days (Figure 93).

The pH in the center of the biofilm and in the bulk fluid increased until it reached a steady value at about 0.8 days. The pH in the biofilm and in the bulk fluid decreased with increasing flow rate (Figures 94 and 95). The pH in the biofilm and in the bulk appeared to be identical until the two graphs are overlaid (Figure 96). At higher flow rates, the pH in the biofilm was slightly higher than the pH in the bulk fluid. Since the biofilm reached steady state in less than two days, the graphs usually showed data only up until two days. In this way, the area of the graph where the changes occur was more easily visible.

Next, the utilization of free calcium ions in the bulk fluid was investigated. For the column system, there were less calcium ions in the bulk fluid at low flow rates than at higher flow rates (Figure 97). The results were the same for calcium utilization in the flat

plate reactor system: the lower the flow rate, the less calcium ions in the bulk fluid (Figure 98). When the two reactor systems were compared, it is found that there were more free calcium ions in solution at low flow rates in the flat plate reactor than in the column system (Figure 99). In each system, the free calcium concentration was higher at the start of the trial and less at the end, indicating that calcium was being precipitated. In the column system, the calcium concentration reached a steady value in about 0.4 days. In the flat plate reactor, the calcium concentration reached a steady value in 0.1 days.

Since it was apparent that calcium was being consumed in both systems, it was logical that the amount of precipitate formed in the bulk fluid would be investigated next. In the column system, at low flow rates, the precipitate concentration increased in the bulk fluid until it reached a steady value at about 0.8 days (Figure 100). At the higher flow rates, the precipitate remained at a constant steady value throughout the BAM trial, although the precipitate concentration in the bulk fluid decreased with increasing flow rate. The trends were the same in the flat plate reactor: the precipitate concentration decreased with increasing flow rate, although the concentration of precipitate throughout the trial remained relatively constant, even at the low flow rate (Figure 101). In comparing the two systems, it was found that the precipitate concentration in the bulk fluid in the column system was higher than the concentration in the flat plate system at every flow rate.

Discussion

The pH results obtained from this modeling project were expected. The pH results obtained in the lab follow the same trend. A gradual increase in pH is seen within the first day or two and then it remains fairly constant throughout the course of the experiment. The pH obtained from the lab experiments is usually not as high as what was seen with the BAM model, but an initial concentration of hydrogen ions was not specified, so this result is not as surprising. It was also expected that the pH in the biofilm would be higher at every flow rate because the reaction that increases the pH occurs intracellularly, not in the bulk fluid, and ions the diffuse out into the bulk fluid. This was only seen at the higher flow rates, indicating that the flow was so fast that the ions did not get the opportunity to make their way into the bulk fluid. At a slower flow rate, the media has more contact time with the biofilm, allowing for this diffusion to occur, and that is why there is no noticeable difference between the pH values in the biofilm and the bulk fluid at the 0.15 mL/min flow rate.

The result that there was less free calcium in the bulk fluid at lower flow rates was also not surprising. Once again, at a lower flow rate, the media has more contact time with the biofilm, allowing for more ions to diffuse into the biofilm and be utilized. At higher flow rates, the media slides past the biofilm faster and the ions can't diffuse into the biofilm as fast. The fact that not as much calcium is being utilized in the flat plate reactor system at the lower flow rate is probably due to the lower surface area to volume ratio. There is not as much area for the biofilm to grow on in the flat plate system, so there is not as much biofilm in the flat plate reactor as in the column reactor. It has been

seen that at higher flow rates not as much calcium is used and therefore it would be assumed that not as much precipitate is formed, which is what is seen in both reactor systems. There is more free calcium in the bulk fluid of the flat plate reactor and therefore less precipitate. This result makes sense with what was seen in the other trials.

Conclusions

The results of this modeling project indicate that the maximum calcium utilization and maximum precipitate formation occur at lower flow rates. At higher flow rates, the nutrients essential for biofilm growth and biomineralization cannot diffuse into the biofilm at the rate they are needed, reducing the bacteria's efficiency at plugging the reactors. The results obtained from the model confirm results obtained from actual lab experiments, and indicate that a continuous flow system might be more effective at plugging the column than a pulse flow system.

APPENDIX B

RAW DATA TABLES

Effluent Data

Table 19: Compiled effluent data for the first 1mm *S. pasteurii* column.

Day	Plate Counts (LOG CFU/mL)	stdev	OD600	stdev	pH	Flow Rate (mL/s)	Dissolved Calcium (mg/L)	Total Calcium (mg/L)	Ammonium-N (mg/L)	stdev	Volume exchanged (mL)
0			0.46		7.01						
1	8.62	0.05	0.31	0.01	9.43	1.58			10578	0	11.25
2			0.11	0.00	9.38	1.51			1666	0	8
3	8.21	0.21	0.09	0.00	9.36	1.76			4510	0	10.5
4	8.25		0.10	0.00	9.34	1.63			5333	0	10
5	8.67	0.05	0.10	0.00	9.27	1.56			5739	0	20
8	7.36	0.12	0.08	0.01	9.28	1.52	8	22	9194	0	12
9			0.08	0.00	9.35	1.57	14	24	9861	0	9.5
10	6.97	0.16	0.06	0.00	9.27	1.42			9780	0	11
11	6.68	0.14	0.05	0.00	9.32	1.57	8	19	9998	0	12.5
12	6.62	0.26	0.05	0.00	9.29	1.44			6974	0	7.75
14							12	81			8
15			0.10	0.01	9.18	1.78			7971	0	9
16	7.12	0.13	0.08	0.00	9.21	1.48			7772	0	9
17	7.49		0.10	0.00	9.35	1.60	13	24	9456	0	7.75
18	7.56	0.06	0.08	0.01	9.31	1.50			6662	0	7.5
19	7.10	0.10	0.08	0.00	9.39	1.47	9	54	7099	0	9.25
20	7.44	0.05	0.06	0.00	9.41	1.40	7	16	6518	0	7.25
22	7.32	0.03	0.06	0.00	9.38	1.42	8	24	8919	0	7.5
23	7.27	0.08	0.05	0.00	9.40	1.46	7	22	9275	0	7.25
24	7.10	0.24	0.26	0.02	9.26	1.55			8988	0	7.5
25	7.45	0.10	0.13	0.03	9.38	1.47					7.5
26	7.35	0.07	0.05	0.00	9.28	1.37			9848	0	8.25
29	7.38	0.03	0.07	0.04	9.17	1.52			11532	0	12.5
36			0.05	0.00	9.35	1.46			11832	0	7.5

Table 20: Complied effluent data for the second 1 mm *S. pasteurii* column.

Day	Plate Counts (LOG CFU/mL)	stdev	OD600	stdev	pH	Flow Rate (mL/s)	Dissolved Calcium (mg/L)	Total Calcium (mg/L)	Ammonium-N (mg/L)	stdev	Protein (mg/L)	stdev	Volume exchanged (mL)
0			0.39										11.25
1	8.84	0.03	0.28	0.00	9.32	1.50			5548	1742	153	5	8.5
2	7.79	0.07	0.13	0.00	9.62	1.52			9312	707	138	3	10.25
3	7.78	0.28	0.11	0.00	9.60	1.42			7908	992	130	5	9.25
4	7.91	0.16	0.11	0.00	9.69	1.47			9290	644	128	7	13
5	7.16	0.20	0.12	0.00	9.70	1.56			11058	975	132	6	10
8	8.17	0.08	0.14	0.00	9.66	1.47			11067	554	158	9	8.5
9	8.15	0.10	0.14	0.00	9.67	1.46	0	17	8351	1181	142	6	8
10			0.08	0.00	9.65	1.46			7818	2140	125	6	8.75
11			0.09	0.01	9.51	1.55	1	16	9015	2067	109	2	7.75
12	7.57	0.52	0.05	0.00	9.36	1.45			12455	1801	108	4	7.75
15			0.07	0.00	9.30	1.39	0	0	17506	2069	101	2	8
16	7.22	0.19	0.08	0.00	9.30	1.48			13512	2094	106	7	11.25
17	7.38	0.12	0.10	0.01	9.29	1.45			8364	333	135	5	8.25
18			0.08	0.00	9.36	1.48	6	10	11210	175	131	4	13.5
19			0.10	0.00	9.46				10802	617	140	11	11.25

Table 21: Compiled effluent data for third 1 mm *S. pasteurii* column.

Day	Plate Counts (LOG CFU/mL)	stdev	OD600	stdev	pH	Flow Rate (mL/s)	Dissolved Calcium (mg/L)	Total Calcium (mg/L)	Ammonium-N (mg/L)	stdev	Protein (mg/L)	stdev	Volume exchanged (mL)
0			0.40										11.75
1	8.91	0.17	0.26	0.02	9.35	1.53			6468	297	172	3	8
2	8.08	0.58	0.15	0.00	9.29	1.53			11033	397	114	2	7
3	7.83	0.09	0.12	0.00	9.30	1.50			10564	1428	117	10	7
4	8.36	0.06	0.14	0.00	9.45	1.50			9734	799	116	1	6.5
5	8.19	0.14	0.14	0.00	9.45	1.20			9925	1086	127	25	6.5
8	8.36	0.05	0.14	0.01	9.34	1.35	8	21	8370	252	125	7	7
9	8.35	0.11	0.15	0.00	9.42	1.38	8	15	7857	285	121	1	6.75
10	8.38	0.18	0.14	0.00	9.45	1.22			8393	2308	116	2	8
11	7.97	0.07	0.12	0.00	9.42	1.22			9204	805	118	5	7
12	7.56	0.17	0.11	0.00	9.37	1.04	8	16	9441	971	104	4	6.75
15	7.60	0.15	0.11	0.00	9.33	1.23	6	15	10740	983	103	4	6
16	7.31	0.23	0.09	0.00	9.25	1.04			10433	1332	93	2	7
17	7.25	0.03	0.08	0.00	9.30	1.06	35	14	10047	553	110	21	7.25
18	7.23	0.07	0.07	0.00	9.25	0.96	12	17	8719	1251	92	6	8
19	6.93	0.19	0.06	0.00	9.28	1.04	13	20	6354	2344	79	3	6.4
22						0.84							6.5
23						0.81							12.25
24						0.93							11.75

Table 22: Complied effluent data for first *B. sphaericus* #21776 column.

Day	Plate Counts (LOG CFU/mL)	stdev	OD600	stdev	pH	Flow Rate (mL/s)	Dissolved Calcium (mg/L)	Total Calcium (mg/L)	Ammonium-N (mg/L)	stdev	Protein (mg/L)	stdev	Volume exchanged (mL)
0													9
1	8.09	0.09	0.32	0.01	9.29	1.51			11987	814	191	7	6.75
2	7.76	0.09	0.13	0.00	9.32	1.51			7587	856	142	32	8.54
3	7.68	0.15	0.10	0.00	9.34	1.54			10761	439	123	3	8
4	6.34	0.23	0.10	0.00	9.29	1.56			10415	1583	116	7	4.5
5	6.75	0.18	0.12	0.00	9.23	1.49			9380	589	132	1	7.75
8	8.85	0.11	0.11	0.00	9.20	1.60			8750	81	122	2	8
9	7.79	0.12	0.11	0.01	9.32	1.89	300	300	11622	967	130	7	7.4
10			0.09	0.00	9.21	1.57			7004	6402	100	6	9
11			0.07	0.00	9.27	2.08			10799	1446	93	6	9
12	6.96	0.19	0.08	0.00	9.24	2.11	300	300	10465	1606	87	2	8.75
15	7.04	0.26	0.07	0.00	9.31	1.98			9524	1381	79	7	8.5
16	7.34	0.07	0.09	0.00	9.28	2.05			9461	313	82	4	8.5
17	7.30	0.12	0.07	0.00	9.27	2.09	350	300	10846	882	83	6	8.5
18	7.54	0.07	0.06	0.00	9.29	2.09			10247	600	79	4	8.5
19	7.73	0.08	0.07	0.00	9.34	2.08			9692	610	69	13	8
20									10559	732			8.5
22	7.18	0.08	0.06	0.00	9.30	1.91	300	300	10247	802	85	6	8.5
23	7.27	0.12	0.06	0.00	9.17	2.02			8607	611	64	3	9
24	7.16	0.12	0.06	0.00	9.14	2.06			8722	219	63	5	9.25
25	7.15	0.08	0.06	0.00	9.31	2.09	300	300			66	3	7.75
26						2.08							8.75
29						1.88							7.75
30						1.89							8.75
34						1.71							9.25
35						2.01							8.75
36						2.01							9
37						2.02							6.75

Table 23: Compiled effluent data for second *B. sphaericus* #21776 column.

Day	Plate Counts (LOG CFU/mL)	stdev	OD600	stdev	pH	Flow Rate (mL/s)	Dissolved Calcium (mg/L)	Total Calcium (mg/L)	Ammonium-N (mg/L)	stdev	Protein (mg/L)	stdev	Volume exchanged (mL)
0			0.39										8.75
1	8.58	0.05	0.31	0.01	9.32	1.46			7275	467	188	2	9
2	7.92	0.14	0.12	0.00	9.64	1.74			9502	775	126	3	9.75
3	7.64	0.05	0.11	0.00	9.61	1.85			10581	911	128	3	8.5
4	7.51	0.31	0.10	0.00	9.69	1.63			8650	565	124	7	8.5
5	7.34	0.23	0.09	0.00	9.70	1.66			10029	1211	116	7	8.25
8	7.59	0.20	0.09	0.00	9.65	1.67			11479	1156	111	13	8.75
9	7.73	0.18	0.09	0.00	9.67	1.68	0	9	9156	1331	123	3	8
10			0.08	0.00	9.63	1.61			10830	984	115	3	7.75
11			0.09	0.00	9.54	1.91	0	4	9944	883	117	32	8
12	7.65	0.11	0.05	0.00	9.37	1.85			13858	725	97	6	7.75
15			0.07	0.00	9.32	1.75	0	0	15417	2397	100	39	8.5
16	7.39	0.07	0.07	0.00	9.30	1.95			13693	1805	98	4	7.25
17	7.44	0.09	0.08	0.00	9.35	1.79			8479	884	98	3	15
18			0.07	0.00	9.42	1.95	7	15	9951	828	91	5	7.75
19			0.08	0.00	9.47				11762	963	124	1	8.75

Table 24: Compiled effluent data for first *B. sphaericus* #21787 column.

Day	Plate Counts (LOG CFU/mL)	stdev	OD600	stdev	pH	Flow Rate (mL/s)	Dissolved Calcium (mg/L)	Total Calcium (mg/L)	Ammonium-N (mg/L)	stdev	Protein (mg/L)	stdev	Volume exchanged (mL)
0					5.94								7.5
1	9.43	0.11	0.33	0.01	9.34	1.42			10200	1094	173	8	15
2	8.81	0.16	0.09	0.00	9.04	1.71			10824	937	92	6	11
3	8.05	0.16	0.05	0.00	8.73	1.69			4491	185	43	2	8
4	7.79	0.63	0.05	0.00	8.82	1.60			4279	658	45	3	8
5	6.95	0.14	0.05	0.00	8.73	1.64			4104	149	42	3	7.75
8	6.65	0.24	0.04	0.00	9.02	1.64			5878	833	39	3	8
9	6.62	0.09	0.04	0.00	9.02	1.63	350	400	6200	225	42	3	7.2
10	5.74	0.11	0.04	0.00	8.87	1.59			3830	3643	27	5	7.75
11	6.91	0.15	0.04	0.00	8.58	1.62			6907	1432	21	4	7.5
12	6.64	0.28	0.04	0.00	8.53	1.66	600	600	5180	250	15	1	8.5
15	6.49	0.12	0.04	0.00	8.93	1.61			6097	769	23	2	7.75
16	6.28	0.17	0.04	0.00	8.88	1.65			5342	137	27	2	9.5
17	6.16	0.22	0.04	0.00	8.86	1.71	350	350	6596	965	32	0	7.5
18	6.06	0.15	0.04	0.00	8.68	1.67			5171	645	23	3	7.75
19	6.36	0.10	0.04	0.00	8.69	1.70			5626	180	20	2	8.75
20	6.05	0.14											8
22	7.05	0.21	0.04	0.00	8.97	1.55	450	350	6056	814	29	1	7.75
23			0.04	0.00	9.07	1.74			7425	1327	48	2	7.5
24			0.04	0.00	9.01	1.72			5454	203	38	2	7.5
25			0.04	0.00	8.94	1.69	350	350	3945	187	34	3	7.5
26						1.69							7.5
29						1.55							7
30						1.64							6.75
34						1.33							7.5
35						1.46							7.75
36						1.62							7.5
37						1.63							15

Table 25: Compiled effluent data for second *B. sphaericus* #21787 column.

Day	Plate Counts (LOG CFU/mL)	stdev	OD600	stdev	pH	Flow Rate (mL/s)	Dissolved Calcium (mg/L)	Total Calcium (mg/L)	Ammonium-N (mg/L)	stdev	Protein (mg/L)	stdev	Volume exchanged (mL)
0			0.36										9.75
1			0.30	0.00	9.29	1.28			6465	902	136	2	10
2	8.55	0.06	0.10	0.00	9.36	1.41			6811	235	90	3	9.25
3	8.31	0.05	0.12	0.00	9.60	1.40			11313	692	114	3	14.25
4	7.91	0.09	0.10	0.00	9.64	1.45			8510	297	110	7	9.25
5	7.39	0.27	0.12	0.00	9.70	1.38			11154	677	118	7	7.5
8	7.83	0.05	0.11	0.00	9.63	1.23			10075	937	113	13	10.5
9	7.85	0.23	0.10	0.00	9.66	1.37	12	22	7883	654	112	3	7.75
10			0.08	0.00	9.62	1.37			9090	648	103	3	8.75
11			0.09	0.00	9.53	1.48	0	3	10188	1694	118	32	8.75
12	7.77	0.12	0.06	0.00	9.36	1.46			12211	1433	87	6	7.25
15			0.07	0.00	9.30	1.34	0	0	12261	469	116	39	8.5
16	7.42	0.04	0.08	0.00	9.33	1.47			12997	617	97	4	8.75
17	7.54	0.36	0.07	0.00	9.31	1.45			9461	829	104	3	9
18			0.07	0.00	9.37	1.38	8	7	9461	546	113	5	15
19			0.06	0.00	9.43				10082	1531	107	1	9.75

Table 26: Compiled effluent data for only *B. subtilis* trial.

Day	Plate Counts (LOG CFU/mL)	stdev	OD600	stdev	pH	Flow Rate (mL/s)	Dissolved Calcium (mg/L)	Total Calcium (mg/L)	Ammonium-N (mg/L)	stdev	Volume exchanged (mL)
0			0.42		7.02						7.5
1	5.59	0.13	0.11	0.00	7.23	1.18			3581	146	11
2	5.83	0.26	0.05	0.00	7.38	1.62			76	60	8.5
3	6.08	0.10	0.04	0.00	7.36	1.66			1292	125	8.75
4					7.41	1.65			1442	78	17
5	5.94	0.06	0.04	0.00	7.35	1.87			1529	39	10
8	6.10	0.10	0.04	0.00	7.27	1.67	711	676	3537	583	8.25
9	6.18	0.16	0.05	0.00	7.51	1.49	766	788	3331	404	7.5
10	6.11	0.11	0.05	0.00	7.70	1.60			2583	22	7.5
11					7.74	1.56	766	786	2820	515	8
12	6.99	0.09	0.06	0.00	7.77	1.63			2171	244	8.5
14							889	913			8
15			0.06	0.00	7.60	1.69			1984	92	8
16			0.05	0.00	7.68	1.64			1716	742	7.75
17			0.05	0.00	7.66	1.66	789	842	4554	2072	7.25
18	6.70	0.12	0.05	0.00	7.67	1.58			2458	1218	11
19	7.34		0.05	0.00	7.72	1.58	750	864	2009	32	8
20	6.30	0.21	0.04	0.00	7.77	1.59	776	915	2028	197	7.5
22	6.84	0.32	0.05	0.00	7.80	1.56	787	1015	2408	138	8
23	6.97	0.11	0.04	0.00	7.80	1.64	779	891	2234	37	7.5
24	6.23	0.28	0.04	0.00	7.62	1.58			3213	1178	10
25	6.89	0.23	0.05	0.00	7.82	1.63					15.5
26	7.09	0.08	0.05	0.00	7.72	1.61			3213	202	7.5
29	6.69	0.09	0.05	0.03	7.77	1.55			3687	298	9
36					7.59	1.52			3550	400	7.5

Table 27: Compiled effluent data for first 0.1 mm *S. pasteurii* column

Day	Plate Counts (LOG CFU/mL)	stdev	OD600	stdev	pH	Flow Rate (mL/s)	Dissolved Calcium (mg/L)	Total Calcium (mg/L)	Ammonium-N (mg/L)	stdev	Protein (mg/L)	stdev	Volume exchanged (mL)
0			0.40										8.5
1	8.81	0.25	0.33	0.02	9.41	0.05			7783	1001	193	4	9
2	7.63	0.24	0.11	0.00	9.39	0.05			10092	297	93	9	8.5
3	7.79	0.03	0.12	0.00	9.45	0.05			10173	853	108	1	8.75
4	7.87	0.16	0.10	0.00	9.45	0.05			9926	1312	98	4	8.5
5	7.23	0.17	0.08	0.00	9.45	0.05			8636	818	92	1	8
8	7.60	0.17	0.08	0.00	9.38	0.04	8	18	10466	1252	87	4	8.5
9	7.15	0.17	0.06	0.00	9.45	0.03	10	24	9483	1096	89	2	8.75
10	6.55	0.10	0.05	0.00	9.45	0.01	7	11	8983	403	108	15	8.5
11	6.28	0.27	0.05	0.00	9.42	0.00	6	11	10624	386	83	5	5
12						0.00							8.5

Table 28: Compiled effluent data for second 0.1 mm *S. pasteurii* column.

Day	Plate Counts (LOG CFU/mL)	stdev	OD600	stdev	pH	Flow Rate (mL/s)	Dissolved Calcium (mg/L)	Total Calcium (mg/L)	Ammonium-N (mg/L)	stdev	Protein (mg/L)	stdev	Volume exchanged (mL)
0			0.40										9
1	9.10	0.10	0.31	0.02	9.41	0.05			7052	1546	198	22	8
2	7.95	0.13	0.13	0.00	9.39	0.05			13570	1300	96	5	7.25
3	7.94	0.13	0.13	0.00	9.45	0.05			10605	805	99	2	7
4	7.90	0.09	0.14	0.00	9.45	0.04			9908	734	96	3	6.5
5	7.93	0.12	0.12	0.00	9.42	0.05			11661	1501	106	1	6.5
8	7.82	0.19	0.11	0.01	9.33	0.04	7	11	10144	141	105	3	7
9	7.64	0.13	0.10	0.00	9.41	0.05	9	19	11524	1601	103	2	7.5
10	7.61	0.13	0.11	0.00	9.43	0.04			9805	602	109	5	7.5
11	7.09	0.07	0.08	0.00	9.44	0.02			14278	2022	88	3	7.75
12	6.93	0.20	0.06	0.00	9.41	0.03	7	12	9553	409	93	12	7
15	7.27	0.20	0.08	0.00	9.42	0.03	7	11	12072	145	88	7	7
16	6.78	0.15	0.06	0.00	9.32	0.02			10612	824	140	93	6.5
17	6.81	0.10	0.06	0.00	9.30	0.01	6	12	10504	1249	128	49	6.5
18	6.86	0.24	0.06	0.00	9.30	0.01	13	39	7481	473	84	4	6.75
19	7.73	0.28	0.05	0.00	9.24	0.00	14	17	6811	2236	65	15	6.2
22						0.00							6.5
23						0.01							6.5
24						0.00							9

Table 29: Compiled effluent data for first 1 mm control column.

Day	OD600	stdev	pH	Flow Rate (mL/s)	Dissolved Calcium (mg/L)	Total Calcium (mg/L)	Ammonium-N (mg/L)	stdev	Volume exchanged (mL)
0			7.13						10.75
1	0.04	0.00	7.02	1.42			6381	0	9
2	0.04	0.00	7.79	1.54			4298	0	10.5
3	0.04	0.00	7.70	1.54			3949	0	8.5
4	0.04	0.00	7.63	1.46			1885	0	14
5	0.04	0.00	7.61	1.64			2645	0	7
8	0.04	0.00	6.73	1.21			5171	0	8.5
9	0.04	0.00	7.36	1.52	776	943	4685	0	9.5
10	0.04	0.00	7.56	1.52			2271	0	10.5
11	0.04	0.00	7.58	1.47			4223	0	7.5
12	0.04	0.00	7.54	1.40			2365	0	7.8
14					901	1114			7.25
15	0.04	0.00	7.36	1.54			1760	0	7.5
16	0.04	0.00	7.60	1.47			3824	0	8.75
17	0.04	0.00	7.62	1.44	777	1005	2371	0	9
18	0.04	0.00	7.62	1.52			3157	0	8
19	0.04	0.00	7.70	1.49	767	994	3618	0	10.5
20	0.04	0.00	7.65	1.48	773	959	2932	0	8.25
22	0.04	0.00	7.54	1.39	820	991	4205	0	8.25
23	0.04	0.00	7.61	1.52	803	967	4997	0	9.8
24	0.04	0.00	7.44	1.48			3799	0	12
25	0.04	0.00	7.78	1.60					12
26	0.04	0.00	7.67	1.57			4604	0	11.5
29	0.04	0.03	7.63	1.50			5838	0	9.5
36	0.04	0.00	7.85	1.49			5053	0	15

Table 30: Compiled effluent for second 1 mm control column.

Day	OD600	stdev	pH	Flow Rate (mL/s)	Dissolved Calcium (mg/L)	Total Calcium (mg/L)	Ammonium-N (mg/L)	stdev	Protein (mg/L)	stdev	Volume exchanged (mL)
0											7.25
1	0.04	0.00	7.42	1.15			4354	462	30	0	7.5
2	0.04	0.00	7.47	1.59			6717	573	49	3	7.75
3	0.04	0.00	7.70	1.72			2848	57	54	2	7.5
4	0.04	0.00	8.06	1.64			3075	44	56	2	9
5	0.04	0.00	8.28	1.64			3275	126	53	2	7
8	0.04	0.00	8.78	1.53			6714	370	55	2	7.25
9	0.04	0.00	8.60	1.52	300	400	6480	276	50	2	7
10	0.04	0.00	8.48	1.59			4803	1627	52	2	8
11	0.04	0.00	8.53	1.73			4862	704	35	1	8
12	0.04	0.00	8.11	1.68	1200	1250	3814	408	33	1	7.25
15	0.04	0.00	9.11	1.45			4117	849	59	2	7.5
16	0.13	0.00	8.70	1.59			4254	868	42	2	7.5
17	0.04	0.00	8.51	1.61	1350	1300	5398	1679	34	1	9.5
18	0.04	0.00	8.50	1.66			3053	154	34	1	7.5
19	0.04	0.00	8.60	1.73			6733	792	40	1	7.25
20							3141	62			8
22				1.60	1300	1300	6568	1648			7.25
23				1.66			3063	421			7.75
24				1.55			3287	239			7.75
25				1.69	1300	1300					7.5
26				1.78							8.5
29				1.60							6.75
30				1.68							7.75
34				1.45							8
35				1.67							7.25
36				1.66							7.25
37				1.66							7.5

Table 31: Compiled effluent data for third 1 mm control column.

Day	OD600	stdev	pH	Flow Rate (mL/s)	Dissolved Calcium (mg/L)	Total Calcium (mg/L)	Ammonium-N (mg/L)	stdev	Protein (mg/L)	stdev	Volume exchanged (mL)
0											10.5
1	0.04	0.00	8.51	1.01			1681	273	24	2	10
2	0.04	0.00	8.20	1.04			3265	398	21	4	9.5
3	0.04	0.00	7.61	1.07			3615	372	34	3	9
4	0.04	0.00	7.49	1.01			5164	167	42	4	9
5	0.04	0.00	7.32	0.94			3758	163	46	1	9.5
8	0.04	0.00	7.44	0.98			7303	860	39	1	8.75
9	0.05	0.00	7.39	1.03	6	14	6764	1786	46	9	8
10	0.11	0.00	7.61	1.04			3446	743	83	58	8.25
11	0.08	0.00	7.84	1.06	697	668	5114	125	49	38	7.75
12	0.08	0.00	8.00	1.07	423	376	6611	835	64	57	7.5
15	0.06	0.00	8.07	1.00			12186	2518	38	38	9.25
16	0.07	0.00	8.06	1.00	273	300	11853	1894	24	1	9
17	0.07	0.00	8.08	0.99			5036	769	46	30	9.25
18	0.08	0.00	8.18	1.10	536	515	4107	342	58	36	7.75
19	0.09	0.00	8.17				8675	550	39	6	10.5

Table 32: Compiled effluent data for 0.1 mm control column.

Day	OD600	stdev	pH	Flow Rate (mL/s)	Dissolved Calcium (mg/L)	Total Calcium (mg/L)	Ammonium-N (mg/L)	stdev	Protein (mg/L)	stdev	Volume exchanged (mL)
0											9
1	0.04	0.00	8.51	0.05			3863	307	24	2	7.75
2	0.04	0.00	8.20	0.05			2067	224	21	4	8
3	0.04	0.00	7.61	0.05			2708	245	34	3	6.8
4	0.04	0.00	7.49	0.05			2399	281	42	4	7
5	0.04	0.00	7.32	0.05			2529	93	46	1	6.25
8	0.04	0.00	7.44	0.05	19	34	2263	32	39	1	7.5
9	0.05	0.00	7.39	0.06	16	23	2646	175	46	9	7.5
10	0.11	0.00	7.61	0.05			1897	246	83	58	7.5
11	0.08	0.00	7.84	0.05			2153	267	49	38	8
12	0.08	0.00	8.00	0.05	996	972	1966	319	64	57	7
15	0.06	0.00	8.07	0.05	1007	970	2759	64	38	38	7
16	0.07	0.00	8.06	0.05			2361	258	24	1	7.25
17	0.07	0.00	8.08	0.04	984	957	2228	414	46	30	7.5
18	0.08	0.00	8.18	0.05	928	953	2035	505	58	36	7.25
19	0.09	0.00	8.17	0.05	993	951	2340	191	39	6	6.5
22				0.04							7.25
23				0.04							7.5
24				0.04							9

Destructive Sampling Data

Table 33: Compiled destructive sampling data for all 1 mm *S. pasteurii* columns.

***S. pasteurii* 1 mm #1**

Calcium

	Calcium (mg/L)	Total Volume (L)	Calcium (mg)	gr bead	Calcium (mg/gr bead)
Top	216	0.002	0.432	0.28	1.54
Middle	105	0.002	0.210	0.06	3.5
Bottom	75	0.002	0.149	0.38	0.4

Protein

	Protein (mg/gr bead)
Top	0.025
Middle	1.7
Bottom	0.069

Plate Counts

	Log CFU/gr bead
Top	**
Middle	7.64
Bottom	7.26

** There is no data for this section due to an unreadable agar plate

Direct Counts

	Log Total cells/gr bead
Top	15
Middle	9.8
Bottom	7.4

Graphing Data

	Top	Middle	Bottom	
Plate Counts		7.64	7.26	Log CFU/gr bead
Plate Count Std Dev		0.054	0.15	
Direct Counts	15	9.83	7.36	log total cells/gr bd
S. pasteurii Calcium #1	1.54	3.5	0.4	mg/g bd
Protein	0.025	1.7	0.069	mg/g bd
Protein Std Dev	0.0	2.5	0.0	

S. pasteurii 1 mm #2

Calcium

	Calcium (mg/L)	Total Volume (L)	Calcium (mg)	gr bead	Calcium (mg/gr bead)
Top	36	0.002	0.0718	0.62	0.12
Middle	46	0.002	0.0930	0.93	0.10
Bottom	36	0.002	0.0722	1.02	0.07

Protein

	Protein (mg/gr bead)
Top	0.057
Middle	0.038
Bottom	0.081

Plate Counts

	Log CFU/gr bead
Top	7.9
Middle	7.93
Bottom	7.63

Direct Counts

	Log Total cells/gr bead
Top	10
Middle	9.4
Bottom	9.3

Graphing Data

	Top	Middle	Bottom	
Plate Counts	7.9	7.93	7.63	Log CFU/gr bead
Plate Count Std Dev	0.060	0.077	0.091	
Direct Counts	10	9.4	9.3	log total cells/gr bd
DC Std Dev	0.27	0.19	0.11	
S. pasteurii Calcium #2	0.12	0.10	0.07	mg/gr bd
Protein	0.057	0.038	0.081	mg/gr bd
Protein Std Dev	0.001	0.006	0.004	

S. pasteurii 1 mm #3

Calcium

	Calcium (mg/L)	Total Volume (L)	Calcium (mg)	gr bead	Calcium (mg/gr bead)
Top	93	0.002	0.185	0.77	0.24
Middle	103	0.002	0.205	0.92	0.22
Bottom	61	0.002	0.122	0.76	0.16

Protein

	Protein (mg/gr bead)
Top	0.10
Middle	0.065
Bottom	0.074

Plate Counts

	Log CFU/gr bead
Top	8.102
Middle	7.8
Bottom	8.04

Direct Counts

	Log Total cells/gr bead
Top	10
Middle	9.2
Bottom	9.2

Graphing Data

	Top	Middle	Bottom	
Plate Counts	8.102	7.8	8.04	Log CFU/gr bead
Plate Count Std Dev	0.05	0.15	0.12	
Direct Counts	10	9.2	9.2	log total cells/gr bd
DC std dev	0.15	0.068	0.14	
S. pasteurii Calcium #3	0.24	0.22	0.16	mg/gr bd
Protein	0.10	0.065	0.074	mg/gr bd
Protein Std Dev	0.008	0.047	0.013	

Table 34: Compiled destructive sampling data for both *B. sphaericus* #21776 columns.

***B. sphaericus* #21776 #1**

Calcium

	Calcium (mg/L)	Total Volume (L)	Calcium (mg)	gr bead	Calcium (mg/gr bead)
Top	95	0.002	0.191	0.48	0.40
Middle	48	0.002	0.096	0.48	0.20
Bottom	36	0.002	0.072	0.8	0.090

Protein

	Protein (mg/gr bead)
Top	0.071
Middle	0.12
Bottom	0.18

Plate Counts

	Log CFU/gr bead
Top	7.26
Middle	7.43
Bottom	7.44

Direct Counts

	Log Total cells/gr bead
Top	11
Middle	9.7
Bottom	9.5

Graphing Data

	Top	Middle	Bottom	
Plate Counts	7.26	7.43	7.44	Log CFU/gr bead
Plate Count Std Dev	0.12	0.066	0.084	
Direct Counts	11	9.7	9.5	log total cells/gr bd
DC Std dev	0.18	0.15	0.13	
B. sphaericus #21776 Calcium #1	0.40	0.20	0.090	mg/gr bd
Protein	0.071	0.12	0.18	mg/gr bd
Protein Std Dev	0.00675	0.072	0.080	

B. sphaericus #21776 #2

Calcium

	Calcium (mg/L)	Total Volume (L)	Calcium (mg)	gr bead	Calcium (mg/gr bead)
Top	115	0.002	0.231	0.83	0.28
Middle	94	0.002	0.188	0.7	0.27
Bottom	70	0.002	0.140	0.6	0.23

Protein

	Protein (mg/gr bead)
Top	0.047
Middle	0.042
Bottom	0.056

Plate Counts

	Log CFU/gr bead
Top	6.8
Middle	8.24
Bottom	7.49

Direct Counts

	Log Total cells/gr bead
Top	9.1
Middle	9.1
Bottom	9.2

Graphing Data

	Top	Middle	Bottom	
Plate Counts	6.8	8.24	7.49	Log CFU/gr bead
Plate Count Std Dev	0.1	0.101	0.22	
Direct Counts	9.1	9.1	9.2	log total cells/gr bd
DC Std dev	0.10	0.24	0.25	
B. sphaericus #21776 Calcium #2	0.28	0.27	0.23	mg/gr bd
Protein	0.047	0.042	0.056	mg/gr bd
Protein Std Dev	0.00539	0.00153	0.00034	

Table 35: Compiled destructive sampling data for both *B. sphaericus* #21787 columns.

***B. sphaericus* #21787 #1**

Calcium

	Calcium (mg/L)	Total Volume (L)	Calcium (mg)	gr bead	Calcium (mg/gr bead)
Top	780	0.002	1.56	0.93	1.7
Middle	710	0.002	1.42	0.86	1.7
Bottom	715	0.002	1.43	1.46	0.98

Protein

	Protein (mg/gr bead)
Top	0.14
Middle	0.34
Bottom	0.16

Plate Counts

	Log CFU/gr bead
Top	7.77
Middle	7.9
Bottom	7.79

Direct Counts

	Log Total cells/gr bead
Top	9.9
Middle	9.3
Bottom	9.2

Graphing Data

	Top	Middle	Bottom	
Plate Counts	7.77	7.9	7.79	Log CFU/gr bead
Plate Count Std Dev	0.082	0.11	0.098	
Direct Counts	9.9	9.3	9.2	log total cells/gr bd
DC Std Dev	0.20	0.08	0.11	
B. sphaericus #21787 Calcium #1	1.7	1.7	0.98	mg/gr bd
Protein	0.14	0.34	0.16	mg/gr bd
Protein Std Dev	0.094	0.14	0.053	

B. sphaericus #21787 #2

Calcium

	Calcium (mg/L)	Total Volume (L)	Calcium (mg)	gr bead	Calcium (mg/gr bead)
Top	116	0.002	0.232	0.77	0.30
Middle	79	0.002	0.158	0.75	0.21
Bottom	69	0.002	0.139	0.77	0.18

Protein

	Protein (mg/gr bead)
Top	0.034
Middle	0.042
Bottom	0.061

Plate Counts

	Log CFU/gr bead
Top	6.71
Middle	7.01
Bottom	7.53

Direct Counts

	Log Total cells/gr bead
Top	10
Middle	9.3
Bottom	9.3

Graphing Data

	Top	Middle	Bottom	
Plate Counts	6.71	7.01	7.53	Log CFU/gr bead
Plate Count Std Dev	0.13	0.17	0.14	
Direct Counts	10	9.3	9.3	log total cells/gr bd
DC Std Dev	0.089	0.10	0.085	
B. sphaericus #21787 Calcium #2	0.30	0.21	0.18	mg/gr bd
Protein	0.034	0.042	0.061	mg/gr bd
Protein Std Dev	0.00303	0.00390	0.00182	

Table 36: Compiled destructive sampling data for both 0.1 mm *S. pasteurii* columns.

***S. pasteurii* 0.1 mm #1**

Calcium

	Calcium (mg/L)	Total Volume (L)	Calcium (mg)	gr bead	Calcium (mg/gr bead)
Top	414	0.002	0.828	0.73	1.1
Middle	148	0.002	0.296	0.74	0.40
Bottom	79	0.002	0.158	0.42	0.38

Protein

	Protein (mg/gr bead)
Top	0.10
Middle	0.11
Bottom	0.15

Plate Counts

	Log CFU/gr bead
Top	5.79
Middle	5.39
Bottom	**

** There is no data for this section due to an unreadable agar plate

Direct Counts

	Log Total cells/gr bead
Top	10
Middle	9.1
Bottom	9.5

Graphing Data

	Top	Middle	Bottom	
0.1 #1 Plate Counts	5.79	5.39		Log CFU/gr bead
Plate Count Std Dev	0.053	0.3		
0.1 #1 Direct Counts	10	9.1	9.5	log total cells/gr bd
DC std dev	0.268	0.201	0.252	
0.1 #1 Calcium	1.1	0.40	0.38	mg/gr bd
0.1 #1Protein	0.10	0.11	0.15	mg/gr bd
Protein Std Dev	0.013	0.009	0.104	

S. pasteurii 0.1 mm #2

Calcium

	Calcium (mg/L)	Total Volume (L)	Calcium (mg)	gr bead	Calcium (mg/gr bead)
Top	97	0.002	0.194	1.16	0.17
Middle	67	0.002	0.133	1.11	0.12
Bottom	62	0.002	0.124	1.16	0.11

Protein

	Protein (mg/gr bead)
Top	0.17
Middle	0.094
Bottom	0.14

Plate Counts

	Log CFU/gr bead
Top	9.23
Middle	7.62
Bottom	8.34

Direct Counts

	Log Total cells/gr bead
Top	11
Middle	9.4
Bottom	9.1

Graphing Data

	Top	Middle	Bottom	
0.1 #2 Plate Counts	9.23	7.62	8.34	Log CFU/gr bead
Plate Count Std Dev	0.13	0.24	0.13	
0.1 #2 Direct Counts	11	9.4	9.1	log total cells/gr bd
DC std dev	0.12	0.0738	0.0779	
0.1 #2 Calcium	0.17	0.12	0.11	mg/gr bd
0.1 #2 Protein	0.17	0.094	0.14	mg/gr bd
Protein Std Dev	0.00462	0.0526	0.0209	

Table 37: Compiled destructive sampling data for all control columns.

Control #1 (1 mm bead pack)

Calcium

	Control Calcium (mg/L)	Total Volume (L)	Calcium (mg)	gr bead	Calcium (mg/gr bead)
Top	5	0.002	0.0095	0.12	0.079
Middle	7	0.002	0.0141	0.1	0.14
Bottom	15	0.002	0.0294	0.21	0.14

Protein

	Protein (mg/gr bead)
Top	0.036
Middle	0.32
Bottom	0.13

Graphing Data

	Top	Middle	Bottom
Control Calcium #1	0.079	0.14	0.14
Control Protein	0.036	0.32	0.13
Protein Std dev	0.014	0.47	0.20

Control #2 (1 mm bead pack)

Calcium

	Control Calcium (mg/L)	Total Volume (L)	Calcium (mg)	gr bead	Calcium (mg/gr bead)
Top	40	0.002	0.079	0.69	0.11
Middle	40	0.002	0.081	1.19	0.068
Bottom	212	0.002	0.424	0.89	0.48

Protein

	Protein (mg/gr bead)
Top	0.29
Middle	0.069
Bottom	0.15

Graphing Data

	Top	Middle	Bottom
Control Calcium #1	0.11	0.068	0.48
Control Protein	0.29	0.069	0.15
Protein Std dev	0.061	0.0059	0.17

Control #3 (1 mm bead pack)

Calcium

	Control Calcium (mg/L)	Total Volume (L)	Calcium (mg)	gr bead	Calcium (mg/gr bead)
Top	319	0.002	0.638	0.71	0.90
Middle	254	0.002	0.508	0.58	0.88
Bottom	189	0.002	0.377	0.59	0.64

Protein

	Protein (mg/gr bead)
Top	0.041
Middle	0.051
Bottom	0.073

Graphing Data

	Top	Middle	Bottom
Control Calcium #3	0.90	0.88	0.64
Control Protein	0.041	0.051	0.073
Protein Std dev	0.0048	0.0012	0.019

Control #4 (0.1 mm beadpack)

Calcium

	Control Calcium (mg/L)	Total Volume (L)	Calcium (mg)	gr bead	Calcium (mg/gr bead)
Top	52	0.002	0.103	0.82	0.13
Middle	193	0.002	0.386	0.97	0.40
Bottom	33	0.002	0.066	0.46	0.14

Protein

	Protein (mg/gr bead)
Top	0.16
Middle	0.087
Bottom	0.042

Graphing Data

	Top	Middle	Bottom
Control Calcium #4	0.13	0.40	0.14
Control Protein	0.16	0.087	0.042
Protein Std dev	0.0039	0.0138	0.0009

Table 38: Compiled destructive sampling data for only B. subtilis column.

B. subtilis

Calcium

	Calcium (mg/L)	Total Volume (L)	Calcium (mg)	gr bead	Calcium (mg/gr bead)
Top	9	0.002	0.0171	0.11	0.16
Middle	15	0.002	0.0307	0.3	0.10
Bottom	27	0.002	0.0548	0.31	0.18

Protein

	Protein (mg/gr bead)
Top	0.31
Middle	1.5
Bottom	0.33

Plate Counts

	Log CFU/gr bead
Top	7.32
Middle	6.01
Bottom	5.86

Direct Counts

	Log Total cells/gr bead
Top	8.8
Middle	8.2
Bottom	7.8

Graphing Data

	Top	Middle	Bottom	
Plate Counts	7.32	6.01	5.86	Log CFU/gr bead
Plate Count Std Dev	0.26	0.14	0.091	
Direct Counts	8.8	8.2	7.8	log total cells/gr bd
Direct Counts Std Dev	0.235	0.277	0.353	
B. subtilis Calcium	0.16	0.10	0.18	mg/gr bd
Protein	0.31	1.5	0.33	mg/gr bd
Protein Std Dev	0.0336	1.85	0.484	

APPENDIX C

PROTEIN COMPARISON

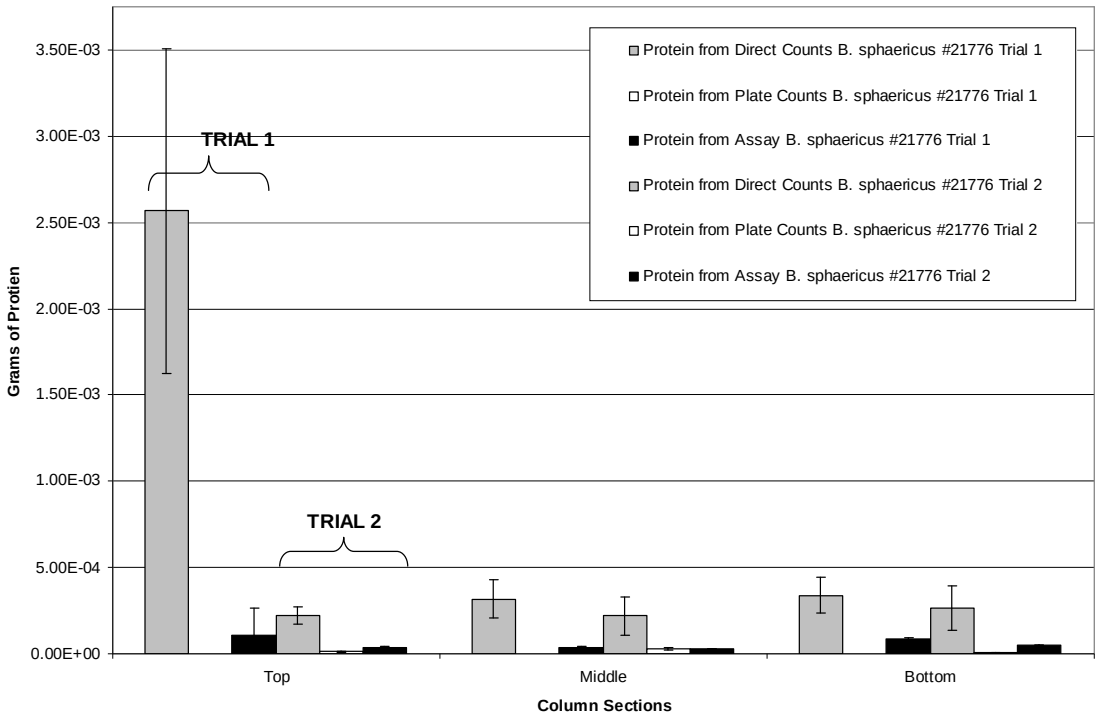

Figure 103: Estimated mass of protein based on plate counts, direct counts, and the Coomassie protein assay for all *B. sphaericus* #21776 trials. Error bars represent one standard deviation.

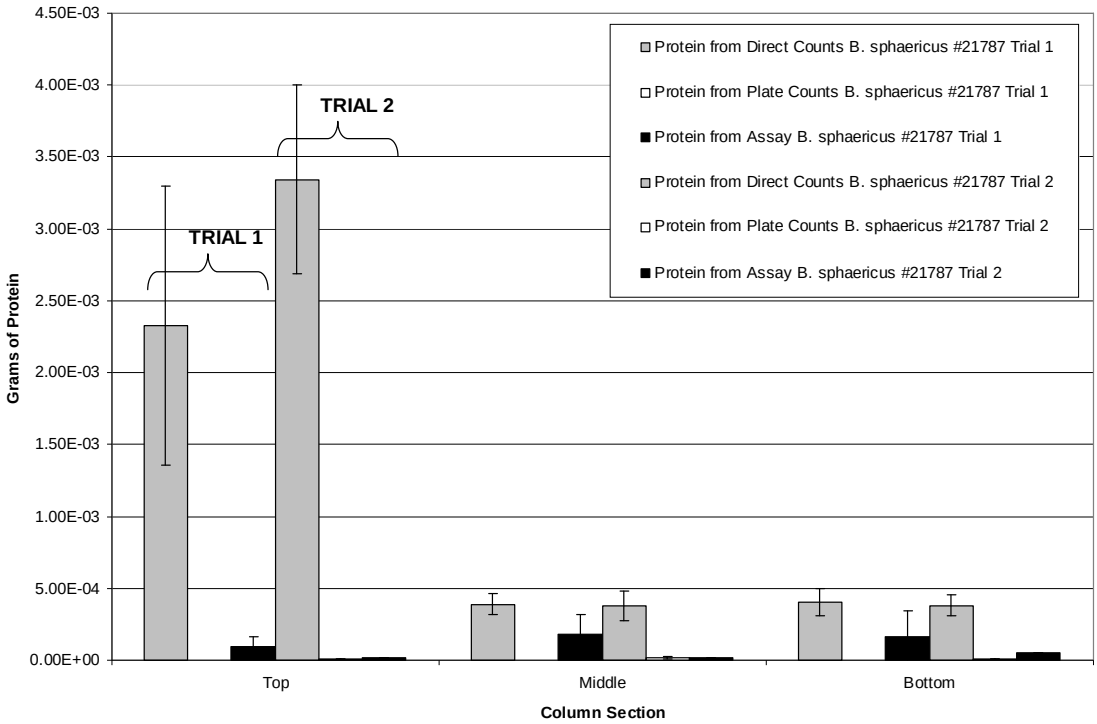

Figure 104: Estimated mass of protein based on plate counts, direct counts and the Coomassie protein assay for all *B. sphaericus* #21787 trials. Error bars represent one standard deviation.

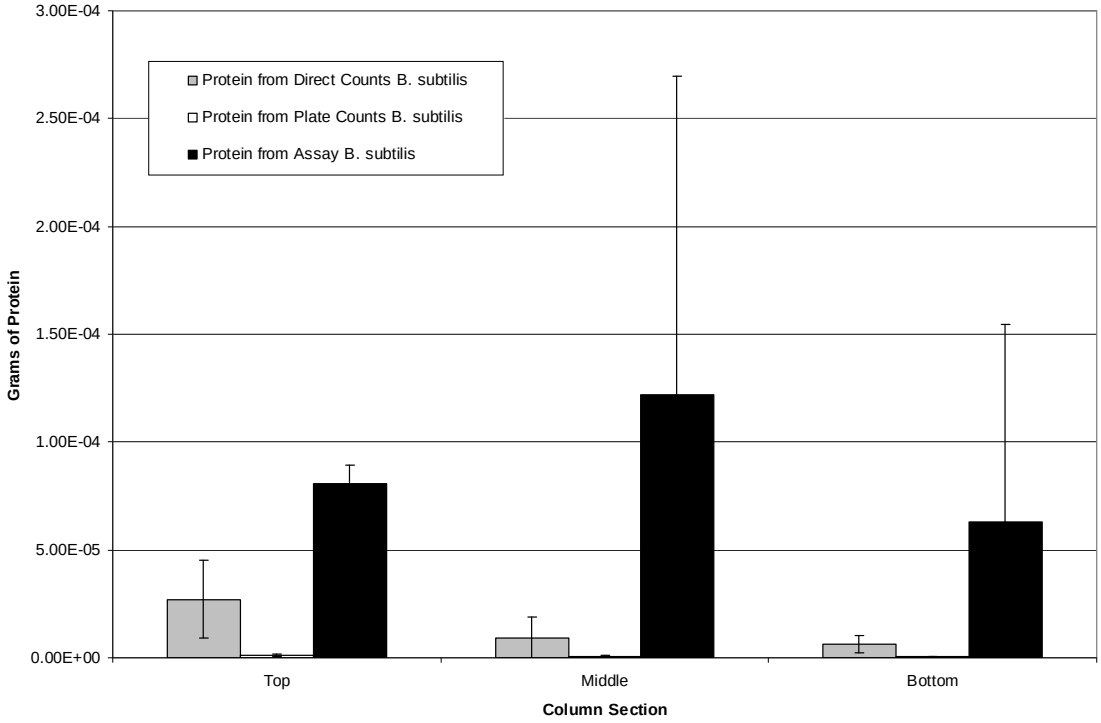

Figure 105: Estimated mass of protein based on plate counts, direct counts and the Coomassie protein assay for only *B. subtilis* trial. Error bars represent one standard deviation.

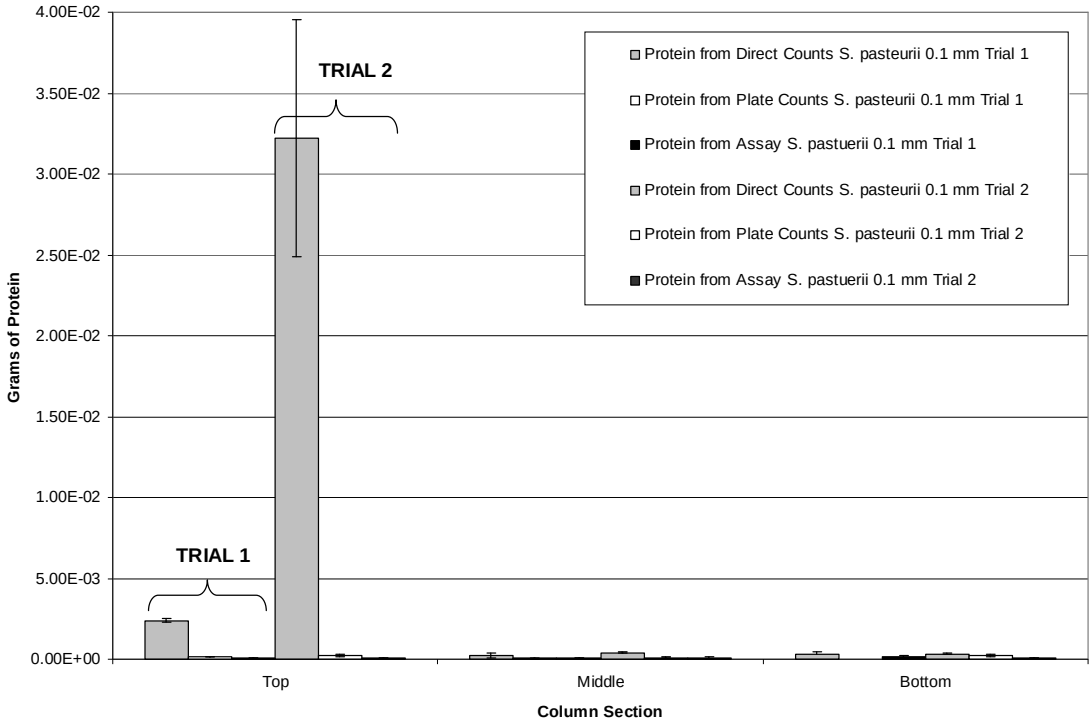

Figure 106: Estimated mass of protein based on plate counts, direct counts and the Coomassie protein assay for both 0.1 mm *S. pasteurii* columns. Error bars represent one standard deviation.

APPENDIX D

CALCIUM ANALYSIS

In order to understand the distribution of calcium in the pulse-flow column system, a mass balance on calcium for each column was performed.

First, the mass of calcium entering the column over the entire calcium sampling period was calculated. The total volume of CMM+ pumped into the column was calculated by adding up the effluent sample volumes for the time period for when calcium was sampled only. The influent concentration of calcium for each column is 1000 (mg/L). Due to errors in making the CMM+ medium, the influent concentration for the control #1 column is 1100 mg/L and the influent concentration for the control #2 column is 1300 mg/L. The total mass of calcium added to the column was calculated as follows:

$$\text{mass of Ca} = \text{total volume of medium exchanged} \quad \text{x} \quad \text{inf luent concentration } \frac{\text{mg}}{\text{L}}$$

The mass of calcium in the column effluent was calculated by multiplying the amount of calcium in each effluent sample. This was done by multiplying the volume of effluent collected by the calcium concentration obtained from the ICP-MS measurement from each day. Values for days that had no ICP-MS measurements were estimated by taking the average of the measurements on the day before and the day after. The total mass of calcium in the effluent was found by adding up the mass of calcium precipitated out each day.

$$\text{mass of Ca} = \text{effluent ICP} - \text{MS measurement } \frac{\text{mg}}{\text{L}} \quad \text{x} \quad \text{effluent sample volume (L)}$$

Subtracting the total mass of calcium in the effluent samples from the total mass of calcium in the influent yields the total mass of calcium that is retained in the column.

Using the destructive sampling data for each column that details how much calcium was found in each column section, the mass of calcium deposited on just the beads is calculated: The mass of calcium per gram of bead for each column section was averaged over the whole column and multiplied by the mass of beads in the column.

$$\left(\frac{(\text{top} + \text{middle} + \text{bottom}) \dfrac{\text{mg Ca}}{\text{gr bead}}}{3} \right) \text{X } 29.5 \frac{\text{gr beads}}{\text{column}} = \frac{\text{mg Ca}}{\text{column}}$$

Subtracting the mass of calcium that is retained on the beads from the total mass of accumulated calcium leave the mass of calcium that is retained on other parts of the system such as the column walls, silicon tubing, fittings, and glass pieces.

Calcium mass balances for each column are tabulated below.

Table 39: Calcium mass balance for all three *S. pasteurii* trials.

Trial	**Influent Calcium (mg)**	**Effluent Calcium (mg)**	**Accumulated Ca (mg)**	**Calcium Retained on Beads (mg)**	**Calcium Retained on System Parts (mg)**
1	116	3.8	112	54	58
2	68	0.64	68	11	57
3	70	1.1	69	8.3	61

Table 40: Calcium mass balance for both *B. sphaericus* #21776 trials.

Trial	Influent Calcium (mg)	Effluent Calcium (mg)	Accumulated Ca (mg)	Calcium Retained on Beads (mg)	Calcium Retained on System Parts (mg)
1	110	33	77	6.8	70
2	64	0.38	63	7.7	56

Table 41: Calcium mass balance for both *B. sphaericus* #21787 trials.

Trial	Influent Calcium (mg)	Effluent Calcium (mg)	Accumulated Ca (mg)	Calcium Retained on Beads (mg)	Calcium Retained on System Parts (mg)
1	104	43	61	41	19
2	69	0.47	69	6.8	62

Table 42: Calcium mass balance for both 0.1 mm *S. pasteurii* trials.

Trial	Influent Calcium (mg)	Effluent Calcium (mg)	Accumulated Ca (mg)	Calcium Retained on Beads (mg)	Calcium Retained on System Parts (mg)
1	34	0.53	33	19	15
2	70	1.2	69	4.7	64

Table 43: Calcium mass balance for single *B. subtilis* trial.

Trial	Influent Calcium (mg)	Effluent Calcium (mg)	Accumulated Ca (mg)	Calcium Retained on Beads (mg)	Calcium Retained on System Parts (mg)
1	107	91	16	4.3	12

Table 44: Calcium mass balance for all control trials.

Trial	Influent Calcium (mg)	Effluent Calcium (mg)	Accumulated Ca (mg)	Calcium Retained on Beads (mg)	Calcium Retained on System Parts (mg)
1	118	107	11	3.5	7.6
2	130	114	16	5.9	10
3	68	20	48	24	24
4 (0.1 mm)	73	48	24	4.6	20

This data suggests that that more calcium accumulates in the columns inoculated with ureolytic bacteria. All 1 mm columns inoculated with a ureolytic bacteria, except for the first *S. pasteurii* trial accumulate between 63 and 77 mg. This is significantly higher than the amount of calcium accumulated in the control columns or the columns inoculated with B, *subtilis*, a non-ureolytic organism. Therefore, the ureolytic bacteria are able to establish a viable biofilm community that utilizes urea and promotes the precipitation of calcium carbonate.

REFERENCES CITED

1. Montana State University. (2005). Retrieved 9/27/07 from http://www.montana.edu/zert/home.php

2. Rosenberg, Matt (2008). *Current World Population: Current population and world population growth since the year one*. Retrieved 7/3/08 from http://geography.about.com/od/obtainpopulationdata/a/worldpopulation.htm

3. United States Statistics Division. (2003). [Data table of 2003 CO_2 emission per country]. Retrieved 9/07 from http://unstats.un.org/unsd/environment/air_co2_emissions.htm

4. Yoon, J, Lee, K, Weiss, N, Kho, Y.H., Kang, K.H., and Park, Y. (2001). *Sporosarcina aquimarina* sp. nov., a bacterium isolated from seawater in Korea, and transfer of *Bacillus globisporus* (Larkin and Stokes1967), *Bacillus psychrophilus* (Nakamura 1984) and *Bacillus pasteurii* (Chester 1898) to the genus *Sporosarcina* as *Sporosarcina globispora* comb. nov., *Sporosarcina psychrophila* comb.nov. and *Sporosarcina pasteurii* comb. nov., and emended description of the genus *Sporosarcina*. *International Journal of Systematic and Evolutionary Microbiology, 51(3),* 1079-1086.

5. White, C.M., Strazisar B.R., Granite, E.J., Hoffman, J.S., & Pennline, H.W. (2003). Separation and Capture of CO2 from Large Stationary Sources and Sequestration in Geological Formation-Coal beds and Deep Saline Aquifers. *Journal of the Air and Waste Management Association, 53,* 645-715.

6. Statoil. (2000). Carbon dioxide storage prized. Retrieved 6/08 from http://www.statoil.com/statoilcom/SVG00990.NSF?OpenDatabase&artid=01A5A730136900A3412569B90069E947

7. Van Lith Y., Warthmann R., Vasconcelos C., McKenzie J.A. (2003). Microbial fossilization in carbonate sediments: a result of the bacterial surface involvement in dolomite precipitation. *Sedimentology, 50(2),* 237-245.

8. Hammes F., Boon N., de Villiers J., Verstraete W., Siciliano S.D. (2003). Strain-Specific Ureolytic Microbial Calcium Carbonate Precipitation. *Applied and Environmental Microbiology, 69(7),* 4901-4909.

9. Harter, Thomas. (2003). Groundwater quality and Groundwater Pollution. University of California Department of Agriculture and Natural Resources. Publication 8084, FWQP Reference Sheet 11.2 Retrieved 5/08 from http://groundwater.ucdavis.edu/Publications/Harter_FWQFS_8084.pdf

10. Clanton, B., Fowler, T., and Hays, K. (2007). Underground CO_2 storage can be done "off the shelf" says UT prof. *Houston Chronicle Online Blog*. Retrieved 10/07 from http://blogs.chron.com/newswatchenergy/archives/2007/09/underground_co2.html

11. Schultze-Lam S., Fortin D., Davis B.S., Beveridge T.J. (1996). Mineralization of bacterial surfaces. *Chemical Geology, 132,* 171-181.

12. Stocks-Fischer S., Galinat J.K., Bang S.S. (1999). Microbiological precipitation of $CaCO_3$. *Soil Biology and Biochemistry, 31(11),* 1563-1571.

13. Mitchell A.C., Ferric F.G. (2006). The influence of *Bacillus pasteurii* on the Nucleation and Growth of Calcium Carbonate. *Geomicrobiology Journal, 23(3 &4),* 213-226.

14. Ehrlich, HL. (2002). *Geomicrobiology* (4th Ed.). New York: Marcel Dekker Inc.

15. Todar, Kenneth. 2005. *Todar's Online Textbook of Bacteriology*. Retrieved 6/07 from http://textbookofbacteriology.net/Bacillus.html

16. Fujita Y., Ferris F.G., Lawson R.D., Colwell F.S., Smith R.W. (2000) Calcium Carbonate Precipitation by Ureolytic Subsurface Bacteria. *Geomicrobiology Journal, 17(4),* 305-318.

17. Mitchell A.C., Ferris F.G. (2006). Effect of Strontium Contaminants upon the Size and Solubility of Calcite Crystals Precipitated by the Bacterial Hydrolysis of Urea. *Environmental Science Technology, 40(3),* 1008-1014.

18. MacLeod F.A., Lappin-Scott H.M., Costerton J.W. (1988). Plugging of a Model Rock System Using Starved Bacteria. *Applied and Environmental Microbiology, 54(6),* 1365-1372.

19. Ferris F.G., Stehmeier L.G. (1992). United States Patent: Bacteriogenic Mineral Plugging. Patent Number: 5,143,155.

20. Ferris FG, Stehmeier LG, Kantzas A, Mourits FM. 1996. Bacteriogenic Mineral Plugging. *The Journal of Canadian Petroleum Technology,* 56-61.

21. Jonkers H.M, Schlangen E. (2007). Retrieved 6/10/2008 from http://www.tudelft.nl/live/pagina.jsp?id=3cf7b0b5-a317-4320-9246-ab8b156b75c2&lang=en

22. Ramachandran S.K., Ramakrishnan V., Bang S.S. (2001). Remediation of Concrete Using Micro-organisms. *ACI Materials Journal*; *98,* 3-9.

23. Rodriguez-Navarro C., Rodriguez-Gallego M., Chekroun K.B., Gonzalez-Muñoz M.T. (2003). Conservation of Ornamental Stone by *Myxococcus xanthus*-Induced Carbonate Biomineralization. *Applied and Environmental Microbiology, 69(4),* 2182-2193.

24. Bachmier K.L., Williams A.E., Warmington J.R., Bang S.S. (2002). Urease activity in microbiologically-induced calcite precipitation. *Journal of Biotechnology, 93(2)*, 171-181.

25. Gollapudi U.K., Knutson C.L., Bang S.S., Islam M.R. (1995). A new method for controlling leaching through permeable channels. *Chemosphere, 30(4)*, 695-705.

26. Vandevivere P., Baveye P. (1992). Relationship Between Transport of Bacteria and Their Clogging Efficiency in Sand Columns. *Applied and Environmental Microbiology, 58(8)*, 2523-2530.

27. Murray J., Irvine R. (1889/1890). On Coral Reefs and other Carbonate of Lime Formations in Modern Seas. *Proceedings of the Royal Society of Edinburgh, 17*, 79-109.

28. Kawaguchi T., Decho A.W. (2002). A laboratory investigation of cyanobacterial extracellular polymeric secretions (EPS) in influencing $CaCO_3$ polymorphism. *Journal of Crystal Growth, 240(1&2)*, 230-235.

29. Beveridge T.J. (1988). The bacterial surface: general consideration towards design and function. *Canadian Journal of Microbiology, 34(4)*, 363-372.

30. Ghannoum M.A., O'Toole G.A. (Eds.) (2004). *Microbial Biofilms*. Washington, D.C.: ASM Press.

31. Mitchell A.C., Ferris F.G. (2005). The coprecipitation of Sr into calcite precipitates induced by bacterial ureolysis in artificial groundwater: Temperature and kinetic dependence. *Geochimica et Cosmochimica Acta, 69(17)*, 4199-4210.

32. Hammes F., Seka A., Van Hege K., Van de Wiele T, Vnaderdeelen J., Siciliano S.D., Verstraete W. (2003). Calcium Removal from industrial wastewater by biocatalytic $CaCO_3$ precipitation. *Journal of Chemical Technology and Biotechnology, 78(6)*, 670-677.

33. Leonard J. (1986). Increased rate of EOR brightens outlook. *Oil and Gas Journal*, April, *84*, 71-101.

34. Arcangeli, J.P., Arvin E. (1995). A membrane de-oxygenator for the study of anoxic processes. *Water Research, 29(9)*, 2220-2222.

35. What is carbon sequestration? National Energy Technology Laboratory (NETL). Retrieved 6/26/08 from http://www.netl.doe.gov/technologies/carbon_seq/FAQs/carbon-seq.html.

36. Loxnachar, T.E., Brown, K.W., Cooper, T.H., Milford, M.H. (1999). *Sustaining Our Soils and Society*. American Geological Institute, Soil Science Society of America, USDA Natural Resource Conservation Service publication. Retrieved 6/26/08 from http://www.co.portage.wi.us/groundwater/undrstnd/soil.htm

37. Calcite. Retrieved 6/29/08 from Wikipedia: http://en.wikipedia.org/wiki/Calcite

38. (2002). Physical Properties. Retrieved 6/29/08 from http://odp.pangaea.de/publications/197_IR/chap_03/c3_8.htm

39. McConnell, David. (2000). *The Good Earth*. McGraw-Hill, Inc. Retrieved 6/29/08 from http://www.mhhe.com/earthsci/geology/mcconnell/demo/prop.htm

40. Bang, S, and Bang, S. (2008). Microbial Dust Suppression [Abstract]. National Science Foundation Grant Award #0725398. Retrieved 7/08 from http://www.nsf.gov/awardsearch/showAward.do?AwardNumber=0725398

41. pH. Retrieved 12/4/07 from Wikipedia: http://en.wikipedia.org/wiki/PH

42. Stewart, P.S. (2003). Diffusion in Biofilms. *Journal of Bacteriology, 185(5),* 1485-1491.

43. Stewart, P.S. (1997). A Review of Experimental Measurements of Effective Diffusive Permeabilities and Effective Diffusion Coefficients in Biofilms. *Biotechnology and Bioengineering, 59(3),* 261-272.

44. Westrin, B.A., and Axelsson, A. (1991). Diffusion in gels containing immobilized cells: A critical review. *Biotechnology and Bioengineering, 38(5),* 439-446.

45. (2008). DuPont Dust Suppression: Effective Solutions for a Serious Problem. Retrieved 7/23/08 from http://www2.dupont.com/Products_and_Services /en_AU/products/dustsuppression.html

46. Dust and Potential Health Problems. Alaska Department of Environmental Conservation. Retrieved on 7/23/08 from http://www.dec.state.ak.us/air/anpms/as /doc/w13NOV06-Dust&Health.pdf

47. "Nucleic Acid and Protein Content of a Bacterial Cell." (2000) Roche Diagnostic Corporation. Retrieved 11/12/08 from http://www.roche-applied-science.com/labfaqs/p5_4.htm

48. Joint Departments of the Army and Air Force USA. (1987). Technical Manual TM 5-830/AFM 88-17, Dust Control for Roads, Airfields, and Adjacent Areas, Unified Facilities Criteria (UFC), Chapter 3. Retrieved 7/23/08 from http://www.tpub.com/content/UFC1/ufc_3_260_17/